

MOLECULAR BEAM STUDIES OF MODEL NSR CATALYSTS

Daniel Archard

A thesis submitted for the degree of Doctor of Philosophy at
Cardiff University

May 2008

UMI Number: U585110

All rights reserved

INFORMATION TO ALL USERS

The quality of this reproduction is dependent upon the quality of the copy submitted.

In the unlikely event that the author did not send a complete manuscript and there are missing pages, these will be noted. Also, if material had to be removed, a note will indicate the deletion.



UMI U585110

Published by ProQuest LLC 2013. Copyright in the Dissertation held by the Author.
Microform Edition © ProQuest LLC.

All rights reserved. This work is protected against
unauthorized copying under Title 17, United States Code.



ProQuest LLC
789 East Eisenhower Parkway
P.O. Box 1346
Ann Arbor, MI 48106-1346

DECLARATION

This work has not previously been accepted in substance for any degree and is not being concurrently submitted in candidature for any degree.

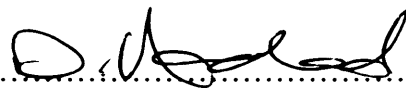
Signed (candidate)

Date 28-08-08

STATEMENT 1

This thesis is the result of my own investigations except where otherwise stated.


Other resources are acknowledged by footnotes giving explicit references. A bibliography is appended.

Signed (candidate)

Date 28-08-08

STATEMENT 2

I hereby give consent for my thesis, if accepted, to be available for photocopying and for inter-library loan, and for the title and summary to be made available to outside organisations.

Signed (candidate)

Date 28-08-08

ACKNOWLEDGEMENTS

Firstly I would like to thank Professor Michael Bowker at Cardiff University for taking me on as his PhD student and for all the assistance and help that he has given me during the course of my studies. His knowledge and experience in the fields of surface science and NO_x catalysis has been invaluable. I would also like to thank my co-supervisor Dr. Phil Davies for the assistance, encouragement and ideas that he has contributed during this time.

This project was jointly funded by the EPSRC and Toyota Japan and I am grateful for their support.

For their advice concerning Low Energy Electron Diffraction and general help with mechanical issues the following people at Cardiff deserve special mention: Dr Albert Carley, Dr Christian Morgan, Dr David Morgan, Dr Federico Grillo, Dr Alistar McDowell, Dr Matt Hall and Professor Gary Attard.

Lastly I would like to thank every friend, family member and work colleague in Cardiff and Swansea who has contributed to this research and my personal development over the last three years. I am happy to say that there are too many of these people to mention individually.

ABSTRACT

The adsorption and reaction of various simple molecules (O_2 , NO , CO and NO_2) commonly associated with gasoline engine exhaust catalysis were investigated on a model catalytic system under ultra-high vacuum conditions using a variety of surface science techniques including molecular beam scattering and temperature programmed desorption. The model catalytic surfaces studied were clean $\text{Pt}(111)$, $\text{K}/\text{Pt}(111)$ and $\text{BaO}/\text{Pt}(111)$ surfaces. The alkaline and alkaline earth metal surfaces were prepared by metal vapour deposition (in an oxygen background in the case of BaO) and annealing. Also investigated was the ability of each of the catalytic surfaces to oxidise NO and CO and to store and reduce NO_2 . It was found that the clean $\text{Pt}(111)$ surface was effective at oxidising CO provided the oxygen was in an adsorbed atomic form. $\text{Pt}(111)$ was also found to be effective in the reduction of NO_2 . NO and O_2 were found to react in a gas phase reaction that made mixed molecular beam studies problematic however it was found when beaming NO with a background pressure of O_2 that no $\text{Pt}(111)$ catalysed surface reaction was observed. It was found that dosing K onto the $\text{Pt}(111)$ surface increased the sticking coefficient of oxygen greatly and that more than a monolayer of K on the surface catalysed the reduction of NO to N_2 . Unlike the $\text{Pt}(111)$ surface, $\text{K}/\text{Pt}(111)$ was capable of storing NO_2 without it being immediately reduced. Potassium peroxide however was found to prevent NO_2 storage. In a similar fashion to K , NO_2 was stored on BaO , being released as NO and O_2 on heating. NO is partially reduced to N_2O by the BaO surface at ambient temperature with increased temperature favouring complete reduction to N_2 .

CONTENTS

1	AN INTRODUCTION TO SURFACE SCIENCE AND NSR CHEMISTRY	<i>1</i>
2	EXPERIMENTAL: SURFACE SCIENCE EQUIPMENT AND TECHNIQUES	<i>26</i>
3	THE BEHAVIOUR OF Pt(111) IN THE Pt(111)/BaO NSR CATALYST	<i>62</i>
4	THE EFFECT OF POTASSIUM ON THE SURFACE CHEMISTRY OF NO, CO AND O₂ ON Pt(111) AND ITS SUITABILITY AS A POTENTIAL NO_x STORAGE COMPONENT	<i>115</i>
5	THE EFFECT OF Ba AND BaO ON THE SURFACE CHEMISTRY OF NO, CO AND O₂ ON Pt(111), AND THE SUITABILITY OF BaO AS A NO_x STORAGE COMPONENT IN THE NSR CATALYST	<i>185</i>
6	CONCLUSIONS AND FUTURE WORK	<i>232</i>

1. AN INTRODUCTION TO SURFACE SCIENCE AND NSR CHEMISTRY

1.1	<i>Surface Science</i>	2
1.2	<i>Surface Reactions and Processes Under Ultrahigh Vacuum</i>	6
1.2.1	<i>The single crystal surface</i>	6
1.2.2	<i>The Miller index</i>	6
1.2.3	<i>Surface structure and topography</i>	8
1.2.4	<i>Adsorption processes</i>	9
1.2.5	<i>Physisorption</i>	11
1.2.6	<i>Chemisorption</i>	12
1.2.7	<i>Kinetics of surface adsorption processes</i>	13
1.2.8	<i>Adsorption isotherms</i>	14
1.2.9	<i>The surface</i>	17
1.3	<i>The NSR Process</i>	17
	REFERENCES	24

1. AN INTRODUCTION TO SURFACE SCIENCE AND NSR CHEMISTRY

1.1 Surface science

A catalyst is a substance that affects the rate at which a chemical reaction reaches its equilibrium position. Although the catalyst participates in the reaction it is regenerated intact at the end of the reaction and does not undergo a permanent chemical change. In effect, the catalyst lowers the activation energy barrier to reaction, thus speeding up the reaction.

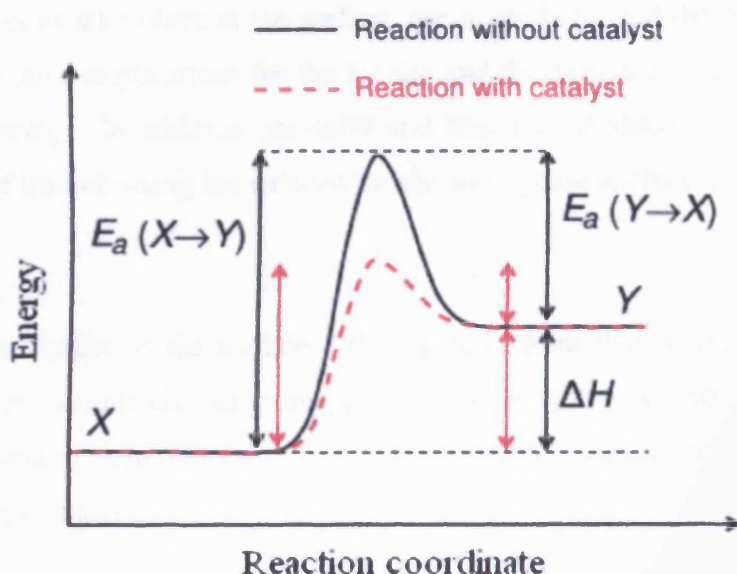


Figure 1.1 - Catalyst-lowered activation energy. Adapted from image created by Brian Kell, University of Nebraska–Lincoln.¹

It does this without altering the equilibrium composition of the final state, as the energetics of the final and initial states are unchanged. In addition to this the catalyst may also be able to increase the selectivity of a particular process towards a desired product by lowering the activation energy barrier to formation of the desired product whilst having a lesser effect on the activation energy of formation of the unwanted side product. An example of this is the catalytic formation of acrolein from propylene despite the combustion process being far more thermodynamically favourable². Catalysis of some kind is necessary in the majority of industrial chemical processes and without biological catalysts, enzymes, life would not exist.

Catalysts are particularly useful from an environmental point of view as, in addition to removal of unwanted polluting by-products from a process they can also be used to tune a process so that the unwanted products are not produced in the first place, as well as making the process more energy efficient, making it occur at a lower temperature². For instance the Haber process, which uses an iron catalyst to react hydrogen and nitrogen to produce ammonia has enabled the cost effective production of fertilizer and is of massive industrial importance.

Heterogeneous reactions are reactions that take place in systems in which there are at least two different phases present. The reaction occurs at the interface between these phases. In catalytic chemistry the role of the catalytic surface is crucial. Reactions take place at the surface, not in the bulk, and the properties of the surface have major implications for the kinetic and thermodynamic parameters of the reaction occurring. In addition gas-solid and liquid-solid phase catalysis gives the opportunity of immobilising the catalyst on the solid phase surface and hence reusing it.

The energetics at the surface differs greatly from that of the bulk. Surface atoms are not completely surrounded by their neighbours and therefore have unsatisfied bonding requirements. This is manifest in a 'desire' to react, with great implications for catalysis.

It follows from this that understanding the processes occurring at the surface is essential for improving and optimising catalysed chemical processes. This has led to the development of the branch of physical chemistry known as surface science. Surface science allows the investigation of model surfaces through single crystals and nanoparticulate arrays on an atomic scale. Through observing processes such as adsorption and desorption, surface decompositions and catalysed reactions and surface diffusion a picture of the overall mechanisms taking place can be proposed and developed. Building an understanding of the fundamental processes occurring on an atomic scale is necessary before scaling up and interpreting observations made on a macroscopic scale in catalytic reactors.

The first surface science experimental observations date back almost two centuries³ with Davey's observations of the impairment of catalytic activity of a platinum wire by the growth of a carbide film. However, it was Langmuir's work on surface adsorbate coverage⁴ and dissociative chemisorption⁵, the development of the Langmuir-Hinshelwood theory^{6,7}, the work by Eley and Rideal leading to the Rideal-Eley mechanism⁸, Lennard-Jones' work on activated adsorption⁹, and the work on adsorption via physisorption and/or chemisorption by Taylor¹⁰, that set the foundations for surface science as it is today.

Later on in the twentieth century surface science changed dramatically with the advent of scanning tunnelling microscopy (STM). Invented by Binnig and Rohrer^{11,12} in 1983, STM allowed a three-dimensional map of a section of the surface under scrutiny to be produced. Shortly after this it was demonstrated that matter could be manipulated on the atomic scale¹³.

Possibly the principal utilisation of surface science is that of as an aid to understanding the processes in heterogeneously catalysed reactions. Perhaps one of the best examples of the practical use of surface science with regards to heterogeneous catalysis is the improvement in the industrial process for the production of ethylene oxide. Via optimisation of the oxidation catalyst a large increase in product selectivity was attained. The original process used a silver catalyst but it was discovered by chance that the addition of chlorine enhanced the yield of ethylene oxide over combustion products significantly. This led to the surface investigation of chlorine atoms on a silver surface, which has helped develop the oxidation catalyst and led to the invention of introducing microscopic amounts of chlorine into the gas feed¹⁴.

Analysis of catalytic reactions is generally done under vacuum pressures to minimise contamination of the process. Simple kinetic theory (see pages 10 and 27) tells us that at a pressure of 1×10^{-6} mbar a surface experiences $\sim 10^{15}$ collisions from gas molecules per square centimetre every second. If one assumes a sticking probability of unity the surface would develop a complete monolayer of adsorbed gas molecules in as little as one second. It follows from this that reducing the pressure will increase the time that the surface remains 'clean' and uncontaminated. Modern

ultrahigh vacuum (UHV) systems are capable of maintaining a system pressure of as little as 10^{-11} mbar. Under these conditions surfaces will remain clean for several hours¹⁵.

Since the 1950's there has been a continued increase in the number of techniques available to chemists for the study of surfaces. These generally measure only a single, or at most a few properties of the surface. These may include surface compositions and structures, chemical properties, oxidation states or electronic properties. The resolution obtainable is constantly improving as surface chemistry strives for an understanding of the processes occurring at the molecular level. As no single technique provides a definitive picture of the surface it is necessary to utilise complementary combinations of surface science techniques¹⁹.

Due to their nature as particles, atoms, ions and electrons are of immense use as probes of surface structure and reactivity, as they can penetrate the surface by no more than a few angstroms. Depending on wavelength photons may also be used for the examination of surfaces and high-energy photons (X-Rays) are useful for examination of bulk structure and properties. Photons can also be employed at higher pressures due to the lower scattering cross sections exhibited.

It is worth noting that applying surface science data directly to real industrial catalytic processes may be problematic due the vast differences in pressures encountered and non-uniformity in catalysts and reagents. Surface science is thus at its most useful as an aid to determining the fundamental reaction steps occurring in model systems, the data from which can then be taken and scaled up to the macroscopic scale.

1.2 Surface reactions and processes under ultra-high vacuum

1.2.1 The single crystal surface

The work presented in this thesis is concerned with the interaction of various gases with a clean and metal vapour-dosed single crystal surface. Many metals, semi-conductors and insulators can be grown as single crystals, which can then be specifically cut to reveal faces with a specific Miller index. Metal single crystals are generally grown by the gradual drawing of a rod of metal from a molten mass¹⁵.

The platinum single crystal used in the experiments has been cut from a larger crystal that has been aligned using Laue X-Ray back scattering such that the desired crystallographic plane is left exposed. The cutting technique used is usually a grinding or spark erosion technique. The angle at which the cut is made determines the topography of the crystal surface^{15,20}.

The advantage of using a single crystal as a reaction surface is one of simplicity. A carefully prepared single crystal surface is the closest approximation attainable to the ideal surface (one that consists of a perfectly periodic array of surface atoms). However, the three dimensional periodicity and properties associated with the bulk material do not abruptly terminate at the crystal surface. Instead there is a gradual transition region in which the chemical, geometric and electronic properties are different from those encountered in the bulk¹⁶. A low index single crystal surface plane has a limited number of adsorption sites to which molecules can bind. This allows the analysis of the fundamental processes occurring when a molecule collides with the surface.

1.2.2 The Miller index

The Miller index is a notation that is used to describe a given lattice plane. It is a measure of where the lattice plane intersects the x y and z crystallographic axis. Hence the (111) face of platinum used in the work contributing to this thesis cuts the x y and z-axis of the unit cell at equal distances from the point of origin.

The Miller index is the reciprocal of these intercepts ie.

Axis	Intercept	Reciprocal
x	1	$1/1 = 1$
y	1	$1/1 = 1$
z	1	$1/1 = 1$

In cases where reciprocals result in fractional indices it is convention to multiply by the highest denominator to remove the fractions.

The low index Miller indices (100), (110), and (111) for a primitive cubic system are shown below.

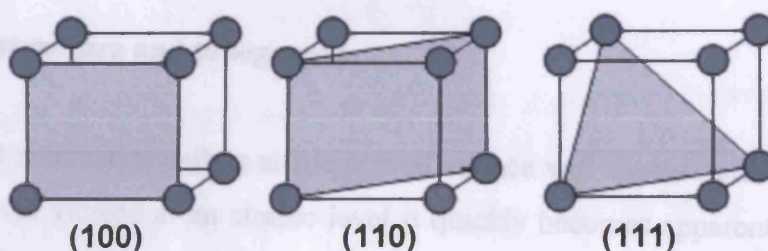


Figure 1.2 – The (100), (110) and (111) surfaces of a fcc cubic crystal. Adapted from ‘Surface Chemistry’ by Elaine McCash.¹⁵

The different Miller indices have different packing of surface atoms. The (110) surface is the most open surface structure, then the (100), with the (111) surface being the most close packed. When performing surface studies it is important that the crystal plane under study be known as the packing of the surface has a marked effect on the reactivity of the surface. For instance Pt(110) readily adsorbs O_2 with an appreciable sticking coefficient, whereas the more closely packed Pt(111) adsorbs O_2 with a very small initial sticking coefficient (~ 0.07).¹⁷

The single crystal surfaces typically used for studies in surface science are well defined and are generally body centred cubic (bcc) or face centred cubic (fcc) in three-dimensional structure.

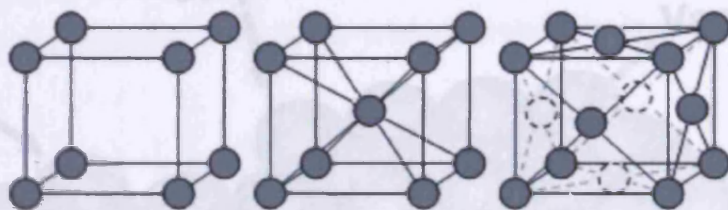


Figure 1.3 - The simple cubic (sc), body centred cubic (bcc) and face centred cubic (fcc) crystal lattices. Adapted from 'Surface Chemistry' by Elaine McCash¹⁵ and 'An Introduction to Surface Chemistry' by Dr Roger M. Nix¹⁸.

Sample preparation is an important aspect of surface science. Ion bombardment and/or heat/chemical treatment is required to remove impurities from the surface and the bulk of the crystal. Thin film adlayers may then be added to the surface by chemical vapour deposition or by straight vapour phase deposition.

1.2.3 Surface structure and topography

Viewed macroscopically a single crystal surface will appear perfectly flat and uniform, however viewed at an atomic level it quickly becomes apparent that this is not the case. Crystals are typically cut to within 0.5% of the desired plane and since the atom is the smallest viewable building block of the surface this creates a terraced surface. In addition to this there may be other defects such as surface vacancies, kinks and adatoms present. The Terrace-Step-Kink (TSK) model best explains this.

1.2.4 Adsorption processes

Adsorption is the outcome of a molecule in an atomic collision in which the final result is the sticking of the molecule to the surface. Adsorption is not the only possibility for the collision event however, the molecule may be reflected back into the vacuum with its energy intact (elastic scattering) or may lose or gain energy in the

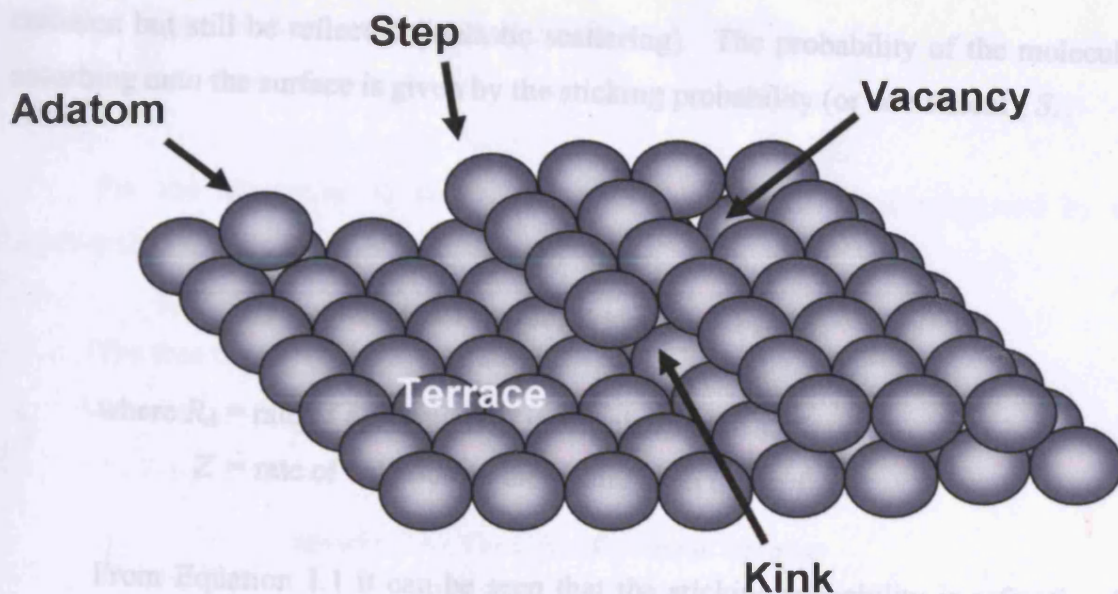


Figure 1.4 - Some of the defects found at a surface. Adapted from 'Surface Science' by Kurt Kolasinski³¹.

This model relies upon the assumption that atoms are perfectly rigid and do not move and that they behave as if they were contained within the bulk. The reactivity of each site depends upon the number of surrounding atoms. Adatoms have the fewest neighbours whilst the atoms making up the terraces have the greatest. At equilibrium up to 20% of surface atoms might be in step sites and 5% at kinks on a rough surface^{19,20}.

A problem with this model is that real catalysts generally exhibit some mobility of surface atoms. Reconstructions can be induced by atomic movement from bulk sites to surface sites or via contractions in the selvedge (near surface) region^{21,22}. Defects are also generally produced during cutting and polishing of the crystal.

1.2.4 Adsorption processes

Adsorption is the outcome of a molecular or an atomic collision in which the final result is the sticking of the molecule to the surface. Adsorption is not the only possibility for the collision event however; the molecule may be reflected back into the vacuum with its energy intact (elastic scattering) or may lose or gain energy in the

collision but still be reflected (inelastic scattering). The probability of the molecule adsorbing onto the surface is given by the sticking probability (or coefficient), S .

$$S = \frac{R_A}{Z}$$

Equation 1.1 - The Sticking Probability

where R_A = rate of adsorption of molecules by the surface

Z = rate of collision of molecules with the surface

From Equation 1.1 it can be seen that the sticking probability is a fractional quantity. A sticking probability of one represents total adsorption whereas a sticking probability of zero indicates the total reflection of the gas phase species. The value of the sticking probability depends upon many variables such as the temperature of the surface, the energy of the adsorbing molecule, the surface coverage of adsorbed species and the nature of the system and crystal face under study.

As molecules continue to adsorb onto the surface more surface adsorption sites become occupied and the sticking probability decreases. The fraction of surface sites occupied is given by the surface coverage, θ , which is defined as

$$\theta = \frac{N_{ads}}{N_s} = \frac{\text{Number of adsorbed surface species}}{\text{Total number of available adsorption sites}}$$

Equation 1.2 – The Surface Coverage

The rate at which collisions take place can be given by the Hertz-Knudsen equation

$$Z = \frac{P}{(2m\pi kT)^{1/2}}$$

Equation 1.3 – The Hertz-Knudsen Equation²⁰

where P = pressure

m = mass of impacting atom or molecule

k = Boltzmann constant ($1.38066 \times 10^{-23} \text{ J K}^{-1}$)

T = temperature

For the adsorption to spontaneously occur it must be accompanied by a negative change in the free energy of the system ie. $\Delta G < 0$

The free energy change is given by the Gibbs-Helmholtz equation

$$\Delta G = \Delta H - T\Delta S$$

Equation 1.4 – The Gibbs-Helmholtz Equation

where ΔG = Gibbs free energy change

ΔH = change in enthalpy

T = temperature

ΔS = entropy change

As adsorbing molecules must have a negative free energy change, and the loss of freedom encountered on adsorption makes the entropy change when adsorbing negative it is obvious that the change in enthalpy must also be negative (an exothermic reaction). However, certain endothermic adsorptions are known, but these tend to be concerned with dissociative adsorption in which the system actually gains in disorder despite the fragments being bound ($\Delta S = +ve$). An example of an endothermic surface adsorption is the dissociative adsorption of hydrogen on glass. In this case the translational freedom of the adsorbate has actually increased upon adsorption with respect to the gas phase²³.

1.2.5 Physisorption

Physisorption is the rather weak adsorption that occurs as a result of the conflict between relatively weak attractive forces between the adsorbate and the surface (such as Van-der-Waals forces) and the repulsive forces associated with close proximity between the two species.

As there is no change in the bonding within molecules which undergo physisorption, physisorption is always exothermic. Despite this the change in enthalpy that accompanies the reaction is low.

In the potential energy diagram shown in Figure 1.5 a physisorbed molecule occupies a potential well in which it oscillates, with the oscillation energy dependent upon the temperature of the surface. If the molecule has sufficient energy supplied to it to overcome the energy barrier in the well it may emerge from the well and desorb from the surface or go on to undergo stronger bonding with the surface.

The surface residence time (τ) of the physisorbed molecule thus depends on the temperature of the surface and can be given by the Frenkel equation.

$$\tau = \tau_0 \cdot \exp\left(\frac{E_D}{R.T}\right)$$

Equation 1.5 – The Frenkel Equation^{31,24}

where τ = the surface residence time

τ_0 = the time of one vibration

E_D = desorption energy

Since energy of desorption is typically low (typically < 20 kJ mol⁻¹) surface residency times are also very short, normally around 10⁻⁸ s at room temperature³¹.

Physisorbed species generally exhibit a slight coverage dependence of the heat of desorption due to increased electric polarisation effects as the molecules become more densely packed on the surface¹⁵. Physisorption occurs regardless of the nature of the surface and adsorbate or the topography of the surface.

1.2.6 Chemisorption

Chemical adsorption (chemisorption) is the process by which adsorption occurs via formation of a strong bond between the surface and the adsorbate. As a

new bond is being formed chemisorption is characterised by the transfer of electrons between the adsorbate and the surface.

The bonds formed by chemisorbing molecules are stronger than the forces causing physisorption. This is reflected in the much greater changes in enthalpy and heats of adsorption (ΔH_{ads}) that occur. Due to the large negative enthalpy change that occurs when a species is chemisorbed (generally $\geq 100 \text{ kJ mol}^{-1}$), chemisorption is an exothermic process. The bonding that occurs may be either ionic or covalent in character or a mixture of both³¹.

Unlike physisorption, chemisorbing species usually display a degree of specificity in the level of interaction with a particular surface. In addition to the chemical character of the adsorbate the surface geometry may also effect the adsorption process.

Chemisorbed species generally exhibit a strong heat of desorption dependency on surface coverage. Due to charge transfer between adsorbed species and the surface setting up permanent dipoles and the electrostatic repulsion that exists between similarly charged species, formation of subsequent dipoles at the surface becomes less favourable, reflected in lower heats of desorption. Electrostatic coupling between closely packed adsorbates may also effect the heat of desorption for a particular species from the surface.

Chemisorption may be subdivided into dissociative and molecular chemisorption, referring to whether the molecule remains intact on adsorption (molecular chemisorption) or dissociates on adsorption (dissociative chemisorption).

1.2.7 Kinetics of surface adsorption processes

The rate of chemisorption varies greatly from system to system; this is largely controlled by the magnitude of the activation energy barrier. This is reflected in the Lennard Jones model; a one-dimensional potential energy diagram.

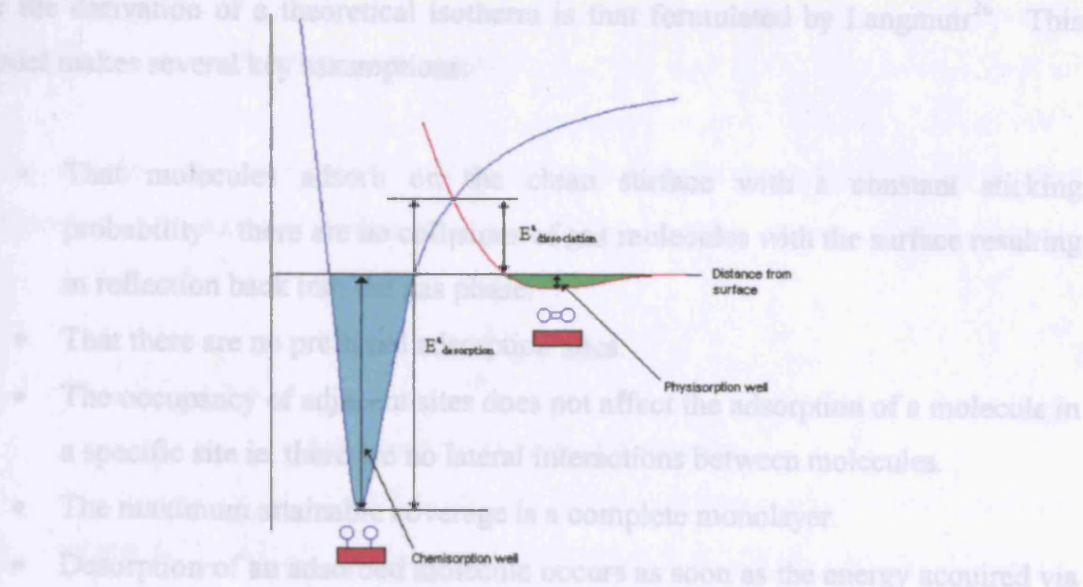


Figure 1.5 - Precursor mediated dissociative chemisorption of a diatomic molecule. Adapted from 'Surfaces' by Gary Attard and Colin Barnes²⁰.

The above Lennard-Jones diagram is a plot of the potential energy against the distance from the crystal surface for a chemisorbing oxygen molecule. It can clearly be seen that there are two distinct oxygen species present, the gas phase and physisorbed dioxygen species and the surface-bonded atomic oxygen. Figure 1.5 demonstrates that there is little to no energetic barrier to physisorption (the precursor state), making this a non-activated process. However for chemisorption to occur there is an energetic barrier to dissociation, $E_{a,dis}$, which must be overcome. This requirement for an input of energy establishes the precursor state as having a finite existence. If $E_{a,dis}$ is positive, the process is referred to as activated adsorption. Processes where the adsorbing molecule encounters no energetic barrier as it moves closer to the surface are termed non-activated adsorptions. From the Lennard-Jones diagram it can be seen that for the gas phase molecule to approach the surface closely enough to chemisorb, the physisorbed approach curve offers the lowest energy pathway.

1.2.8 Adsorption isotherms

An isotherm is a depiction of the relationship between the quantity of gas adsorbed as a function of pressure at a constant temperature²⁵. The simplest model

for the derivation of a theoretical isotherm is that formulated by Langmuir²⁶. This model makes several key assumptions:

- That molecules adsorb on the clean surface with a constant sticking probability – there are no collisions of gas molecules with the surface resulting in reflection back into the gas phase.
- That there are no preferred adsorption sites.
- The occupancy of adjacent sites does not affect the adsorption of a molecule in a specific site ie. there are no lateral interactions between molecules.
- The maximum attainable coverage is a complete monolayer.
- Desorption of an adsorbed molecule occurs as soon as the energy acquired via lattice vibrations is equal to the heat of adsorption.
- A gas phase molecule encountering an adsorbed species will be reflected back into the gas phase with no loss of energy.
- At equilibrium the rate of adsorption into unoccupied sites equals the rate of desorption from occupied sites.

Applying the above assumptions to a system comprising of the adsorption of a gaseous phase onto a perfect surface at a temperature T and a pressure P with N adsorption sites per unit area and N_s occupied surface sites per unit area gives a rate of adsorption of

$$\frac{d\theta}{dt} = k_a P(N - N_s)$$

Equation 1.6 - The rate of adsorption for a Langmuirian system

where θ = surface coverage (as defined in Equation 1.2)

this can also be expressed as

$$\frac{d\theta}{dt} = k_a P N (1 - \theta)$$

Equation 1.7 - The rate of adsorption

where

k_a = adsorption rate constant

By the same logic the rate of desorption is directly proportional to the number of adsorbed species on the surface ie.

$$-\frac{d\theta}{dt} = k_d N\theta$$

Equation 1.8 - The rate of desorption

where

k_d = rate constant for desorption

Since, at equilibrium, the number of desorbing species equals the amount of adsorbing species, putting the two expressions equal to each other and rearranging yields

$$\theta = \frac{Kp}{1 + Kp}$$

Equation 1.9 – Derived Langmuir Isotherm

where

$$K = k_a k_d$$

The Langmuir model does however deviate from real-world systems in several aspects as it fails to take into account non-uniformity of the surface, the effects caused by geometric factors and the changes in adsorption energy as a function of surface coverage due to lateral interactions between adsorbed surface species. In addition to this the Langmuir isotherm also ignores the possibility of surface mobility; this is especially important when considering desorption of products which are the result of a dissociative adsorption and must recombine before they desorb. A further problem with the Langmuir model is that it does not take into account the possibility of larger adsorbed molecules blocking adjacent adsorption sites; this is especially a problem when considering adsorption of aromatic rings and other large organic molecules.

It is worth noting that several other isotherm models exist which partially compensate for shortcomings in the Langmuir model such as the adsorption of greater than a monolayer (Brunauer-Emmett-Teller isotherm) or for adsorption sites not being equivalent (Temkin and Freundlich isotherms). These isotherms also rely upon certain similar assumptions to the Langmuir isotherm, however they do give accurate results when used in the specified conditions¹⁶.

1.2.9 The surface

Possibly the most important concept behind surface science is the realisation that the atoms at the surface have lower coordination numbers (are surrounded by less neighbours) than the atoms in the bulk. This lower coordination number has a variety of consequences that make surfaces desirable for study.

The electronic structure of the surface is different from that of the bulk. Whereas bulk metals exhibit overlap of energy levels forming 'bands' of electron energy levels, surface atoms have specific discrete energy levels. In addition to this the atoms at the surface are often at a much higher energy than those in the bulk. This can lead to different crystallographic structures at the surface when compared to that of the bulk, due to reconstructions to minimise the surface energy. The lower coordination number of the atoms at the surface may also be made manifest in a favourable adsorption of gases, which may go on to react¹⁵.

1.3 The NSR process

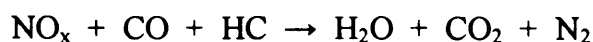
Since the Industrial Revolution there has been a large amount of damage done to the environment by the reckless use of raw materials such as fossil fuels as well as a lack of regard for 'cleaning up' after industrial processes. There has been government environmental legislation in Britain in one form or another since as early as the 1200's when laws were first introduced to limit the burning of coal in cities. More recently due to heavy smogs, particularly in London, Tokyo and Los Angeles, countries have brought in increased legislation to tackle airborne pollutants.

In the last decade there has been an increasing awareness of the need for a reduction in the levels of greenhouse gases, particularly the CO₂ that is produced as a by-product of human industry. In the automotive industry this has been manifest in the desire of manufacturers to produce cleaner and more fuel-efficient cars. One development that has the potential to greatly cut CO₂ emissions is the lean burn engine. Via a more complete combustion process in an environment of excess oxygen the lean burn engine can offer up to 30% decreased fuel consumption when compared to a traditional stoichiometric engine²⁷. Decreased fuel consumption reduces the volume of CO₂ produced per journey and the oxidising atmosphere effectively eliminates hydrocarbon and CO emissions.

Nitric oxides (NO_x) are a major constituent of all automotive pollutants. NO_x is believed to make soil and ground water more acidic via atmospheric transformation to nitric acid, HNO₃, which is then precipitated as acid rain. NO_x has also been linked to the accumulation of ozone at ground level observed in certain regions of the world, via reaction of photo-free radicals with oxygen. Emitted NO is also oxidised in the atmosphere to NO₂, a gas that has been proven to have adverse effects upon the respiratory system and to increase the risk of development of respiratory allergies. Studies have shown that that NO_x levels of 0.05 ppm are harmful for healthy people; for people with respiratory disorders these levels are still too high^{28,29}. Exhaust emissions of NO_x and particulate matter (PM) from heavy-duty diesel vehicles from 2007 will have to be reduced to 10% of maximum 2003 levels³⁰.

Normal automobile engines are operated at very close to stoichiometric conditions of air:fuel, approximately 14.5:1. Under these conditions the engine produces large quantities of NO_x, CO and short chain hydrocarbons. In addition to this, in the past it has been common practice to add trace amounts of organo-lead compounds (usually tetra-ethyl lead) into gasoline as an anti-knock component; despite being present in low concentrations on average each engine releases several kilograms of lead into the environment each year².

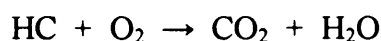
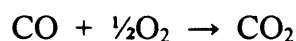
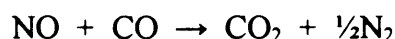
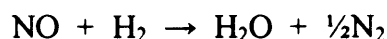
Currently the catalyst present in the majority of automotive catalytic converters is the three-way catalyst, so named because it facilitates the simultaneous oxidation of carbon monoxide and hydrocarbons (HC) and reduction of NO ie.



Scheme 1.1 – Three-way catalyst overall operation

The three-way catalyst is composed of a mixture of platinum, palladium and rhodium dispersed on a Al_2O_3 support³¹. It is important for the catalyst and the monolith support that it is mounted on to have both high mechanical and high thermal strength. The high resistance to thermal shock and expansion is necessary as car engines operate over a wide temperature range and can change temperature greatly in a very short space of time. In addition to the components mentioned above certain manufacturers also add oxygen storage media such as ceria to maintain oxidation during low air: fuel operating conditions².

The NO_x conversion shown in scheme 1.1 occurs through a number of fundamental steps



Scheme 1.2 – NO_x conversion of the three-way catalyst

The NO reduction reactions are mainly carried out over the rhodium component in the catalyst and the oxidation over the platinum.

Normal combustion produces an exhaust gas mixture that contains balanced amounts of CO, H_2 and hydrocarbons to enable the reduction of NO_x ³². Such is the efficiency of the three-way catalyst that the pollutants present can be almost completely transformed into CO_2 , N_2 and H_2O , however a surplus of oxygen present in the exhaust of the engine will prevent the reduction of NO_x ⁴³. One problem with the three-way catalyst is that at present the light-off temperature, the temperature at

which the catalyst begins to work, is rather high. When the exhaust temperature is below the light off temperature pollutants pass unchecked through the exhaust.

Since 1984 it has been known that combustion of the unburnt hydrocarbons which are present in the exhaust of a traditional engine can increase engine efficiency by up to 30%. This is achieved via combustion of the fuel in an environment of excess oxygen (lean environment)(25:1 or above air: fuel ratios), unlike the stoichiometric air: fuel ratios (14.5:1) used in conventional gasoline engines. From both an environmental and economical point of view this is advantageous; however it necessitates the development of a new exhaust catalytic technology to prevent the engine pollutants from passing into the atmosphere, as existing catalytic technologies are inoperable under oxidising conditions. Various alternatives to the three-way catalyst have been proposed, most of which operate around reducing nitric oxides directly³³, either via injection of ammonia or urea or over a Cu/zeolite catalyst³⁴. However all of these catalysts have several serious problems associated with their usage such as narrow temperature windows of operation, low durability and low catalytic activities³². The zeolite-based catalysts, at one point the most promising, in particular have been proven to have an unsatisfactory hydrothermal resistance³⁵.

Direct NO reduction to N₂ and O₂ is a catalytic option that is attractive for its simplicity; however the decomposition reaction is thermodynamically unfavourable and the supported platinum and palladium catalysts which have been tried rapidly lose efficiency due to oxygen poisoning^{36,37,38}. At elevated temperatures it has been suggested that the desorption of O₂ from the catalyst is the rate determining step for the reaction³⁹.

Perhaps the most promising technology, and one that is currently in use in Japan is NO_x Storage and Reduction (NSR). This catalyst system was first introduced by Toyota in the early 1990's^{40,41}. The NSR catalyst is a combination of a modification of the lean burn catalyst and a change in the mode of engine operation. It comprises of a precious metal to oxidise/reduce NO_x (typically a Pt/Rh mix; Platinum is normally chosen due to its high NO oxidation ability and rhodium for reduction ability), an alkali or alkaline earth metal oxide (barium oxide is generally chosen due to ease of nitrate formation) and a high surface area substrate upon which

the catalyst is supported (normally γ -alumina providing a surface area in excess of $200 \text{ m}^2 \text{ g}^{-1}$)^{27,42}. The storage component must be capable of storing NO_x and releasing it at temperatures of 300-600 °C. Barium and strontium are good examples of such metals.

The engine operates under predominantly oxygen rich (lean) conditions, during which NO_x is stored as nitrate on a NO_x storage medium (barium oxide). Every few minutes a spike of fuel is injected into the combustion mix (rich conditions). This provides a reducing environment, with hydrocarbons, carbon monoxide and hydrogen being present without being oxidised. Under these conditions the stored NO_x is released from the storage component and reduced over the precious metal component of the catalyst, to be passed out of the exhaust as N_2 , CO_2 and H_2O . Regeneration of the NO_x trap is essential for freeing NO_x storage sites for continued catalytic use. Although this oscillation of combustion conditions is employed during normal driving, during the initial period of engine operation (warm-up) a constant air: fuel ratio is employed. This coincides with large production of pollutant but allows the engine to reach normal working conditions where the excess oxygen environment can be used as rapidly as possible. Although developed to remove NO_x from lean burn gasoline engines it seems likely that NSR catalysts have a role to play in NO_x emission control in diesel engines too⁴³.

A problem with the NSR catalyst is that it is easily poisoned by sulphur present in fuel. This is due to the enhanced stability of sulphate species over nitrate species when bonding with barium oxide, with the consequence that the NO_x trap cannot be regenerated under normal operating conditions and no further nitrate can be stored. This is not so much of a problem in Japan, where the fuel sulphur content is much lower, but it has delayed the import of the lean burn engine to the European and American markets. There are desulphation procedures which have been proven to be effective in removing stored SO_x such as regeneration under high temperature; however this reduces the working life of the catalyst and as such is not a viable option for high-sulphur containing fuels⁴². It has been theorised that transitions from surface to bulk sulphates and the size of the sulphate particles also increase the difficulty of regenerating the NO_x trap⁴⁴. As well as sulphur contamination, CO_2 has displayed an

affinity for binding to NO_2 adsorption sites⁴⁵ with the consequent blocking of those sites.

The role of each component in the NO_x storage catalysis has been investigated separately. Takahashi *et al.*⁴⁶ have shown that the conversion of nitric oxides to nitrogen takes place over the noble metal sites in the catalyst. They have also shown that the quantity of NO_x stored increases with increasing oxygen content and reported IR evidence that NO_x is stored as nitrate. It is worth noting that the group used barium instead of barium oxide, possibly necessitating the oxidation of barium as the first step of NO_x storage. However evidence is provided which argues against this by Li *et al.*⁵⁰ who note that despite the NO_x storage capacity increasing with increasing oxygen concentration, a pre-oxidised surface has a lesser storage capacity than a pre-reduced surface. Other groups have also confirmed the storage of the NO_x as nitrate⁴⁷.

It is generally assumed that NO_x is stored via the reaction of adsorbed NO_2 (created from reaction of adsorbed NO and atomic oxygen) and NO with BaO to form $\text{Ba}(\text{NO}_2)_2$ (from reaction with NO) and $\text{Ba}(\text{NO}_3)_2$ (from reaction with NO_2)⁵⁰. However this is by no means certain. The above hypothesis assumes that BaO is the storage component, rather than possibly being a hydroxide or carbonate species, and rules out the possibility of storage occurring directly via NO rather than necessitating the preliminary oxidation step. In addition to this the form that NO_x is stored on the storage component is by no means certain, although it has been reported as $\text{Ba}(\text{NO}_3)_2$ ⁴⁸. The initial oxidation step over the Pt metal centre has been shown to be the rate-determining step⁴⁹. However the fact NO is released in addition to NO_2 being stored when a stream of NO_2 is passed over a NO_x trap catalyst hints at a more complex redox process occurring⁴⁹.

It is generally assumed that the stored NO_x is released in the reverse process of that described above with the stored NO_x being released as NO_2 and NO and reduced over the noble metal component of the catalyst (Rh in the Toyota catalyst) by the reducing agent.

It has been found that both BaO and BaAl₂O₄ are efficient at storing NO_x. However stable carbonates form more readily on BaO, with the effect of poisoning the catalyst. Although it has been proven that both store NO_x as nitrate, the nitrate formed on BaAl₂O₄ is bonded through the nitrogen whereas the BaO-nitrate species is not. This has implications with regard to SO_x poisoning^{50,51}. There has also been evidence reported in the literature of NO_x being stored as nitrite at lower adsorption temperatures (below 200 °C)⁵⁰. The presence of oxygen in the exhaust stream inhibits the release of stored NO_x and the presence of CO₂ promotes it³⁴.

From the above it is apparent that detailed knowledge, with regards to the mechanism of NO_x storage and reduction, is essential for optimising the NSR catalyst. This project aims to provide enhanced understanding of some of the fundamental steps involved.

REFERENCES

1. http://en.wikipedia.org/wiki/Image:Activation_energy.svg
2. Bowker, M., *The Basis and Applications of Heterogeneous Catalysis*, OUP, 1998.
3. Davy, H., *Phil. Trans. R Soc.*, **107**, 1817, 77.
4. Langmuir, I., *J. Chem. Soc.*, **38**, 1916, 221.
5. Langmuir, I., *J. Chem. Soc.*, **34**, 1912, 860 & 1310.
6. Langmuir, I., *Trans. Faraday Soc.*, **17**, 1922, 607 & 621.
7. Hinshelwood, C.N. *Annual Reports Chemical Society, London*, **24**, 1928, 335.
8. Eley, D.D., Rideal, E.K., *Nature*, **146**, 1940, 401.
9. Lennard-Jones, J.E., *Trans. Faraday Soc.*, **A178**, 1941, 429.
10. Taylor, H.S., *J. Am. Chem. Soc.*, **53**, 1931, 578.
11. Binnig, G., Rohrer, H., Gerber, C., Weibel, *Phys. Rev. Lett.*, **49**, 1982, 57.
12. Binnig, G., Rohrer, H., *Rev. Mod. Phys.*, **71**, 1999, S324.
13. Eigler, D.M., Schweizer, E.K., *Nature*, **344**, 1990, 524.
14. Campbell, C.T., *Appl. Surf. Sci.*, **19**, 1932, 32.
15. McCash, E. M., *Surface Chemistry*, OUP, 2001.
16. Ertl, G., Küppers, J., *Low Energy Electrons and Surface Chemistry*, 2nd edition, VCH, 1985.
17. King, D.A., *CRC Crit. Rev Solid State Mater. Sci.*, **7**, 1979, 167.
18. <http://www.chem.qmul.ac.uk/surfaces/scc/>
19. Somorjai, G.A., *Introduction to Surface Chemistry and Catalysis*, J. Wiley and sons Ltd., 1994.
20. Attard, G., Barnes, C., *Surfaces*, OUP, 1998.
21. Tanaka, H., Yoshinobu, Kawai, M., *Surf. Sci. Lett.*, **327**, 1995, L505.
22. Harris, P.J.F., *Nature*, **323**, 1986, 792.
23. Roberts, M.W., McKee, C.S., *The Chemistry of the Metal-Gas Interface*, OUP, 1978.
24. Adamson, A.W., *Adsorption of Gases and Vapors on Solids in Physical Chemistry of Surfaces*, Wiley, 1982.
25. Thompkins, F.C., *Chemisorption of Gases on Metals*, Academic Press, 1978.
26. Langmuir, I., *J. Amer. Chem. Soc.*, **40**, 1918, 1361.
27. Fridell, E., Skoglundh, M., Westerberg, B., Johansson, S., Smedler, G., *Journal of Catalysis*, **183**, 1999, 196.
28. Chiron, M., *Stud. Surf. Sci.*, **30**, 1987, 1.
29. Olsson, L., *Kinetic Studies of NO Oxidation and NO_x Storage on Pt/BaO/Al₂O₃ catalysts*, Dpt. Chem. React., Chalmers University of Technology, Sweden.
30. Environmental Protection Agency (EPA), vol. **2003**, 2003.
31. Kolasinski, K.W., *Surface Science*, John Wiley & Sons, 2002.
32. Masahiko, T., Matsumoto, S., *Topics in Catalysis*, **28**, 2004, 151.
33. Anderson, J.A., Bachiller-Baeze, B., Fernandez-Garcia, M., *Phys. Chem. Chem. Phys.*, **5**, 2003, 4418.
34. Kabin, K.S., Muncrief, R.L., Harold, M.P., *Catalysis Today*, **96**, , 2004 79.
35. Torre-Abreu, C., Ribeiro, M.F., Enriques, C., Ribeiro, F.R., *Cat. Lett.*, **43**, 1997, 25.
36. Wang, X., Sigmon, S.M., Spivey, J.J., Lamb, H.H., *Cat. Today*, **96**, 2004, 11.
37. Hightower, J.W., Van Leirsburg, D.A., Kimilish, R.L., Larson, J.G., *The Catalytic Chemistry of Nitrogen Oxides*, Plenum Press, New York, 1975, 63.
38. Burch, R., Watling, T.C., *Catt. Lett.*, **37**, 1996, 51.
39. Furusawa, T., Aika, K., *Bull. Chem. Soc. Jap.*, **73**, 2000, 795.

-
40. Toyota Patent, European Patent Application no. 0573 672A1, 1992.
 41. Miyoshi, European Patent Application no. 0 669 157 A1, 1995.
 42. Poulston, S., Rajaram, R.R., *Catalysis Today*, **81**, 2003, 603.
 43. Yu, R.C., Cole, A.S., Stroia, B.J., Huang, S.C., Howden, K., Chalk, S., SAE Paper 2002-01-1867, 2002.
 44. Liu, Z., Anderson, J.A., *Journal of Catalysis*, **228**, 2004, 243.
 45. Rodrigues, F., Juste, L., Potvin, C., Tempe, J.F., Blanchard, G., Djega-Mariadassou, G., *Cat. Lett.*, **72**, 2001, 59.
 46. Takahashi, N., Yokota, K., Sugiura, M., Kasahara, K., SAE Technical Paper Series No. 950809, 1995.
 47. Bognor, W., Kramer, M., Krutzsch, B., Pischinger, S., Voigtlander, D., Wenninger, G., Wirbeleit, F., Brogan, M.S., Brisley, R.J., Webster, D.E., *Appl. Catal. B*, **7**, 1995, 153.
 48. Takahashi, N., Shinjoh, H., Iijima, T., Suzuki, T., Yamazaki, K., Yokota, K., Suzuki, H., Miyoshi, N., Matsumoto, S., Tanizawa, T., Tanaka, T., Tateishi, S., Kasahara, K., *Catal. Today*, **27**, 1996, 63.
 49. Broqvist, P., Panas, I., Fridell, E., Persson, H., *J. Phys. Chem., B*, **106**, 2002, 137.
 50. Li, X., Meng, M., Lin, P., Fu, Y., Hu, T., Xie, Y., Zhang, J., *Topics in catalysis*, **22**, 2003, 111.
 51. Matsumoto, S., Ikeda, Y., Suzuki, H., Ogai, M., Miyoshi, N., *Appl. Catal. B*, **25**, 2000, 115.

2. EXPERIMENTAL: SURFACE SCIENCE EQUIPMENT AND TECHNIQUES

2.1	<i>Introduction</i>	27
2.1.1	<i>The analysis chamber</i>	27
2.1.2	<i>Quadrupole mass spectrometry (QMS)</i>	32
2.1.3	<i>K and Ba sources</i>	33
2.1.4	<i>Crystal cleaning</i>	34
2.2	<i>Experimental Techniques</i>	35
2.2.1	<i>Molecular beam experiments</i>	35
2.2.2	<i>Temperature programmed desorption experiments</i>	45
2.2.3	<i>Auger electron spectroscopy (AES)</i>	49
2.2.4	<i>Low energy electron diffraction (LEED)</i>	53
	<i>REFERENCES</i>	61

2. EXPERIMENTAL: SURFACE SCIENCE EQUIPMENT AND TECHNIQUES

2.1 Introduction

A relatively young discipline, surface science is a field that has grown immensely since its inception in the 1960s. There are multiple techniques available to the surface scientist for the investigation and characterisation of a surface and examining the reactions catalysed by the surface. It is worth noting that no single technique is capable of providing all the information needed to form a complete picture of what exactly is happening at the surface. For this reason multiple analysis techniques providing complementary information are often employed. For instance STM (Scanning Tunnelling Microscopy) will show a nanoscale picture of the surface but provides little information on the nature of the species being viewed whereas XPS (X-Ray Photoelectron Spectroscopy) will identify the species present at the surface but will give no indication on their topographical structure. For this reason XPS and STM are techniques which are often used in tandem to provide complementary information. This chapter lists and describes the experimental apparatus and surface analytical techniques used in the gathering of the data presented in later chapters and gives an overview of the theory behind the techniques.

2.1.1 The analysis chamber

If an idealised reaction on a prepared surface is to be studied accurately it is important that the surface be unaffected by chemical species other than those being studied. Using equation 1.3 (page 10) it can be calculated that a background pressure of 1×10^{-8} mbar CO in the chamber thus gives a molecular flux of approximately 10^{13} molecules $\text{cm}^{-2}\text{s}^{-1}$ at 300 K. If one assumes that the concentration of atoms present at the surface is approximately 1×10^{15} molecules cm^{-2} and that the sticking probability of CO on the surface is unity, an atomically clean surface (less than 1% contamination) can be maintained for only 1 second and a complete monolayer of adsorbed CO will form in under two minutes.

It follows that in order to simplify the analysis of the reactions being studied one must endeavour to remove all the potential contaminants and non-participating species from the reaction. This allows measurements to be made on atomically clean surfaces. To this end studies are conducted under ultra high vacuum conditions (UHV). Ultra high vacuum is a designation given to a pressure in the range $1 \times 10^{-9} - 1 \times 10^{-12}$ torr ($1.33 \times 10^{-9} - 1.33 \times 10^{-12}$ mbar). Under these sorts of pressures the mean free path of the gas molecules is very large, making molecule-surface collisions more significant than molecule-molecule conditions. A further advantage of ultra high vacuum is that the molecules, ions and electrons used as probes in many surface analytical techniques have a longer undisturbed trajectory with decreasing pressure.

The apparatus used consisted of a main chamber that was pumped using a liquid nitrogen trapped oil-vapour diffusion pump and a Leybold turbomolecular pump, both of which were backed by Leybold and Edwards rotary pumps. Oil diffusion pumps operate by heating an oil reservoir to produce a stream of vapour that carries residual gas molecules in the chamber towards an exhaust, from which it is pumped by a backing rotary vane pump. The oil vapour is re-condensed on the body of the pump, which is water-cooled. The liquid nitrogen cold trap condenses out contaminants from the back streaming oil, and prevents oil vapour from diffusing into the main analysis chamber. The choice of oil employed in the diffusion pump is critical as it must possess an extremely low vapour pressure (better than 10^{-9} torr) at ambient temperature and be resistant to damage caused by heating as well as being relatively unreactive to gases encountered in the vacuum chamber. The oil chosen for use was Santovac 5 polyphenyl ether oil (Monsanto Corp.) possessing a vapour pressure of $\sim 4 \times 10^{-10}$ mbar at 298 K¹.

The turbomolecular pumps operate in a similar manner to a turbine, with rotating assemblies of blades spinning at high speeds (50,000-100,000 rpm). Molecules entering the intake of the pump are impacted by the blades and have a velocity imparted to them, being moved to the exhaust, where they are then removed by the backing pumps.

Rotary pumps operate by removing gas cyclically from a system and removing it to an outlet. Unlike the turbomolecular and oil diffusion pumps mentioned above

the rotary pumps are able to operate at standard pressure without damage to themselves. This makes them essential components for 'roughing out' the system (bringing the internal pressure to a level where the other pumps can safely operate) in addition to removing the pumped gas from the outlets of the other pumps.

The chamber was also equipped with a ThermoVacuum Generators titanium sublimation pump (TSP), which provided high speed pumping and a lower ultimate base pressure than the oil diffusion pump and turbomolecular pumps alone. The titanium sublimation pump operates by putting a high current through thick titanium-molybdenum filaments. As the filaments heat via resistive heating they start to sublime titanium, which then coats the walls of the chamber and forms stable compounds with contaminants, permanently trapping them. The titanium sublimation pump is only effective at chamber pressures of $\sim 1 \times 10^{-8}$ mbar or below. The combined pumping systems are easily capable of keeping the main chamber at a pressure of 1×10^{-10} mbar or lower.

The combination of these pumping techniques was effective at removing almost all gaseous contaminants from the chamber. The major residual gases present in the system were from atmospheric hydrogen and helium, both of which have slow pumping speeds with the available vacuum pumps, and carbon monoxide which is produced from heated filaments in the chamber (e.g. ionisation gauges, mass spectrometer filaments, heater filaments etc.)².

It is worth noting that all of the pumps mentioned above have an effective pressure range that they can safely be operated in. Operation of the pumps above this range at best will trip safeguards to shut the pumps down, and at worst will result in damage to the pumps. The oil in the oil diffusion pump in particular is susceptible to 'cracking' if heated at high pressures. The oil diffusion pump should not be used at pressures above 10^{-3} mbar, the turbomolecular pumps 10^{-2} mbar and the titanium sublimation pump 10^{-8} mbar. As all of these pressures are lower than atmospheric pressure the system must be thoroughly roughed with roughing pumps. These are typically one or two vane rotary vane pumps that can pump from atmospheric pressures to 10^{-3} mbar. These pumps are also used to back the oil diffusion and turbomolecular pumps.

The molecular beam enclosure was kept under a reduced pressure of 1×10^{-7} mbar via twin rotary-backed turbomolecular pumps and could be isolated from the main chamber by means of a gate valve.

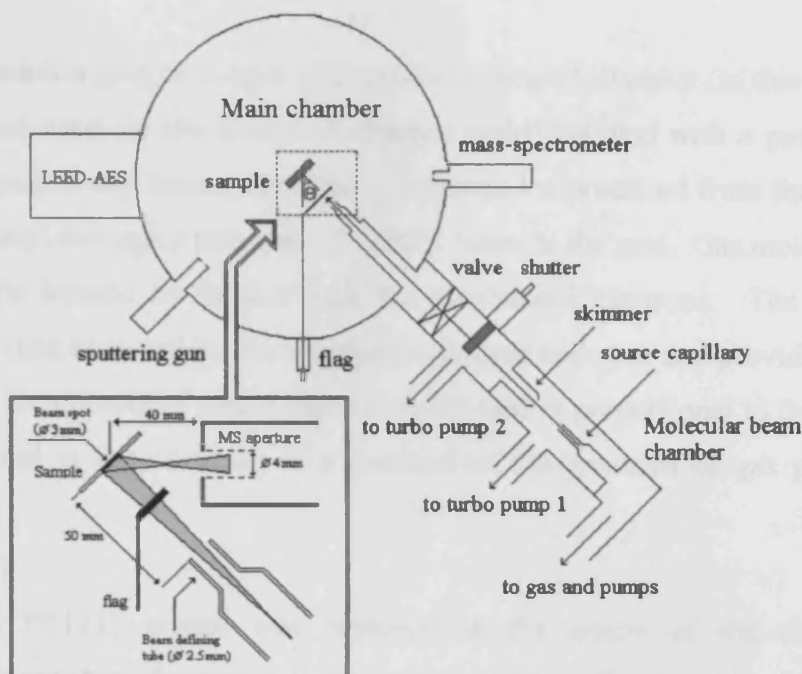


Figure 2.1. Schematic of the experimental apparatus setup in the ultra high vacuum chamber used for the experiments contained in this thesis.

It is impossible to achieve ultra high vacuum conditions without subjecting the system to ‘baking out’, or heating the system to around 450 K for 12-24 hours. This temperature is hot enough to desorb the majority of contaminant gases that contribute strongly to the residual pressure (especially water) from the chamber walls. Following this the equipment inside the ultra high vacuum chamber needs to be ‘degassed’, when all the filaments are operated for at least an hour directly after baking when the chamber is still hot. This is necessary to remove all contaminants from the interior surfaces of the chamber, which might adsorb onto the prepared surface of the crystal.

The pressure in the ultra high vacuum chamber was measured by a Pirani gauge for pressures ranges of $\sim 10^0$ to 10^{-3} mbar and an ionisation gauge for pressures of 10^{-4} to 10^{-11} mbar.

The Pirani gauge operates by measuring the increase in resistance of a length of heated wire as heat dissipation is reduced with lowered pressure. However the pirani gauge is unsuitable for precise measurements as different gases exhibit different thermal conductivities.

Ionisation gauges consist of a resistively heated filament (in this case thoriated tungsten was used for the increased electron yield) coupled with a positively biased grid and a negatively biased collector. Electrons are produced from the filament and are accelerated through a potential of ~ 150 V towards the grid. Gas molecules present may thus be ionised by impact with the accelerated electrons. The positive ions created are then attracted by the negatively charged collector and provide an electrical signal. As the number of ions created and detected is proportional to the pressure the signal created at the collector is a measure of the pressure of gas present in the chamber.

The Pt(111) crystal was mounted in the centre of the chamber on a manipulator capable of rotating about the azimuthal and polar axis. Rotation about both axes could be controlled by automated stepper motors for use in angle resolved experiments; however all the work presented in this thesis was performed with the crystal surface directly facing either the molecular beam (for sticking experiments) or facing the mass spectrometer (for temperature programmed desorption experiments).

The crystal was held in place by two 0.15 mm tungsten wires threaded through four holes bored in the crystal surface. These wires also provided resistive heating with the temperature ramp set to 1 K/s for most experiments. The temperature of the crystal could be lowered to 130 K by cooling with liquid nitrogen through a sealed pipe connected to the sample mount via a sapphire thermal switch and copper braid. The temperature of the crystal could be measured by a K-type thermocouple placed in another hole bored in the edge of the crystal.

Gases could be dosed onto the crystal surface either via leak valves (background dosing) or by using the thermal molecular beam. The molecular beam was sharply collimated to give a final circular spot of 3 mm in diameter. The beam was normally operated at 50 mbar source pressure, which translated to a gas pressure

of approximately 2×10^{-8} mbar at the crystal surface. The gases used in the experiments contained in this thesis were O₂ (99.999%, Argo International Ltd.), CO (99.5%, Argo International Ltd.), Ar (99.999%, Argo International Ltd.), NO (99.0%, Argo International Ltd.) and NO₂ (99.5%, BDH Chemicals Ltd.).

The vacuum chamber was also equipped with a PSP ISIS 3000 argon ion sputter gun for crystal cleaning and a ThermoVacuum Generators rear view retarding field analyser for low energy electron diffraction and auger electron spectroscopy experiments.

2.1.2 Quadrupole mass spectrometry (QMS)

Mass spectrometry is perhaps the most widely used scientific analytical technique. The sample under examination is ionised (and thus has a charge imparted to it) and the resultant ions are separated according to their different mass: charge ratios. This separation is generally done via the manipulation of the ionised gas through differing spatial trajectories.

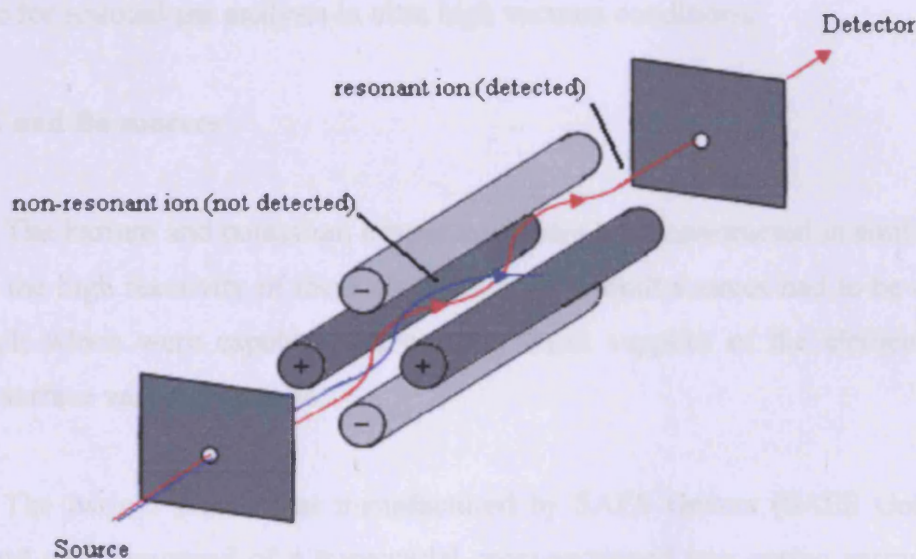


Figure 2.2. A quadrupole mass spectrometer.

As Figure 2.2 shows the quadrupole mass spectrometer separates ions by two perpendicular fluctuating electrical fields of variable strength between two pairs of

opposing poles. One pair of rods has an applied potential of $+(U + V \cos(\omega t))$ and the other $-(U + V \cos(\omega t))$, where U is the DC voltage, $V \cos(\omega t)$ is the AC voltage of frequency ω and amplitude V and t is the time. The potential difference applied to each pair of rods is varied sinusoidally as $\cos(\omega t)$ cycles with time. Ions are created by the source and accelerated down the spectrometer towards the detector. The fluctuating electric fields ensure that the ion travels in a spiral path with trajectories dependent upon the mass: charge ratio of the ions. As the field strength is varied ions with too small a mass: charge ratio develop a greater path radius and so do not reach the detector, making it possible to 'scan' through the available mass: charge ratios by varying the strength of the electric fields created. Only ions of a specific mass: charge ratio will pass through the quadrupole filter and reach the detector. There are two scanning modes commonly used; holding ω constant and varying U and V , or holding U and V constant and varying ω .

The quadrupole mass spectrometer is commonly used for UHV applications due to its relatively low cost and power demands and ease of use. It typically provides a lesser resolution than the larger magnetic sector analysers but is more suitable for residual gas analysis in ultra high vacuum conditions.

2.1.3 K and Ba sources

The barium and potassium evaporators were both constructed in similar ways. Due to the high reactivity of these elements custom-built sources had to be designed and built which were capable of depositing clean supplies of the element on the crystal surface with high purity.

The barium source was manufactured by SAES Getters (SAES Getters GB Ltd.) and was composed of a trapezoidal cross-sectioned iron casing surrounding a BaAl_4 alloy wire with a nickel reactant. The filament was resistively heated by putting 10 Amps of current through it, causing the casing to increase to over 1073 K in temperature. At this temperature the nickel reacts with the aluminium alloy in an exothermic reaction that raises the temperature of the wire to approximately 1523 K. The chemical reaction produces barium vapour, which is emitted through an aperture machined along the axis of the casing.

The potassium source was manufactured by SAES Getters (SAES Getters GB Ltd.) and was composed of a trapezoidal cross-sectioned metal container provided with a slit to allow evaporation of the alkali metal vapour. Contained within the casing was a potassium chromate of formula K_2CrO_4 and a reducing agent. The filament was resistively heated by putting 7 A of current through it, heating it to over 500 °C and causing the reducing agent to break down the chromate and irreversibly sorb all chemically reactive gases produced during the reduction reaction and evaporating the metal from the doser in a similar manner to that of the barium doser.

Both sources were mounted on a normal high current four terminal ultra high vacuum feedthrough and were enclosed in a custom built stainless-steel cylindrical metal shield with an aperture cut into the far end to allow directional dosing of the crystal. The shield was necessary to prevent unwanted metal deposition onto the internal surfaces in the vacuum chamber. The crystal was held at a distance of 80 mm from the deposition source whilst dosing. During the deposition of both of these metals the pressure in the system increased to not more than 5×10^{-9} mbar.

2.1.4 Crystal cleaning

The Pt(111) single crystal (5N purity, Metal Crystals & Oxides Ltd.) was cleaned by cycles of argon ion sputtering (1.0×10^{-5} mbar, 500-1000 eV, $6 \mu A/cm^2$, 30 min) to remove unwanted impurities and adsorbates as well as some of the Pt(111) surface atoms. This left a very rough surface rather than the smooth (111) plane required so the crystal was then annealed in O_2 (2.5×10^{-8} mbar, 500 °C, 20 min) followed by annealing in oxygen at lower temperature (2.5×10^{-8} mbar, 300 °C, 20 min) to remove residual carbon. The oxygen was then removed and the crystal flashed (700°C, 2 min) to remove platinum oxide. Cleanliness of the surface was ascertained by achieving a smooth Auger spectrum where the only major feature was a Pt (MNN) peak at 69 eV and an absence of a C (KLL) peak at 275 eV. In addition to this the periodicity of the surface was ascertained by achieving a (1 x 1) LEED pattern. An alternative method of checking for carbon contamination was to dose oxygen onto the surface followed by a linear temperature ramp. CO and CO₂ being evolved in the desorption trace is indicative of the presence of carbon at the surface.

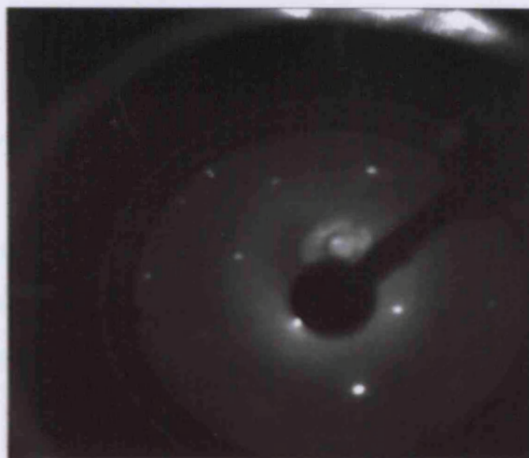


Figure 2.3. A (1 x 1) LEED pattern of the clean Pt(111) crystal surface.

2.2 Experimental techniques

2.2.1 Molecular beam experiments

The molecular beam is a tool of surface science that has been in use since before 1920 and remains useful to the current date. However it is only in the last twenty-five years that they have commonly been applied to surface studies having been used previously in He atom scattering structural determining experiments¹⁵.

The first effusive molecular beam was developed using sodium atoms by Dunnoyer in 1911³. The technology was developed by Knudsen⁴ and Wood⁵ and was first used to investigate gas-solid systems in 1915. The molecular beam was first used to accurately examine gas adsorption by Bell and Gomer in 1966⁶. In 1972 a molecular beam system which collimated the beam through a series of five differentially pumped chambers utilising liquid nitrogen cooling was developed by King and Wells⁷. This design was later refined by King and Bowker⁸ into a molecular beam system with only three differentially pumped stages similar to that used in the course of the experiments here.

The molecular beam used in the experiments described in this thesis was a thermal nozzle source designed and built by Dr R. Bennett at the University of Reading, based on earlier King and Bowker designs (see Figure 2.1)^{7,8,11}. The beamline was composed of two stainless steel six way cross-junctions and a stainless

steel four-way junction connected linearly. The four-way junction was at the end of the beamline and was backed by a Leybold rotary pump and acted as the source chamber. Both six way junctions were pumped by Leybold turbomolecular pumps, which were backed by Leybold rotary vane pumps. One junction acted as the beam production chamber and one defined and resolves the beam. The combined pumping speed of the two turbomolecular pumps has been calculated to be approximately 18 L s^{-1} .⁹ The entire beamline could be isolated from the main chamber by means of a fast acting gate valve.

The molecular beam is exactly as described; a straight, narrow, well-defined beam of atoms or molecules propagating into the vacuum chamber and colliding with a prepared sample. When combined with ultra high vacuum conditions the individual molecules in the molecular beam do not interact with each other or with any other residual molecules in the chamber.

The molecules comprising thermal molecular beams (so called because the beam molecules collide many times with the source capillary and so are at thermal equilibrium with the source) have a Boltzmann-like internal energy distribution. However, by increasing the pressure in the source by many orders of magnitude to create a supersonic beam (so called as the molecular velocity is greater than the speed of sound) and combining with laser photo-excitation of the beam molecules, it is possible to specifically access any of the quantum energy states of the beam molecules. Supersonic molecular beams typically use pressures of several atmospheres in the source and nozzles of $\sim 0.1 \text{ mm}$ in diameter to produce a molecular velocity greater than the speed of sound. Despite the much higher kinetic energies that supersonic beams can develop they are designated 'cold' beams due to the small range of velocities of the individual molecules in the beam and the associated non-Maxwellian distributions of energies as well as the cooling due to gas expansion. Supersonic beams are more difficult to operate and require much more pumping and hence energy than thermal beams, however they do allow the study of adsorption processes that require a high activation energy input and are simply not accessible to thermal beams. In addition to this supersonic molecular beams put all beam molecules in their quantum ground states (unless it is specifically being varied), and so allow the contribution of each quantum state to adsorption and reaction to be

determined¹¹. This can be desirable as the quantum energy state of the beam molecule can greatly effect the nature of the adsorption and surface reaction occurring. This makes molecular beams an invaluable tool for investigating the kinetics of surface reactions such as activation energies of adsorption and sticking probabilities. It is worth noting that unlike beams of electrons or ions, changing the direction of propagation of the molecular beam may be problematic¹⁰. Due to the non-penetrative nature of the molecules used molecular beams are extremely surface sensitive, more so than the Auger electron spectroscopy or low energy electron diffraction techniques also used in performing experiments contained in this thesis, in which the electrons are able to penetrate the surface to some extent.

The molecular beam reactor allows the study of controlled reactions between gas molecules impinging on prepared single crystal surfaces. The beam of molecules is produced by the thermal expansion of a gas through a small aperture and successive evacuated regions until a single beam of molecules travelling with idealised velocity in a specific direction is achieved. Molecular beams make dosing of gases on crystals and prepared crystal surfaces simple and straightforward, allowing the easy investigation of reactions between adsorbed molecules. The low flux of molecules impacting on the surface allows the assumption that all molecules in the beam arrive intact on the surface and that the molecules will only interact with the surface and each other on the crystal and not in the beam itself, or on any other part of the apparatus. This allows the assumption that the beamed molecules will either adsorb (via physisorption or chemisorption) or be reflected back into the vacuum. In addition to this the molecular beam may be used to perform sequential dosing experiments that allow a surface to be analysed further after a reaction with another molecule. As a method of dosing gas onto a surface, when compared with direct dosing via a leak valve for temperature programmed desorption experiments, the molecular beam allows more control over the collision rate and spatial distribution and is thus more accurate. It also allows the collection of reaction data at temperatures above the normal molecular desorption temperature. It is worth noting however that, neglecting surface diffusion, the area of the crystal dosed by the molecular beam is much smaller than the entire crystal surface (effected via background dosing). This can lead to contaminants adsorbed from the background giving false signals of the same order of

magnitude as the results from the molecular beam experiment, leading to confusing experimental results.

This assumption that beam molecules are either adsorbed or reflected allows simple measurement of sticking probabilities as well as the variation of sticking probability with adsorbate surface coverages to be determined. In addition it is often possible to observe evolution of products desorbing from a molecular beam reaction.

Molecular beams may be classified according to the source used to introduce gas into the beamline. In an effusive source molecular beam the beam gas effuses from an aperture and the pressure of the gas source is varied to give a Knudsen number of $K > 1$ (the mean free path of the individual molecules in the beam is greater than the diameter of the aperture used to create the beam). The distribution of energies of the molecules in the beam is Boltzmann-like¹¹. In the effusive source beam the molecular flow is described as 'free' and the properties of the beam are directly controlled by the temperature of the walls of the beam apparatus and the pressure of the source. This enables the intensity of the beam and energy of the molecules in beam to be varied easily. A nozzle source molecular beam utilises a skimmer to eliminate molecules moving in directions other than the direction of beam propagation from becoming part of the beam.

The thermal molecular beam has the same temperature as the nozzle or orifice used to create the beam and typically creates beam fluxes $10^{17} - 10^{18}$ molecules $\text{m}^{-2} \text{s}^{-1}$ ($0.01 - 0.1 \text{ ML s}^{-1}$ relative to the surface density of Pt(111) assuming unit sticking probability, calculated via integration of oxygen sticking curves on Pd(110)). Thermal molecular beams produce a beam flux that is several orders of magnitude lower than the flux produced by a supersonic molecular beam. Note that the amount of pumping required is directly proportional to the pressure of gas in the source with greater source pressures giving a greater beam intensity at the cost of due a larger volume of non-beam molecules that need to be removed. As a result of this supersonic molecular beams, in addition to being more problematic to create, require greater pumping speeds and more pumped regions than the simpler thermal molecular beams¹¹.

The molecular beams used in the experiments were created by the thermal expansion of the gases in the source through a nozzle and a skimmer and a series of apertures and gate valves. The source was equipped with two 5 L gas reservoirs that could be connected together or used independently; these allowed simultaneous dosing of a mixture of gases onto the sample. If a mixture of gases was used for the experiments the operator must ensure that sufficient time has passed to ensure a thorough mixing of the gases prior to the experiment. Another effect of the reservoirs was to stabilise the source pressure and hence beam signal during the course of the experiments. In general, 50 mbar of gas was used in the experiments in this work. This pressure was found to give the greatest signal to noise ratio without anomalous gas flow occurring in the beam. The gas from the source effuses through a quartz capillary, which was equipped with a platinum wire for heating the beam by resistive heating (increasing the energy of the beam molecules) and a chromel-alumel thermocouple for measuring the temperature of the quartz. The source capillary is mounted on a manipulator that is capable of moving in three dimensions to align the capillary with the skimmer for maximum beam signal. The beam of molecules is thermalised by collision with the walls of the capillary. A conical skimmer and series of apertures cut down the number of 'out of beam' molecules before the gas passes to the next chamber. Molecules that are not part of the beam do not pass through successive apertures and are pumped away by attached rotary pump backed turbomolecular pumps. The beam enters the UHV chamber via a final aperture, which gives the shape of the final beam spot on the sample surface. The nozzle on the molecular beam used in the gathering of the data in this thesis produced a circular beam spot of diameter 3 mm (confirmed by monitoring the change in LEED pattern with variation of vertical and horizontal displacement for molecular beam dosed O_2 on $\text{Pd}(110)$). There is a distance of 50 mm between the final capillary and the crystal in the chamber. The molecular beam was equipped with Pirani and ionisation gauges in the final chamber to measure the in-beam pressure. All beam pressures used generated pressures of between 10^{-8} mbar and 10^{-7} mbar on the ionisation gauge mounted in the second six way cross junction in the beamline.

When designing the beam it is important that the sizes of the transmission holes in the skimmer, nozzle and source capillary have been chosen so that the beam spot on the sample is sufficiently large that accurate sticking measurements may be

obtained whilst ensuring that the pressure rise due to beaming (out of beam molecules arriving in the analysis chamber) is as small as possible.

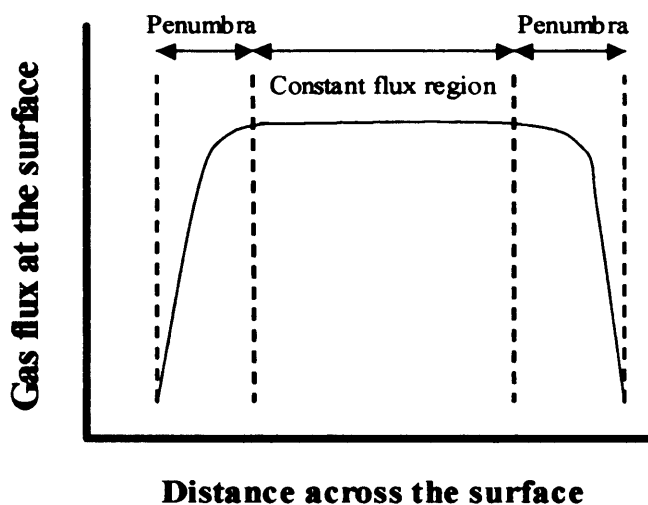


Figure 2.4 - The gas flux across the crystal surface with respect to the distance across the surface.

To maximise accuracy for molecular beam sticking experiments the penumbra (see Figure 2.4) must be as small as possible and the constant flux region across the sample as flat as possible, so that an accurate coverage dependence of sticking probability can be obtained. The penumbra can be minimised either by using a very small diameter source and a low source pressure or by ensuring that the collimator is positioned as close to the sample as possible or by a combination of the above. A skimmer-nozzle distance of 15 mm was used in all of the molecular beam experiments contained in this thesis.

The molecular beam was also equipped with a shutter, which acts as an on/off switch for the beam of molecules, and a flag made of gold foil between the nozzle and the crystal in the main chamber itself, which provided a measure of the total reflection of the beam. Reflected beam or product molecules were measured by quadrupole mass spectrometry.

The typical molecular beam experiment produces a mass spectrometer trace similar to that shown in Figure 2.5 below. This is a similar approach to that described by King and Wells)^{12,13}.

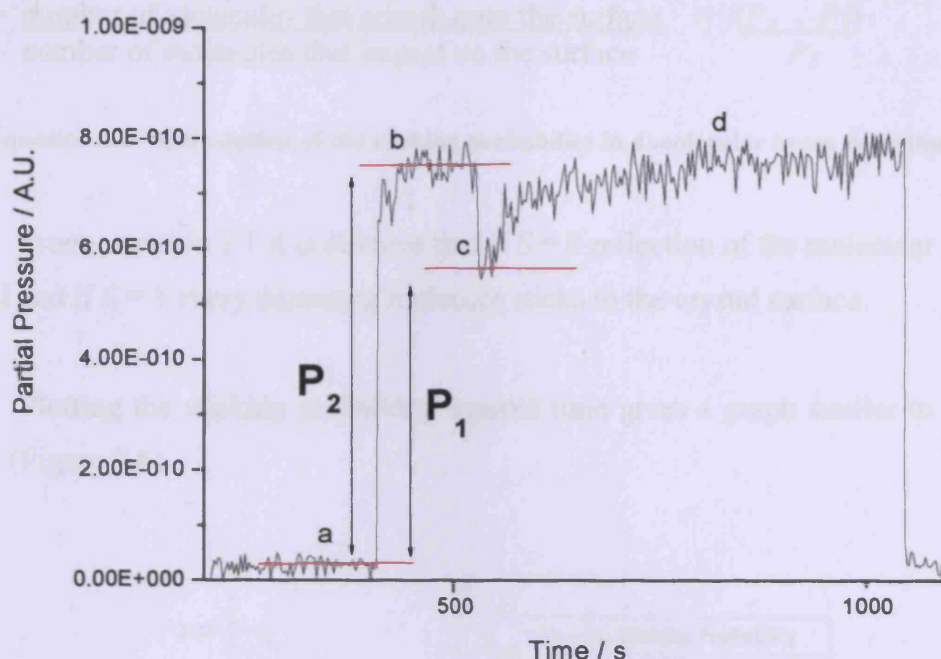


Figure 2.5 – A molecular beam of O_2 adsorbing on K/Pt(111) surface.

At time *a* the beam flag is closed and the mass spectrometer detects only the residual gases in the chamber. At time *b* however the beam flag is opened and the beam enters the chamber where it impacts with the gold flag. Being inert the adsorption of the molecular beam by the flag is negligibly small and this allows a measurement of the total reflection pressure, P_2 . At time *c* the chamber flag is opened, allowing the beam to travel to the crystal surface where it is adsorbed according to the sticking probability of the system. After a set amount of time the pressure either reaches the total reflection pressure and the surface is saturated, or a lesser pressure, indicative of some more complicated steady-state process occurring.

The most common measurement with the molecular beam is the sticking coefficient. The sticking probability/coefficient (*S*) is a measure of the probability of a given molecule adsorbing following a single collision with a surface. It depends upon a variety of parameters such as nature of the system under study, the excitation (vibrational, rotational, translational) of the beam molecules quantum modes, the surface coverage and the temperature that the surface is held at. The sticking probability is a function of the two partial pressures given in Figure 2.5 ie

$$S = \frac{\text{number of molecules that adsorb onto the surface}}{\text{number of molecules that impact on the surface}} = \frac{(P_2 - P_1)}{P_2}$$

Equation 2.1 – Calculation of the sticking probability in a molecular beam experiment.

From equation 2.1 it is obvious that if $S = 0$ reflection of the molecular beam is total and if $S = 1$ every incoming molecule sticks to the crystal surface.

Plotting the sticking probability against time gives a graph similar to the one below (Figure 2.6).

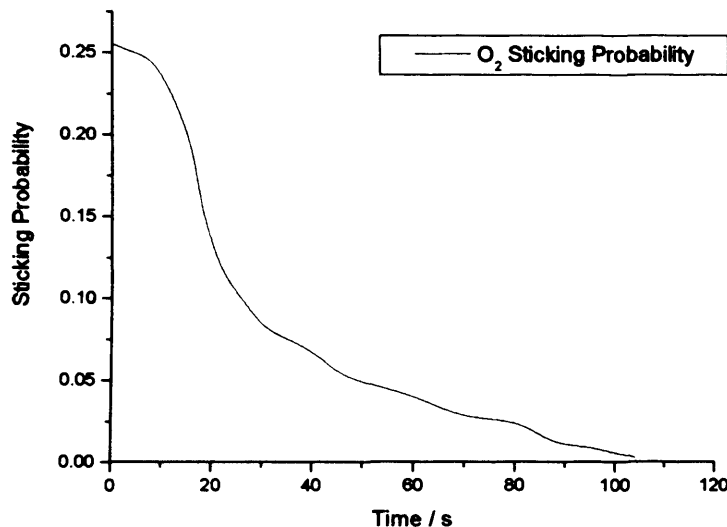


Figure 2.6 - A transformation of Figure 2.5 into a sticking probability vs time curve.

For a simple surface adsorption of the type $X_{(g)} \rightarrow X_{(s)}$ applying

$$\text{Surface coverage, } N_{ads} = Z \int S(t) dt$$

Equation 2.2 – Calculation of the total number of adsorbed molecules from the beam flux and sticking probability

Where N_{ads} = number of adsorbed molecules

Z = beam flux of molecular beam

allows the integration of Figure 2.6 to give the coverage of beam molecules adsorbed (Figure 2.7) ¹¹.

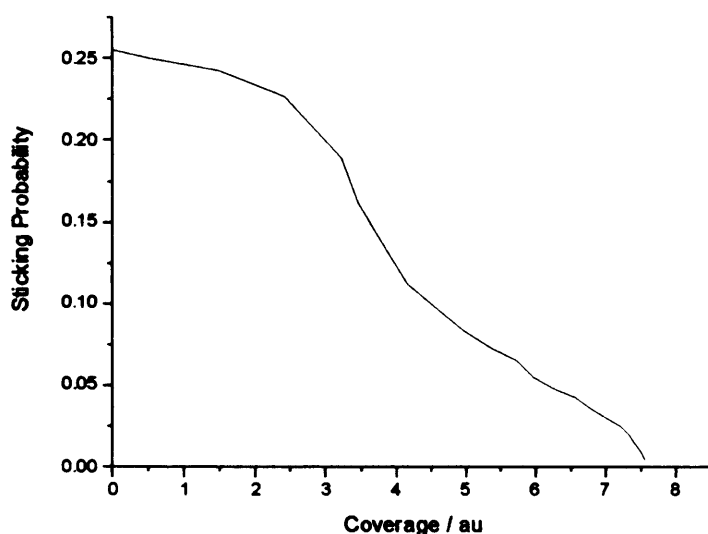


Figure 2.7 - The sticking probability vs adsorbate coverage.

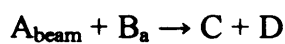
This data can then be correlated with previously obtained molecular beam curves or LEED images to provide the absolute coverage in monolayers.

Precise measurements can be made in this fashion and the kinetics deduced. In addition to this the shape of the sticking curve gives information on the type of adsorption mechanism occurring. In cases where there is an immediate reaction on beam incidence with the surface the reduction in beam sticking probability is often accompanied by the release of products. Sticking probability measurements also allow adsorption trends with regards to temperature and system to be determined. Should there be an activation energy barrier to adsorption it can be overcome by raising the temperature of the beam.

The shape of the curve relating the sticking probability with adsorbate coverage can also give an indication into the nature of the fundamental steps occurring in the adsorption process. For instance, precursor-mediated chemisorption generally exhibits a large initial sticking probability with a sizeable initial plateau region due to the stability and mobility of the precursor state. However for activated adsorption the sticking curve generally exhibits a more linear decrease in sticking

probability with increasing surface coverage (the square root of the coverage if the adsorption is dissociative).

Molecular beams are also commonly used as a tool to probe surface reactions between molecules adsorbing onto the surface. This can either be achieved by pre-covering the crystal surface with a known coverage of one reactant via background dosing through a fine leak valve or by using both reactants in the molecular beam simultaneously. Thus, for a reaction;



Where A_{beam} = reactant present in beam

B_{a} = reactant adsorbed on the surface

C and D = products

There are three possible outcomes;

- (i) A may adsorb onto the surface and react with B
- (ii) A may directly react with adsorbed B without adsorbing
- (iii) Both (i) and (ii) may occur

If during the course of the molecular beam experiment A adsorbs to high surface coverage (case (i) or (iii) occurs) equation 2.2 becomes

$$\theta_{A,t} = Z \int \{S_{A,t} - R_t\} dt$$

Equation 2.3

where S = Sticking probability of A

R = Reaction probability of A and B

Note that the coverage of adsorbed A is dependent upon both the reaction with B and the sticking probability of A. However in practice it is often difficult to differentiate between the two processes and applying the equation becomes problematic.

A common addition to molecular beam systems is a rotating chopper. The 'chopper' periodically blocks the beam and this has the effect of pulsing it. Such beams are commonly used to maximise the data gained from systems exhibiting fast transient adsorption behaviour^{11,14}. Isothermal transient measurements normally involve gas pre-dosed onto the surface before being exposed to a molecular beam of another species. If the two species react on the crystal surface the order in which the products are desorbed from the surface as the temperature is ramped gives an indication of the relative strengths of the different product-surface bonds and the ratio of the integrals of the desorption peaks gives information on the stoichiometric ratios of the products (assuming equal sensitivities to mass spectrometry). A mixed beam of reactants can be used to give isothermal steady state measurements in which, after an initial transient region, the evolution of products and consumption of reactants (and hence the coverages of each) has reached a steady state. Repetition of these experiments at several different temperatures allows a rate-temperature graph to be calculated, which can then be used to determine the energetics of the reaction. An alternative to this is the pseudo-steady state reaction in which a linear increase of temperature is applied during the experiment to continually disturb the steady state. The pseudo-steady state experiment may be complicated by transient adsorption and desorption processes which can be problematic to identify due to the temperature ramp and thus make it hard to analyse; however it typically produces rate-temperature relationship information at a much faster rate than steady state reaction experiments.

2.2.2 Temperature programmed desorption experiments

In addition to the molecular beam technique mentioned above it is also possible to use the UHV chamber for Temperature Programmed Desorption (TPD) studies. This involves measuring the products coming off the surface via mass spectrometry as the temperature of the surface is increased steadily (ramped). It is possible to repeat this at a variety of adsorbate surface coverages to build up a more detailed understanding of a particular system. Temperature programmed desorption is extremely useful in the determination of various kinetic and thermodynamic parameters of a reaction system. Analysis of desorption data can provide information on both the coverage of an adsorbate and the strength of the adsorbate-surface bond.

This information can then be used to deduce rate mechanisms and activation energies for reaction.

The crystal surface is background-dosed with the desired gas through the fine leak valve for a given pressure and time, which produces the required coverage of the reaction surface (generally given in Langmuirs, where $1 \text{ L} = 1.33 \times 10^{-6} \text{ mbar s}$). For TPR (temperature programmed reaction) experiments the reactant must be stable at the adsorbing temperature, often necessitating cooling. A linear temperature ramp (1 K s^{-1} was used in all the temperature programmed desorption experiments contained in this thesis) is applied to the crystal and the amount and identity of desorbing species analysed via quadrupole mass spectrometry. The temperature at which the created species are desorbed can be related directly to the adsorbate/product-surface bond strength in an Arrhenius-type rate equation for the desorption process. It is worth noting that this rate equation contains a contribution from the initial surface coverage as well as an exponential factor and Arrhenius constant ie. in the case of a surface desorption $N_{(a)} \rightarrow S + N_{(g)}$ ¹⁵

$$-\frac{d[N_{(a)}]}{dt} = k_d [N_{(a)}]^n = A [N_{(a)}]^n \exp\left(\frac{-E_d}{RT}\right)$$

Equation 2.4

Where S = surface adsorption site

n = order of desorption process

A = Pre-exponential factor

k_d = rate constant of desorption

N_{ads} = concentration of adsorbate molecules present on surface

E_d = activation energy for desorption

The rate of desorption is also related to the heating rate, dT/dt , ie.

$$-\frac{dN}{dT} = -\frac{dN}{dt} \cdot \frac{dt}{dT} = -\frac{dN}{dt} \cdot \frac{1}{\beta}$$

Equation 2.5

where β = heating rate

Putting this into equation 2.4 gives

$$-\frac{dN}{dT} = \frac{AN^n}{\beta} \exp\left(\frac{-E_d}{RT}\right)$$

Equation 2.6

As the maximum desorption rate occurs where $\frac{d^2 N_{ads}}{dt^2} = 0$ and $\frac{d^2 N_{ads}}{dT^2} = 0$

differentiating equation 2.6 and putting it equal to zero allows the temperature at which the maximum desorption rate occurs (the maximum point of the curve), T_{max} , to be determined ie.

$$n N_{ads}^{n-1} \frac{dN_{ads}}{dT} = -N_{ads}^n \frac{E_d}{RT_{max}^2}$$

Equation 2.7

Putting equation 2.6 into equation 2.7 gives

$$\frac{A n N_{ads}^{n-1}}{\beta} \exp\left(\frac{-E_d}{RT_{max}}\right) = \frac{E_d}{RT_{max}^2}$$

Equation 2.8

or in first order form

$$\frac{A}{\beta} e^{\frac{-E}{RT_{max}}} = \frac{E_d}{RT_{max}^2}$$

Equation 2.9

As equation 2.8 shows the dependence of T_{max} with adsorbate coverage depends upon on the order of the desorption (see Figure 2.8).

The desorption spectra obtained are typically plotted as mass spectrometer intensity against sample temperature. The measured signal from the mass spectrometer undergoes a marked increase at the temperature that is sufficient to overcome the activation energy for the desorption process. As with all peaks, a

maximum is observed, after which the signal decreases. Initially the shape of the desorption curve is governed by the exponential $e^{(-E_d/RT)}$ term of equation 2.4 due to the low desorption rate and hence small change in surface coverage of adsorbate that occurs in this region. As the desorption rate increases however, the surface coverage of adsorbate decreases, leading N_{ads} to dominate the equation.

Analysis of temperature programmed desorption experiments for different initial coverages of a particular species allows the order of reaction and the pre-exponential factor to be deduced. Substitution of these values into the above equation allows the energy of desorption to be calculated.

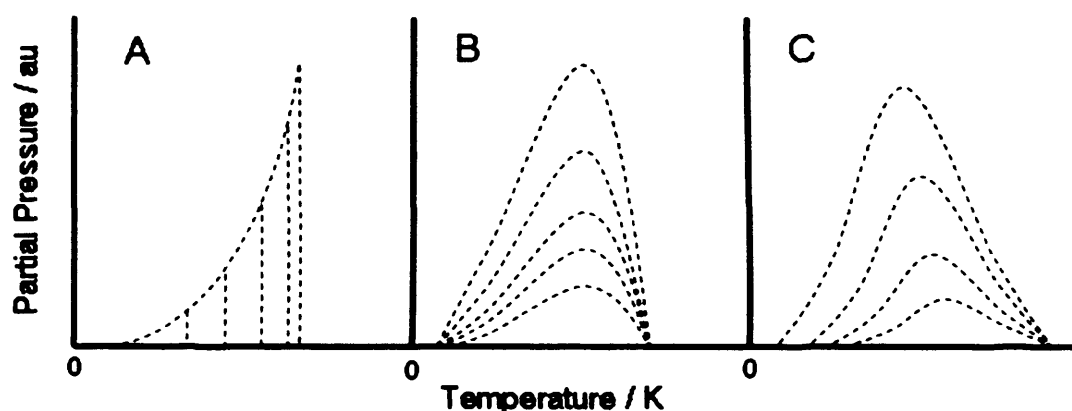


Figure 2.8 - The theoretical shapes of zero order (A), first order (B) and second order (C) desorption peaks. Figure adapted from diagrams present in tutorials on Michigan State University website by Simon J. Garrett.¹⁶

As Figure 2.8 shows the order of desorption has a definite effect on the shape of the desorption peaks. A zero order desorption exhibits a gradual increase in desorption rate up until the curve reaches a temperature where all the adsorbate has desorbed and there is a sudden drop in the desorption rate. The temperature at which the maximum desorption occurs increases with increasing initial surface coverage for a zero order desorption. A first order desorption process displays a profile that is asymmetrical but lacks the sudden drop off of the zero order desorption process. The temperature of the maximum desorption for a first order desorption process is independent of surface coverage. A second order desorption process gives a peak that is symmetrical and has a maximum desorption temperature that shifts to lower temperature with increasing surface coverage. Second order desorption peaks are commonly observed due to recombination of atoms following dissociative adsorption.

It is worth noting that there may be additional features such as species in different adsorption states, molecules adsorbed in precursor states and lateral interactions between adsorbed species which may add to the complexity of the recorded spectra^{15,20,23}.

The area underneath a desorption peak is directly proportional to the amount of gas desorbing from the surface, and hence the surface coverage of the adsorbed species. Provided the pumping speed of the analysis chamber has been maintained at a constant rate it is possible to obtain absolute coverages from known coverages (commonly determined using LEED) ie.

$$\theta = \frac{\text{Integral of unknown temperature programmed desorption curve}}{\text{Integral of known temperature programmed desorption curve}} \times \theta$$

Equation 2.10

where θ = absolute coverage for known system

θ = absolute coverage for unknown system

In systems where temperature programming leads to a surface reaction or when adsorption is not completely reversible the technique is termed temperature programmed reaction spectroscopy (TPRS or TPR). Temperature programmed reaction spectroscopy is especially useful for separating and examining the different components of complex systems and determining the individual surface reactions occurring as part of the system.

2.2.3 Auger electron spectroscopy (AES)

One of the more widely used surface science techniques is that of Auger electron spectroscopy (AES). In addition to the qualitative analysis of the sample the apparatus used for the generation of Auger spectra can be easily modified and used to give LEED patterns, saving space and money. Before the widespread use of x-ray photoelectron spectroscopic (XPS) techniques Auger electron spectroscopy was the principle tool for the examination of the elemental composition of a surface.

The original observation of the Auger effect was made by Pierre Auger in 1925¹⁷. Development of Auger electron spectroscopy as an experimental technique was limited by difficulties involved with producing and maintaining a suitable vacuum due to the limited vacuum technology available at the time. It wasn't until 1953 that the Auger transitions were first identified by Lander¹⁸. The next important advance came in 1968 when it was demonstrated that the resolution of the received spectrum could be enhanced greatly by differentiation of the energy distribution of the detected electrons¹⁹.

Auger electron spectroscopy is a method that is able to provide an elemental analysis of a sample. It relies on the Auger process (Figure 2.9, below), which is described below.

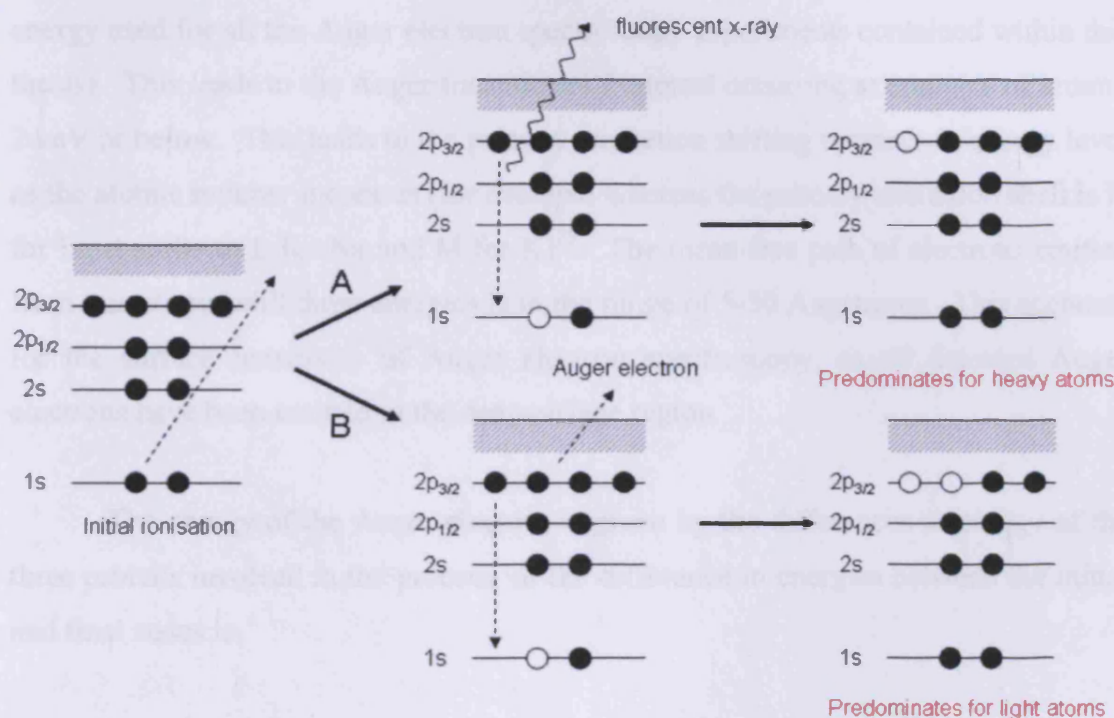


Figure 2.9 - The competing relaxation processes of x-ray fluorescence (path A) and Auger electron emission (path B).

In this process an initial ionisation of a low-lying orbital occurs by an incident beam of high-energy electrons, photons or ions. This creates an excited species in an unstable state. Relaxation from this excited state occurs via a less-bound electron from a higher energy level dropping down to fill the hole created in the lower energy level. This creates an excess of energy in the atom, which is removed via expulsion

of another (less strongly bound) electron from a higher-lying orbital, leaving a doubly-ionised final state. Although Auger spectroscopy may be used to detect any element heavier than hydrogen and helium the excited atom may also relax through a competing process called X-ray fluorescence with the loss of Auger signal. In this process instead of the Auger electron being emitted the excess energy is lost as a photon. This allows X-ray fluorescence spectroscopy to give complementary data to that of Auger electron spectroscopy. Since the Auger process depends upon the three separate energy levels of the emitting atom it is highly element specific as no two elements have identical energetics of electron energy levels.

Due to the nature of the physical apparatus used in the Auger experiment, beam energies of about 3 keV are normally used (2.7 keV was the primary beam energy used for all the Auger electron spectroscopy experiments contained within this thesis). This leads to the Auger transitions of interest occurring at energies of around 2 keV or below. This leads to the primary excitation shifting upwards in energy level as the atomic number increases (for example whereas the primary excitation shell is K for Li, it shifts to L for Na and M for K)²³. The mean free path of electrons emitted from transitions with these energies is in the range of 5-50 Angstroms. This accounts for the surface sensitivity of Auger electron spectroscopy, as all detected Auger electrons have been emitted in the near-surface region.

The energy of the Auger electron is given by the differences in energy of the three orbitals involved in the process, or the difference in energies between the initial and final states ie.

$$E_{\text{AUGER}} = E_x - E_y - E_z = E_{(\text{INITIAL})}^+ - E_{(\text{FINAL})}^{2+}$$

Equation 2.11

where E_{AUGER} = kinetic energy of emitted Auger electron

E_x = energy level of primary hole

E_y = energy level of electron filling primary hole

E_z = energy level of Auger electron origin

As the orbitals differ in energy between elements the emitted electrons occur at kinetic energies characteristic of the elements emitting for an excitation beam of known energy.

The Auger electron spectrum plot is a function of signal intensity against electron energy with characteristic energy peaks identifying individual elements. Unfortunately when the surface is bombarded with the exciting electrons from the primary beam electrons arising from the Auger process are not the only electrons encountered. The majority of the electrons detected are secondary electrons that have lost energy via such processes as plasmon excitations and interband transitions. In order to increase the resolution of the Auger peak against this large background the Auger spectrum is differentiated.

The exact energy change accompanying a specific Auger transition can be very difficult to calculate due to the multitude of electronic effects and final state energies that have to be taken into account. It falls outside the scope of this thesis to provide a detailed accounting of the energetics of the various Auger processes encountered due to the limited resolution obtainable with the Auger optics used. In this thesis Auger electron spectroscopy was used only for elemental detection and analysis of the surface composition.

As shown in Figure 2.9 the excited atom may also relax via loss of the excess energy as an x-ray photon. This relaxation process is in competition with the Auger process as a means of returning to a more stable conformation and the extent to which a given atom will fluoresce or emit Auger electrons varies according to the atomic number of the element in question (Figure 2.10).

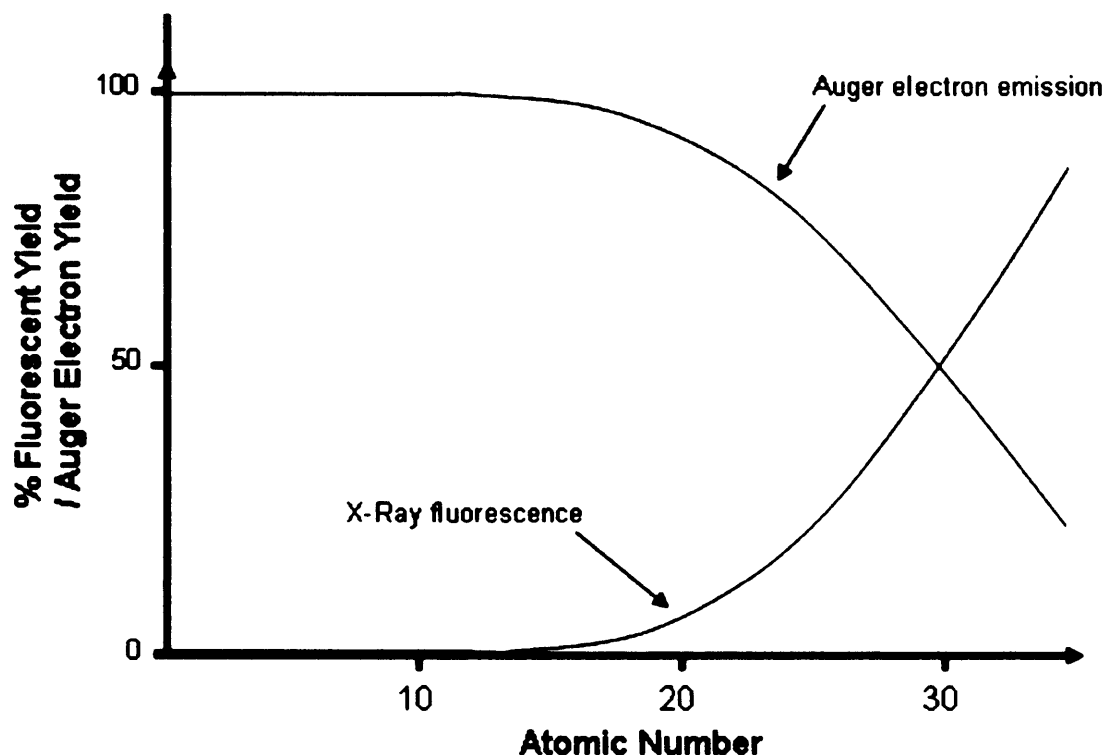


Figure 2.10 - Probability of Auger emission vs x-ray fluorescence with atomic number. Adapted from 'Surfaces' by Gary Attard and Colin Barnes.²⁰

Due to its nature there were problems using Auger emission with barium. Due to its high atomic weight, barium produces a very weak peak in the Auger spectrum, almost to the extent that it may also be considered 'Auger invisible.' This was not a problem however with the potassium system that was also studied in this thesis.

2.2.4 Low energy electron diffraction (LEED)

Low energy electron diffraction (LEED) is a fundamental crystallographic technique that can be utilised to provide accurate structural analysis. It is the most commonly used analytical technique when providing information about the structure of the near-surface region of a single crystal. However with reference to this project LEED is only applicable to check the periodicity of the surface being studied and of adsorbates deposited on the surface.

The first LEED experiment was in 1927 in the USA, when Germer and Davisson recording patterns from electron beams between 15-200 eV diffracted by a nickel foil. They observed an angular variation of the reflected electron flux and

explained their data in as being due to diffraction of the electron beam by crystallites in the nickel²¹. A short time after this Thomson observed diffraction patterns from a platinum film using a more energetic electron beam between 30000-60000 eV²². These experiments were the first experimental proofs of the validity of the de Broglie equation (equation 2.12)²³. Due to the advances in UHV equipment and technology that occurred at this time, the next major development in the LEED experiment occurred in the 1960's, enabling the production of a powerful and surface sensitive technique for examining adsorbate structure and ordering²⁴.

The LEED experiment operates by firing a beam of electrons of between 20 and 500 eV in kinetic energy perpendicularly towards the target. These electrons have a mean free path of between 5 and 10 Å and so will interact with the first 1-2 layers of the surface but lack the energy to penetrate deeper to any significant degree. Diffraction from x-rays has been used for many years as an experimental analytical technique but due to their nature x-rays are scattered poorly by matter and therefore penetrate deeply into the bulk of the solid and are not surface sensitive. Electrons reaching the detector from atoms further from the surface have generally lost energy via inelastic collisions and so are not detected. The inelastic mean free path of the electrons in a solid does not depend greatly on the identity of the solid under study, the major factor being the energy of the incident beam of electrons²³.

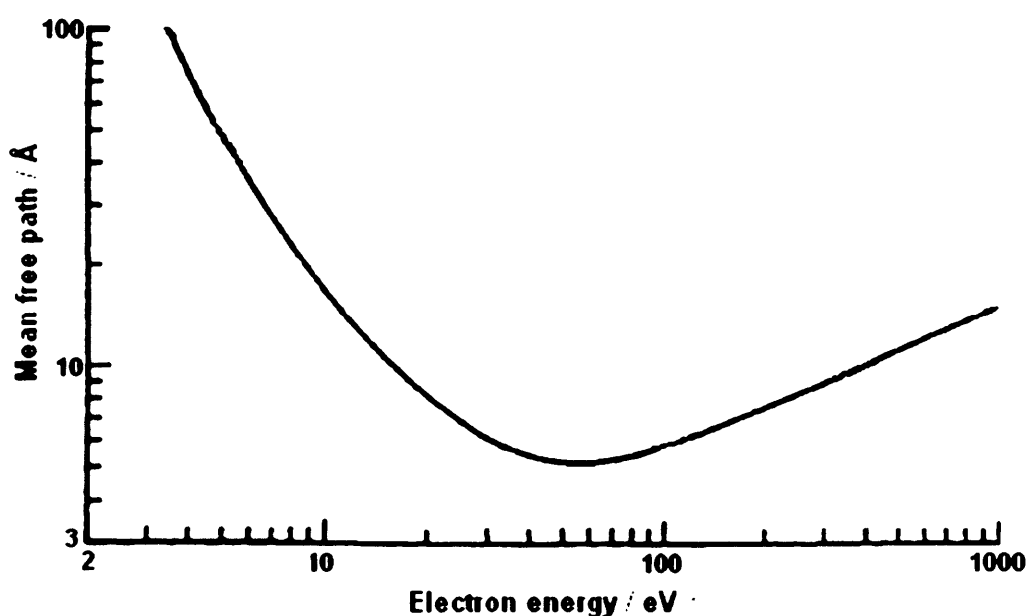


Figure 2.11 - The variation of the inelastic mean free path with electron energy. Adapted from 'An Introduction to Surface Chemistry' by Dr Roger M. Nix²⁵, 'Surfaces' by Gary Attard and Colin Barnes²⁰, and 'Auger Electron Spectroscopy (AES)' by Simon J. Garrett¹⁶.

The wavelength of the diffracted electrons obey the de Broglie relationship ie.

$$\lambda = \frac{h}{p}$$

Equation 2.12 – The de Broglie equation

where : λ = electron wavelength

h = Planck's constant

p = momentum of electron

Since the momentum of the electron is equal to the product of the mass of the electron and the velocity that it is moving with, and the kinetic energy of the electron can be given by classical kinetic energy methods and is also the product of the charge on the body and the accelerating voltage equation 2.12 can be rewritten as

$$\lambda = \frac{h}{mv} = \frac{h}{(2mE_k)^{1/2}} = \frac{h}{(2meV)^{1/2}}$$

Equation 2.13

Where : v = velocity of electron

m = mass of electron

E_k = kinetic energy of the electron

e = charge on electron

V = accelerating voltage

Substituting values for the above constants ($h = 6.62 \times 10^{-34}$ J s, $m = 9.11 \times 10^{-31}$ kg, $e = 1.60 \times 10^{-19}$ C) and cancelling allows the following relationship to be obtained:

$$\lambda = \left(\frac{150.6}{E} \right)^{1/2}$$

Equation 2.14

where λ is the wavelength of the electron in angstroms and E in the energy of the electron in electronvolts.

As the lattice spacings between the layers of atoms in most crystals (0.4- 2.7 Å) are of the same order of magnitude of the de Broglie wavelengths of the incident electrons, electrons of energy 30 – 500 eV are elastically back-scattered by the crystal surface. In crystals with a regularly repeating surface unit the converging diffracted electron beams superimpose to give a large signal in areas of constructive interference and thus a bright LEED spot is observed. Secondary electrons are removed by energy filtering grids in front of the fluorescent screen. The diffracted electrons produce a diffraction pattern of a two-dimensional surface as the reciprocal lattice of the actual crystal surface.

The constructive interference that arises from diffraction of a beam of electrons from a one-dimensional lattice is governed to the Bragg relationship for normal incidence.

$$\text{Path difference} = n\lambda = a \sin \theta$$

Equation 2.15 – The Bragg relationship for normal incidence.

Where n = order of diffraction

λ = de Broglie wavelength of electron beam (constant for elastically scattered electrons)

a = lattice constant

θ = scattering angle from surface

As a result of this there are specific areas of constructive interference where diffracted beams from specific scattering angles converge (see Figure 2.13). The diffraction pattern obtained is sharp where the surface is well ordered over regions much larger than the wavelength of the incident electrons. Poorly ordered surfaces however tend to give a diffraction pattern with diffuse spots. As the energy of the electron beam is increased the wavelength and diffraction angle of the beam

decreases. This is reflected in the compression of the LEED pattern and the modulation of the intensity of the discrete beams.

An alternative way of explaining LEED theory for regularly arranged one- and two-dimensional lattices is with reciprocal lattice (vector) analysis¹⁵. This mode of analysis is often more useful than Bragg-like equations when analysing two-dimensional lattices. As a LEED pattern is a reciprocal image of the two dimensional surface arrangement of atoms or molecules, Laue theory, which is based upon complex exponential phase factors, states that the difference in the two wavevectors is equal to a reciprocal lattice vector²⁶.

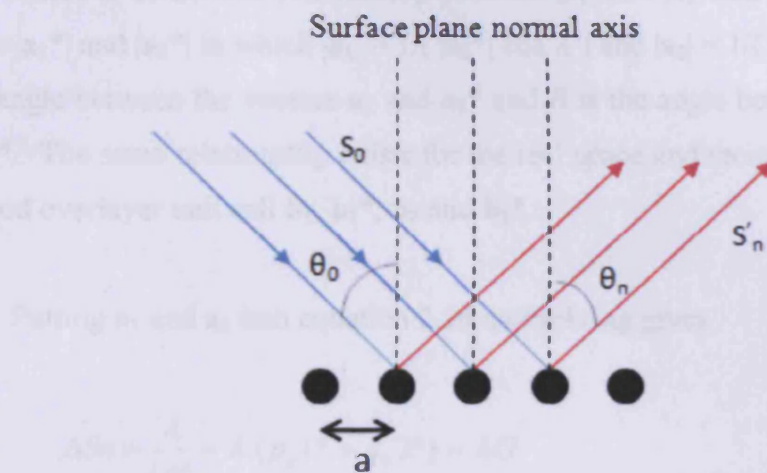


Figure 2.12 – Diffraction of an incident beam of electrons from a one dimensional array of metal ion cores. Figure adapted from ‘Surface Chemistry’ by Elaine M. McCash¹⁴.

The Laue condition states that

$$n\lambda = a(\sin \theta_n - \sin \theta_0) = a.\Delta S_n$$

Equation 2.16

and that the 2-D reciprocal lattice vector relating points in the reciprocal lattice can be expressed as

$$G = p\mathbf{a}_1^* + q\mathbf{a}_2^*$$

Equation 2.17

Where p and q are integers and G is the two-dimensional reciprocal lattice vector. The reciprocal lattice is defined by the reciprocal vectors \mathbf{b}_1^* and \mathbf{b}_2^* for the adsorbate and \mathbf{a}_1^* and \mathbf{a}_2^* for the substrate. The reciprocal vectors (\mathbf{a}_1^* , \mathbf{a}_2^* , \mathbf{b}_1^* and \mathbf{b}_2^*) are related to the real space vectors (\mathbf{a}_1 , \mathbf{a}_2 , \mathbf{b}_1 and \mathbf{b}_2) by a scalar product relationship :

$$\begin{aligned}\mathbf{a}_1 \cdot \mathbf{a}_2^* &= \mathbf{a}_1^* \cdot \mathbf{a}_2 = 0, \quad \mathbf{b}_1 \cdot \mathbf{b}_2^* = \mathbf{b}_1^* \cdot \mathbf{b}_2 = 0 \\ \mathbf{a}_1 \cdot \mathbf{a}_1^* &= \mathbf{a}_2 \cdot \mathbf{a}_2^* = 1, \quad \mathbf{b}_1 \cdot \mathbf{b}_1^* = \mathbf{b}_2 \cdot \mathbf{b}_2^* = 1\end{aligned}$$

Equation 2.18

There is an inverse relationship between $|\mathbf{a}_1|$ and $|\mathbf{a}_2|$ and the reciprocal space vectors $|\mathbf{a}_1^*|$ and $|\mathbf{a}_2^*|$ in which $|\mathbf{a}_1| = 1/(|\mathbf{a}_1^*| \cos A)$ and $|\mathbf{a}_2| = 1/(|\mathbf{a}_2^*| \cos B)$ where A is the angle between the vectors \mathbf{a}_1 and \mathbf{a}_1^* and B is the angle between the vectors \mathbf{a}_2 and \mathbf{a}_2^* . The same relationship exists for the real space and reciprocal vectors for the adsorbed overlayer unit cell \mathbf{b}_1 , \mathbf{b}_1^* , \mathbf{b}_2 and \mathbf{b}_2^* .

Putting \mathbf{a}_1 and \mathbf{a}_2 into equation 2.16 and solving gives

$$\Delta S n = \frac{\lambda}{|a|} = \lambda (p_a \mathbf{1}^* + q_a \mathbf{2}^*) = \lambda G$$

Equation 2.19

thus creating a relationship between the reciprocal lattice of the surface and the observed diffraction pattern. When the adsorbate reciprocal lattice is superimposed on the surface reciprocal lattice this allows a theoretical LEED pattern to be obtained¹⁵.

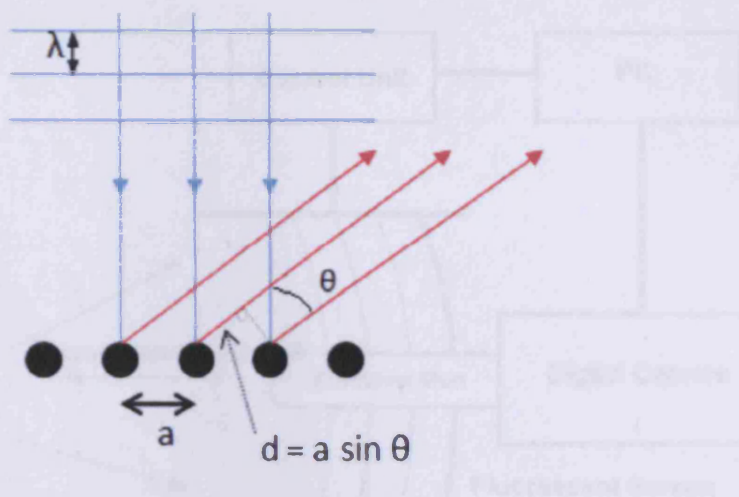


Figure 2.13 - Diffraction of a beam of electrons perpendicular to the plane of the surface. Figure adapted from 'An Introduction to Surface Chemistry' by Dr Roger M. Nix.²⁷

Analysis of the positions of the spots in the diffraction pattern created gives information on the size and geometry of the substrate and adsorbate unit cells and any surface reconstructions induced by adsorption. In addition to this comparison of the experimental LEED pattern and theoretically calculated LEED pattern can give information on defects at the surface.

It is also possible to use LEED in a quantitative manner by recording the intensities of the diffracted beams as a function of the electron energy of the incoming beam of electrons. This produces I-V curves that can give a more accurate view of the atomic positions and bond lengths when compared with theoretically generated I-V curves.

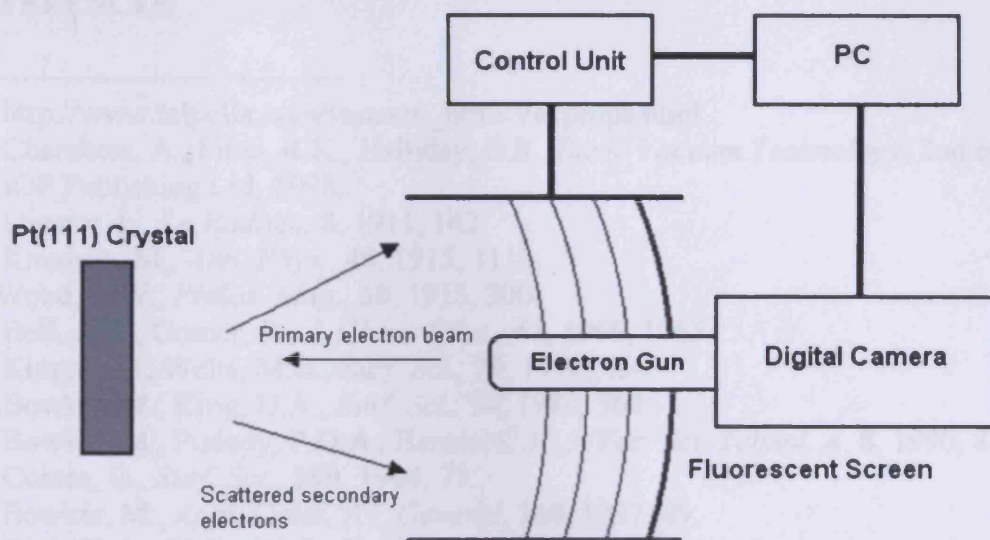


Figure 2.14 - A schematic of the LEED apparatus used in the experiments.

The LEED apparatus shown above uses an electron gun to produce a beam of electrons, which are directed at the sample. To prevent the build-up of charge at the sample surface the sample is earthed. As the beam of electrons hits the sample a portion of the beam is scattered. Electrons scattered in the backwards direction toward the LEED apparatus are collected by a series of concentric grids. The scattered electrons may either be elastic in nature (kinetic energy has been conserved) or inelastic (some kinetic energy has been imparted to the sample). Despite making up less than 1% of the received back-scattered electrons, it is the elastically scattered electrons that create the diffraction pattern. Inelastically scattered electrons have to be filtered out by the central grids, which are held at a variable negative potential. The elastically scattered electrons impact on a phosphor screen, inducing a fluorescent pattern of bright spots. The pattern is generally photographed to give recordable quantitative results. In the LEED experiments contained in this thesis a digital camera was used which was directly interfaced to a computer allowing for simple image capture and manipulation.

REFERENCES

1. http://www.telpella.com/vacuum_html/Vacpmps.html
2. Chambers, A., Fitch, R.K., Halliday, B.S., *Basic Vacuum Technology*, 2nd edition, IOP Publishing Ltd, 1998.
3. Dunnor, L., *Le Radium*, **8**, 1911, 142.
4. Knudsen, M., *Ann. Phys.*, **48**, 1915, 1113.
5. Wood, R.W., *Philos. Mag.*, **30**, 1915, 300.
6. Bell, A.A., Gomer, R., *J. Chem. Phys.*, **44**, 1966, 1065.
7. King, D.A., Wells, M.G., *Surf. Sci.*, **29**, 1972, 454.
4. Bowker, M., King, D.A., *Surf. Sci.*, **94**, 1980, 564.
9. Bowker, M., Pudney, P.D.A., Barnes, C.J., *J. Vac. Sci. Technol. A*, **8**, 1990, 816.
10. Comsa, G., *Surf. Sci.*, **299**, 1994, 77.
11. Bowker, M., *Appl. Catal. A : General*, **160**, 1997, 89.
12. King, D.A., Wells, M.G., *Surf. Sci.*, **29**, 1972, 454.
13. Alnot, P., Cassuto, A., King, D.A., *Farad. Disc. Chem. Soc.*, **87**, 1989, 219.
14. McCash, E., M., *Surface Chemistry*, OUP, 2001, 146
15. Woodruff D.P. and Delchar, T.A., *Modern Techniques of Surface Science*, Cambridge University Press, 2nd Edition, 1994.
16. <http://www.cem.msu.edu/%7Ecem924sg/LectureNotes.html>
17. Auger, P., *J. Phys. Radium*, **6**, 1925, 205.
18. Lander, J.J., *Phys. Rev.*, **91**, 1953, 1382.
19. Harris, L.A., *J. Vac. Sci. and Tech.*, **39**, 1974, 11, 23.
20. Attard, G., Barnes, C., *Surfaces*, OUP, 17, 1998.
21. Davisson, C.J., Germer, L.H., *Phys. Rev.*, **30**, 1927, 705.
22. Thompson, G.P., *Nature, Lond.*, **120**, 1972, 802.
23. Kolasinski, K.W., *Surface Science*, Wiley, 2002.
24. Germer, L.H., Hartman, C.D., Scheiber, E.J., *Rev. Sci. Inst.*, **31**, 1960, 112.
25. <http://www.chem.qmul.ac.uk/surfaces/scc/>
26. Clarke, L.J., '*Surface Crystallography: An Introduction to Low Energy Electron Diffraction*', Wiley, 1985.
27. <http://www.chem.qmul.ac.uk/surfaces/scc/>

3. THE BEHAVIOUR OF Pt(111) IN THE Pt(111)/BaO NSR CATALYST

3.1	<i>Introduction</i>	63
3.2	<i>Literature Review</i>	63
3.3	<i>Results and Discussion</i>	77
	<i>3.3.1 Auger spectrum and LEED of clean Pt(111)</i>	77
	<i>3.3.2 CO adsorption on Pt(111)</i>	78
	<i>3.3.3 NO adsorption on Pt(111)</i>	82
	<i>3.3.4 Molecular beams of NO₂ on Pt(111) held at increasing surface temperature</i>	85
	<i>3.3.5 Mixed molecular beams of NO₂ and O₂ on Pt(111)</i>	92
	<i>3.3.6 CO oxidation on Pt(111)</i>	101
	<i>3.3.7 NO reduction on Pt(111)</i>	106
3.4	<i>Summary of Conclusions</i>	110
	<i>REFERENCES</i>	112

3.1 Introduction

This chapter is primarily concerned with the interactions and reactions between CO, NO and O₂ and the platinum (111) crystal surface. The systems described in this chapter are relatively simple when compared with the K/Pt(111) and BaO/Pt(111) systems examined in chapters 4 and 5, but a detailed understanding of the reaction processes that the basic surface undergoes is essential when examining the more complex systems.

3.2 Literature Review

NO adsorption on platinum group metal surfaces has attracted much research interest due to its importance in environmental catalysis. Platinum group metals commonly form the active centres in the automotive catalytic converters found in lean-burn and non lean-burn gasoline engines. One of the major pollutants present in the exhaust fumes of such engines is NO. Platinum, palladium and rhodium are used in catalytic converters for the conversion of NO_x CO and unburnt hydrocarbons to N₂, CO₂ and H₂O. Under exhaust gas temperatures of 300 – 600 °C (measured at the oxygen sensor) these catalysts have proven themselves to be both efficient and reliable.¹

Early studies of NO adsorption on Pt(111) reported that the crystal surface was able to decompose NO². Since then however, multiple studies have shown this conclusion to be false, with the general consensus being that NO decomposition only occurs in small amounts (<1-2% of NO), if at all, and is therefore likely to be due to defects in the crystal surface^{5,6,20,23,26}. In particular high-resolution x-ray photoelectron and temperature programmed desorption studies performed by Zhu *et al* have shown that NO dissociation does not occur on the (111) surface of platinum³. Out of the basic planes it has been shown that the (100) face of platinum binds NO the most strongly and that the Pt(100) face also causes the greatest amount of NO dissociation. During temperature programmed desorption the desorbing atomic nitrogen and oxygen desorb associatively to form N₂ and O₂²⁰. Using high-resolution electron energy loss spectroscopy (HREELS) and infrared adsorption spectroscopy (IRAS) on NO adsorption at ~100 K Ibach and Lehwald observed two molecular N-O

stretching frequencies. Based on this work they proposed an adsorption model for NO on Pt(111) in which NO molecules adsorb as single molecules at low coverages but as dimers at higher coverages⁴. However, this model has been questioned by Hayden⁵ and Gland and Sexton⁶ who by comparing the observed vibrational frequencies with those of co-ordinated nitrosyl complexes found that although there were two different NO-Pt species present (with preferred states at different coverages), the N-O IR stretching frequencies were more characteristic of species bound in on-top sites and bridge sites. Using this evidence, a model was proposed in which NO adsorbs in the bridge site at low coverages but shifts to on-top sites at higher coverages^{6,7,8}. This model has been partially supported by x-ray photoelectron spectroscopy measurements^{9,10} in which O1s peaks were identified at different binding energies at low to intermediate coverages and assigned to on-top (higher coverages) and bridge sites (lower coverages), and a single broad peak identified at saturation coverage. However there were still inconsistencies between the infrared adsorption spectroscopy and high-resolution electron energy loss spectroscopy spectra at close to saturation coverages, particularly as the x-ray photoelectron data did not support the conversion of bridge-bonded to on-top NO theory.

More recently LEED¹¹ evidence supported by ab initio total energy calculations using spin-density functional theory with generalised gradient approximations¹² has suggested that the preferred binding site of NO at low coverages is in fact the fcc hollow site, with a c(2 x 2) structure being formed at 0.25 ML coverage (where 1 ML is defined as 1 adsorbate atom per surface atom). This model was supported by scanning tunnelling microscopy, dynamic LEED-IV, infrared adsorption and high-resolution electron energy loss spectroscopy evidence from Matsumoto *et al.*^{13,14} who showed that at low coverage NO adsorbs on the threefold fcc-hollow sites. However from 0.25 ML to 0.5 ML on-top adsorption sites begin to be populated in addition to the fcc-hollow sites. At the saturation coverage of 0.75 ML NO populates the hcp and fcc hollow sites as well as well as on-top sites. This study also showed that NO adsorbs upright on both of the hollow adsorption sites but is tilted at the on-top site¹⁶. It is worth noting that NO adsorbed at the hcp hollow site desorbs at 190 K and NO in the on-top site at 275 K. The only desorption site which is occupied at room temperature is the fcc hollow site, which desorbs at 320 K^{15,23}. This model is supported by x-ray photoelectron spectroscopy data¹⁵ and density

functional theory calculations¹⁶ which explains the observations that led to the proposal of the dimer⁴ and bridge-bonded models⁶ as being due to the change in electronic states induced by the on-top bonded NO causing a shrinking of the fcc hollow species vibrational peak. This model has also been supported by near edge x-ray absorption fine structure (NEXAFS) data provided by Zhu *et al*¹⁷.

An alternative model for NO saturation coverage at 0.75 ML has been constructed by Metka *et al.*¹⁸ based on LEED measurements and in situ SFG (Sum Frequency Generation). The model is based on the (2 x 2) unit cell and contains two tilted on-top and one bridge-bonded adsorbed NO surface species. This model appears similar to that used by Kasai *et al.*¹⁹ to explain the saturation NO coverage (0.75 ML) (2 x 2) structure on Pd(111). However the high resolution x-ray photoelectron spectroscopy data gathered by Zhu and co-workers has disproved this model¹⁵.

Despite the differences between these models it is generally agreed that below 300 K NO adsorbs molecularly on the Pt(111) surface through the nitrogen of the NO. The small amounts of O₂ and N₂ from dissociated NO that are sometimes observed are generally attributed to being due to breakdown over defect sites^{6,20}.

It has been shown that NO adsorbs in a (2 x 2) structure when saturated on Pt(111)^{5,6,11,21} however the coverage at which total surface saturation occurs is still a matter of much debate. Whereas Hayden reports a saturation coverage of 0.25 ML⁵ at 95 K, Campbell reports 0.3 ML²², Ranke reports 0.65 ML at 90 K⁹, and Matsumoto 0.74 at 90 K¹⁴. Raising the temperature to 120 K enabled Kiskinova to attain a saturation coverage of 0.54 ML¹⁰. This difference in saturation values can be explained by reference to the above difference in site occupancy; it seems likely that the lower coverages are due to the amount of NO required to fill all adsorption sites at that temperature. A true saturation coverage in which all hcp-hollow sites, on-top sites and fcc-hollow sites are occupied would seem to be at 0.75 ML. This coverage of NO gives a (2 x 2)-3NO structure¹⁵.

It has been found that pre-covering the Pt(111) with a p(2 x 2) coverage (saturation coverage) of atomic oxygen before adsorbing NO on the surface has a

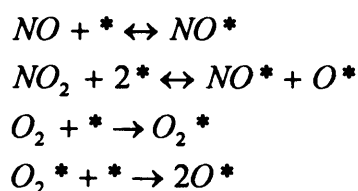
marked effect on the adsorption of NO when compared to that observed when adsorbing on the clean surface. The energetically preferred adsorption site of the atomic oxygen is the fcc hollow site, the preferred low coverage adsorption site for NO. This has the effect of blocking these sites resulting in NO populating on-top sites at low coverages, which was not previously possible. In a similar manner to that seen on the clean surface, at higher NO coverages NO occupies hcp hollow sites although the strength of the Pt-NO bond at the hollow site is weakened by the presence of the atomic oxygen²³. The authors explain this bond weakening as the result of the oxygen reducing electron back-bonding into the $2\pi^*$ antibonding orbitals of the adsorbing NO. It was also found that the total saturation coverage of NO decreased with increasing oxygen coverage and that the presence of oxygen on the surface decreased the measured NO sticking coefficient from 0.96 to 0.88²³.

It is well known that platinum is an efficient catalyst for NO oxidation. However it has been shown by kinetic Monte Carlo simulations and flow reactor experiments²⁴ that, due to the formation of strong oxygen-platinum bonds, at low temperatures the oxidation of NO is actually inhibited. Once the surface coverage of adsorbed oxygen is increased (with a consequent bond weakening effect), platinum lowers the activation energy barrier to the reaction and hence catalyses it. As a result turnover frequencies have a strong temperature dependence²⁴.

Under ultrahigh vacuum conditions NO oxidation after coadsorption with oxygen is not observed due to the fact that the energy of desorption of NO is lower than the activation energy barrier to oxidation^{25,26}. It has been claimed that there may be significant oxygen exchange between adsorbed oxygen and the oxygen in NO, depending upon adsorption conditions^{25,27,28}. However this is at odds with the findings of Schneider *et al.* who found that NO oxidation is actually inhibited by the presence of a platinum catalyst due to the strong Pt-O bonds formed²⁴. The group found that the oxygen has to be adsorbed to a significant coverage before the chemical potential is sufficient for the formation of NO₂ to be favourable. As a result the rate of NO₂ formation was found to depend strongly on O₂ partial pressure, with a 25% O surface coverage being required to make the reaction exothermic. The reason given for the dependence of reaction rate on oxygen coverage was that of O-O and NO-O

repulsive interactions becoming more significant at higher surface coverages and partially compensating for the stability of the Pt-O bond²⁴.

It has been found that the presence of NO₂ inhibits the oxidation of NO over platinum^{29,30}. This effect has been attributed to the powerfully oxidising character of NO₂, which is well known to dissociatively adsorb on platinum, leaving reactive atomic oxygen adsorbed on the surface. This effects the position of the equilibrium constants for the non-dissociative adsorption of O₂ and NO, the first steps of the NO oxidation surface catalysed reaction²⁹.



Scheme 3.1 - Proposed NO oxidation²⁹.

It was found that the rate of NO₂ production was approximately first order with respect to NO and O₂ concentration but almost -1 with respect to NO₂ concentration.

It has been shown that it is possible to adsorb NO₂ molecularly on clean Pt(111) at 100 K with dissociation only occurring as the surface temperature is raised to 170 K³⁰. This molecular adsorption state is bridge-bonded between two platinum atoms via one of the oxygen atoms and the nitrogen atom. It is thought that this species is a precursor in the dissociative adsorption of NO₂. This is evidenced by the fact that at high surface coverages of oxygen atoms (0.75 ML), NO₂ adsorption is only able to occur via the nitrogen atom and dissociation stops³⁰. There was no evidence of a stable NO₃ species produced from the coadsorption of NO₂ and O, despite a precursor NO₃ state being proposed as an intermediate in the desorption of N₂O₄.³⁰

The adsorption and desorption of CO on Pt(111) is one of the classical adsorbate systems dealt with in many textbooks. It is well known that CO adsorbs on bridge sites as well as on top sites of Pt(111) and forms several different coverage

dependent ordered structures³¹. Steininger *et al.* have observed superstructures with a $(\sqrt{3} \times \sqrt{3})R30^\circ$ LEED pattern at coverages of 0.17, 0.22 and 0.33 ML at ~ 100 K³². At around 150 K these superstructures merge into a single diffuse $(\sqrt{3} \times \sqrt{3})R30^\circ$ LEED pattern. Other groups have also observed these features^{33,34,35}. Increasing the temperature and the coverage of CO to about 0.35 ML leads to a $c(2 \times 2)$ pattern forming which increases in clarity to become sharpest at a coverage of 0.5 ML and a temperature of 260-270 K. Greater exposures produce a maximum coverage of around 0.67 ML and exhibit compressed surface structures^{32,36,37}.

There is not complete agreement however as to the binding site occupancy that these structures represent. The generally agreed view is that the LEED patterns observed at lower temperatures and coverages are due to CO binding to on-top adsorption sites. As the temperature and coverage are increased CO starts to be adsorbed in bridge-bonded sites until at around 0.5 ML, after annealing, the number of CO molecules adsorbed in bridge bonded and on top sites is equal^{32,38}. This was confirmed by Meisher *et al.* who, via time resolved electron energy loss spectroscopy (EELS), was able to quantify site partial coverages as a function of enthalpy³⁷.

Work by Ertl *et al.*³⁹, using LEED patterns as calibration for pressure-coverage data which in turn was then used to calculate heats of adsorption, found that CO initially adsorbs with a heat of adsorption of 138 kJ mol^{-1} for zero coverage. This energy decreased monotonically with increasing CO coverage. Calculations performed by Poelsema *et al.* give a similar zero coverage heat of adsorption^{31,40}. However, using direct microcalorimetric measurements Yeo *et al.* found the heat of adsorption to be around 180 kJ mol^{-1} for zero coverage decreasing to about 80 kJ mol^{-1} at full saturation⁴¹. This agrees with the work of Ray and Anderson who, using molecular orbital theory, derived binding energies of 180 kJ mol^{-1} for on-top sites and 112 kJ mol^{-1} for high coordination sites⁴².

A problem with many of the earlier temperature programmed desorption studies of CO on Pt(111) is that they have been adversely affected by the influence of anomalous adsorption/desorption behaviour at defect sites^{35,39}. The energy of CO adsorption was found to be of the order of 67.5 kJ mol^{-1} larger at a step edge than on a flat terrace⁴³. When performed on a surface relatively free of defects, a single

desorption peak is observed in temperature programmed desorption experiments. The temperature of the maximum of this desorption peak shifts to lower temperatures with increasing CO surface coverage. The desorption spectra obtained do not normally show any features giving an insight into the relative site occupancy at a particular coverage^{44,45,46}. This would seem to imply that CO is fairly surface mobile at temperatures above 100 K²⁹. This conclusion is supported by a recent research paper by Kinne *et al.* which observes the CO surface site occupancy be independent of the total coverage (for coverages below ~ 0.35 ML) for surface temperatures above 100 K⁴⁷.

Early studies determined the sticking coefficient of CO on Pt(111) to be a function of CO coverage and temperature in a number of experiments and values for the initial sticking coefficient of between 0.5-0.9 were obtained up to coverages of 0.15-0.4 ML, after which there is a decrease which is roughly linear with increasing CO surface coverage to less than $S = 1 \times 10^{-3}$ at 0.5 ML surface coverage^{32,39,48}. At room temperature several groups have shown a linear decrease in CO sticking coefficient (after an initial plateau region) for coverages up to 0.5 ML^{41,48}. It seems likely that this ambiguity over sticking probability and saturation coverage is due to the presence of surface defects at the crystal surface. However, these studies do all agree on the presence of a noticeable precursor effect, which is responsible for an initial maintenance of sticking probability despite increasing surface coverage.

The first bonding model for the adsorption of CO on Pt(111) was developed by Blyholder in 1964⁴⁹. His model for CO adsorption invoked electron charge transfer from 5σ CO orbitals to the crystal surface and simultaneous electron back donation of electron density into an antibonding $2\pi^*$ resonance of the CO molecule. Although useful, this model assumes that adsorption takes place solely in on-top adsorption sites. This is not a great problem however, due to the high mobility of adsorbed CO species and the established experimental fact that CO tends to preferentially adsorb in on-top sites at low coverages. A problem with this however was that theoretical calculations produced using density functional theory consistently predicted the adsorption of CO in the three-fold hollow site⁵⁰.

Despite numerous density functional theory calculations predicting a bonding preference for the threefold hollow site experimental evidence has consistently pointed towards on-top adsorption at low coverages. This could be explained by the inclusion of relativistic effects⁵¹ but further work needs to be done on this topic as calculated binding energies display marked differences from experimental evidence³¹.

An important part of forming a model for CO and NO oxidation on Pt(111) is the understanding of the adsorption of O₂ on the Pt (111) crystal surface and the growth and behaviour of the oxygen phases formed. This is made more complex by the fact that, at the pressures and temperatures employed in industrial applications, oxygen can exist in a variety of states between chemisorption and bulk oxide⁶⁴. Differences in the state of the oxygen at the surface can have a large effect on the kinetics of the reaction under investigation. For example, the transition of oxygen between differently adsorbed surface states has been shown to induce oscillations in the rate of CO₂ production in CO oxidation on platinum^{52,53}.

The mechanism of O₂ adsorption on Pt(111) has undergone extensive investigation. At low temperatures (< 100 K) O₂ adsorbs into a molecular adsorption state via superoxy or peroxy states^{32,54}. The adsorbed O₂ begins to desorb and dissociate at slightly high temperature (~ 150 K) to generate a coverage of adsorbed atomic oxygen (a single chemisorbed state) of 0.25 ML (where 1 ML is equal to the platinum atom surface density, 1.51×10^{15} atoms cm⁻²) ordered into p(2 x 2) domains. The atomic oxygen is adsorbed at the fcc hollow sites of the platinum⁸¹ at coverages of up to 0.25 ML. Oxygen of coverages of greater than this have been hypothesised to be due to adsorption in the hcp hollow adsorption sites⁵⁵. Temperature programmed desorption⁴⁸ and theoretical simulation⁵⁶ experiments indicate that repulsive interactions exist between the adsorbed oxygen adatoms and that hcp hollow site adsorbed oxygen atoms desorb at lower temperatures than those adsorbed in fcc hollow sites due to the differences in relative bond strengths⁵⁵.

There is however little agreement on the total saturation coverage and the magnitude of the heat of adsorption for O₂ on Pt(111)⁴¹. The majority of research groups agree that oxygen (from O₂) saturates to a maximum coverage of 0.25 ML on Pt(111)^{57,58}; however other groups have reported larger saturation coverages (obtained

by using aggressive molecular oxidants)^{59,79}. This discrepancy has been explained as being due to the low initial sticking coefficient of O₂ for Pt(111) (which decreases further with increasing oxygen surface coverage) leading to surface loading procedures with molecular oxygen being curtailed before saturation is achieved⁴¹. Oxygen has been shown to adsorb much more readily on more open platinum surfaces⁶⁰, however it was found that the oxygen saturation coverage could be doubled using a beam of electrons on an O₂ covered surface⁶¹ and coverages of atomic oxygen as high as 2.4 ML could be produced on Pt(111) when using aggressive molecular oxidants such as NO₂⁶² or ozone,⁶³ and 2.9 ML using a beam of atomic oxygen⁶⁴. Work performed by Segner et al.⁶⁵ has shown that a coverage of atomic oxygen of 0.75 ML can be obtained by the dissociative adsorption of NO₂ followed by heating the surface to 450 K to desorb adsorbed NO. In addition to this, Derry and Ross utilised a combination of relatively high partial pressures of O₂ (~1 x 10⁻³ Pa) and elevated surface temperatures to produce 0.125-0.75 ML surface oxygen coverage⁶⁶. Temperature programmed desorption spectra of the adsorbed oxygen layer indicates that the strength of the Pt-O bond decreases substantially with increasing oxygen surface coverage⁶⁵. However it was shown by Parker *et al.*⁶⁷ that the oxygen atoms remain chemically similar and therefore that the decrease in activation energy for the desorption with increasing oxygen surface coverage was likely to be due to repulsive interactions between the adsorbed atoms, which become more significant with closer packing. In addition, there appears to be no significant penetration of oxygen atoms into the bulk of the crystal. Using temperature programmed desorption, Auger electron spectroscopy⁶⁵ and x-ray photoelectron spectroscopy⁶⁸ it has been shown that, for O_(a) coverages greater than 1 ML, platinum oxide particles begin to form. The formation of platinum oxide particles is accompanied by a disruption in the order of the surface⁶⁴. However, formation of platinum-oxide is contentious as the oxide tends to be associated with silicon or calcium impurities in the crystal surfaces^{68,69,70}. More recently it has been proposed that there is a thermodynamically (not kinetically)-determined transition between a chemisorbed phase and an oxide film that occurs at a critical oxygen surface coverage, θ_c^{thd} .⁷¹ The heat of formation of platinum oxide is less than the heat of formation of the chemisorbed surface phase. However, as the oxygen surface concentration increases the repulsive interactions between the adsorbed oxygen atoms also increase, which has the effect of reducing the differential heat of adsorption until

it becomes more favourable to form an oxide film⁷¹. This has been supported by density functional theory calculations that have shown that adsorption of oxygen via chemisorption onto the surface is initially more favourable than incorporation into the surface region. This is attributed to the energetic cost of distorting the surface lattice and breaking strong metal-metal bonds. Again it was found that there was a critical O surface coverage at which, due to repulsion between the highly electronegative O adatoms, the occupation of sub-surface sites by adsorbing oxygen became more favourable than adsorption into the chemisorbed layer^{72,73}.

The mechanism of oxygen adsorption is probably one of the most studied systems in surface science⁷⁴. It has been found that at low temperatures (< 30 K) a single physisorbed molecular adsorption state exists⁷⁵. At slightly higher temperature (~ 100 K) two separate chemisorbed species can be identified, peroxy-like and superoxy-like (O_2^{2-} and O_2^- respectively)⁷⁶. Molecular beam experiments have confirmed the existence of a precursor adsorption state at low beam energies. The disappearance of this state with increasing beam energy is attributed to the ability of the beam to directly populate the chemisorbed adsorption states⁷⁷. However it is worth noting that the sticking probability of O_2 on Pt(111) is significantly higher in this work than in others, possibly indicating inaccuracy in experimental procedures. Theoretical studies performed by Groß *et al.*⁷⁴ suggest that adsorption into a molecular precursor state is an essential step for the dissociative chemisorption of O_2 on Pt(111). The group also suggest that a cold Pt(111) surface is incapable of dissociating incoming O_2 molecules (even if the incoming molecules have kinetic energies greater than the barrier to dissociation) due to the dissociative adsorption being a two-step process with the precursor state requiring thermal accommodation from the surface to dissociate.

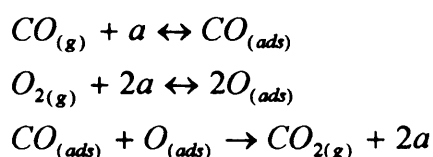
Molecular oxygen adsorbs dissociatively to the Pt(111) surface with a low initial sticking probability (0.06) at 300 K. The initial sticking probability decreases with increasing temperature to as low as 0.025 at 600 K^{48,78}. A similar value of sticking coefficient of 0.08-0.1 has been obtained by Bonzel and Ku, who also noted an exponential decrease in sticking probability with increasing oxygen coverage⁷⁹. Sticking probabilities greater than this are likely due to the presence of defects or increased numbers of steps on the crystal surface⁸⁰. Atomic oxygen has been shown

to desorb at around 700 K giving a value for the energy of desorption of approximately 460 kJ mol^{-1} ⁴⁸. For coverages below 0.5 ML oxygen is adsorbed predominantly into one adsorption state, which desorbs with second order kinetics. Increased oxygen coverage leads to a smooth lowering of the desorption peak. Theoretical molecular orbital studies have given the on-top, bridge and threefold sites binding energies of 400 kJ mol^{-1} , 297 kJ mol^{-1} and 290 kJ mol^{-1} respectively⁴². From this it can clearly be seen that the on-top site is theoretically the most stable. However LEED structural analysis of the $\text{p}(2 \times 2)\text{-O}$ system carried out by Materer *et al.* found that the fcc hollow sites were the preferred binding site for atomic oxygen. The group also noted some oxygen-induced deformations in the first two surface layers of metal atoms⁸¹. Weaver found that oxygen initially adsorbs in a $\text{p}(2 \times 2)$ layer up to a coverage of 0.25 ML. Increasing the coverage of oxygen on the platinum surface beyond this coverage results in a loss in the long-range order of the surface and a higher-density phase is formed. For oxygen coverages of greater than 0.5 ML (created using aggressive molecular oxidants), two separate oxygen states are visible in temperature programmed desorption experiments. These have been assigned to oxygen present in disordered domains and a high-density ordered phase. Increasing the oxygen coverage further to 0.75 ML has been shown to favour the creation of Pt-O particles. These particles undergo decomposition at high temperatures, explosively releasing the stored oxygen as molecular species. The strength of the Pt-O bond has also been shown to decrease with increasing O coverage⁶⁴. Unlike Materer and group⁸¹, the data gathered by Weaver *et al.* indicated that oxygen preferentially adsorbed in the hcp sites rather than fcc adsorption sites⁶⁴. Using XPS, CAICISS (co-axial impact collision ion scattering spectroscopy) and LEED to examine the adsorption of atomic oxygen, Parkinson and co-workers confirmed the existence of two separate adsorbed oxygen species, a chemisorbed species and an oxidic oxygen state. They also found that the penetration of the oxidic species into the first two layers of the platinum surface is most likely occurs via an oxygen-platinum exchange mechanism⁶⁸. It was found that, when heating to 500°C , the oxidic layer decomposed and a $\text{p}(2 \times 2)\text{-O}$ reconstruction was observed again, corroborating the work of Weaver *et al.*^{64,68}.

The oxidation of carbon monoxide by various transition metal surfaces has been studied extensively and are, without doubt, some of the better understood

heterogeneous catalytic reactions. The mechanism of this reaction has attracted much attention due to the oxidation of carbon monoxide in catalytic converters⁴¹. In addition, CO oxidation has attracted much interest due to its similarity to CO oxidation at the electrodes during methanol oxidation in fuel cells⁸². It appears that the same general mechanism is responsible for the oxidation of CO on platinum as on other transition metals^{48,83}.

It has been shown that whereas the initial sticking probability of CO on clean Pt(111) is 0.76 (at ~ 0 K) and displays the Kisliuk-typical shape, the initial sticking probability of CO on a Pt(111) surface pre-saturated with oxygen is 0.70 and declines monotonically with increasing CO coverage⁴¹. The mechanism for the reaction has been the focus of much study and has been established to be of Langmuir-Hinshelwood type, in which the reactants adsorb prior to reaction at the surface⁸⁴. Some of the earlier papers favoured an Eley-Rideal –type mechanism as opposed to, and as well as⁸⁸, the Langmuir-Hinshelwood that has since be proven. In the Eley-Rideal mechanism the CO either reacts directly with chemisorbed oxygen or is weakly held in a transient precursor state prior to reaction. It follows that the deciding factor between which of these reaction schemes occurs is the strength of the CO-metal bond. Measurement of the surface residence time before reaction by molecular beam⁸⁵ and isotopic tracer⁸⁶ studies supported a Langmuir-Hinshelwood mechanism regardless of temperature. The basic steps for the reaction are hence



Scheme 3.2 - The Langmuir-Hinshelwood mechanism for CO oxidation.

where a = free surface adsorption site

From the above it can clearly be seen that CO chemisorbs intact at the surface but the chemisorption of O₂ is preceded by its dissociation into atoms. When atomic oxygen and CO are adsorbed in neighbouring surface sites there is only a small activation energy barrier to reaction and hence high reaction probability (almost 1 for

temperatures below 540 K⁴⁸). As CO₂ has a low surface binding energy, once it is formed desorption is instantaneous. However, this is an over-simplification as various surface processes such as diffusion, adsorbate-adsorbate interactions, adsorption and desorption may participate in and hence affect the reaction⁸⁷.

It can be inferred from Scheme 3.2, that the rate of reaction is governed, to an extent, by the surface concentrations of the adsorbed reactants. Simulations and catalytic studies have shown that there are in fact three distinct regions with different rates of reaction, which can be induced by changing the surface concentrations of CO and O. At a slight increase in CO concentration past optimum conditions an instability in the reaction rate is introduced. Further increase in the CO concentration leads to complete or partial surface poisoning by adsorbed CO. Increasing the CO concentration past this region leads to the formation and stabilisation of densely packed CO islands with the catalysed oxidation reaction only able to take place along the boundaries of these islands. The reaction can however tolerate very much higher gas phase concentrations of oxygen than CO. Under these conditions the surface coverage of O becomes greater than the coverage of CO but the surface remains highly reactive and a high reaction rate is observed. Unlike the CO islands that form with an excess of CO, the oxygen islands formed are more open in structure and CO adsorption and the reaction can proceed unchecked⁸⁷. It follows that the overall rate of reaction under steady-state conditions is determined by the adsorption of CO or O₂, depending upon experimental conditions. The actual reaction step occurring at the crystal surface has been found to occur too rapidly to have an effect on the rate of product formation⁸⁸. Due to the low sticking coefficient of O₂ on Pt(111) under ultrahigh vacuum conditions a surface pre-covering of atomic oxygen is optimal for ensuring an appreciable reaction rate. A coverage of O of 0.25 ML (where 1 ML = the platinum atom surface density, 1.51×10^{15} atom cm⁻²) has been shown to facilitate the oxidation of coadsorbed CO at 295 K, producing CO₂, which immediately desorbs. Oxygen coverages of greater than this have been shown to reduce the rate of reaction by preventing the adsorption of CO⁸⁹, with oxygen coverages of 1.5 ML (cooled to 100 K) producing no appreciable reaction rate. It is worth noting that the efficiency of the poisoning by oxygen species is much less than poisoning by CO however, as a platinum surface with a large coverage of O_a (0.5 ML at 300 K) exhibits only a mild drop in the adsorption coefficient of CO when compared to a clean

surface⁴¹. Theoretical studies have shown that the rate of CO oxidation is mainly determined by the relative rates of oxygen migration and CO adsorption, with high rates of oxygen migration serving to reduce the rate of reaction⁸⁹.

In addition to the rate of reaction, the coverage of CO and O has been shown to effect the energetics with the oxidation of CO requiring an activation energy of 96 kJ mol⁻¹ when both of the reactants are in low concentrations, but at higher concentrations of oxygen on the surface the activation energy is only 47 kJ mol⁻¹. This has been attributed to repulsive interactions between adsorbates. Under these reaction conditions there is a weakly held CO precursor state above the oxygen adlayer. This state facilitates CO chemisorption and so is important in the reaction kinetics. The reduction in the lifetime of the precursor state with increasing temperature is the reason for the reduction in the reaction rate with increasing temperature⁸³.

It has been claimed that the reaction mechanism is basically independent of the surface geometry and that all platinum surfaces exhibit similar reactive regions⁹⁰. However, more recent studies have shown that the kinetics of the reaction are such that rearrangements in the positions of both adsorbed CO and O are possible. Zaera and co-workers found that a higher reaction rate for the oxidation was attainable when the adsorbed oxygen atoms were present as islands rather than distributed evenly across the surface. They attribute this to a lowered CO-binding strength in the vicinity of the islands contributing to lowered reaction activation energy^{91,92}. A problem with this explanation is that it is incompatible with more recent DFT calculations that predict a similar binding energy for CO bound to clean Pt(111) and in the middle of an O island^{93,94}. An alternative explanation may be that CO molecules will oxidise more readily at the periphery of O islands. It has been shown that when adsorbing CO onto an oxygen-covered platinum (111) surface at low temperature two distinct phases form and CO oxidation takes place only at the boundary of these phases^{95,96}. This is likely due to the two phases being mutually incompatible at the phase divide, resulting in a high initial energy which facilitates crossing the activation energy barrier⁹⁵. At higher temperature (close to CO desorption temperature) however the reaction kinetics follow a different pathway. The CO phase becomes less stable as a separate entity and the oxidation therefore

occurs across the surface in a more uniform fashion. Despite this the activation energy is still heavily influenced by the coverage of adsorbed atomic oxygen^{91,92,97}. Using scanning tunnelling microscopy Rhee *et al.* have shown that prior to oxidation, an adsorbed (2 x 2)-3CO surface structure changes into a ($\sqrt{19} \times \sqrt{19}$)-13CO surface structure and that there is a migration from three-fold adsorption sites to bridge sites. During this process the absolute coverage of CO also decreases from 0.75 to 0.68 ML. However, the authors note that the reason for this change is not fully understood⁸².

In addition, it has been shown that the physical states of the adsorbates, the coverage to which they saturate and the sticking probabilities of the individual species as well as interactions between the adsorbate and the surface and the adsorbates themselves may have a large effect on the reactivity of the transition metal catalysed CO oxidation reaction.

3.3 Results and Discussion

3.3.1 Auger spectrum and LEED of clean Pt(111)

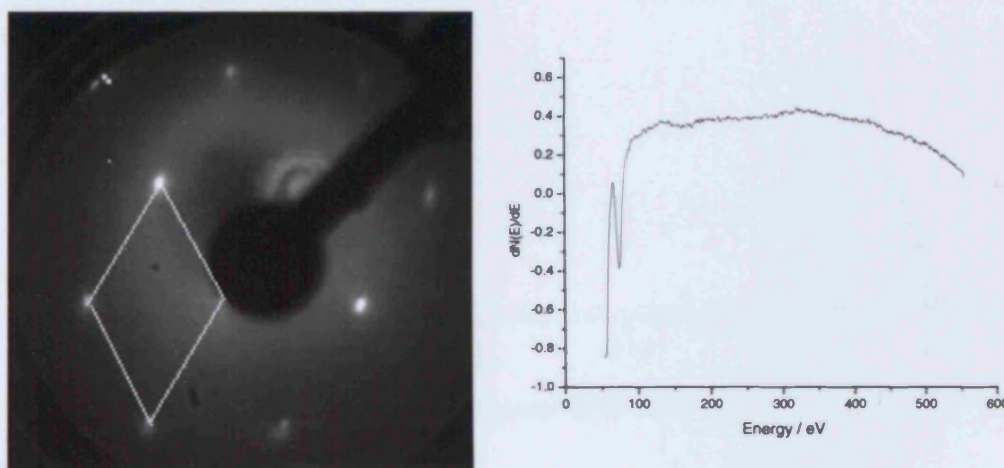


Figure 3.1 – LEED (67 eV, room temperature) and AES of clean Pt(111).

Figure 3.1 shows the Auger spectrum obtained from the Pt(111) crystal after repeated cycles of sputtering and annealing. The MNN transition at 70 eV is clearly seen with no visible peaks due to carbonaceous contamination. The LEED pattern shows a (1x1) pattern with the unit cell marked. There are no additional spots visible. Taken together, these spectra indicate that a clean Pt(111) surface has been prepared

and is free of any contaminants that might complicate the analysis of surface reactions.

3.3.2 CO adsorption on Pt(111)

Sticking probability measurements of CO at the Pt(111) surface are given in Figure 3.2. A variation is observed in sticking probability as a function of coverage for CO beamed on to the Pt(111) surface at different surface temperatures. The initial sticking probability is 0.49 (± 0.02) at 50 °C that (using LEED data from the literature) equates to a 0.5 ML surface CO saturation.

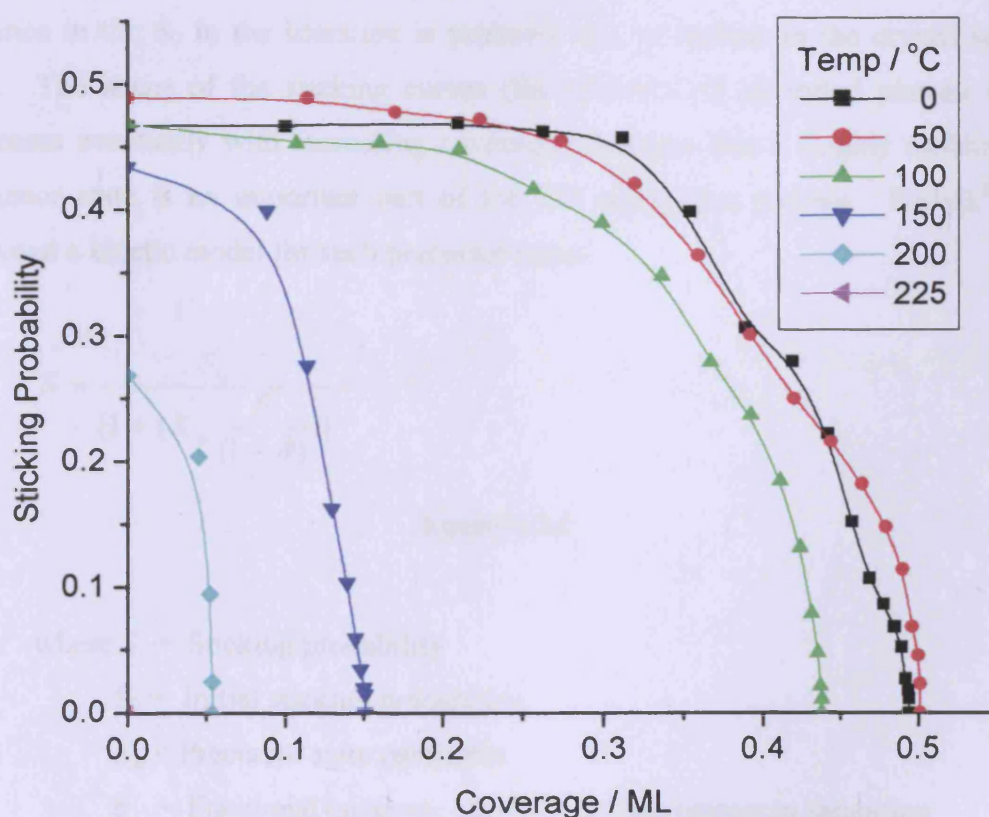


Figure 3.2 - The variation of sticking probability with coverage of molecular beams of CO (50 mbar molecular beam source pressure) on the Pt(111) crystal surface held at different surface temperatures.

Between 0-150 °C, S_0 varies only slightly with an average value of 0.48 ± 0.01 . Beyond 150 °C however S_0 falls off rapidly with increasing surface temperature

and no sticking is observed above 200 °C. Between 0 – 50 °C, CO saturates the surface to the highest coverage, 0.5 ML. This maximum saturation coverage decreases with increasing surface temperature after 50 °C, implying that adsorption processes are in competition with desorption processes at 100 °C and above, with there being no observable CO adsorbed at 225 °C. However, the initial sticking probability only starts to decrease after 150 °C, indicating that surface diffusion is likely to be occurring. The shape of the sticking curves are similar to those reported in the literature, which in general are reported to have an initial level region up until 0.15-0.4 ML followed by a sharp decrease to saturation at 0.5 ML. There is however, a discrepancy between the reported sticking probabilities in the literature and those in Figure 3.2 ($S_0 = 0.5-0.9$ literature values compared to 0.45-0.49 above). The large variance in the S_0 in the literature is probably due to defects in the crystal surface used. The shape of the sticking curves (the presence of an initial plateau which decreases eventually with increasing coverage) indicates that a (highly mobile) CO precursor state is an important part of the CO adsorption process. Kisliuk⁹⁸ has proposed a kinetic model for such precursor states:

$$S = \frac{S_0}{[1 + (K_p \frac{\theta}{1 - \theta})]}$$

Equation 3.1

where S = Sticking probability

S_0 = Initial sticking probability

K_p = Precursor state parameter

θ = Fractional coverage normalised with respect to saturation coverage

A key feature of this model is the precursor state parameter, K_p . If this quantity is much less than 1 it implies that precursor kinetics are an important part of the adsorption process in the system under study. A sticking profile with $K_p = 1$ is displaying simple straightforward Langmuirian kinetics. For the sticking curve measured at 0 °C a K_p value of 0.1 best fits the recorded data (below), indicating that

precursor kinetics and surface mobility make a large contribution to the adsorption of CO on the Pt(111) surface.

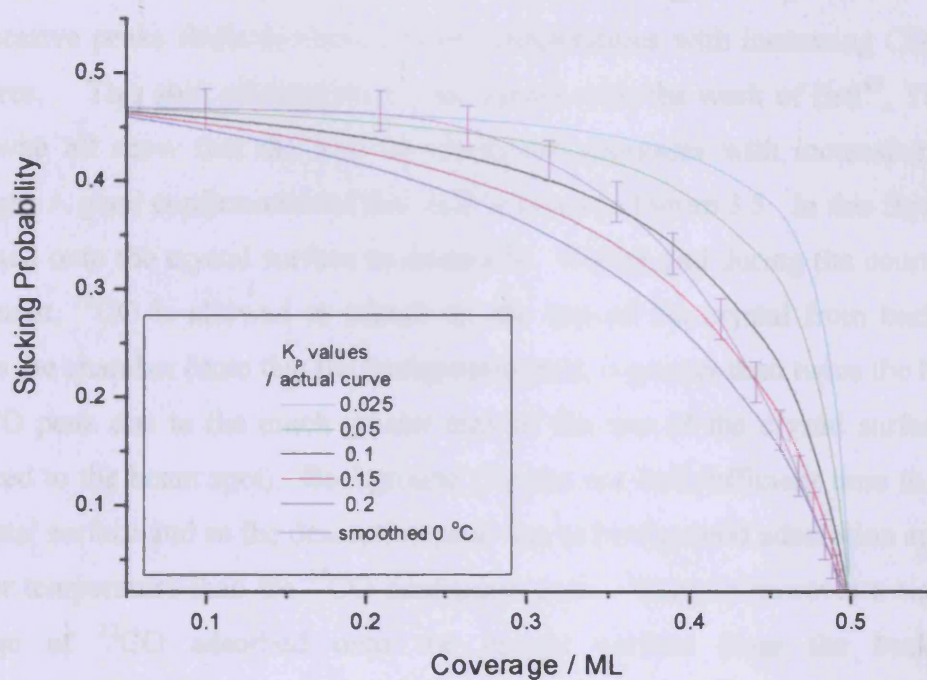


Figure 3.3 – The CO sticking curve modelled with different Kisluik constants to determine which constant fits the data displayed in Figure 3.2 the most closely.

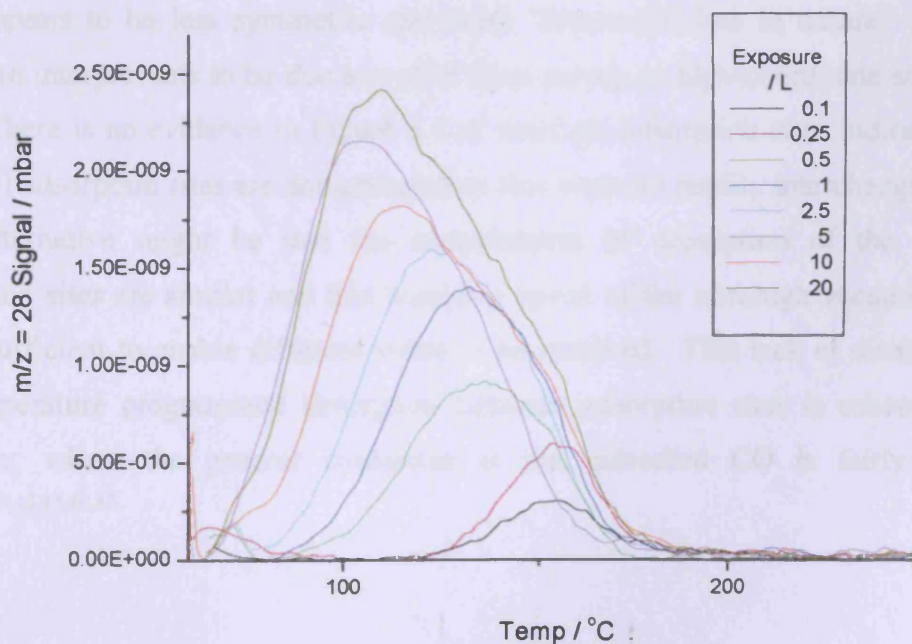


Figure 3.4 – Temperature programmed desorption experiments of CO adsorbed on Pt(111). A temperature ramp of 1 K/s was used in each case.

The temperature programmed desorption shown in Figure 3.4 shows that CO adsorbs reversibly and desorbs with a single low temperature desorption peak. The size and area of the desorption peak grows with increasing coverage and the maxima of successive peaks shifts to slightly lower temperatures with increasing CO surface exposures. This shift of desorption peak agrees with the work of Ertl³⁹, Yeo⁴¹ and Ray⁴² who all show that the heat of adsorption decreases with increasing surface coverage. A good confirmation of this shift is given in Figure 3.5. In this figure ¹³CO is beamed onto the crystal surface to saturation. Before and during the course of the experiment, ¹²CO is allowed to adsorb on the rest of the crystal from background gases in the chamber (note that the background peak is greater than twice the height of the ¹³CO peak due to the much greater area of the rest of the crystal surface when compared to the beam spot). Background CO has not had sufficient time to saturate the crystal surface and so the desorption peak due to background adsorption appears at a higher temperature than the ¹³CO desorption peak. There is however a significant coverage of ¹²CO adsorbed onto the crystal surface from the background, approximately 0.09 ML (where 1 ML equals 1 adsorbate atom per surface atom), or 1/5th saturation coverage (calculated using the relative areas of the desorption peaks in Figure 3.5 and the areas over which ¹²CO and ¹³CO adsorption were occurring and assuming a saturation coverage of 0.5 ML). In addition, the shape of the desorption peak appears to be less symmetric and more ‘first-order’-like in nature. Ray and Anderson interpret this to be due to a shift from on-top to high-coordinate adsorption sites. There is no evidence in Figure 3.4 of multiple adsorption sites indicating that either all adsorption sites are not saturated or that sites are readily interchangeable. A third alternative might be that the temperatures of desorption of the different adsorption sites are similar and that pumping speed of the ultrahigh vacuum system was insufficient to enable different states to be resolved. This lack of distinction in the temperature programmed desorption between adsorption sites is echoed in the literature, where the general consensus is that adsorbed CO is fairly surface mobile^{29,44,45,46,47}.

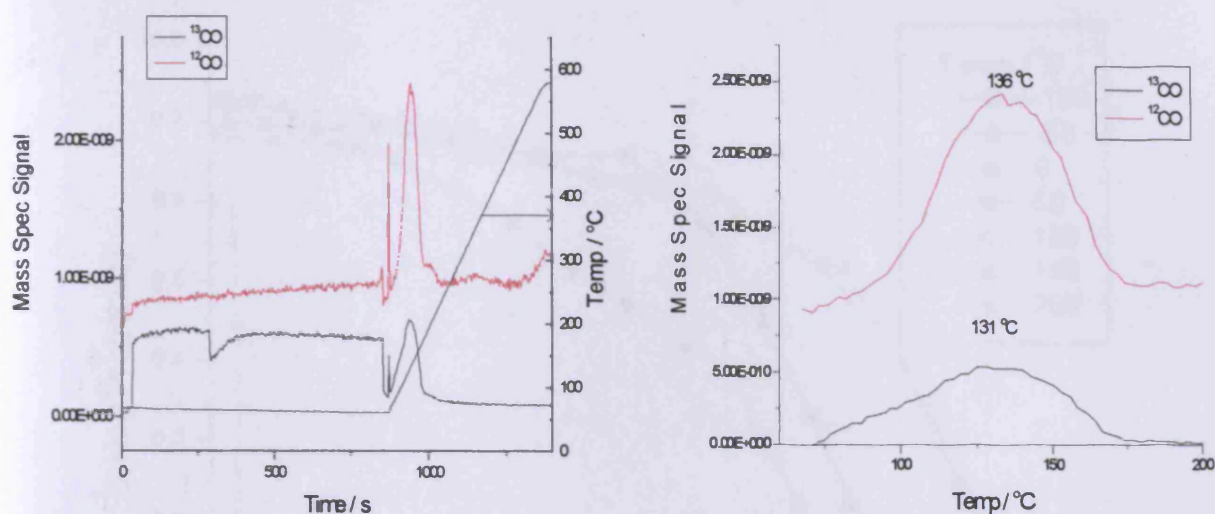


Figure 3.5 – A molecular beam of ^{13}CO (50 mbar molecular beam source pressure) beamed onto the Pt(111) surface to saturation compared to ^{12}CO adsorbing from the background during the course of the experiment and the temperature programmed desorption following the molecular beam experiment (left). The figure on the right is an expansion of the $m/z = 12$ and $m/z = 13$ desorption peaks showing the shift in peak maximum.

3.3.3 NO adsorption on Pt(111)

Figure 3.6 contains molecular beam sticking measurements for the NO/Pt(111) system in which the sticking probability is shown as a function of coverage at different surface temperatures. The initial sticking coefficient is 0.73 at 50 °C (+/- 0.2), which gives a 0.75 ML surface saturation coverage (using data from the literature).

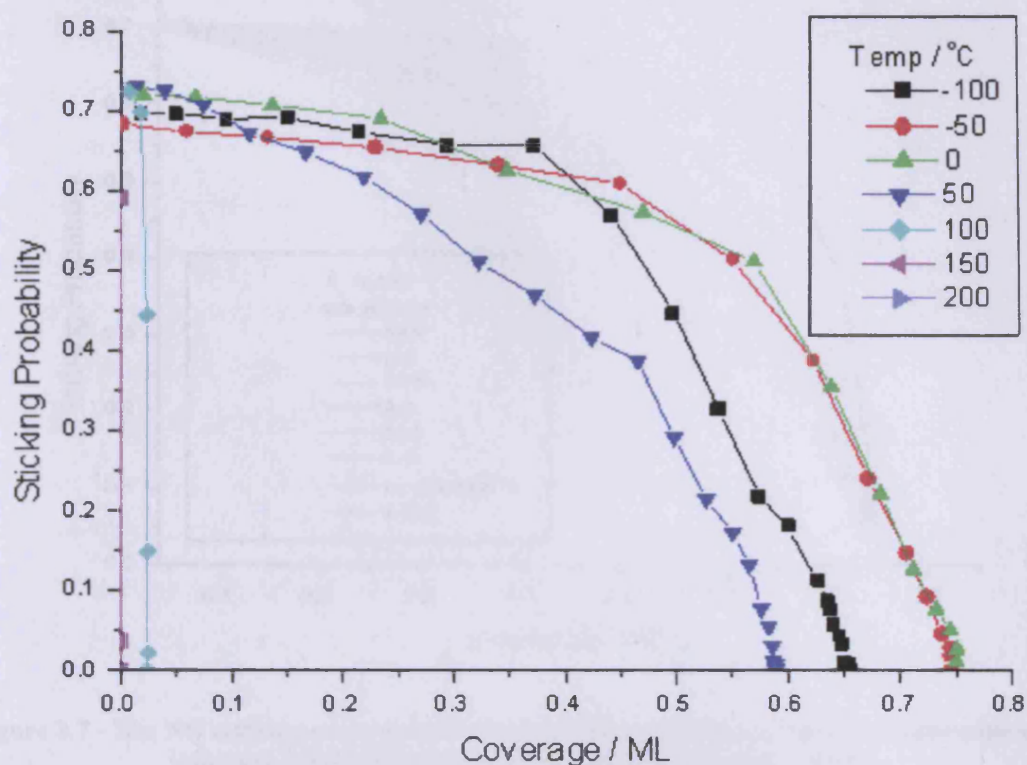


Figure 3.6 – Sticking probability measurements for molecular beams of NO (50 mbar molecular beam source pressure) on Pt(111) with increasing surface temperature.

As with CO cooling the crystal has little effect on S_0 , with NO adsorbing with a large initial sticking probability ($S_0 = 0.71 \pm 0.02$) up to 50 °C. At 100 °C, S_0 starts to fall and NO has stopped adsorbing by 200 °C Pt(111) surface temperature. The maximum saturation coverage attained is 0.75 ML at -50 °C and 0 °C. That maximum saturation of the surface occurs at these temperatures and not lower is likely due to the extra time it takes to reach temperatures below this, as there is increased adsorption of background gases from the chamber that compete with the beam of NO for surface adsorption sites. The presence of the initial plateau indicates that significant precursor kinetics are occurring in the adsorption process. As the temperature is increased it appears to be the lifetime of the precursor state that is decreasing not the adsorption probability into the precursor state, with the plateau region that has constant sticking probability (characteristic of precursor mediated adsorption) reducing in size, not the initial sticking probability. Using the Kisluik equation described in Equation 3.1 a K_p value of 0.175 can be obtained for the sticking profile at 0 °C, indicating a substantial precursor effect in operation.

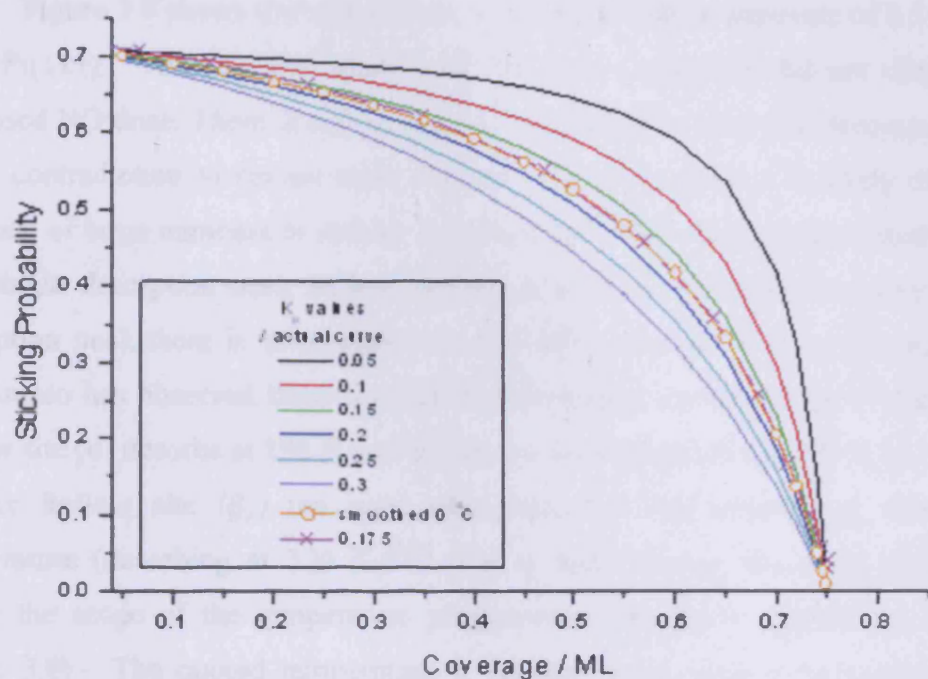


Figure 3.7 - The NO sticking curve modelled with different Kisluik constants to determine which constant fits the data displayed in Figure 3.6 the most closely.

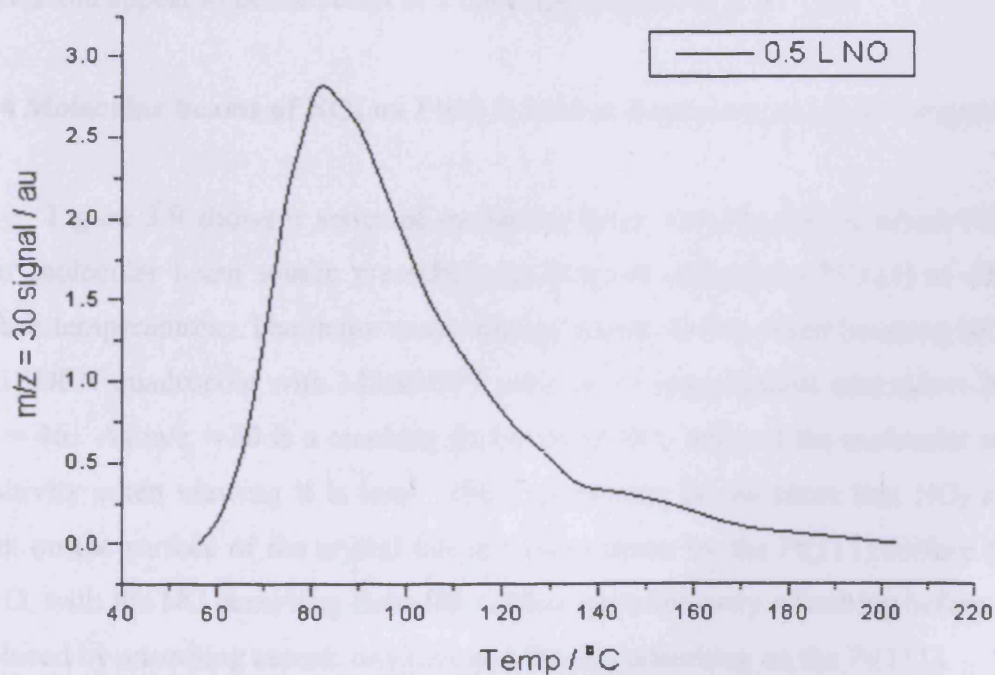


Figure 3.8 – Temperature programmed desorption of NO from Pt(111). A temperature ramp of 1 K/s was used. Differing NO surface exposures produced little effect on the size and maximum of the desorption peak and have been omitted for clarity.

Figure 3.8 shows the temperature of desorption of an exposure of 0.5 L of NO from Pt(111). The size and position of the desorption peak did not change with increased NO dose. There is no evidence of any products from NO decomposition in direct contradiction to certain early studies². This discrepancy is likely due to the presence of large numbers of defects in the crystal used in the previous study. There is a single desorption peak with a maximum at 82 °C. As there is only a single desorption peak there is no evidence of any differences in binding site occupancy. Matsumoto has observed three distinct NO adsorption environments^{13,14} but the hcp hollow site (α) desorbs at 190 K and the on-top adsorption sites at 275 K (β_1), leaving the fcc hollow site (β_2) the only adsorption site that desorbs at above room temperature (desorbing at 320 K)^{15,23} (the α states shown occurs at temperatures below the scope of the temperature programmed desorption experiment shown in Figure 3.8). The quoted temperature is slightly lower than the maximum of the desorption peak in Figure 3.8. Three separate binding site environments have also been observed at different coverages and temperatures by Gorte *et al.*²⁰ at 200, 340 and 400 K, although the higher temperature peaks observed do not appear in the same spectra and appear to be the result of a coverage-dependent peak shift.

3.3.4 Molecular beams of NO₂ on Pt(111) held at increasing surface temperature

Figure 3.9 shows a series of molecular beam experiments in which NO₂ (50 mbar molecular beam source pressure) was beamed onto clean Pt(111) at different surface temperatures. The major mass: charge signal visible when beaming NO₂ and the HIDDEN quadrupole with MASSOFT used in the experiments was $m/z = 30$, not $m/z = 46$. As $m/z = 30$ is a cracking fragment of NO₂ and not the molecular ion the sensitivity when viewing it is less. The experiments below show that NO₂ arrives intact on the surface of the crystal but is broken down by the Pt(111) surface to NO and O, with the NO desorbing from the surface (or transiently adsorbing before being displaced by adsorbing atomic oxygen) and the O_(a) adsorbing on the Pt(111).

When NO₂ was beamed onto the Pt(111) crystal surface at 50 °C an initial sticking was observed. However the $m/z = 30$ signal quickly rose to a value greater than the total reflection observed when the chamber flag was closed. This increased $m/z = 30$ signal was not maintained and fell back to the background level with

continued beaming. A possible explanation for the observed behaviour might be that the NO_2 is broken down to NO and O by the platinum surface. The NO thus produced desorbed immediately (possibly displaced by adsorbing atomic oxygen). As molecular NO also has a mass: charge ratio of 30, NO desorbing from the surface in addition to the reflected NO_2 from the beam gives a greater $m/z = 30$ response to the mass spectrometer than the initial full reflection signal (before the beam flag is opened). The increased $m/z = 30$ signal has the effect of masking observable NO_2 sticking. As NO_2 reduction continues the surface becomes saturated with adsorbed atomic oxygen from the decomposition, tying up further NO_2 adsorption sites and in effect poisoning the surface with regards to NO_2 decomposition. At 50 °C there is also a substantial $m/z = 44$ desorption peak that occurs on adsorption of NO_2 . Given the decomposition of NO_2 by the surface it seems likely that this desorption peak is due to the formation and desorption of CO_2 , created by the reaction of $\text{O}_{(\text{a})}$ from the reduction of NO_2 , and CO adsorbed from the background gases within the chamber. The fact that this peak is greatly reduced in size when beaming at 100 °C and 150 °C and absent for surface temperatures higher than 150 °C would seem to agree with this hypothesis as Figure 3.4 shows that CO desorbs from Pt(111) at these temperatures.

This behaviour continues up until 300 °C where after a $m/z = 32$ desorption signal appears with a slight time delay after the beam of NO_2 first impacts the crystal. The magnitude of the $m/z = 32$ desorption signal relative to the $m/z = 30$ sticking trace grows with increasing temperature. At temperatures of 350 °C or greater the ‘bump’ of $m/z = 30$ that follows the immediate adsorption of NO_2 onto the crystal surface is absent; instead a continuous raised plateau is observed, consistent with steady-state NO_2 breakdown and desorption of decomposition products.

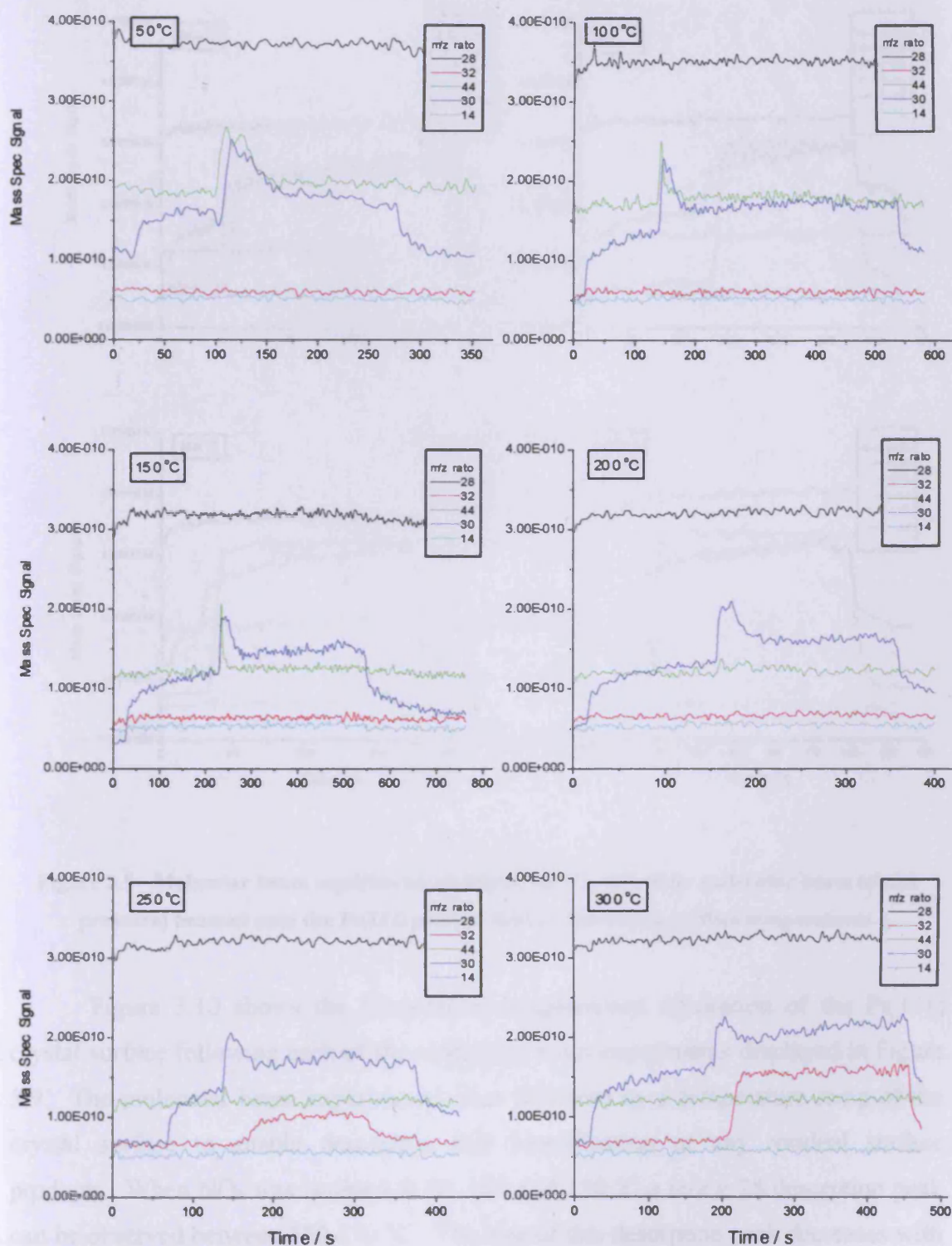


Figure 3.9 – Molecular beams of NO₂ (50 mbar molecular beam source pressure) beamed onto the Pt(111) surface held at increasing surface temperatures.

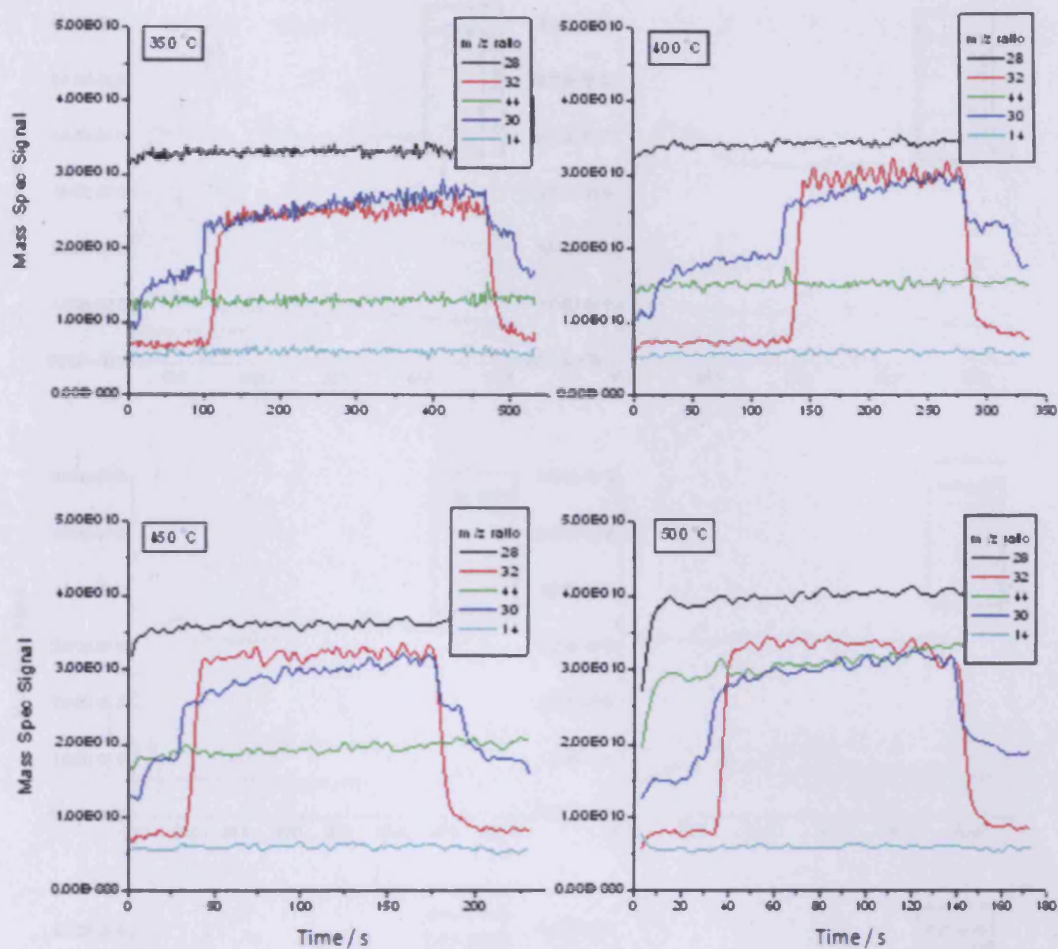


Figure 3.9 - Molecular beam experiments of beams of NO₂ (50 mbar molecular beam source pressure) beamed onto the Pt(111) surface held at increasing surface temperatures.

Figure 3.10 shows the temperature programmed desorption of the Pt(111) crystal surface following each of the molecular beam experiments displayed in Figure 3.9. The molecular beam experiments were followed by a temperature ramp of the crystal surface to enable desorption and identification of any residual surface products. When NO₂ was beamed at 50, 100 and 150 °C a $m/z = 28$ desorption peak can be observed between 150-170 °C. The size of this desorption peak decreases with increasing surface temperature. The origin of this peak is likely from the adsorption of background CO onto the crystal surface. At 50 °C there is also a large $m/z = 44$ peak, again also likely due to background CO adsorbing but this time reacting with adsorbed atomic oxygen from NO₂ breakdown and forming CO₂.

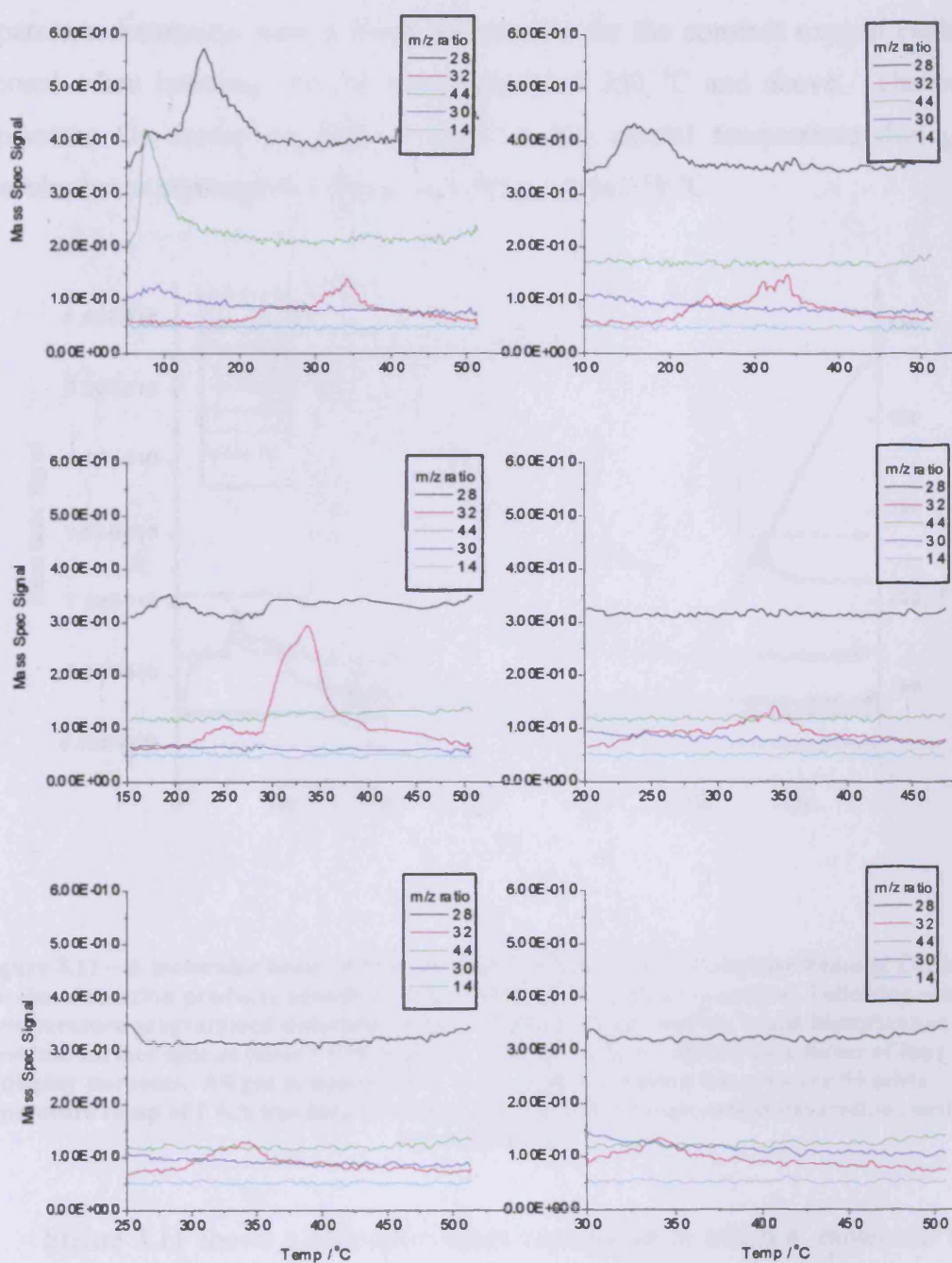


Figure 3.10 – Temperature programmed desorption of the Pt(111) surface immediately following the molecular beam experiments displayed in Figure 3.9. A temperature ramp of 1 K/s was used during each experiment.

The temperature programmed desorptions from the experiments in which NO_2 was beamed onto the Pt(111) surface held at 50, 100, 150 and 200 °C all display a double $m/z = 32$ oxygen desorption feature, with a main high temperature desorption

peak at 340-350 °C that has a lower temperature shoulder at 250-260 °C. This lower temperature desorption state is likely responsible for the constant oxygen evolution observed when beaming NO_2 at temperatures of 250 °C and above. The higher temperature O_2 desorption peak remains as the crystal temperature during the molecular beam experiment is increased further, up to 350 °C.

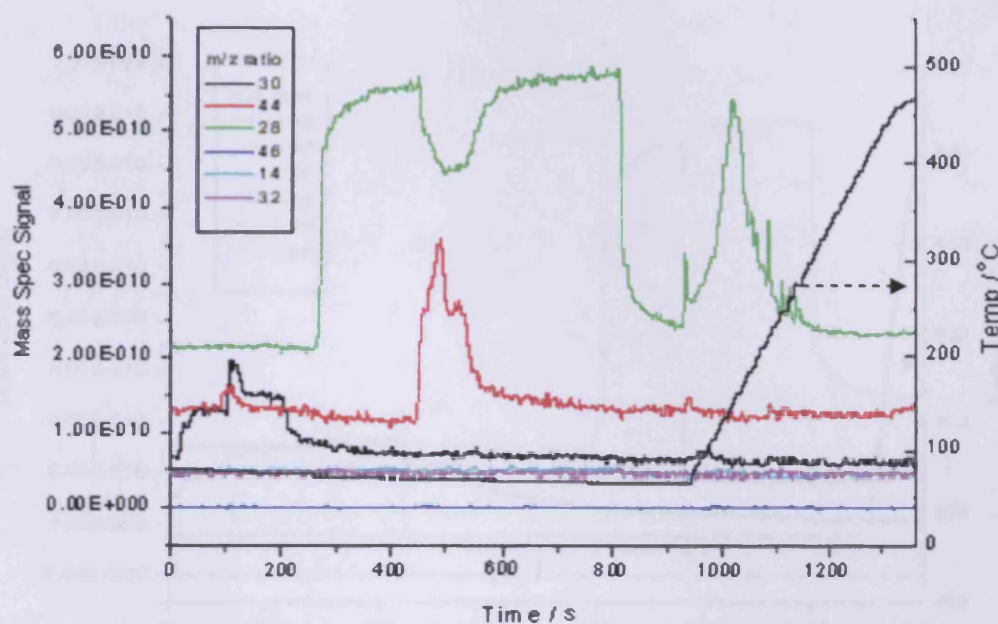


Figure 3.11 – A molecular beam of NO_2 on Pt(111) followed by a molecular beam of CO (as a probe of reaction products adsorbed on the surface) at room temperature. Following this a temperature programmed desorption was performed on the surface to aid identification of residual surface species (time > 950 s). Note that CO trace is reduced by a factor of four for display purposes. All gas pressures used in the molecular beam source were 50 mbar. A temperature ramp of 1 K/s was used during the temperature programmed desorption portion of the experiment.

Figure 3.11 shows a molecular beam experiment in which a molecular beam of NO_2 (beam flag opened at 100 s) is beamed onto the Pt(111) surface at room temperature, followed by a molecular beam of CO (beam flag opened at 450 s) in an attempt to ascertain the surface processes occurring. As before there is a peak in the $m/z = 30$ trace encountered on opening the chamber flag before the $m/z = 30$ returns to its original value (allowing for an increase in the baseline).

Beaming CO onto the surface results in an immediate $m/z = 44$ desorption peak in addition to the extensive CO sticking observed. This is good evidence that

NO_2 has been broken down by the Pt(111) surface, leaving adsorbed atomic oxygen. There appear to be two overlapping $m/z = 44$ desorption peaks, possibly due to oxygen being adsorbed in two separate non-equivalent environments. The temperature programmed desorption part of the experiment (above 950 s) shows only a single $m/z = 28$ desorption peak at 160 °C and the oxygen desorption peaks present in Figure 3.10 are absent.

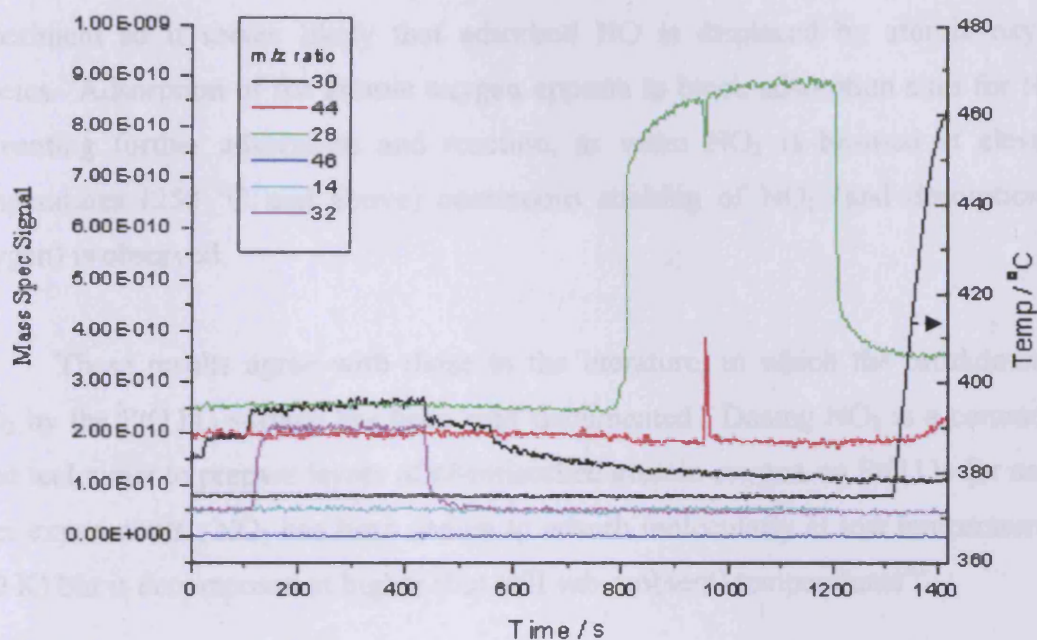


Figure 3.12 – A molecular beam of NO_2 beamed onto the Pt(111) surface held at 375 °C, followed by a molecular beam of CO. Following this a temperature programmed desorption was performed on the surface to aid identification of residual surface species (time > 1310 s). Note that the CO trace is reduced by a factor of four for display purposes. All molecular beams used a pressure of 50 mbar in the molecular beam source. A temperature ramp of 1 K/s was used during the temperature programmed desorption portion of the experiment.

The data shown in Figure 3.12 is from a similar experiment to the one presented in Figure 3.11 with the exception that the reactants were beamed onto a Pt(111) surface that was held at 375 °C. As with Figure 3.11 the NO_2 beaming is comparable to that seen in Figure 3.9, with continuous $m/z = 32$ and 30 desorption signals occurring. When beaming CO however, the size of the $m/z = 44$ desorption peak is much less than that seen in Figure 3.11 and the reduction in reflected CO reaching the mass spectrometer that occurs when the beam of CO hits the crystal surface is much less. Unlike in the temperature programmed desorption part of Figure

3.11 there appear to be no significant desorption peaks present in the temperature programmed desorption in Figure 3.12 (time > 1310 s).

Taken together these experiments provide conclusive evidence that NO₂ is readily broken down by the Pt(111) surface with the desorption of NO and the adsorption of atomic oxygen onto the crystal face. There are no significant NO desorption peaks present in the temperature programmed desorption part of the experiment so it seems likely that adsorbed NO is displaced by atomic oxygen species. Adsorption of the atomic oxygen appears to block adsorption sites for NO₂, preventing further adsorption and reaction, as when NO₂ is beamed at elevated temperatures (250 °C and above) continuous sticking of NO₂ (and desorption of oxygen) is observed.

These results agree with those in the literature, in which the breakdown of NO₂ by the Pt(111) surface has been well documented. Dosing NO₂ is a commonly used technique to prepare layers of chemisorbed atomic oxygen on Pt(111) for use in later experiments. NO₂ has been shown to adsorb molecularly at low temperature (~100 K) but is decomposed at higher (but still sub-ambient) temperatures³⁰.

3.3.5 Mixed molecular beams of NO₂ and O₂ on Pt(111)

Figure 3.13 shows the effect of beaming a molecular beam of NO₂ and O₂ (created by mixing a 1:1 ratio of NO and O₂, 50 mbar total molecular beam source pressure) onto the Pt(111) crystal held at increasing surface temperatures. At 50 °C, when the chamber flag is opened and the beam hits the crystal, there is a rise in the amount of m/z = 30 reaching the detector. After a few seconds this increased m/z = 30 signal has returned to the initial total reflection level. This also occurs for mixed beams at 100 and 200 °C. There is no visible change in the O₂ mass spectrometer signal when beaming at these temperatures, implying that the surface reaction is not between O₂ and NO.

However for temperatures of 300 °C and above constant m/z = 32 and 30 desorption features are observed when the beam hits the crystal surface. At 300 °C there is an initial high point that gradually returns to an increased constant sticking

level; at 400 °C and above this is absent and the magnitude of the constant desorption feature is greater.

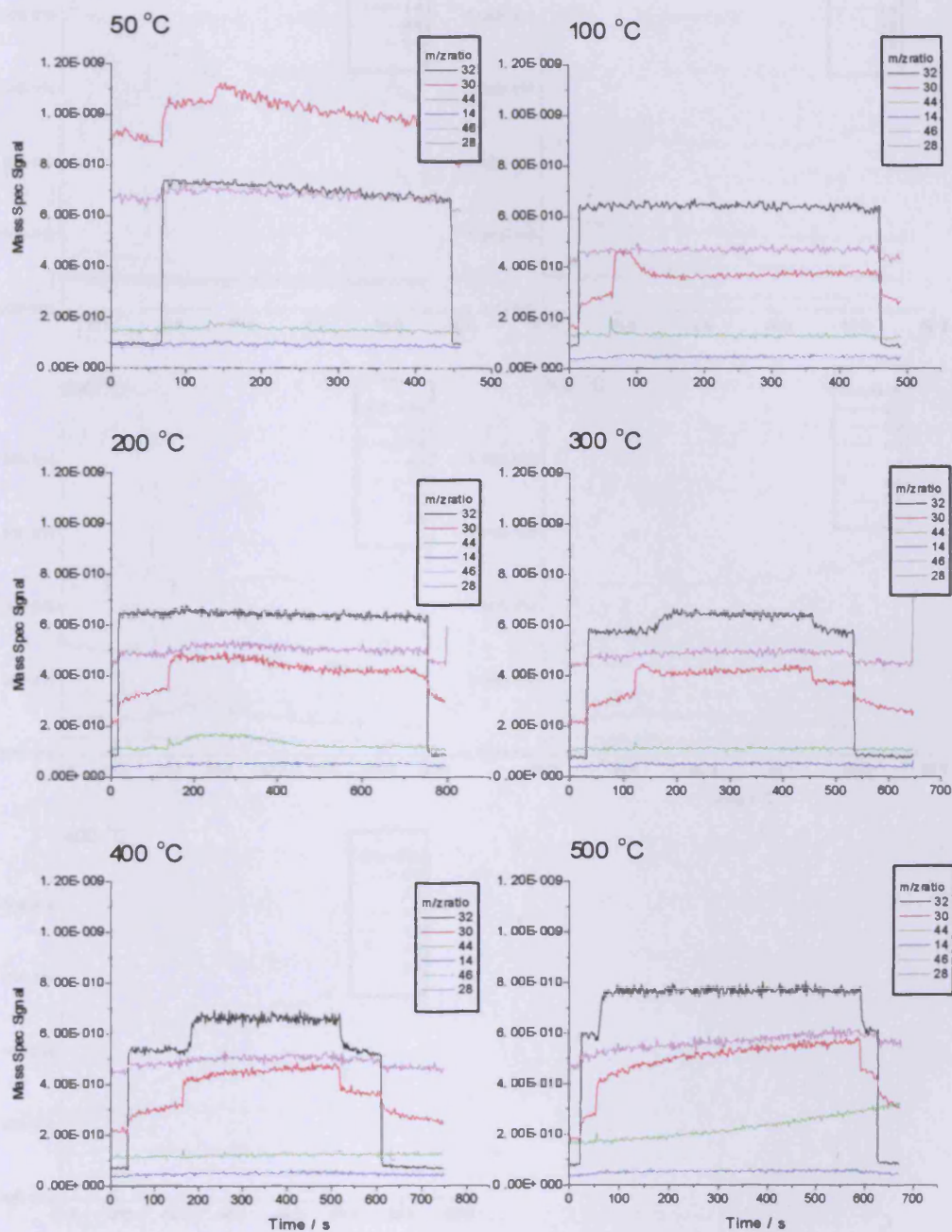


Figure 3.13 - Mixed molecular beams of NO₂ and O₂ (created using a 1:1 mixture ratio of NO and O₂, 50 mbar total molecular beam source pressure) on the Pt(111) crystal surface held at increasing surface temperatures.

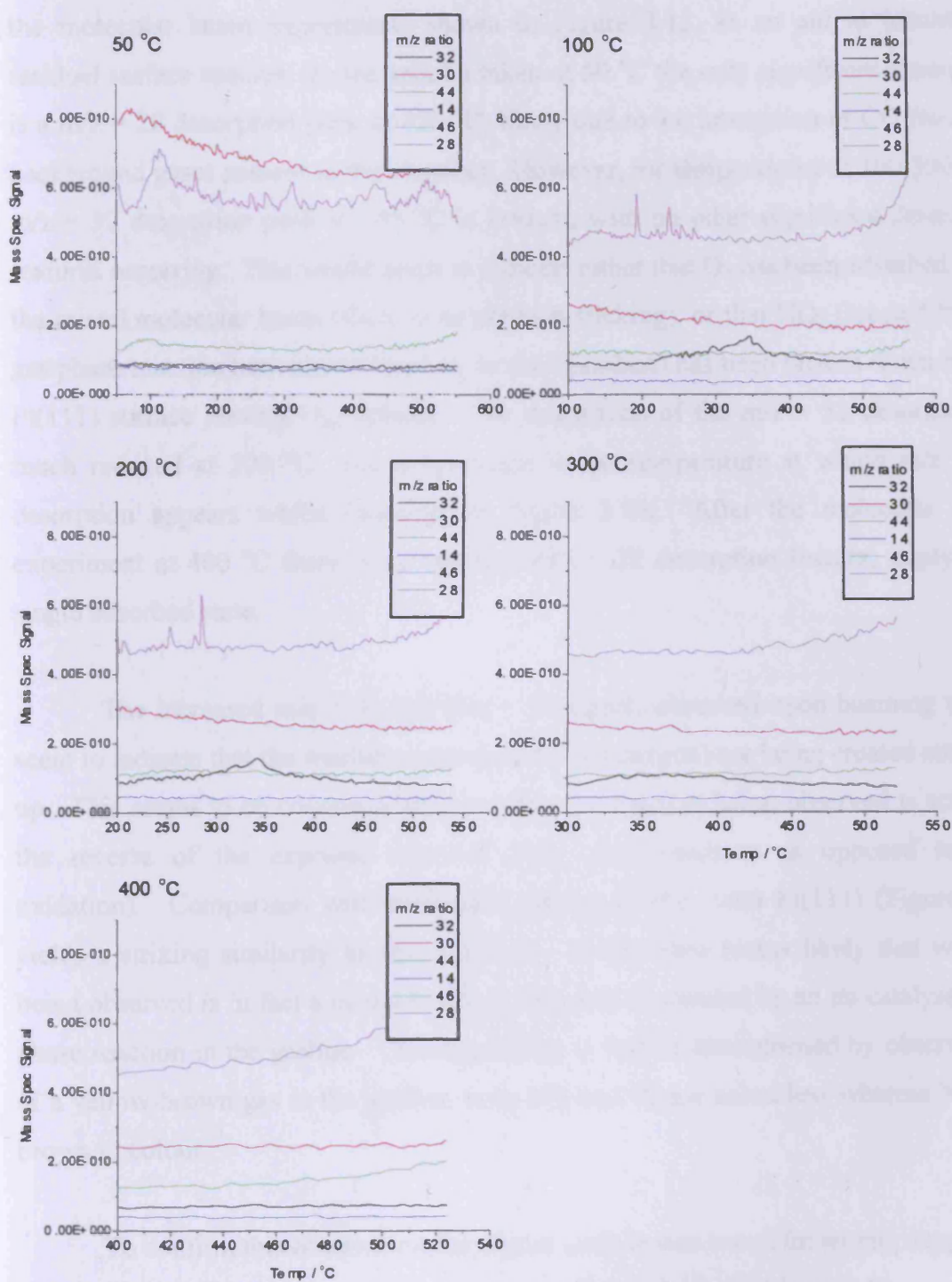
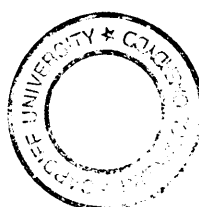


Figure 3.14 – Temperature programmed desorption experiments of the Pt(111) surface immediately following the molecular beam experiments shown in Figure 3.13. A temperature ramp of 1 K/s was used in all cases.

Figure 3.14 shows temperature programmed desorption experiments following the molecular beam experiments shown in Figure 3.13, as an aid to identifying residual surface species. In the spectra taken at 50 °C the only significant desorption is a $m/z = 28$ desorption peak at 120 °C, likely due to the adsorption of CO from the background gases present in the chamber. However, for temperatures of 100-300 °C a $m/z = 32$ desorption peak at 345 °C is evident, with no other significant desorption features occurring. This would seem to indicate either that O_2 has been adsorbed from the mixed molecular beam (there is no obvious sticking), or that NO_2 (created from a gas phase reaction between NO and O_2 in the beamline) has been broken down by the Pt(111) surface leaving $O_{(a)}$ behind. The magnitude of the $m/z = 32$ desorption is much reduced at 300 °C; this temperature is the temperature at which $m/z = 32$ desorption appears whilst beaming in Figure 3.13. After the molecular beam experiment at 400 °C there is no obvious $m/z = 32$ desorption feature, implying a single adsorbed state.

The increased $m/z = 30$ and $m/z = 32$ signals observed upon beaming would seem to indicate that the reactants (nitric oxide and oxygen) are being created not used up. This seems to be counter-intuitive unless the reaction being observed is actually the reverse of the expected reaction (NO_2 decomposition as opposed to NO oxidation). Comparison with molecular beams of NO_2 onto Pt(111) (Figure 3.9) yields a striking similarity in observed data. It therefore seems likely that what is being observed is in fact a mixed beam of NO_2 and O_2 created by an un-catalysed gas phase reaction in the gasline. This hypothesis is further strengthened by observation of a yellow-brown gas in the gasline; both NO and O_2 are colourless whereas NO_2 is brown in colour.

To confirm this observation the crystal surface was tested for atomic oxygen remaining after beaming in a similar manner to Figure 3.11 and Figure 3.12.



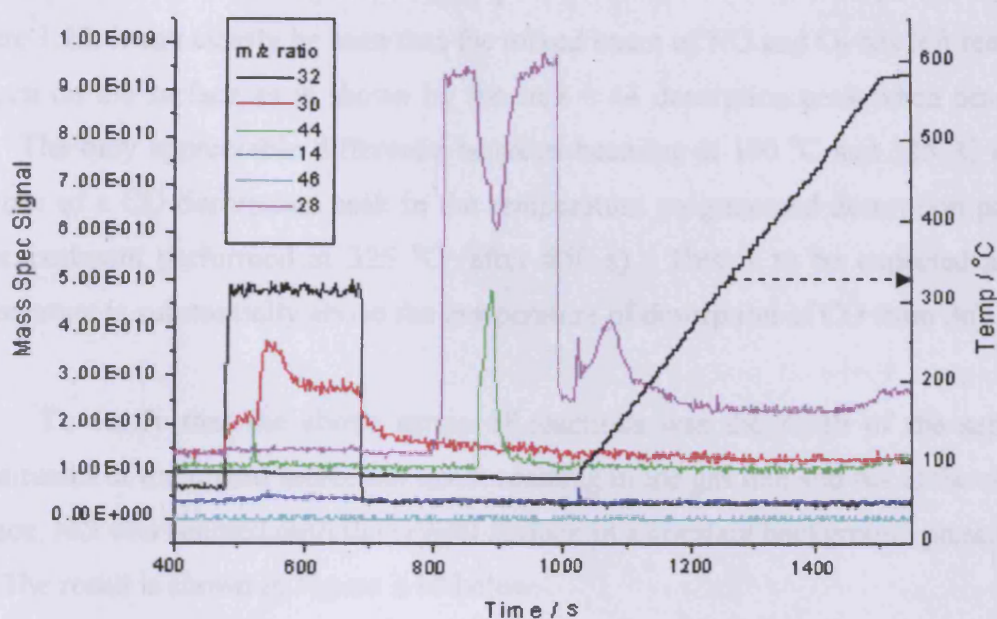


Figure 3.15 – A mixed molecular beam of NO_2 and O_2 (created using a 1:1 $\text{NO}:\text{O}_2$ gas mixture ratio, 50 mbar total beam source pressure) beamed on to Pt(111) surface held between 90-100 °C followed by a beam of CO (50 mbar molecular beam source pressure) as an aid to identify any created surface species. The molecular beam experiment was then followed by a temperature ramp of 1 K/s to identify residual surface species (time > 1040 s). Note that $m/z = 28$ signal has been reduced by a factor of three for display purposes.

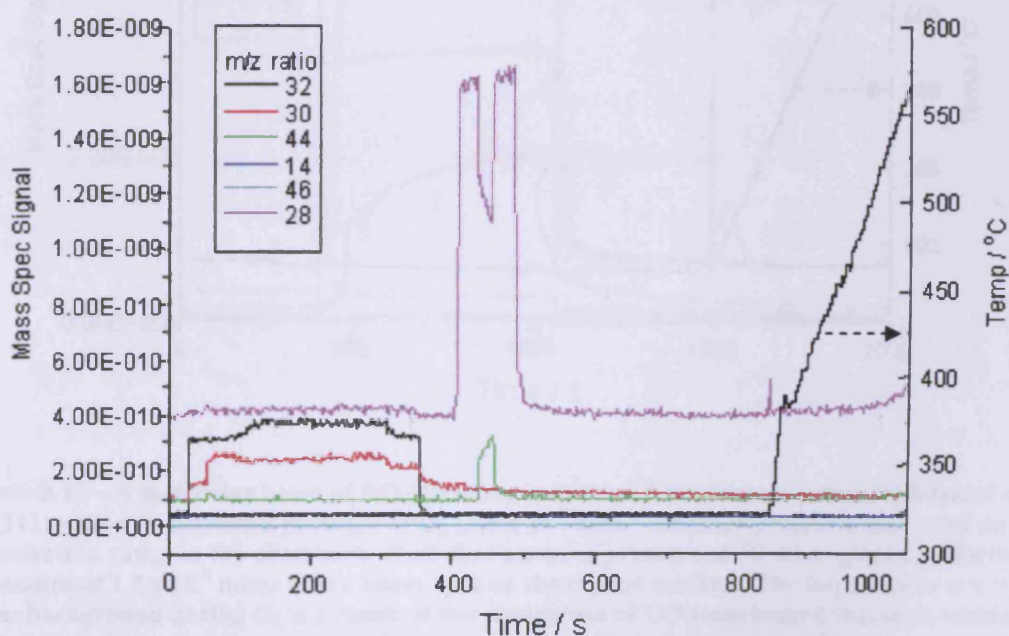


Figure 3.16 - A mixed molecular beam of NO_2 and O_2 (created using a 1:1 $\text{NO}:\text{O}_2$ gas mixture ratio, 50 mbar total molecular beam source pressure) beamed on to a Pt(111) surface held at 325 °C followed by a molecular beam of CO (50 mbar molecular beam source pressure) in a similar manner to Figure 3.15, followed by a temperature programmed desorption (time > 850 s) to identify any residual surface species.

In a similar manner to the examples shown previously in Figure 3.11 and Figure 3.12, it can clearly be seen that the mixed beam of NO and O₂ has left reactive oxygen on the surface as is shown by the $m/z = 44$ desorption peak when beaming CO. The only appreciable difference between beaming at 100 °C and 325 °C is the absence of a CO desorption peak in the temperature programmed desorption part of the experiment performed at 325 °C (after 850 s). This is to be expected as the temperature is substantially above the temperature of desorption of CO from Pt(111).

To verify that the above series of reactions was the result of the separate constituents of the mixed molecular beam reacting in the gas line and not at the crystal surface, NO was beamed onto the crystal surface in a constant background pressure of O₂. The result is shown in Figure 3.17 below.

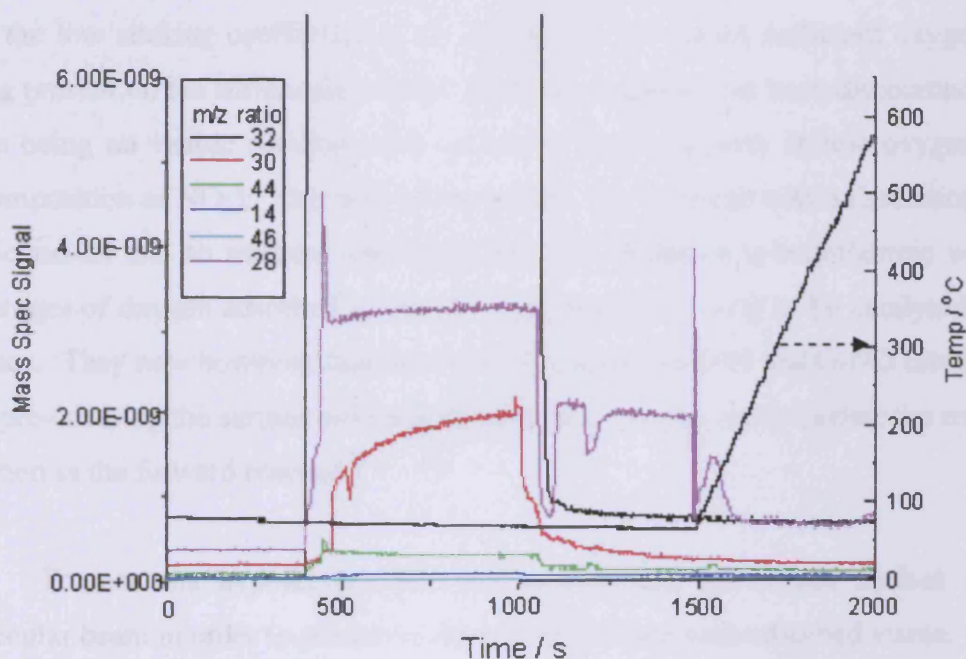


Figure 3.17 – A molecular beam of NO (50 mbar molecular beam source pressure) beamed on to Pt(111) with a background pressure of O₂ (2.5×10^{-8} mbar chamber pressure, measured on the ionisation gauge in the chamber). Note that a source pressure of 50 mbar gives an effective pressure of 2.5×10^{-8} mbar at the beam spot on the crystal surface. The large rise in $m/z = 28$ when background dosing O₂ is a result of the desorption of CO from heated filaments within the chamber. Note that the pressure of CO present is unlikely to cause significant experimental contamination due to the low pressure of CO when compared to the O₂ pressure and the effective pressure from the molecular beam at the crystal surface.

As can be seen there is no ‘bump’ in the $m/z = 30$ signal upon beaming NO and the little CO₂ that is produced on beaming CO is likely due to adsorption of O₂

from the background rather than adsorbed atomic oxygen from the breakdown of NO_2 .

The above experiments show conclusively that NO and O_2 are reacting in the beamline not on the crystal surface to produce NO_2 and that the NO_2 was broken down by the Pt(111) surface to produce NO, which desorbed (possibly following displacement of adsorbed NO by atomic oxygen created by decomposition of NO_2) and atomic oxygen, which was left behind on the surface and only desorbed at elevated temperatures during the temperature programmed desorption following the molecular beam experiment. The fact that NO was not oxidised under ultrahigh vacuum conditions by the Pt(111) surface seems to contradict the generally accepted model for the NO_x storage and reduction catalyst in which NO is oxidised over the platinum centre before being stored as nitrate by the barium oxide. The possibility that the low sticking coefficient of O_2 on Pt(111) prevented sufficient oxygen from being present on the surface for visible oxidation products has been discounted due to there being no visible reaction on a surface pre-covered with atomic oxygen (from decomposition of NO_2). This non-NO oxidation is consistent with a theoretical study by Schneider and co workers who noted that NO oxidation is endothermic with low coverages of oxygen adsorbed on Pt(111) and thus is unlikely to be catalysed by the surface. They note however, that due to highly repulsive O-O and O-NO interactions, that pre-covering the surface with adsorbed atomic oxygen can influence the oxidation reaction in the forward reaction²⁴.

To test this hypothesis, NO_2 was dosed onto the crystal surface via the molecular beam in order to pre-cover the crystal surface with adsorbed atomic oxygen as demonstrated in Figure 3.11, before the surface was heated to 160 °C (above the desorption temperature of NO) to remove adsorbed NO. The surface was then allowed to cool before NO (50 mbar molecular beam source pressure) was beamed onto the prepared surface.

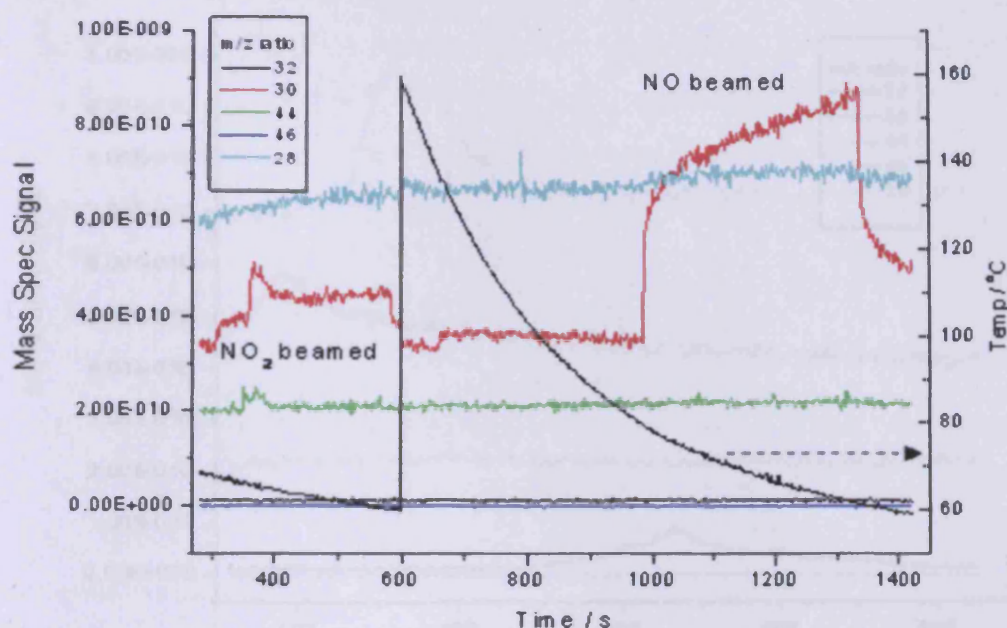


Figure 3.18 – A molecular beam of NO (50 mbar molecular beam source pressure) on the Pt(111) surface pre-covered with $O_{(a)}$ from the dissociative adsorption of NO_2 . Note that the flash in temperature at 600 s is to remove any NO that has been adsorbed from NO_2 breakdown.

From Figure 3.18 it can be seen that there is little or no NO removed from the crystal surface when the crystal is heated to 150 °C, making it likely that adsorbed NO from the breakdown of NO_2 has already been displaced by atomic oxygen. Unsurprisingly the beam of NO displays little adsorption and no reaction products are obvious. The temperature of the sample was then ramped at a rate of 1 K/s to examine the nature of any adsorbed surface species.

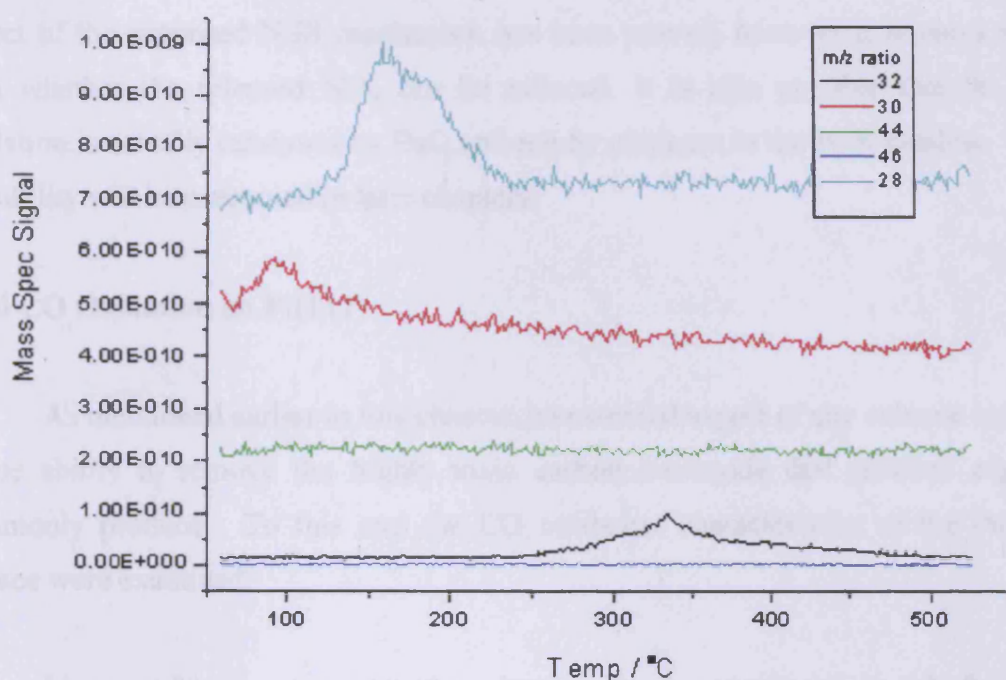


Figure 3.19 – Temperature programmed desorption of Pt(111) surface immediately following the molecular beam experiment shown in Figure 3.18, as an aid in identifying any residual surface species. A temperature ramp of 1 K/s was used in the experiment.

Figure 3.19 is identical to the temperature programmed desorption shown in Figure 3.10. There is a small NO desorption peak at 95 °C, characteristic of molecularly adsorbed NO desorbing from Pt(111), a CO desorption peak at 155-160 °C characteristic of molecularly adsorbed CO desorbing from Pt(111) and an oxygen desorption peak at 338 °C, which is due to the associative desorption of atomic oxygen from the Pt(111) surface. There is no evidence of the NO oxidation predicted by Schneider and group to occur on Pt(111) surfaces with a high $O_{(a)}$ pre-coverage (0.25 ML)²⁴. This lack of reaction of NO and pre-adsorbed O has also been shown by Zhu and co-workers. The only effect on the adsorption of NO that they found was the replacement of fcc adsorbed NO by $O_{(a)}$ due to electronic back-donation into the $2\pi^*$ antibonding orbital of hcp NO, and a consequent large reduction in sticking coefficient⁹⁹.

The above experiments have established that NO_2 is broken down to nitric oxide and oxygen by the platinum surface. This behaviour is expected during the

fuel-rich cycle of the lean burn engine, after the stored NO_x has been released. This aspect of the proposed NSR mechanism has been proved; however it remains to be seen whether the released NO_x can be reduced. It is also possible that the NO oxidation is actually catalysed by BaO and not by platinum in the NSR catalyst. This possibility will be examined in later chapters.

3.3.6 CO Oxidation on Pt(111)

As mentioned earlier in this chapter, an essential aspect of any exhaust catalyst is the ability to remove the highly toxic carbon monoxide that gasoline engines commonly produce. To this end the CO oxidation characteristics of the Pt(111) surface were examined.

Figure 3.20 shows a mixed molecular beam experiment in which equal pressures of CO and O_2 (50 mbar total molecular beam source pressure) were dosed onto the Pt(111) crystal surface held at increasing temperatures. From figure 3.20 it can be seen that both constituents adsorb in a similar manner as they do singly, with CO adsorbing fairly well ($S_0 = 0.36$ at 50 °C) but oxygen not adsorbing to any measurable extent. There is no evidence of any CO oxidation occurring. This is surprising as the NSR catalyst is also required to oxidise CO from the exhaust gases. When one takes into account the CO oxidation that readily occurs in Figure 3.15 it is apparent that CO is readily oxidised by atomic oxygen. It therefore seems likely that the reason that no CO oxidation has occurred in Figure 3.20 is that the low sticking coefficient of oxygen on Pt(111) ensures that only a small amount of oxygen is adsorbed. Any adsorbed $\text{O}_{(a)}$ would also swiftly be eliminated by incoming CO in a clean-off reaction.

The only major features in Figure 3.21 are large CO desorption peaks at 140-155 °C, characteristic of CO reversibly adsorbing on Pt(111). As expected from the lack of adsorption, no other desorption products are visible. The lack of any visible reaction products is not surprising given the lack of O_2 adsorption in Figure 3.20. The CO oxidative ability of the Pt(111) surface has been well documented in the literature; however, from the above it appears that the reaction must follow a Langmuir-like mechanism between molecularly adsorbed CO and adsorbed atomic oxygen rather

than an Eley-Rideal type mechanism between adsorbed CO and molecular oxygen in the gas phase. To investigate this the surface was pre-covered with atomic oxygen (via dissociative adsorption of NO_2 followed by thermal removal of adsorbed NO as demonstrated earlier) and CO (50 mbar molecular beam source pressure) beamed onto the crystal surface (figure 3.22).

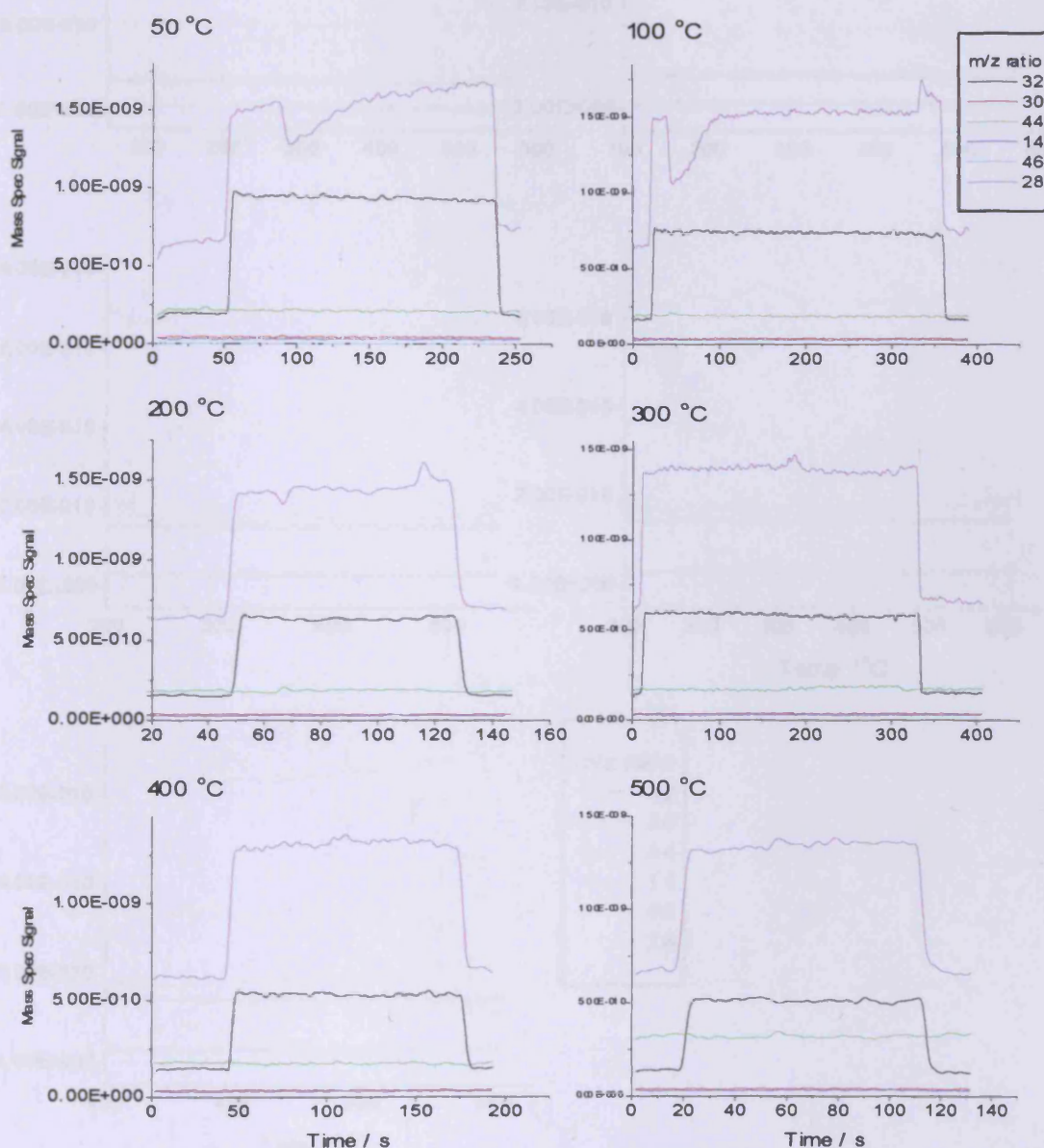


Figure 3.20 - Mixed molecular beams of CO and O₂ (1:1 ratio mixture, 50 mbar total molecular beam source pressure) beamed on to Pt(111) surface held at increasing temperatures.

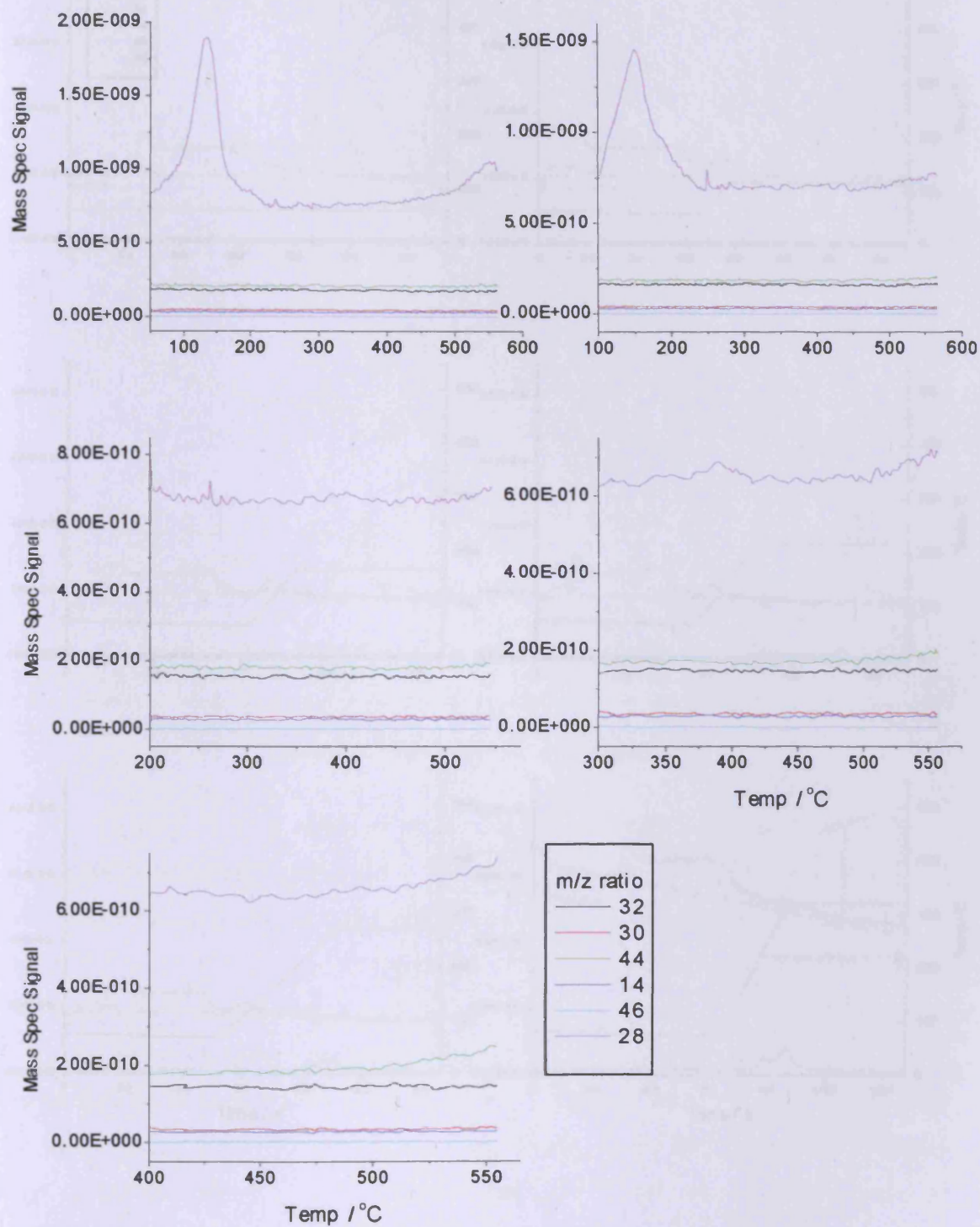


Figure 3.21 – Temperature programmed desorption experiments of the Pt(111) surface following the mixed molecular beam experiments shown in Figure 3.20. A temperature ramp of 1 K/s was used in each experiment.

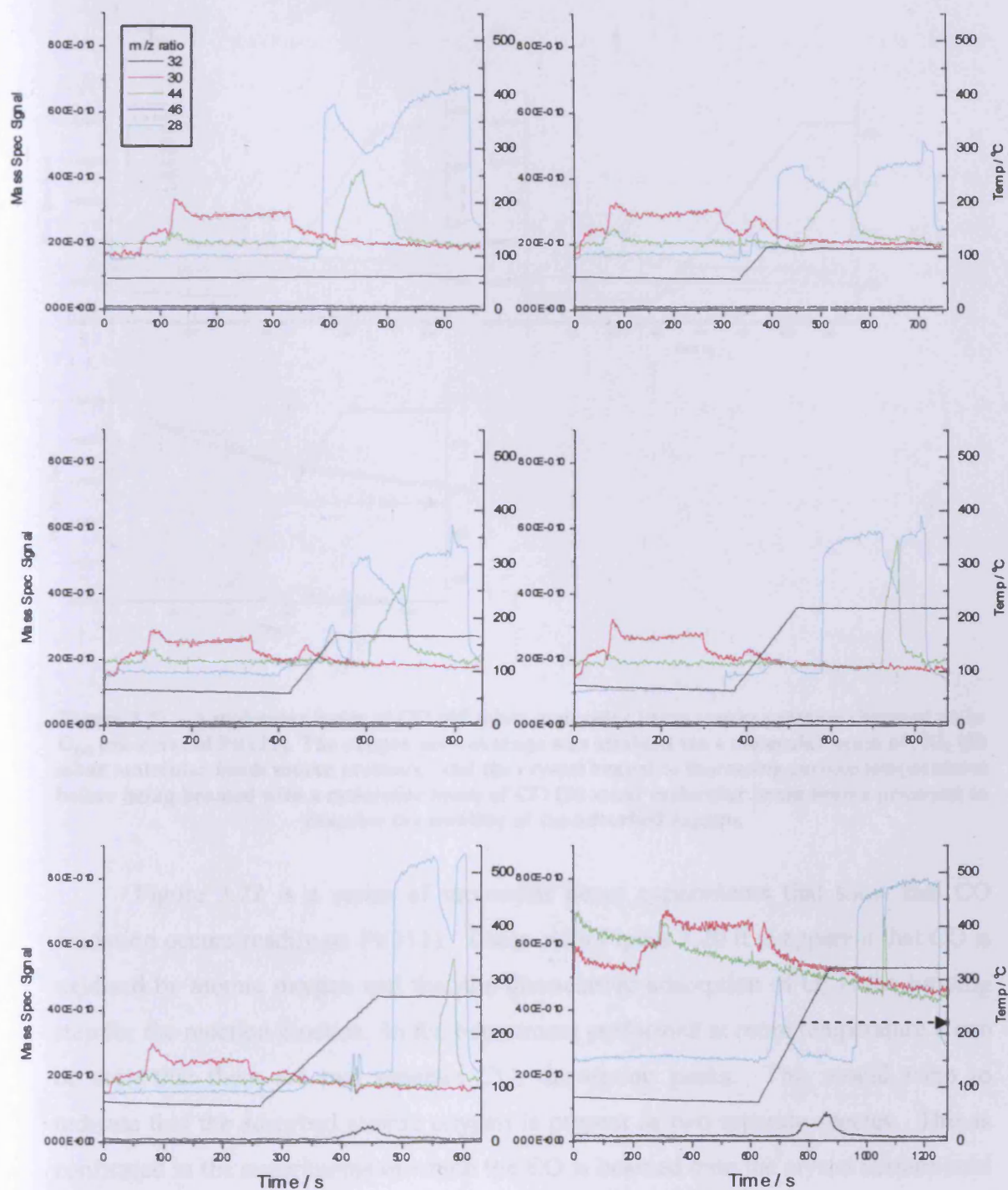


Figure 3.22 – A molecular beam of CO (50 mbar molecular beam source pressure) beamed on to $O_{(a)}$ pre-covered Pt(111). The oxygen pre-coverage was attained via a molecular beam of NO_2 (50 mbar molecular beam source pressure) and the crystal heated to increasing surface temperatures before being beamed with a molecular beam of CO (50 mbar molecular beam source pressure) to examine the stability of the adsorbed oxygen.

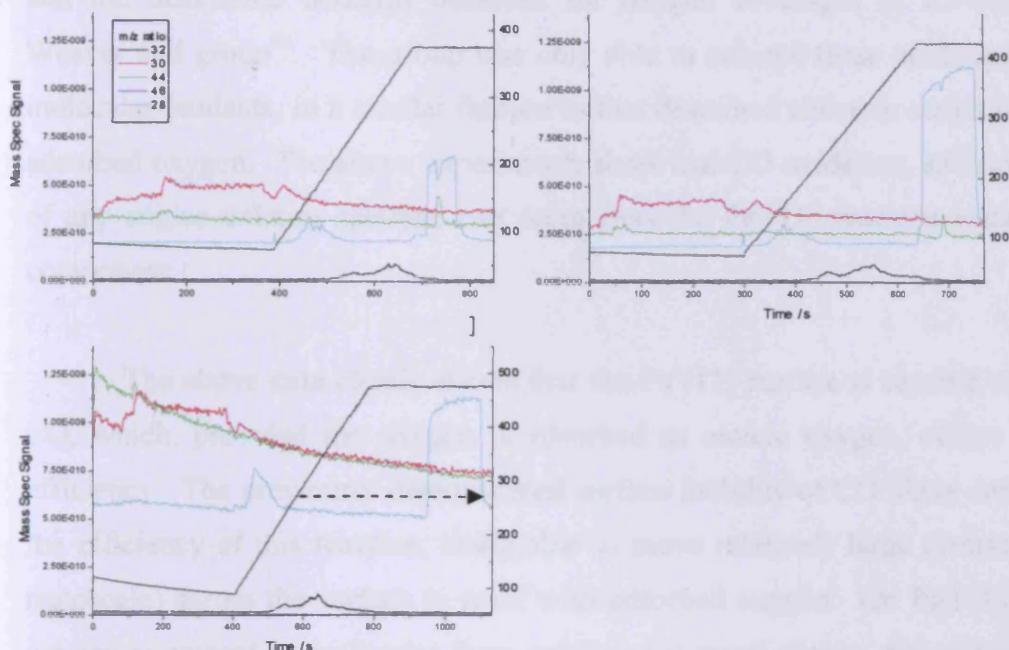


Figure 3.22 – A molecular beam of CO (50 mbar molecular beam source pressure) beamed on to $O_{(a)}$ pre-covered Pt(111). The oxygen pre-coverage was attained via a molecular beam of NO_2 (50 mbar molecular beam source pressure) and the crystal heated to increasing surface temperatures before being beamed with a molecular beam of CO (50 mbar molecular beam source pressure) to examine the stability of the adsorbed oxygen.

Figure 3.22 is a series of molecular beam experiments that show that CO oxidation occurs readily on Pt(111). Taken with Figure 3.20 it is apparent that CO is oxidised by atomic oxygen and that the dissociative adsorption of O_2 is the limiting step for the reaction kinetics. In the experiment performed at room temperature it can be seen that there are two separate CO_2 desorption peaks. This would seem to indicate that the adsorbed atomic oxygen is present as two separate species. This is confirmed in the experiments in which the CO is beamed onto the crystal surface held at temperatures of 270 °C and above. There is also an O_2 desorption peak visible in the temperature ramp to these temperatures (270 °C and above) before onset of beaming CO as well as a single CO_2 desorption peak. There are also two $m/z = 32$ desorption peaks visible for temperatures of 400 °C and above. There is no oxygen left on the surface when CO is beamed at 475 °C as no reaction products are visible in the CO molecular beam experiment following the temperature ramp.

The two separate oxygen species are likely to be the high-density ordered state and the disordered domains observed for oxygen coverages of 0.5-0.75 ML by Weaver and group⁶⁴. The group was only able to achieve these coverages by using molecular oxidants, in a similar fashion to that described above to create the layer of adsorbed oxygen. The above experiments show that CO oxidation, an important part of any engine exhaust catalyst, can occur over the Pt(111) precious metal catalytic component.

The above data clearly shows that the Pt(111) surface is capable of oxidising CO, which, provided the oxygen is adsorbed as atomic oxygen, occurs with high efficiency. The previously demonstrated surface mobility of CO likely contributes to the efficiency of this reaction, being able to move relatively large distances (on the nanoscale) across the surface to react with adsorbed oxygen. On Pt(111), when the oxygen is present in molecular form oxidation is much slower due to the relatively low oxygen sticking coefficient. On these surfaces the adsorption of O₂ could hence be considered to be the rate-limiting step.

3.3.7 NO reduction on Pt(111)

An important aspect of the NSR catalyst is the ability to reduce the NO_x (that has been stored under oxygen-rich conditions) that is released during the fuel-rich phase of engine operation. To this end mixed beams of NO and CO were adsorbed onto the crystal surface and any possible reaction monitored. It is possible that the platinum surface would behave in a similar manner to palladium and rhodium, which both catalyse the reduction of NO to produce a mixture of N₂O and N₂, and N₂ respectively.

From Figure 3.23 it appears that both CO and NO are adsorbing to the crystal surface with initial sticking coefficients characteristic of both species adsorbing on the Pt(111) surface alone. The sticking probabilities of both species diminish with increasing temperature, NO more so than CO. This is to be expected if no reaction is occurring due to the relatively low desorption temperatures of both species (see Figure 3.4 and Figure 3.8). In addition to this it is probable that CO blocks NO

adsorption sites. There is no immediate desorption of any reaction products when beaming.

Figure 3.24 supports the conclusion that there is no surface reaction between adsorbed NO and CO occurring. The only features in the temperature programmed desorption experiments that followed the mixed molecular beam reaction are desorption features due to CO and NO, which both occur at typical temperatures for each of the species desorbing from Pt(111). It is not surprising that the platinum surface does not catalyse the reaction as both rhodium and palladium have been shown to catalyse the breakdown of NO, which is the proposed first step of the reaction whereas on Pt(111) NO is reversibly adsorbed (see Figure 3.6 and Figure 3.8). The atomic oxygen produced by the breakdown of NO by rhodium and palladium reacts with the adsorbed CO and desorbs as CO₂. The lack of reaction between co-adsorbed NO and CO on Pt(111) has also been documented in the literature²⁰. The fact that there is no obvious NO reduction catalysed by the Pt(111) surface has implications for the proposed model for the NSR catalyst as in the Matsumoto model for the NSR catalyst (see page 234) NO₂ released from the BaO NO_x storage component is reduced to N₂ over the platinum metal centre^{13,14}. Previous sections have shown that NO₂ is broken down to NO and O₂ by the Pt(111) surface with great efficiency (see section 3.3.4); it may be that it is the BaO NO_x storage component binds the NO liberated from the breakdown of NO₂ over platinum and catalyses its breakdown. This possibility will be examined in later sections.

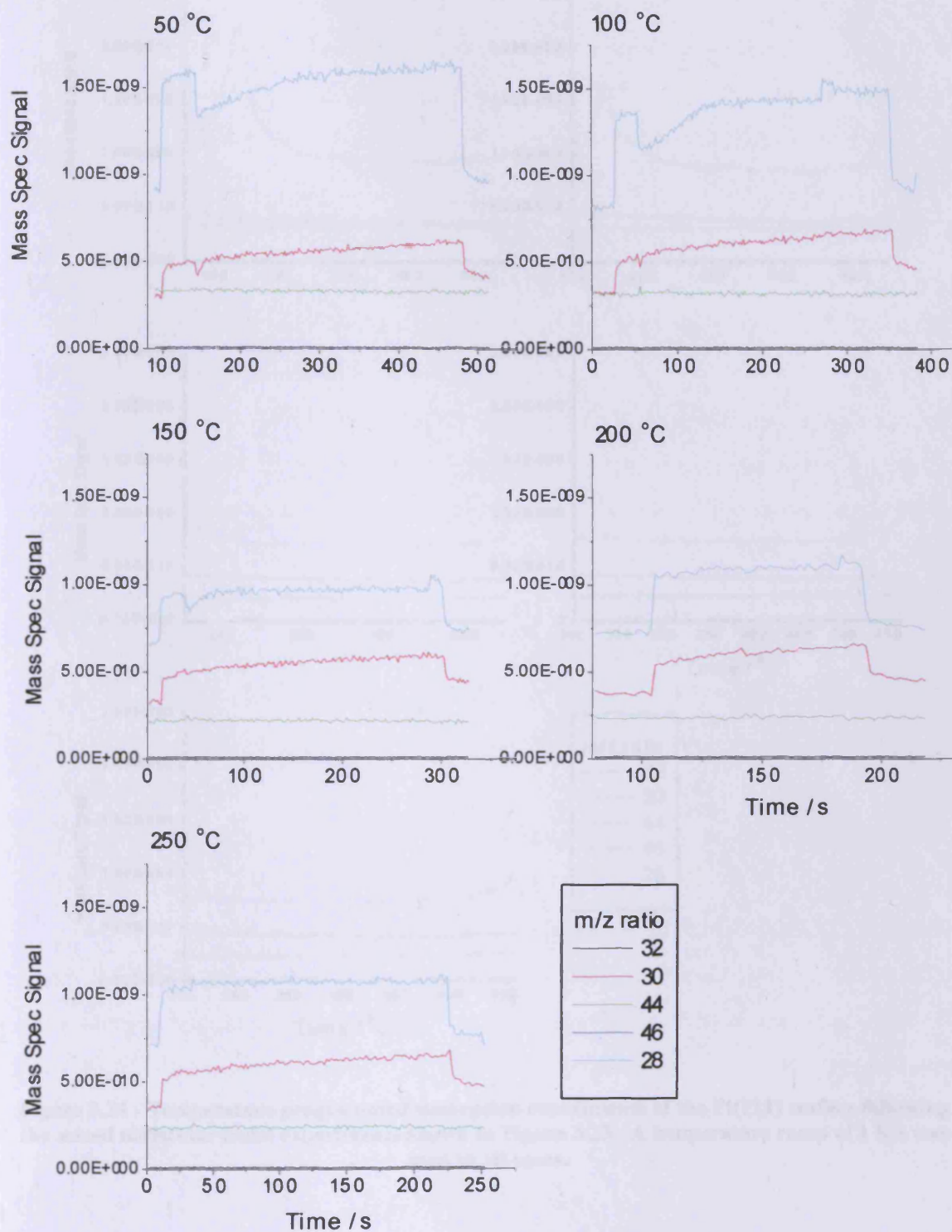


Figure 3.23 - Mixed molecular beams of CO and NO (1:1 gas mixture ratio, 50 mbar total molecular beam source pressure) on Pt(111) with increasing substrate temperature.

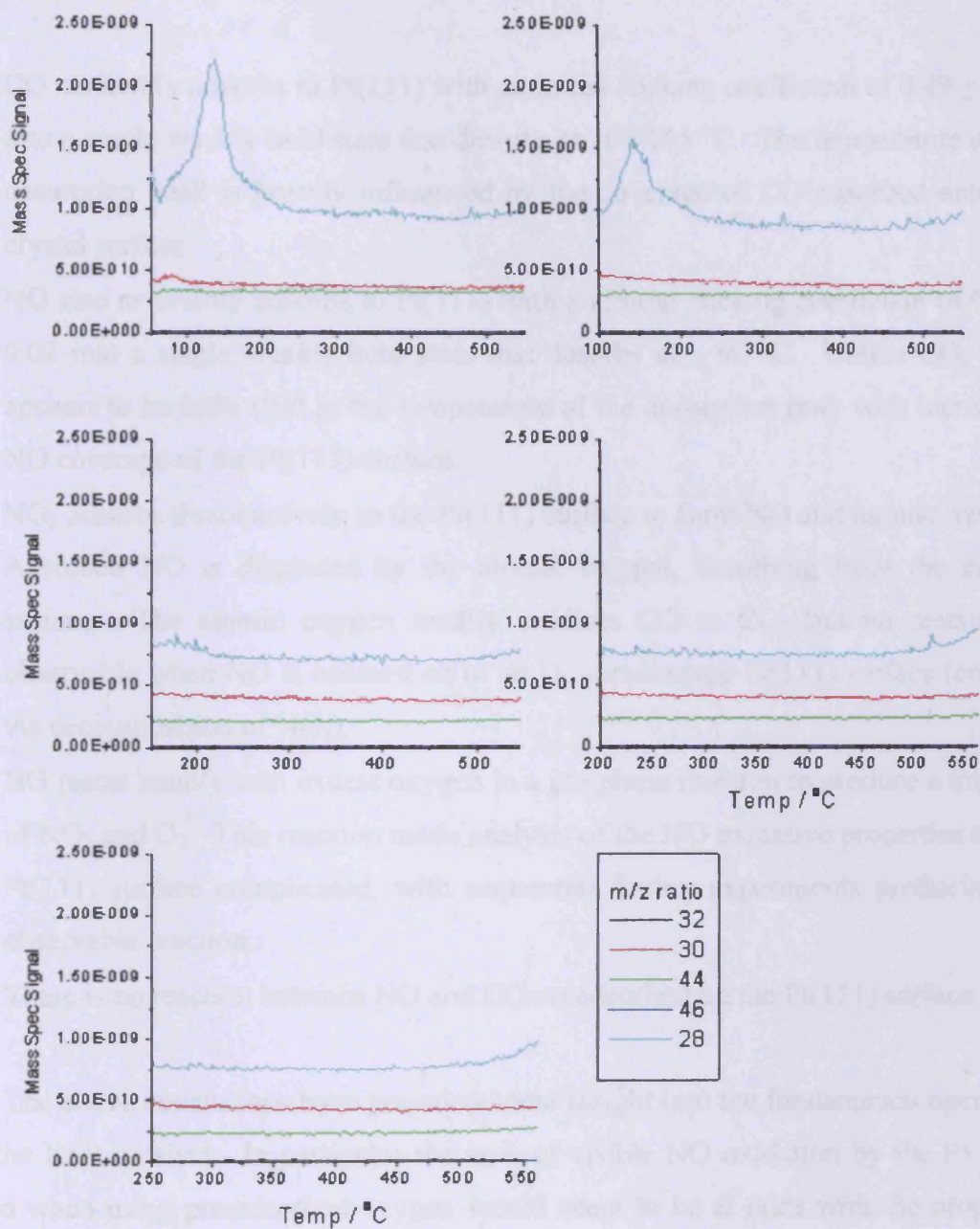


Figure 3.24 - Temperature programmed desorption experiments of the Pt(111) surface following the mixed molecular beam experiments shown in Figure 3.23. A temperature ramp of 1 K/s was used in all cases.

3.4 Summary of Conclusions

- CO reversibly adsorbs to Pt(111) with an initial sticking coefficient of 0.49 ± 0.02 into a single weakly held state that desorbs at 105-155 °C. The temperature of the desorption peak is heavily influenced by the coverage of CO adsorbed onto the crystal surface.
- NO also reversibly adsorbs to Pt(111) with an initial sticking coefficient of 0.71 ± 0.02 into a single weakly held state that desorbs at ~ 90 °C. Unlike CO, there appears to be little shift in the temperature of the desorption peak with increasing NO coverage of the Pt(111) surface.
- NO₂ adsorbs dissociatively to the Pt(111) surface to form NO and atomic oxygen. Adsorbed NO is displaced by the atomic oxygen, desorbing from the crystal surface. The atomic oxygen readily oxidises CO to CO₂ but no reaction is observable when NO is beamed on to an O_(a)-precovered Pt(111) surface (created via decomposition of NO₂).
- NO reacts readily with excess oxygen in a gas phase reaction to produce a mixture of NO₂ and O₂. This reaction made analysis of the NO oxidative properties of the Pt(111) surface complicated, with sequential dosing experiments producing no observable reaction.
- There is no reaction between NO and CO co-adsorbed on the Pt(111) surface

The above conclusions have provided some insight into the fundamental operation of the NSR catalyst. In particular the lack of visible NO oxidation by the Pt(111), even when using pre-adsorbed oxygen would seem to be at odds with the proposed Matsumoto model (see chapter 6), in which NO is oxidised to NO₂ over the platinum in the Pt/BaO/Al₂O₃ exhaust catalyst. However, while this does not happen over the platinum (111) under ultrahigh vacuum conditions the gas phase reaction of NO and O₂ observed in the gasoline indicates that oxidation is favourable and spontaneous given sufficiently high partial pressures of the reactants. The ability of the catalyst to catalyse the back reaction of NO₂ to NO and oxygen has been shown; however an elevated operating temperature (or as shown above, the presence of a reductant such as CO) is necessary to remove the adsorbed oxygen. Both of these criteria would be fulfilled in the fuel-rich operating phase of the lean-burn gasoline engine. The main

contradiction of the Matsumoto model however is the lack NO breakdown in a reducing environment. In the proposed model this occurs over the platinum metal centre; however the results given above have shown that no NO reduction is observed over the (111) face of platinum. It may well be that the presence of barium oxide is necessary for this to occur. This will be investigated in subsequent chapters.

REFERENCES

1. Open University Lab Space
<http://labspace.open.ac.uk/mod/resource/view.php?id=207208>
2. Comrie, C.M., Lambert, R.M., *Surf. Sci.*, **46**, 1974, 61.
3. Zhu, J.F., Kinne, M., Fuhrmann, T., Denecke, R., Steinruck, H.P., *Surf. Sci.*, **529**, 2003, 384.
4. Ibach, H., Lehwald, S., *Surf. Sci.*, **78**, 1978, 1.
5. Hayden, B.E., *Surf. Sci.*, **131**, 1983, 419.
6. Gland, J.L., Sexton, B.A., *Surf. Sci.*, **94**, 1980, 355.
7. Bartam, M.E., Koel, B.E., *Surf. Sci.*, **219**, 1989, 467.
8. Trenary, M., Agrawal, V.K., *Surf. Sci.*, **259**, 1991, 116.
9. Ranke, W., *Surf. Sci.*, **209**, 1989, 57.
10. Kiskinova, M., Pirug, G., Bonzel, H.P., *Surf. Sci.*, **136**, 1984, 285.
11. Materer, N., Barbieri, A., Gardin, D., Starke, U., Batteas, J.D., Van Hove, M.A., Somorjai, G.A., *Surf. Sci.*, **303**, 1994, 319.
12. Ge, Q., King, D.A., *Chem. Phys. Lett.*, **285**, 1998, 15.
13. Matsumoto, M., Tatsumi, N., Fukutani, K., Okano, T., Yamada, T., Miyake, K., Hate, K., Shigekawa, H., *J. Vac. Sci. Technol. A*, **17**, 1999, 1577.
14. Matsumoto, M., Fukutani, K., Okano, T., Miyake, K., Shigekawa, H., Kato, H., Okuyama, H., Kawai, M., *Surf. Sci.*, **454**, 2000, 101.
15. Zhu, J.K., Kinne, M., Fuhrmann, T., Denecke, R., Steinruck, H.P., *Surf. Sci.*, **529**, 2003, 384.
16. Aizawa, H., Morikawa, Y., Tsuneyuki, S., Kukutani, K., Ohno, T., *Surf. Sci.*, **514**, 2002, 394.
17. Zhu, P., Shimada, T., Kondoh, H., Nakai, I., Nagasaka, M., Ohta, T., *Surf. Sci.*, **565**, 2004, 232.
18. Metka, U., Schweitzer, M.G., Volpp, H.R., Wolfrum, J., Warnatz, J., *Phys. Chem.*, **214**, 2000, 865.
19. Kasai, H., Enomoto, Okiji, A., *J. Phys. Soc. Jpn.*, **57**, 1988, 2249.
20. Gorte, R.J., Schmidt, L.D., Gland, J.L., *Surf. Sci.*, **109**, 1981, 367.
21. Materer, N., Barbieri, A., Gardin, U., Starke, U., Batteas, J.D., Van Hove, M.A., Somorjai, G.A., *Phys. Rev. B*, **48**, 1993, 2859.
22. Campbell, C.T., Ertl, G., Segner, J., *Surf. Sci.*, **115**, 1982, 309.
23. Zhu, J.F., Kinne, M., Fuhrmann, T., Tränkenschuh, B., Denecke, R., Steinrück, H.-P., *Surf. Sci.*, **547**, 2003, 410.
24. Ovesson, S., Lundqvist, B.I., Schneider, W.F., Bogicevic, A., *Phys. Rev. B*, **71**, 2005, 115406-1.
25. Sawabe, K., Matsumoto, Y., Yoshinobu, J., Kawai, M., *J. Chem. Phys.*, **103**, 1995, 4757.
26. Bartram, M.E., Koel, B.E., Carter, E.A., *Surf. Sci.*, **219**, 1989, 467.
27. Meier, W.D., Pelak, R.A., Ho, W., *Surf. Sci.*, **359**, 1996, 23.
28. Sawabe, K., K., Matsumoto, Y., *Surf. Sci.*, **303**, 1994, L385.
29. Mulla, S.S., Chen, N., Delgass, W.N., Epling, W.S., Ribeiro, F.H., *Catt. Lett.*, **100**, 2005, 267.
30. Bartram, M.E., Windham, R.G., Koel, B.E., *Langmuir*, **4**, 1988, 240.
31. McEwen, J.-S., Payne, S.H., Kreuzer, H.J., Kinne, M., Denecke, R., Steinruck, H.-P., *Surf. Sci.*, **B545**, 2003, 47.
32. Steininger H., Lehwald, S., Ibach, H., *Surf. Sci.*, **123**, 1982, 264.
33. Poelsema, B., Palmer, R.L., Comsa, G., *Surf. Sci.*, **123**, 1982, 152.

-
34. Tüshaus, M., Schweizer, E., Hollins, P., Bradshaw, A.M., *J. Elec. Spec.*, **44**, 1987, 305.
 35. Hopster, H., Ibach, H., *Surf. Sci.*, **77**, 1978, 109.
 36. Avery, N., *J. Chem. Phys.*, **74**, 1981, 4202.
 37. Mieher, W.D., Whitman, L.J., Ho, W., *J. Chem. Phys.*, **91**, 1989, 3228.
 38. Froitzheim, H., Hopster, H., Ibach, H., Lehwald, S., *Appl. Phys.*, **13**, 1977, 147.
 39. Ertl, G., Neumann, M., Streit, K.M., *Surf. Sci.*, **64**, 1977, 393.
 40. Poelsema, B., Palmer, R.L., Comsa, G., *Surf. Sci.*, **136**, 1984, 1.
 41. Yeo, Y.Y., Vattuone, L., King, D.A., *J. Chem. Phys.*, **106**, 1997, 392.
 42. Ray, N.K., Anderson, A.B., *Surf. Sci.*, **119**, 1982, 35.
 43. Hammer, B., Nielsen, O.H., Nørskov, *Catt. Lett.*, **46**, 1997, 31.
 44. Seebaur, E.G., Kong, A.C.F., Schmidt, L.D., *Surf. Sci.*, **176**, 1986, 134.
 45. Allers, K.-H., Pfnür, H., Menzel, D., *Surf. Sci.*, **291**, 1993, 167.
 46. Gorte, R.J., Schmidt, L.D., *Surf. Sci.*, **11**, 1981, 260.
 47. Kinne, M., Fuhrmann, T., Whelan, C.M., Zhu, J.F., Pantförder, J., Probst, M., Held, G., Denecke, R., Steinrück, H.-P., *J. Chem. Phys.*, **117**, 2002, 10852.
 48. Campbell, C.T., Ertl, G., Kuipers, H., Segner, J., *Surf. Sci.*, **107**, 1981, 207.
 49. Blyholder, G., *J. Chem. Phys.*, **68**, 1964, 2772.
 50. Feibelman, P.J., Hammer, B., Norskov, J.K., Wagner, F., Scheffler, M., Stumpf, R., Watwe, R., Dumesic, J., *J. Phys. Chem. B*, **105**, 2001, 4018.
 51. Geschke, D., Baştuğ, Jacob, T., Fritzsche, S., Sepp, W.-D., Fricke, B., Varga, S., Anton, J., *Phys. Rev. B*, **64**, 2001, 235411.
 52. Colen, R.E.R., Christoph, J., Pena, F., Rotermund, H.H., *Surf. Sci.*, **408**, 1998, 310.
 53. Dicke, J., Rotermund, H.H., Lauterbach, J., *Surf. Sci.*, **454**, 2000, 352.
 54. Nolan, P.D., Lutz, B.R., Tanaka, P.L., Davis, J.E., Mullins, C.B., *J. Chem. Phys.*, **111**, 1999, 3696.
 55. Jerdev, D.I., Kim, J., Batzill, M., Koel, B.E., *Surf. Sci.*, **498**, 2002, L91.
 56. Zhdanov, V.P., Kasemo, B., *Surf. Sci.*, **415**, 1998, 403.
 57. Monroe, D.R., Merril, R.P., *J. Cat.*, **65**, 1980, 461.
 58. Collins, D.M., Lee, J.B., Spicer, W.E., *Surf. Sci.*, **55**, 1976, 389.
 59. Schwaha, K., Bechtold, E., *Surf. Sci.*, **65**, 1977, 277.
 60. Yotsushashi, S., Yamada, Y., *Phys. Rev. B*, **72**, 2005, 033415.
 61. Gland, J.L., *Surf. Sci.*, **93**, 1980, 487.
 62. Dahlgren, D., Hemminger, J.C. *Surf. Sci.*, **123**, 1982, L739.
 63. Saliba, N.A., Tsai, Y.-L., Panja, C., Koel, B.E., *Surf. Sci.*, **419**, 1999, 79.
 64. Weaver, J.F., Chen, J.-J., Gerrard, A.L., *Surf. Sci.*, **592**, 2005, 83.
 65. Segner, J., Vielhaber, W., Ertl, G., *Israel J. Chem.*, **22**, 1982, 375.
 66. Derry, G.N., Ross, P.N., *Surf. Sci.*, **140**, 1984, 165.
 67. Parker, D.H., Bartram, M.E., Koel, B.E., *Surf. Sci.*, **217**, 1989, 489.
 68. Parkinson, C.R., Walker, M., McConville, C.F., *Surf. Sci.*, **545**, 2003, 19.
 69. Niehus, H., Comsa, G., *Surf. Sci.*, **93**, 1980, L147.
 70. Bonzel, H.P., Franken, A.M., Pirug, G., *Surf. Sci.*, **104**, 1981, 625.
 71. Carlisle, C.I., Fujimoto, T., Sim, W.S., King, D.A., *Surf. Sci.*, **470**, 2000, 15.
 72. Ganduglia-Pirovano, M.V., Scheffler, *Phys. Rev. B*, **59**, 1999, 15533.
 73. Todorova, M., Li, W.X., Ganduglia-Pirovano, M.V., Stampfl, C., Reuter, K., Scheffler, M., *Phys. Rev. Lett.*, **89**, 2002, 96103.
 74. Groß, A., Eichler, A., Hafner, J., Mehl, M.J., Papaconstantopoulos, D.A., *Surf. Sci.*, **539**, 2003, L542.

-
75. Luntz, A.C., Grimblot, J., Fowler, D.E., *Phys. Rev. B*, **39**, 1989, 12903.
 76. Eichler, A., Mittendorfer, F., Hafner, J., *Phys. Rev. B*, **62**, 2000, 4744.
 77. Luntz, A.C., Williams, M.D., Bethune, D.S., *J. Chem. Phys.*, **89**, 1988, 4381.
 78. Gland, J.L., *Surf. Sci.*, **75**, 1978, 733.
 79. Bonzel, H.P., Ku, R., *Surf. Sci.*, **40**, 1973, 85.
 80. Hopster, H., Ibach, H., Comsa, G., *J. Cat.*, **46**, 1977, 37.
 81. Materer, S., Stakre, U., Barbieri, A., Döll, R., Heinz, K., Van Hove, M.A., Somorjai, G.A., *Surf. Sci.*, **325**, 1995, 207.
 82. Jung, C., Ku, B., Kim, J., Rhee, C.K., *Chem. Commun.*, 2006, 2191.
 83. Campbell, C.T., Ertl, G., Küppers, H., Segner, J., *J. Chem. Phys.*, **73**, 1980, 5862.
 84. Engel, T., Ertl, G., *J. Chem. Phys.*, **69**, 1978, 1267.
 85. Palmer, L., Smith, J.N., *J. Chem. Phys.*, **60**, 1974, 1453.
 86. Matsushima, T., *Surf. Sci.*, **79**, 1979, 63.
 87. Ehasai, M., Matloch, M., Frank, O., Block, J.H., *J. Chem. Phys.*, **91**(8), 1989, 4949.
 88. Matsushima, T., *Surf. Sci.*, **127**, 1983, 403.
 89. Gerrad, A.L., Weaver, J.F., *J. Chem. Phys.*, **123**, 2005, 224703.
 90. Engel, T., Ertl, G., *Adv. Cat.*, **28**, 1979, 1.
 91. Zaera, F., Liu, J., Xu, M., *J. Chem. Phys.*, **106**, 1997, 4204.
 92. Xu, M., Liu, J., Zaera, F., *J. Chem. Phys.*, **104**, 1996, 8825.
 93. Eichler, A., Hafner, J., *Phys. Rev. B*, **59**, 1999, 5960.
 94. Bleajeley, K., Hu, P., *J. Am. Chem. Soc.*, **121**, 1999, 7644.
 95. Volkening, S., Wintterlin, J., *J. Chem. Phys.*, **114**, 2001, 6382.
 96. Wintterlin, J., Volkening, S., Janssens, T.V.W., Zembelli, T., Ertl, G., *Science*, **273**, 1997, 1931.
 97. Campbell, C.T., Ertl, G., Kuipers, H., Segner, J., *J. Chem. Phys.*, **73**, 1980, 5862.
 98. Kisliuk, P., *J. Phys. Chem. Solids*, **3**, 1957, 95.
 99. Zhu, J.F., Kinne, M., Fuhrmann, T., Trankenschuh, B., Denecke, R., Steinruck, H.-P., *Surf. Sci.*, **547**, 2003, 410.

4. THE EFFECT OF POTASSIUM ON THE SURFACE CHEMISTRY OF NO, CO AND O₂ ON Pt(111) AND ITS SUITABILITY AS A POTENTIAL NO_x STORAGE COMPONENT

4.1	<i>Literature Review</i>	116
4.2	<i>Results and Discussion</i>	126
4.2.1	<i>Dosing K on Pt(111)</i>	126
4.2.2	<i>Adsorption of CO on the K/Pt surface</i>	129
4.2.3	<i>Sticking of O₂ on K dosed Pt(111)</i>	136
4.2.4	<i>Adsorption of NO on K dosed Pt(111) surface</i>	141
4.2.5	<i>Molecular beams of NO on K/Pt(111) surface held at increasing surface temperature</i>	147
4.2.6	<i>Mixed molecular beams of NO₂ and O₂ on different K coverages of the Pt(111) surface</i>	151
4.2.7	<i>Co-dosing O₂ and K at room temperature</i>	157
4.2.8	<i>Mixed molecular beams of NO₂ and O₂ on K₂O₇/K₂CO₃ layer formed at room temperature</i>	165
4.2.9	<i>Mixed molecular beam of CO and O₂ On K₂O₇/K₂CO₃ layer formed at room temperature</i>	167
4.2.10	<i>Co-dosing K and O₂ at 200 °C</i>	168
4.2.11	<i>Molecular beams of CO on K₂O₂ surface created at 200 °C</i>	171
4.2.12	<i>Molecular beams of NO on K₂O₂ surface created at 200 °C</i>	174
4.2.13	<i>Mixed molecular beams of NO₂ and O₂ on K₂O₂ surface created at 200 °C</i>	179
4.3	<i>Summary and Conclusions</i>	180
4.3.1	<i>Platinum (111)/Potassium</i>	180
4.3.2	<i>Platinum(111)/Potassium peroxide</i>	181
	REFERENCES	183

4.1 Literature Review

Transition metal catalysts often have sub-monolayer amounts of alkali metals incorporated due to the ability of the alkali metal to alter and effect the adsorption characteristics of the catalyst. This is believed to occur via the low ionisation potential of the alkali metal leading to the transference of a valence electron from the alkali metal to the transition metal, which sets up a localised dipole. This transfer of electronic charge is normally evidenced by a marked decrease in the workfunction of the transition metal surface. The first demonstration of this effect was the observation of a significant enhancement in electron emission from the transition metal surface upon alkali adsorption¹. The adsorption of the alkali metal onto a metal crystal surface hence normally results in a range of altered properties such as differing adsorption sites and adsorption kinetics, differing vibrational frequencies of adsorbed species and different adsorption sites becoming available. This effect is most pronounced in heterogeneous catalysis where alkali metal promotion is used to increase the selectivity of the catalyst towards certain products.

The K/Pt(111) system is probably the most frequently used system for modelling coadsorption effects especially with regards to O₂ and CO and the alkali induced weakening of the carbon-oxygen bond. In CO hydrogenation reactions the addition of potassium to the active catalyst has been shown to slow down the reaction and shift the equilibrium in favour of the more desirable high molecular weight species².

Alkaline earth metals, most commonly BaO, are frequently used as NO_x storage components in the NSR catalyst. The ability of the storage component of the lean burn catalyst to store NO_x has been the object of several studies. The conclusions that these studies have drawn is that the more basic the storage component the greater the amount of NO_x that can be stored. In particular the work done by Kobayashi et al has shown that in terms of NO_x storage ability K > Ba > Sr ~ Na > Ca > Li ~ Mg³.

Contaminant-free potassium adlayers have been found to be hexagonally ordered on Pt(111) for potassium coverages of $\theta = 0.9-1$. A complete monolayer of

potassium, $\theta = 1$, is equal to 36% of the surface density of platinum atoms or 5.4×10^{14} atoms cm^{-2} . The ordering of the surface was only visible at low temperature and at room temperature more than one complete monolayer of potassium was not attainable. The potassium layer could, however, be thermally stabilised by exposure to oxygen¹².

Early models of potassium adsorption onto the Pt(111) surface assumed the charge transfer model as proposed by Gurney⁴, in which the adsorbing potassium donates electron density to the surface from an s-orbital. Repulsion between the resulting dipole species formed leads to the adsorbate being spread evenly over the surface rather than clumping into islands. In this model potassium atoms adsorb with a sticking probability that is independent of coverage and at a constant rate⁵.

However work carried out by Lehmann *et al*⁶ and Muller⁷ in the later half of the 1990's has shown that for low coverages of potassium (less than 0.2 ML) potassium is absorbed into sub-surface sites and migrates to the surface upon adsorbing above a critical amount. However, while Lehmann states that all potassium is absorbed below 0.22 ML coverage with no measurable activation energy barrier, Muller has observed an initial adsorption of potassium up to 0.1 ML (where 0.33 ML is equal to a complete adlayer being deposited) on the surface, after which there is a migration to subsurface sites in the second layer on the Pt crystal, due to an activation energy barrier. The fact that there have been LEED observations of a (3x3) pattern at low coverages and that there is no evidence of potassium incorporation below the surface at 100 K would seem to argue against the blanket statement made by Lehmann and co-workers^{8,9}.

The behaviour of K/Pt(111) appears to be characteristic for alkali metal adsorption, with adsorbed species exhibiting strong repulsive forces between themselves and large dipole moments at low coverages. As the coverage of alkali metal increases metallization and the formation of ordered overlayers are observed^{10,11}. With the increasing coverage the (initially ionic) potassium becomes more neutral due to depolarisation effects^{12,13}. Many early studies have claimed that potassium adsorbs regularly to the surface with a sticking coefficient that is independent of coverage¹⁴⁻¹⁵ however more recent work has suggested that the rate of

potassium adsorption is much more rapid at lower coverages.^{13,16,17} This may be due to an enhanced sticking coefficient at these coverages or to incorporation of potassium into the surface.

The adsorption of potassium onto Pt(111) has been shown to reduce the work function of the surface greatly, due to the partly ionic nature of potassium atoms at lower coverages^{13,15}. Early work by Kiskinova and colleagues showed that the decrease in work function reaches a minimum at 0.5 ML, where after it increases to that of almost bulk potassium at 1 ML (as defined by the authors, where 1 ML = 1 complete adlayer).¹⁸

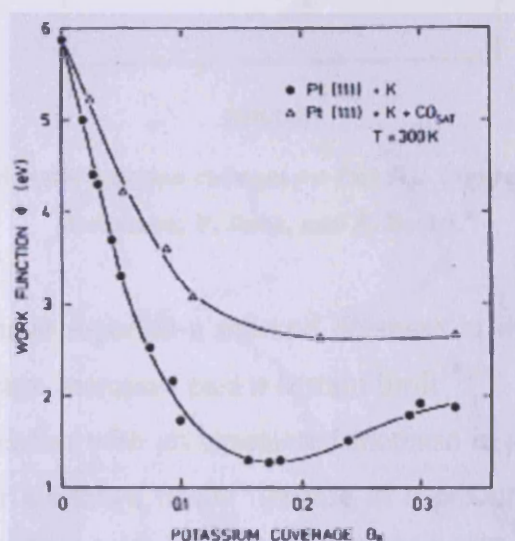


Figure 4.1 - Work function of Pt(111) surface as a function of potassium coverage prior to CO exposure and after saturation with CO at 300 K. Figure taken from paper by M. Kiskinova, G. Pirug and H.P. Bonzel.¹⁸

This is due to a large charge transfer from the adsorbed potassium to the platinum surface at low coverages with the consequent formation of highly ionised adatoms. Due to repulsion between similarly charged species it would be expected for an uniform distribution of potassium at this coverage. The increase in workfunction is due to the adlayer becoming depolarised. In this phase of adsorption the repulsive interactions become less significant so a non-uniform distribution of adsorbed species would be expected^{15,18}. The workfunction of the saturated surface is less than the workfunction of the clean Pt(111) surface. Whilst broadly agreeing with this model, the point at which the minimum occurs in the workfunction curve has

been disputed in a more recent paper by Lehmann and colleagues, who place the minimum workfunction much closer to the point of monolayer formation.⁶

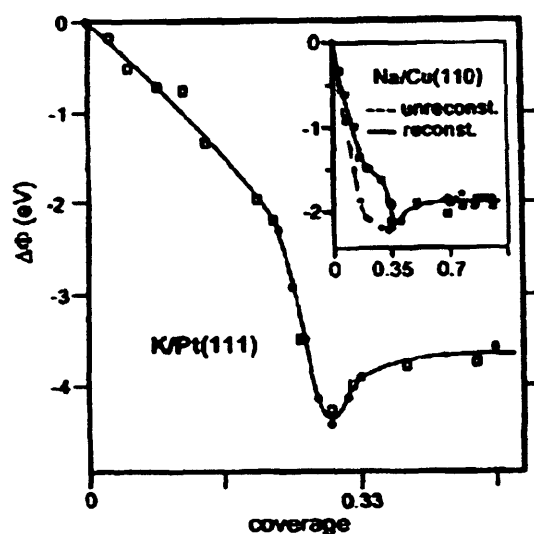


Figure 4.2 – K induced work function changes on Pt(111). Figure taken from paper by J. Lehmann, P. Roos, and E. Bertel.⁶

Many authors have reported a marked decrease in the sticking coefficient of CO as potassium coverage increases past a certain limit^{18,20}. Whether this is due to an increase in potassium radius with an associated increase in site blocking of platinum CO adsorption sites, or a change in the lifetime of a precursor state¹⁸ remains to be seen. Below this limit ($\theta_K = 0.19$) the initial sticking coefficient is independent of K coverage. It is worth noting that although the initial sticking coefficient changes from almost 1 to less than 0.25 as this threshold is passed the saturation coverage of CO still remains high and in fact appears to increase with increasing potassium coverage¹⁸.

It has been shown that the coadsorption of potassium and carbon monoxide increases the heat of adsorption of CO and causes a decrease in the strength of the C-O double bond¹⁹. This is in agreement with observations that the increased temperature of desorption observed in temperature programmed desorption experiments with potassium was due to an increased C-Pt bond strength²⁰. This C-O bond weakening has been shown to be caused by the potassium causing an enhancement in electron back-donation from the platinum surface into 2π antibonding orbitals on the CO and simultaneous strengthening of the C-Pt bond^{18,21}. The

decrease in the strength of the C=O bond results in an increased dissociation probability²². Despite this, dissociative adsorption of CO on K covered Pt(111) does not occur at 300 K¹⁸.

Two different binding sites are observed for the adsorption of CO on Pt(111); a linear and a bridged site with the on-top sites filling before adsorption in the bridged sites. However only one adsorption site is observed for a monolayer of potassium and the binding energy observed is close to that seen for CO bidentate (bridge-bonded) adsorption on Pt(111). This has been interpreted as a shift in favoured binding site from linear to bridged with increasing potassium coverage^{1,18,22,23}. It has been observed that potassium promoted binding sites fill before other binding sites for low K coverages¹⁸. It has also been shown that CO adsorption on the potassium adatoms does not occur²⁴. Theoretical studies have shown that the CO binds in a vertical rather than horizontal fashion through the carbon²³.

CO adsorption on moderate potassium coverages induces an increase in the workfunction of the surface, unlike that of CO on Pt(111), when adsorption decreases the work function². The magnitude of the workfunction increase is directly proportional to the K coverage for $\theta_K < 0.17$. These workfunction changes are connected with K-promotion of CO species. At higher potassium coverages there is a further workfunction increase that has been attributed to adsorption of CO between almost metallic-like K atoms causing electronic charge to be passed from the K to the Pt and into the $2\pi^*$ CO orbitals. This movement of charge means that the K atoms in the local vicinity of the adsorbed CO become more ionic and hence have a lower workfunction. The smaller size of the ionised potassium frees more space for adsorption of further CO with further workfunction effects¹⁸.

Adsorption of CO onto a K covered surface has been shown to re-order the surface into CO + K islands with a fixed stoichiometry (dependent on initial K coverage), leaving free platinum surface. This is likely due to strong attractive interactions between the coadsorbed species. However, at low coverages CO and K do not simultaneously desorb. This would seem to indicate that the adsorbed species interact via coulombic interactions rather than via the formation of an oxocarbon (salt-like) compound. Further exposure to CO leads to an increase in island size with a

consequent increase in CO: K ratio. At $\theta_K \leq 0.11$ the coverage of potassium is insufficient to cover the whole surface with CO + K islands regardless of ratio, with the result that CO adsorbs on exposed Pt(111)¹⁹. As the K coverage increases the maximum of the CO desorption peak shifts to higher temperature, with larger CO exposures broadening the desorption peak. The magnitude of the temperature shift corresponds to a binding energy of approximately 104.6 kJ mol⁻¹ from CO on clean Pt(111) to 150.6 kJ mol⁻¹ for CO on a monolayer of K (assuming a pre-exponential factor of $1 \times 10^{13} \text{ s}^{-1}$). The total amount of CO adsorbed also decreases with increasing K coverage. No ordered LEED patterns are observed when co-dosing CO and K¹. Despite CO and K not appearing together in temperature programmed desorption experiments the temperatures of the desorption peaks are strongly dependent on both CO and K coverage. This is consistent with the proposed model of CO-K and CO-Pt interactions. The presence of potassium on the surface of Pt(111) increases the temperature of desorption of CO. Windham and co-workers have proposed that this is due to a reduction in the pre-exponential factor, in addition to an increase in the activation energy for desorption¹⁹.

Dosing potassium on to the surface has a marked effect on the vibrational stretching frequency of adsorbed CO species. Bridge-bonded CO decreases from 1870 cm⁻¹ on clean Pt to 1560 cm⁻¹ on 0.6 ML of K. At constant potassium coverages the vibrational stretching frequency of adsorbed CO increases substantially with increasing CO coverage¹.

For coverages of potassium greater than 0.15 ML there is a small amount of atomic exchange in the desorbing CO. However the magnitude of the atomic exchange is much less than that seen for similar experiments on potassium on Ru²⁵, Rh²⁶, or Ni²⁶. As these four systems are very similar in essence it seems likely that the same exchange pathways are occurring on the surface but the concerted exchange mechanism proposed by Lee *et al.*²⁶, with weakening of C-O and C-substrate bonds, is simply less favoured on Pt(111).

The general conclusion for the model of CO bonding to K/Pt(111) is that it occurs via electron donation from the highest occupied molecular orbital of CO (5σ) to the transition metal surface. This has the follow on effect of electron back-donation

into the LUMO of CO ($2\pi^*$) leading to a strengthening of the M-C bond and weakening of the C-O bond. The potassium added to the surface acts as an electron donor, affecting the back-donation to CO. Electron density is passed from the potassium to the metal surface with electrons from the metal electrostatically shielding the positive charge created. The dipole thus created lowers the work function of the surface. The surfeit of electron density at the surface results in an enhanced back-donation upon adsorption of CO. An important implication of this model is the molecular orbital consideration, which involves a shift of preferred binding site from on-top to three-fold hollow for potassium-influenced platinum²³. This has been confirmed experimentally by Somorjai and co-workers^{1,12,22}.

Potassium has been found to form various ordered overlayers with different coverages on Pt(111). At $\theta_K = 0.33$ a $\sqrt{3} \times \sqrt{3}R30^\circ$ LEED pattern is observed indicating a close packed surface arrangement with a coverage of 0.33 when compared to the platinum surface. No LEED patterns are commonly observed at lesser coverages, although (3×3) , (2×2) , $(\sqrt{7} \times \sqrt{7})R19$ and $(3/2 \times 3/2)$ patterns have been claimed for coverages of less than a monolayer²⁷. Some groups have also observed more complicated structures evolving with higher coverages^{14,12,15}. In addition it has been noted that at temperatures above 420 K (when the potassium starts to desorb) the $\sqrt{3} \times \sqrt{3}R30^\circ$ spots become gradually weaker and no further LEED patterns are observed¹⁶. As the coverage of the potassium overlayer increases the heat of desorption for potassium from the Pt(111) surface decreases. Temperature programmed desorption studies have shown a remarkable variance in the temperature of desorption from 1000 K for coverages of less than 0.1 ML to 400 K for monolayer coverages (251 kJ mol⁻¹ for $\theta_K < 0.1$ to 83.7 kJ mol⁻¹ for $\theta_K = 2$). This has been attributed to partial ionisation of the adatoms and repulsive lateral interactions becoming more important with increased occupancy of adsorption sites¹². It is worth noting that layers of potassium greater than a monolayer are only readily formed at lower temperatures and layers formed at room temperature are rarely very pure¹⁸.

The ordering of the alkali metal layer on the transition metal is strongly temperature dependent. At 100 K several different LEED patterns have been observed including a (2×2) , (3×3) , and $(\sqrt{7} \times \sqrt{7})R19.1^\circ$.¹⁴ Potassium adsorbs in the hcp hollow site on Pt(111) in both the (2×2) and $(\sqrt{3} \times \sqrt{3})R30^\circ$ phases²⁸. There is

an energy difference of 1.4 kJ mol^{-1} between the hcp site and the fcc adsorption site due to the antibonding character of the HOMO Pt *d* orbital.

When taken with the work of Brodén *et al*¹¹ and Lehmann *et al*¹³, this suggests that potassium is absorbed into the platinum surface at low coverages of potassium ($\theta_K < 0.22$). They suggest that the incorporation requires little activation and may occur at temperatures as low as 100 K.^{14,12,15} This incorporation of potassium has been confirmed by scanning tunnelling microscopy experiments that show a potassium-induced reconstruction of surface steps with some buckling outwards of localised surface regions²⁸. The fact that at room temperature adsorption of potassium onto Pt(111) causes a compressive surface stress, whereby at lower temperatures the tensile stress of the surface was found to increase, would seem to support this model, the compressive and tensile stresses created being due to incorporated K atoms and surface-bonded atoms respectively²⁹.

However Hannon *et al*²⁸ have found that the adsorption of potassium is an activated process and can only take place at coverages of $\theta_K = 0.1$ or higher (where $\theta_K = 0.33$ is equal to a complete adlayer). They have suggested that substitutional adsorption takes place below this coverage with the K adsorbing at surface hollow sites and forming an ionic bond with the platinum surface. Above this coverage the group noticed a slow migration of potassium to sub-surface sites in the second platinum layer. This is in direct contradiction to the charge-transfer model proposed by Gurney *et al*³⁰ in which the alkali metal partially donates an *s* electron to the surface, giving rise to a permanent dipole. Island formation is restricted in this model due to strong repulsive interactions between partially ionised adsorbed alkali metals.

It has frequently been found that the presence of oxygen, either bonded as an oxide or coadsorbed with the alkali metal, is able to accentuate the catalytic effect of the catalyst¹⁰. Oxygen adsorbs very readily on this potassium monolayer and induces a contraction, making the potassium coverage higher in the local vicinity when co-dosing. Exposure to oxygen makes a layer of adsorbed potassium (provided coverage $> 0.2 \text{ ML}$) more thermally stable, reflected in an increase in the heat of desorption¹² (105 kJ mol^{-1} for a monolayer of pure potassium to 209 kJ mol^{-1} for the same coverage after exposure to oxygen).

Two adsorbed oxygen states are commonly observed, a potassium-oxygen bonded state and a more loosely held platinum-oxygen state. Temperature programmed desorption studies have shown a simultaneous desorption of molecular oxygen and potassium with low potassium coverages also producing some weakly bound oxygen¹². The Pt-O state is similar to that obtained for chemisorbed O₂ on Pt(111) and it has been claimed that the K-O state is not K₂O¹⁰. However adsorption stoichiometries of 2:1 are observed and other groups suggest the existence of K₂O species for potassium coverages of less than a monolayer¹². The work of Brodén *et al*¹¹ shows that potassium oxide does not exist at monolayer coverages. They theorize that oxygen is chemisorbed to the substrate and incorporated into the substrate lattice or present as a substrate-metal oxide.

In addition to this, the work of More *et al* shows that substitutional or subsurface incorporations do not occur at reduced temperatures.²⁷ Pirug *et al*¹⁰ also noted that exposure to oxygen caused the ($\sqrt{3} \times \sqrt{3}$)R30° LEED pattern to disappear, with greater exposures also causing a weakening of the Pt(111) substrate spots and an increase in background, indicating a loss of surface order. However annealing this layer brought an ordering of the surface with a (4 x 4) LEED pattern being observed. It has been suggested that in addition to potassium-bonded species being formed the potassium is able to reduce the dissociation barrier of O₂ resulting in atomic oxygen being created and spilling over to free platinum binding sites¹⁰.

Oxygen monolayers form much more readily on potassium-dosed platinum than on platinum alone. In addition to the lower sticking coefficient exhibited by oxygen for platinum ($S_0 = 0.02-0.06$) this also may be due to the clean-off reactions with CO and H₂ which readily occur on the platinum surface not occurring with potassium¹⁰. The authors also report an increase in initial sticking probability to close to 1 for oxygen adsorbing onto a monolayer of potassium on platinum.

Temperature programmed desorption experiments involving co-adsorbed potassium and oxygen on Pt(111) show a shift to lower desorption temperatures for O₂ with increasing potassium coverage, however the magnitude of the shift is much less than that exhibited for pure potassium (251 kJ mol⁻¹ at 0.1 ML to 209.2 kJ mol⁻¹ at 3 ML)¹².

In catalytic reactor studies platinum has been shown to be very active in the reduction of NO, but tends to exhibit poor selectivity for N₂, with N₂O being the major product³¹. The (111) face of platinum however is much more reluctant to dissociate NO as back donation into the 2 π^* orbital of the molecularly bonded NO is symmetry forbidden, thus disfavouring dissociation (dissociation is possible at elevated temperature \sim 1200 K). Although energetically the dissociation of NO on Pt(111) is exothermic, it has been shown that NO adsorbs reversibly at room temperature. However, addition of $\theta_K = 0.18$ potassium surface coverage induces dissociation of NO with the products, N and O, being adsorbed.^{6,7} This is attributed to a potassium-induced lowering of the activation energy for dissociation²⁰. A strengthening of the M-N bond has also been reported³². This is reflected in an increase in the desorption temperature of NO from the surface³³. N₂O desorption has also been observed at the same temperature as NO desorption in the K/Pt(111) system; this has been attributed to a nitrite species (NO₂)³⁴.

It has been found that potassium, when dosed on platinum, greatly effects the selectivity of the reduction of NO to N₂, with the selectivity being proportional to the total potassium surface coverage. On coverages of a monolayer or greater reduction to N₂ greatly dominates.²¹ It would appear that this is due to a synergistic mechanism in which each of the metallic centres is responsible for a different component of the reduction; Pt for reducing NO to N₂O and K for reducing N₂O to N₂. However, it was noted that the two metals have to be in intimate contact for efficient reduction to occur, implying simultaneous participation of both metals in the reaction mechanism.³⁵ In addition to this the NO dissociation has been shown to occur at temperatures below 300 K³⁶. Films of other alkali metals, in particular sodium, exhibit similar behaviour with regard to NO reduction when dosed on Pt(111)³².

NO adsorbing on Pt(111) induces a small initial increase in workfunction followed by a slightly larger decrease after $\theta_{NO} = 0.2$. However when 0.36 ML of potassium is dosed onto the surface, adsorbing NO induces a large increase in the workfunction of the surface with increasing NO coverage. This increase in the magnitude of the workfunction change with the addition of alkali metals to the transition metal surfaces appears to be quite common.³⁷

Atomic oxygen adsorbed on the surface from the dissociative adsorption of NO has been shown to be able to react with another adsorbed NO molecule to produce a potassium-stabilised NO_2^- species. The formation of this species is facilitated by high temperatures.²⁰ Note that due to the demonstrated ability of Pt(111) to break down NO_2 (see chapter 3), the existence of this species on a potassium free surface is highly unlikely. NO_2^- can also be produced on the K/Pt(111) system by the sequential dosing of O_2 and NO.²⁰

With regards to its proposed use in this project as a potential candidate for an alternative NO_x trap, potassium has been shown to offer several advantages over BaO in regards to NO_x storage ability. In particular many studies have shown that potassium nitrates are more stable at higher temperatures than barium nitrates and that the NO_x storage ability of a potassium storage component is greater than for a BaO one^{38,39,40,41}. In addition to this the stability of the barium containing storage component in the catalytic converter wash-coat limits the NO_x trap to operating temperatures between 200–450 °C⁴². Wash-coats containing alkali metal components have been shown to be stable up to 575 °C^{38,39}.

4.2 Results and Discussion

4.2.1 Dosing K on Pt(111)

Potassium was dosed onto the surface at 300 K for increasing lengths of time using a custom built SAES getter source heated to over 1200 K and positioned in front of the crystal. After outgassing the differential pressure rise was 2×10^{-9} mbar during the course of the depositions, the majority of which was due to hydrogen desorption from the doser. The growth of the potassium adlayer was charted using the Pt_{MNN} 69 eV and K_{LMM} 272 eV Auger signals. The surface was heated to 550 °C and sputtered and annealed in between each dosing to make certain of the removal of all the potassium used in previous experiments from the surface.

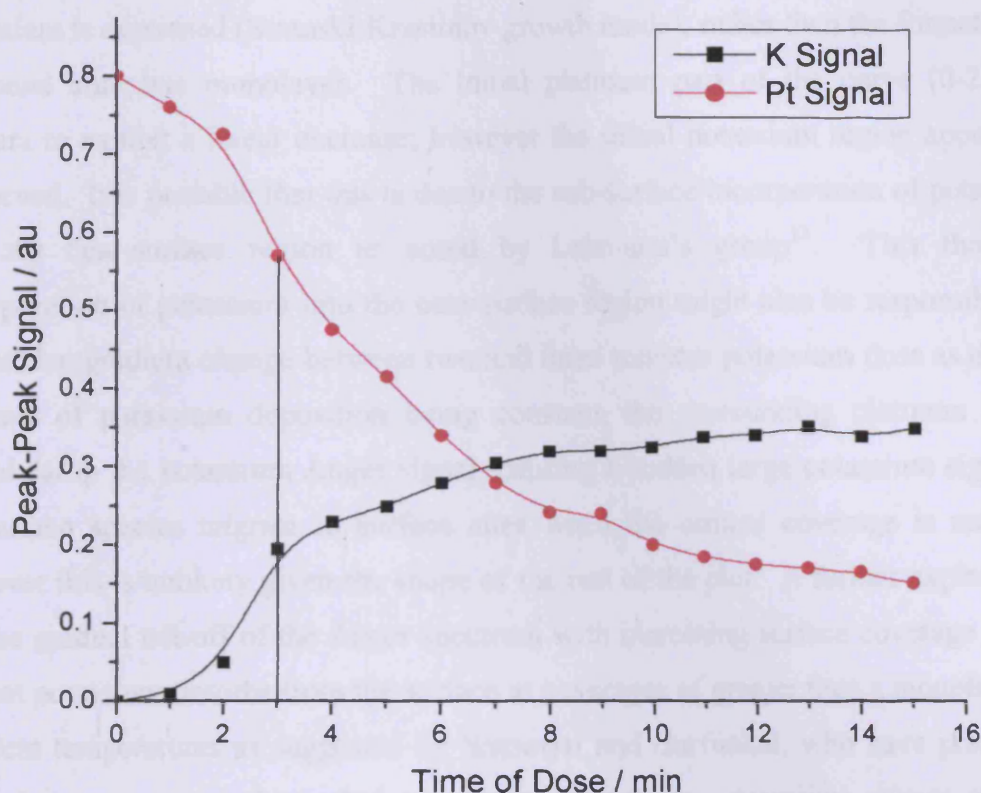


Figure 4.3 – the change in the relative Auger signals of K and Pt with increasing K surface coverage. The point of monolayer completion is also shown.

Figure 4.3 shows two intersecting curves. The growth curve is due to the increasing amount of potassium that is deposited on the crystal surface with increasing time of potassium dose, and the decaying curve is due to the increasing amounts of potassium obstructing the passage of the Auger electrons from the platinum to the electron detecting grids of the retarding field analyser. The curves show that there is a relatively slow initial increase in Auger signal until two minutes potassium surface dose. Between two and three minutes there is a large increase in the K signal and consequent reduction in the Pt signal. After this jump there is a slow increase in K signal that appears to tail off towards a maximum with increasing time. This sudden 'jump' in signal is likely due to the adsorbed potassium changing state from ionic to metallic as described in the literature¹³. Due to the chemisorption experiments contained later in this section (Figure 4.6 and Figure 4.9) three minutes was determined as the dosing time required for completion of one full potassium layer. The gradual curve that appears to level off after the completion of the layer is

characteristic of islands of potassium being formed, which grow in size as further potassium is deposited (Stranski-Krastinov growth mode), rather than the formation of a second complete monolayer. The initial platinum part of the curve (0-2 min) appears to exhibit a linear decrease; however the initial potassium region appears to be curved. It is possible that this is due to the sub-surface incorporation of potassium into the near-surface region as noted by Lehmann's group¹³. This theorised incorporation of potassium into the near-surface region might also be responsible for the sudden gradient change between two and three minutes potassium dose as despite the rate of potassium deposition being constant, the surrounding platinum atoms would damp the potassium Auger signal, causing a sudden large potassium signal as subsurface species migrate to surface sites when the critical coverage is reached; however this is unlikely given the shape of the rest of the plot. A further explanation for the gradual tail-off of the Auger spectrum with increasing surface coverage might be that potassium desorbs from the surface at coverages of greater than a monolayer at ambient temperatures as suggested by Somorjai and Garfunkel, who have presented data that appears to show that no further potassium adsorption occurs after a monolayer deposition¹². While this does not agree with the data shown in Figure 4.3 (and the textual descriptions in later works) as there is no abrupt limit to the growth of the K signal, a plot of the relative peak ratios of the two major peaks in the Auger spectrum (Figure 4.4) produces a much more similar trend to another plot published in the paper in which a constant increase in K:Pt signal is observed that can be grouped into several discrete regions¹².

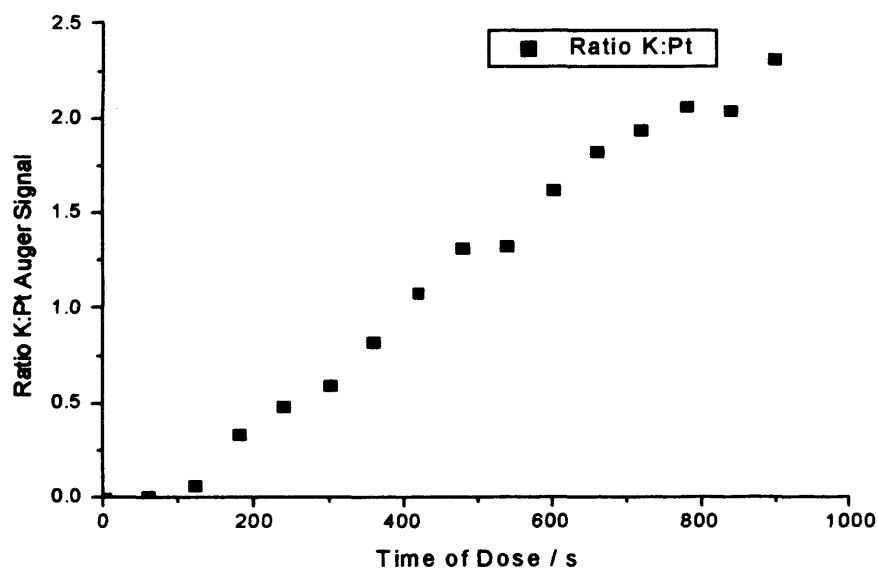


Figure 4.4 - K 252 eV to Pt 64 eV peak: peak ratios.

4.2.2 Adsorption of CO on the K/Pt surface

As shown in chapter 3, CO adsorbs with relatively high initial sticking probability ($S_0 = 0.45 \pm 0.02$) on Pt(111) at 300 K. It was found that the initial sticking probability of CO on high doses of potassium was negligibly small. This allowed the growth of the surface to be charted to complement the Auger data shown in Figure 4.3.

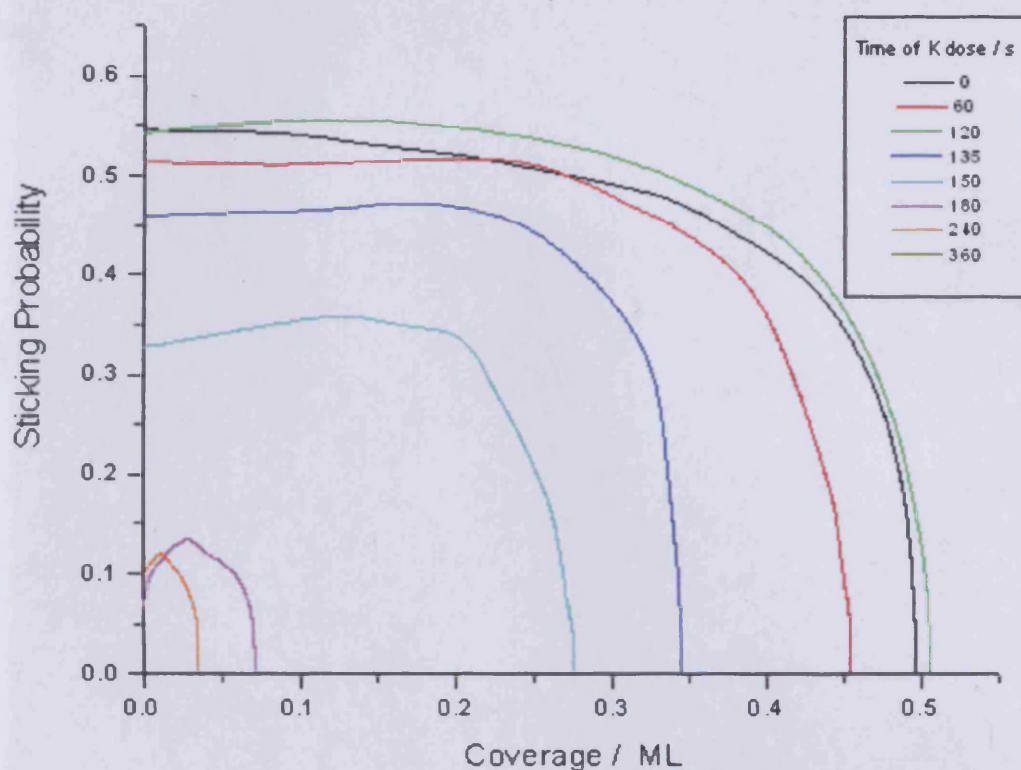


Figure 4.5 – The variation in the sticking probability of molecular beams of CO (50 mbar molecular beam source pressure) with CO coverage for increasing K coverages of the Pt(111) crystal surface.

Figure 4.5 indicates that surface doses of potassium up to 120 s appear to adsorb roughly the same amount of CO as the clean surface, have similarly shaped uptake curves and saturate to roughly the same amount CO coverage (the total coverage achieved at 120 s potassium dosing time is actually larger than that achieved at 60 s dosing time). As the potassium surface dose is increased further there is a large decrease in the saturation coverage and sticking coefficient until no CO adsorption is visible at 360 s of potassium surface dose. This decrease in CO sticking with increased potassium surface coverage has been reported in the literature, with a reduction in measured sticking coefficient but a relatively stable total saturation coverage. However, the authors note that much greater CO exposures are required to reach these coverage than at lower θ_K ¹⁸. All the sticking profiles have an initial plateau followed by a steep decrease indicating that precursor kinetics are an important part of this system (K_p is small). CO adsorbs less as the potassium layer

becomes less polar. To aid analysis of the growth of the potassium on the surface the initial sticking coefficient, S_0 , was plotted against time of dose (Figure 4.6).

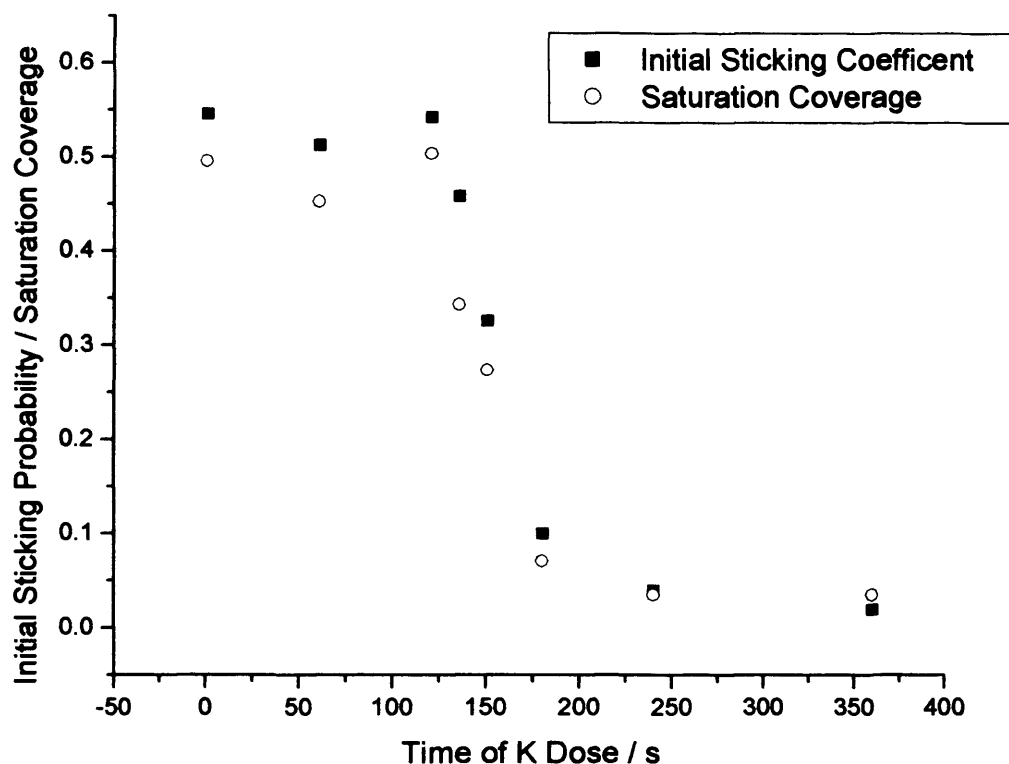


Figure 4.6 - The initial sticking probability of molecular beams of CO plotted against time of potassium dose of Pt(111) crystal surface.

Figure 4.6 shows that the initial sticking probability remains fairly constant between 0.5 and 0.55 for doses of K up to 120 s. After this time there is a sharp decrease in the initial sticking probability. It is possible that this is due to a complete layer of potassium having been deposited at this point, however taking Figure 4.3 into account it seems as if the abrupt gradient change at 180 s potassium dose is due to the first layer nearing completion (adsorbed ionic potassium atoms becoming more metallic-like as they are packed more tightly onto the crystal surface), with the platinum (111) being completely covered by 240 s potassium dose. This behaviour has been noticed by other groups, with White and co workers observing that the CO adsorption at K coverages in excess of a full layer ($\theta_K = 0.49$, where $\theta_K = 0.33$ equals a complete K coverage of the Pt(111) surface) is extremely slow. This is rationalised as the reluctance of CO to adsorb on potassium that is metallic in character⁴³.

The plateau of constant sticking probability with initial potassium surface coverage has been noted by Kiskinova and co-workers who have postulated that it is due to a potassium-induced increase in the lifetime of a CO precursor species. The authors also ascribe the sudden drop in the sticking coefficient to be due to a change from ionic potassium to metallic potassium, which induces a drop in the precursor state lifetime. In addition to these observations, due to the repulsive forces between adsorbed potassium ions, spacing between the adatoms would be maximised, potentially leaving CO adsorption sites on platinum unobstructed. That CO still adsorbs (albeit in relatively small quantities) after a complete monolayer of adsorbed potassium indicates that some sort of K-CO species is being formed, or possibly K-induced CO decomposition (however this is unlikely as there is no evidence of decomposition products whilst beaming or in the temperature programmed desorption following the beam experiment, and it has been observed in the literature that no CO dissociation occurs on K-promoted Pt(111)¹⁸). As further potassium is added to the surface the sticking probability of CO decreases further, indicating that this adsorption takes place on thin films of potassium polarised by the platinum surface rather than on the more bulk metallic-like potassium, which occurs in the growth of islands. The decrease in initial sticking coefficient can therefore be directly related to the polarity of the adlayer. As the islands grow in size the total CO adsorbed at saturation decreases due to the increasing metallic character of the potassium. The shape of Figure 4.6 is related to the changes in work function observed when dosing potassium onto the Pt(111) surface. Both Windham¹⁵ and Pirug¹⁶ have observed a decrease in workfunction with increasing potassium up to half a complete monolayer of potassium, after which the workfunction increases to resemble bulk potassium. The rise from the minimum in the workfunction curve reported by Kiskinova and colleagues, at which point metallic potassium begins to form, appears at a point coincident with the fall in sticking probability in Figure 4.6. It therefore appears that the decrease in sticking probability of CO is caused by the metallic potassium, possibly due to blocking of CO adsorption sites on the Pt(111).

All of the curves for different K coverages in Figure 4.5 have an initial plateau region and in some cases appear to transiently increase in sticking probability as the beam is impacting with the surface. This is indicative of precursor state adsorption kinetics playing a part in the adsorption, with CO having an appreciable physisorbed

lifespan before adsorbing in a more permanent chemisorbed fashion. The fact that all of the adsorption profiles look similar and merely decrease in magnitude with increasing potassium surface coverage lends itself to the explanation that the reduced CO adsorption coefficient, which occurs at potassium dosings of 120 s and greater, is merely due to surface potassium blocking adsorption sites on the platinum. The minor change in adsorption profiles and sticking probabilities of CO for dosings of less than this can be explained by invoking the sub-surface adsorption of K as described by Hannon²⁸ and Lehmann¹³ in which the initial adsorbed potassium migrates to sub-surface sites, leaving CO adsorption sites un-obstructed for adsorption.

The temperature programmed desorption spectra recorded after the molecular beam experiments shown in figure 4.5 (Figure 4.7) show several interesting features that help to clarify the adsorption processes that are occurring in this system. With no potassium surface coverage there is just a single CO desorption environment at relatively low temperature ($\sim 120^\circ\text{C}$, characteristic of CO desorbing from Pt(111) – see section 3.3.2). As 60 s potassium is dosed onto the surface another separate CO desorption peak occurs at higher temperature (180°C) with a shoulder at 220°C . The magnitude of the desorption peak associated with CO on Pt(111) has decreased compared to the clean platinum, which is to be expected considering the reduced platinum surface area available for adsorption. When potassium is dosed onto the surface for 120 s the peak resulting from CO desorption from platinum is greatly reduced in size and the CO desorption peak has shifted to higher temperature (290°C). This would seem to indicate that the observed reduction in initial sticking coefficient and absolute adsorption observed in Figure 4.5 and Figure 4.6 is simply due to potassium on the surface blocking adsorption sites for CO on un-promoted platinum. The desorption peak at 290°C is present for all potassium coverages of greater than a monolayer, indicating that CO does adsorb on potassium, but not as well as on Pt(111). This feature has been observed by Somorjai and co-workers, however they have interpreted it as being a gradual shift of the potassium-influenced CO-Pt rather than as a K-CO species²². Crowell *et al.*¹ observed that no CO adsorption took place on multilayer potassium. This, combined with the presence of K-CO desorption peaks in the temperature programmed desorption experiments following beaming (Figure 4.7), reinforces the earlier assertion that potassium surface

growth occurs via a Stranski-Krastanov growth mode. Interestingly this conclusion also contradicts the conclusions of Somorjai and Garfunkel who stated that multiplayer potassium formation was not possible at room temperature¹².

Kiskinova and co-workers have observed, using ultraviolet photoelectron spectroscopy and x-ray photoelectron spectroscopy, two separate CO environments when adsorbing CO on potassium pre-covered Pt(111). They state that the initial CO adsorption takes place into a potassium-influenced site on the platinum, followed by adsorption on the clean platinum. Adsorption in the potassium-influenced adsorption sites has a greater adsorption energy than adsorption in the platinum sites alone ($< 200 \text{ kJ mol}^{-1}$ compared to 138 kJ mol^{-1} for CO on clean Pt(111)). They also observe exchange in the relative populations of clean and potassium-influenced sites as the surface potassium coverage increases¹⁸. These conclusions aid rationalisation of Figure 4.7. At 60 s dose two separate CO environments are visible, a lower temperature desorption peak at 125°C resulting from CO adsorption on Pt(111), and a higher temperature CO desorption peak at 183°C that is therefore due to the adsorption of CO on the electronically perturbed platinum immediately adjacent to potassium. As the surface dose is increased to 120 s both of these environments are drastically reduced in size and a new desorption peak at 277°C , that is obviously due to CO adsorption on K, has appeared. All potassium doses greater than this lack the lower temperature desorption peaks associated with CO on Pt(111) and only show the single higher temperature desorption peak associated with potassium. This supports the earlier conclusions about the time of dose at which completion of a full monolayer occurs. That there is still CO desorption from all potassium surface dosings despite the limited CO sticking observed at higher K coverages suggests that CO has been adsorbed from the background gases in the chamber during deposition of the potassium layer.

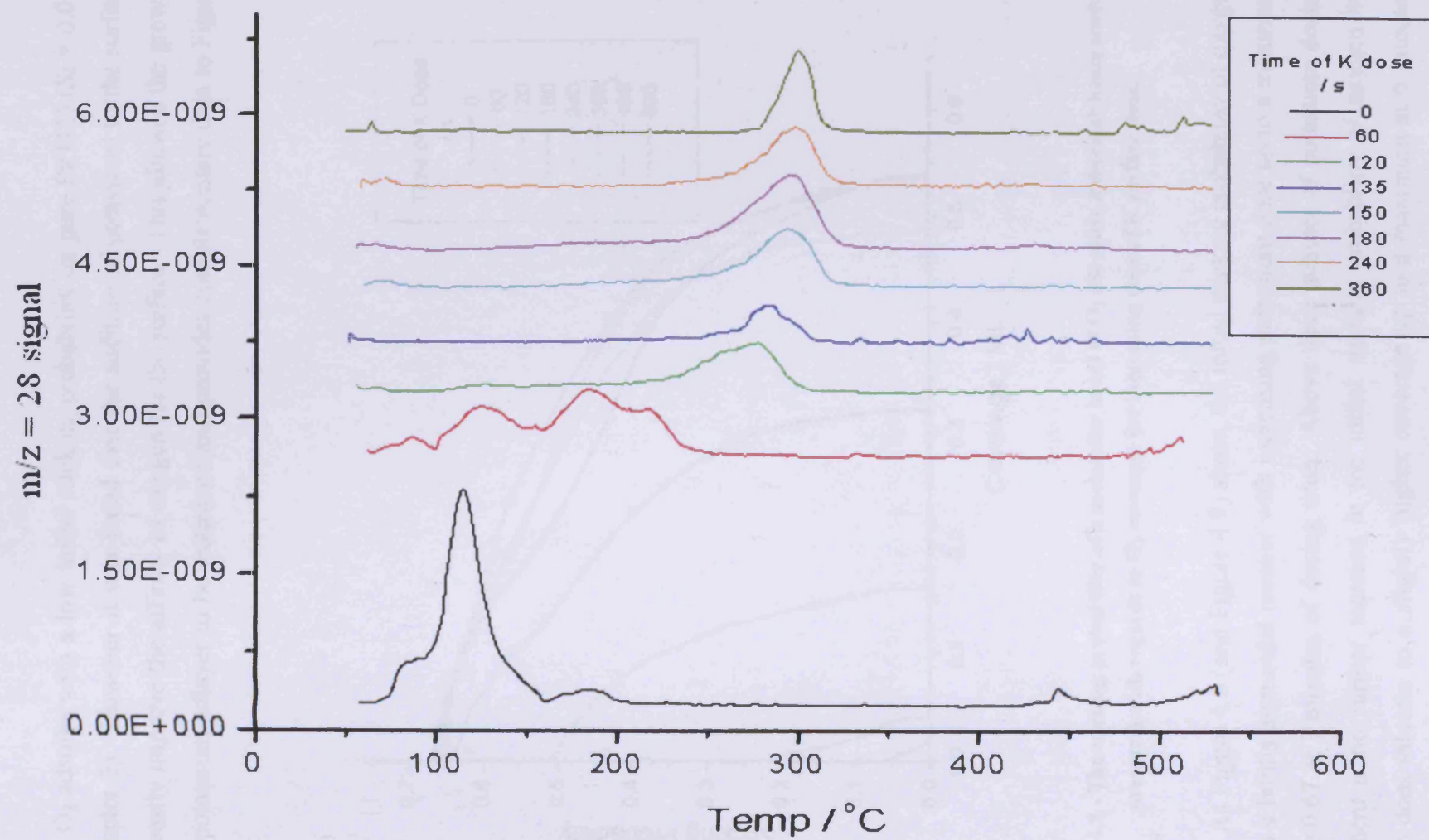


Figure 4.7 – Temperature programmed desorption of the crystal surface following the molecular beam experiments shown in Figure 4.5

4.2.3 Sticking of O₂ on K dosed Pt(111)

O₂ adsorbs with a low initial sticking probability on pure Pt(111) ($S_0 = 0.06$, see chapter 3). However it was found that the addition of potassium to the surface could vastly improve the affinity of oxygen for the surface. This allowed the growth of the potassium adlayer to be examined and provides complementary data to Figure 4.3.

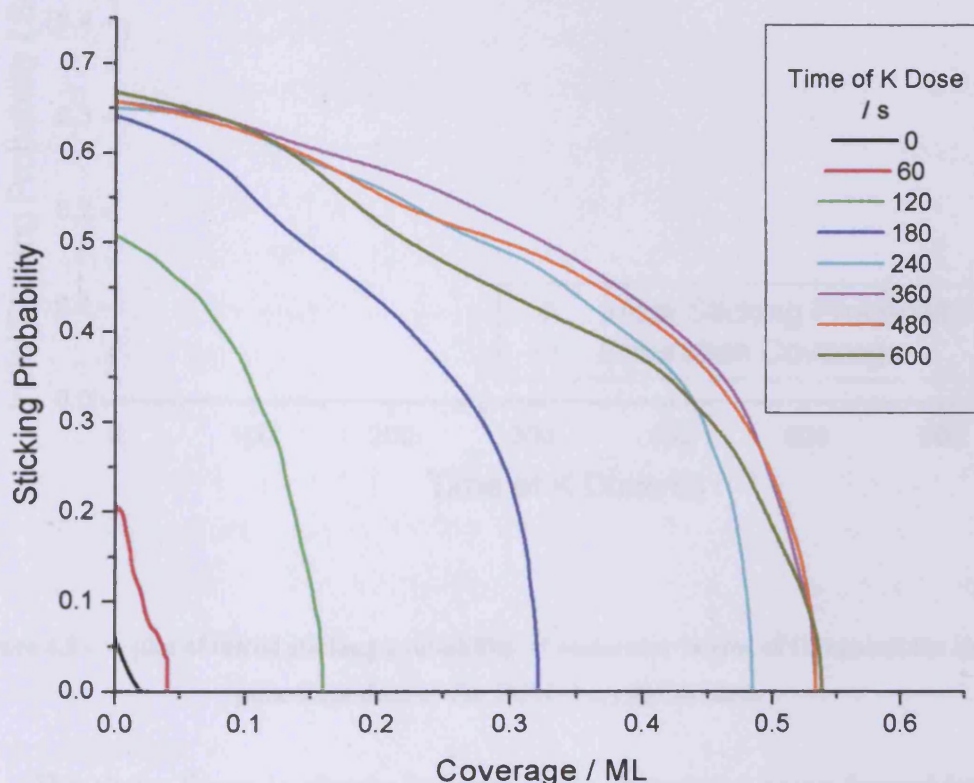


Figure 4.8 - The sticking probability of a molecular beam of O₂ (50 mbar molecular beam source pressure) with regards to O₂ coverage for increasing time of K surface dose.

As Figure 4.8 (and Figure 4.9) show, the initial sticking probability of oxygen rises in a faintly sigmoidal manner with increasing potassium dose up to a maximum of $S_0 = 0.67$ at 3 minutes of dosing time. Above three minutes of potassium dosing time there is no further increase in the initial sticking probability of oxygen but oxygen does saturate to a slightly higher coverage up to a maximum at 6 minutes.

Plotting the initial sticking probability and saturation of O₂ against the time of potassium dose gives Figure 4.9 (below).

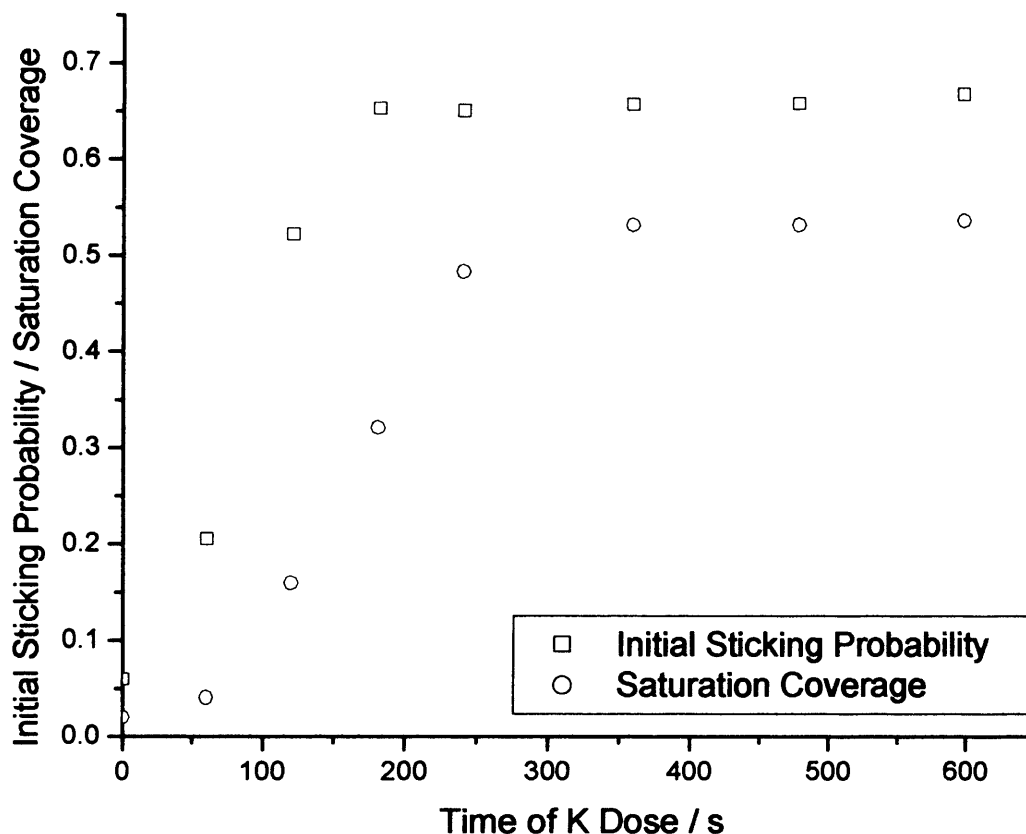


Figure 4.9 – A plot of initial sticking probability of molecular beams of O₂ against the time of potassium dose of the Pt(111) crystal surface.

The above figure is clearly indicative of a monolayer being formed by 180 s dose. However, if the growth mode is Stranski-Krastanov as Figure 4.3 suggests, one would expect a more gradual levelling off of both the initial sticking probability and saturation coverage towards a plateau rather than the abrupt gradient change (observed for O₂ initial sticking probability at 180 s K dose and O₂ saturation coverage at 240 s K dose) observed in Figure 4.9. However this may not be the case as, unlike the Auger data shown in Figure 4.3, deposition of potassium onto the surface would have the effect (neglecting oxygen penetration of the surface) of obstructing the potassium below it, muting the predicted gradual gradient change. The sigmoidal shape of the initial curve (sub-monolayer coverages) is a possible

indication of potassium being adsorbed into subsurface sites or of adsorbed CO from the background being removed in a clean-off reaction.

The constant plateau that is observed in Figure 4.9 for both the O₂ initial sticking probability and the coverage to which it saturates would appear to indicate that O₂ adsorption is occurring via formation of an oxide of potassium for surface coverages in excess of a monolayer. However, adsorption may still be occurring via K-induced charge transfer or K-mediated adsorption followed by spillover at lower coverages. These two mechanisms are unlikely at monolayer coverages or above as potassium has been shown to completely cover the platinum surface (Figure 4.3), making potassium-induced dissociation followed by spillover unlikely. Potassium also becomes more metallic in character at higher coverages, thus reducing charge transfer to the platinum surface, although it is worth noting that it may be possible were the potassium adlayer to undergo any sort of contraction. Unlike the case for CO, there is no sudden change in the sticking profile of Figure 4.9 as the adsorbed potassium adatoms change from ionic to metallic in character.

The work of Pirug¹⁰ has shown that potassium adatoms induce O₂ dissociation with the result of atomic oxygen binding on the Pt(111) surface rather than with the potassium. However Brodén has provided evidence that dosing oxygen onto the surface of a complete layer of potassium disrupts the monolayer (and induces a contraction) and that although oxygen is stored, it is not stored as platinum oxide¹⁰. Together, this indicates that the adsorption of O₂ on K/Pt(111) is not as simple as Figure 4.9 implies, with multiple adsorption mechanisms being responsible for the oxygen adsorption.

Examining the temperature programmed desorption experiments that were carried out following the molecular beam experiments in Figure 4.8 (Figure 4.10) provides information on the mechanism of oxygen adsorption on K/Pt(111). With no potassium present on the surface, due to the very low initial sticking coefficient of O₂ on Pt(111), no O₂ desorption is evident. As O₂ has a finite adsorption coefficient on Pt(111) ($S_0 = 0.06$) it seems likely that the lack of a desorption peak is due to a CO clean-off reaction. With 60 s potassium dosed onto the surface there is a desorption peak at 325 °C with a higher temperature shoulder. Increasing the potassium surface

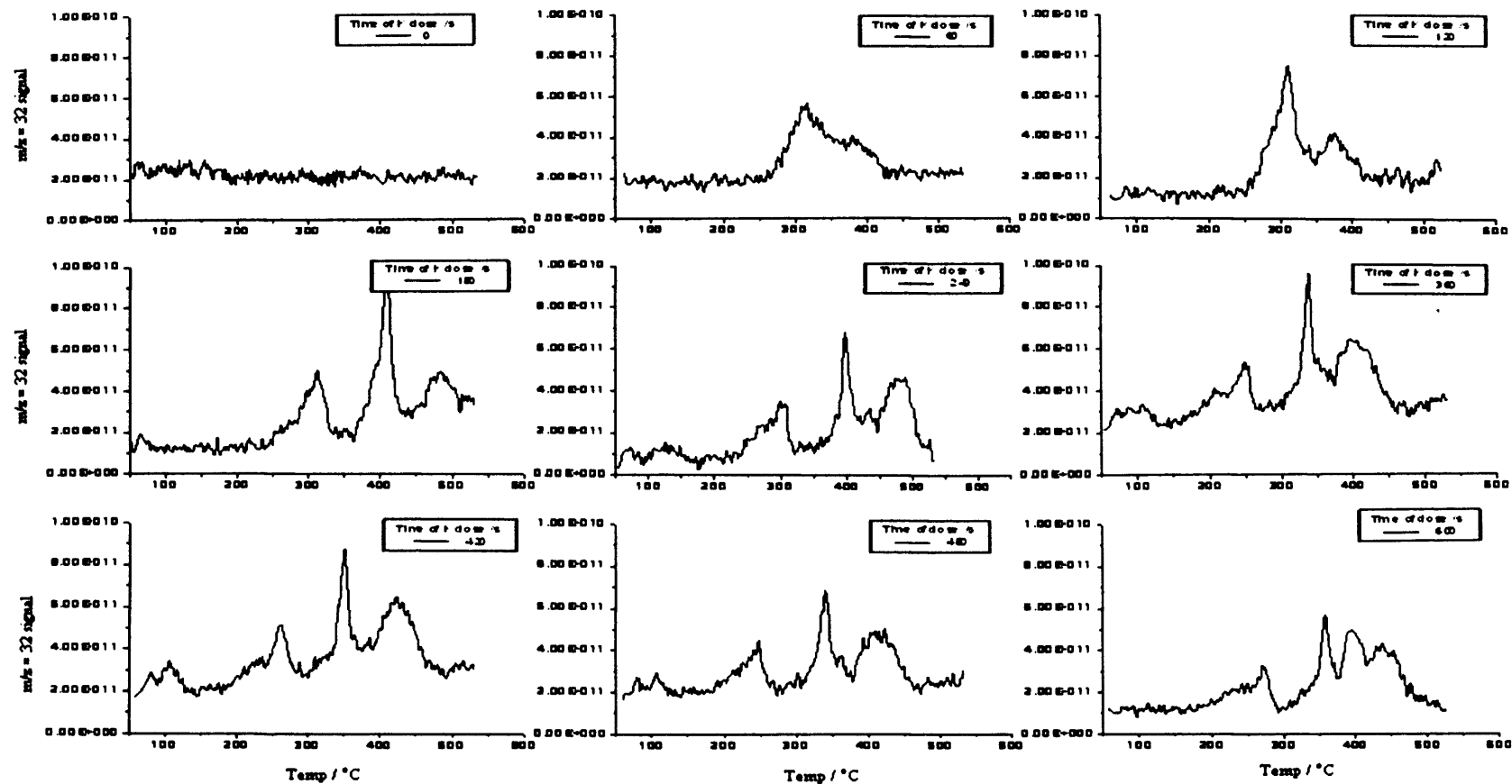


Figure 4.10 –Temperature programmed desorption of O₂ following the molecular beam experiments shown in Figure 4.8.

coverage resolves this shoulder and shifts it to higher temperatures. With three minutes of potassium dose another oxygen desorption peak at 480 °C becomes visible. Taken together it seems as if the initial $m/z = 32$ desorption peak at 325 °C is a result of the desorption of atomic oxygen created by a potassium-induced reduction in the barrier to O_2 dissociative adsorption (this peak is noted in temperature programmed desorption spectra of potassium oxide by Somorjai *et al.*¹², who also note that it disappears for potassium coverages of greater than a monolayer). The fact that this peak does not disappear in the temperature programmed desorption experiments shown in Figure 4.10 is due to a difference in experimental procedure – in our experiments the potassium layer was deposited before oxidation by the molecular beam. This peak is therefore evidence of the contraction that occurs when oxidising a layer of potassium (a contraction in a complete monolayer of potassium of the magnitude described by Brodén and co-workers would leave 25% of the underlying platinum surface exposed)¹⁰. This chemisorbed oxygen-platinum species has also been noted by Bonzel *et al.*¹¹ when examining oxygen adsorption on potassium-covered Pt(111). The smaller size of the oxide allows atomic oxygen adsorption on the exposed Pt(111). Garfunkel and Somorjai also note that potassium desorption occurs at the same temperature as the highest temperature oxygen desorption peak, making it likely that the peak at ~ 480 °C is due to a potassium oxide species decomposition. If so, it is worth noting that this species only occurs after a complete monolayer of potassium has been deposited, indicating that the potassium oxidation does not occur if the potassium is ionic in character. However, Brodén and co-workers have provided evidence that potassium oxide does not form on Pt(111). They theorise that this state is due to oxygen incorporation into the platinum surface¹¹. It seems likely that, as they deposited the potassium at 600 K, only sub-monolayer coverages of potassium were formed; these were shown to be reluctant to oxidise (making the sticking observed in the early parts of Figure 4.8 and Figure 4.9 to be likely to K-induced O_2 dissociation and spillover of atomic oxygen to platinum adsorption sites). The mid-temperature peak is likely to be due to a substrate-metal-oxide species as theorised by Brodén *et al.*¹¹. The formation of potassium oxide at half-monolayer coverages has been proven by Cassuto and co workers. Using UPS they proved that molecular oxygen adsorbs via dissociative adsorption on a potassium-promoted Pt(111) surface and that the atomic oxygen produced either chemisorbs on the potassium/platinum or forms potassium oxide⁴⁴. They also

formed potassium peroxide and superoxide species at 95 K. It is an established fact that O_2 molecularly adsorbs in the form of O_2^- on Pt(111) as a precursor to dissociative adsorption⁴⁵. The adsorption is facilitated by partial transfer of electronic charge into a π^* antibonding orbital on the oxygen molecule. It is therefore to be expected that the enhanced back-donation from the platinum as a result of increased local electron density provided by adsorbed potassium would reduce the barrier to sticking by stabilising the precursor state as a species and reducing the barrier to dissociation. This is evidenced by the increased sticking of O_2 that is visible with low coverages of surface potassium and the temperature programmed desorption experiment evidence that the oxygen is present as a Pt-O species.

Due to the agreement between Figure 4.3, Figure 4.9 and Figure 4.10 it was concluded that a full monolayer of potassium ($\theta_K = 0.33$) has been deposited at three minutes of dosing time. This will be used as a reference point for monolayer completion in future experiments.

4.2.4 Adsorption of NO on K dosed Pt(111) surface

Potassium was dosed onto the Pt(111) surface (held at 300 K) for differing lengths of time using a custom built SAES getter source. NO (50 mbar molecular beam source pressure) was beamed onto the surface at room temperature and the sticking probability was measured as described earlier.

Figure 4.11 shows that the initial sticking coefficient of NO on the surface varies only slightly as the potassium surface coverage is increased, remaining constant (within experimental error) at $S_0 \sim 0.5$. There is relatively little change in saturation coverage compared with CO and O_2 adsorption.

It is a well-documented ability of the K/Pt(111) system to reduce NO. This, combined with the adsorption on potassium-free and potassium-locally influenced platinum as well as adsorption effects due to the changing ionic character of the potassium adatoms adds complexity to the adsorption process.

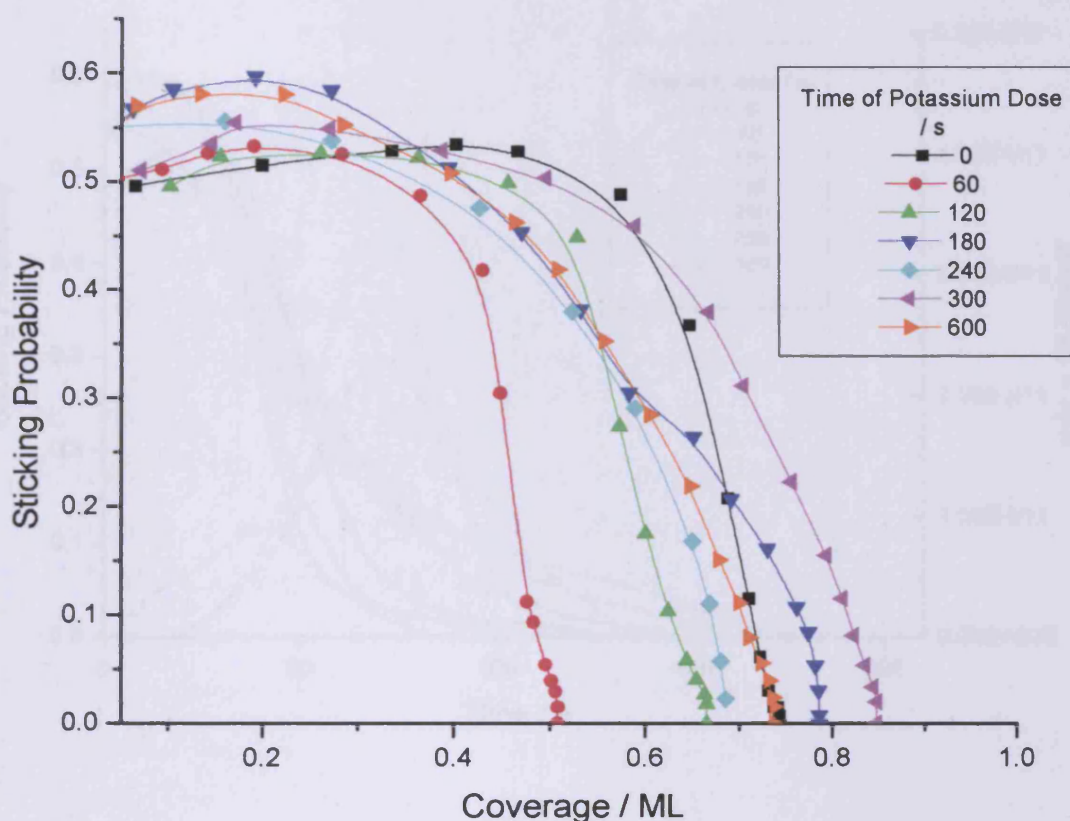


Figure 4.11 – The variation of sticking probability with coverage for molecular beams of NO (50 mbar molecular beam source pressure) on increasing potassium surface coverages of Pt(111).

It was found that $m/z = 28$ was desorbed after a short time lag when beaming NO for certain K coverages. This did not occur on clean Pt(111), making it unlikely that the identity of the desorbing species was CO from the surface in a displacement reaction. It was therefore concluded that the identity of the desorbing species was N_2 from NO dissociative adsorption.

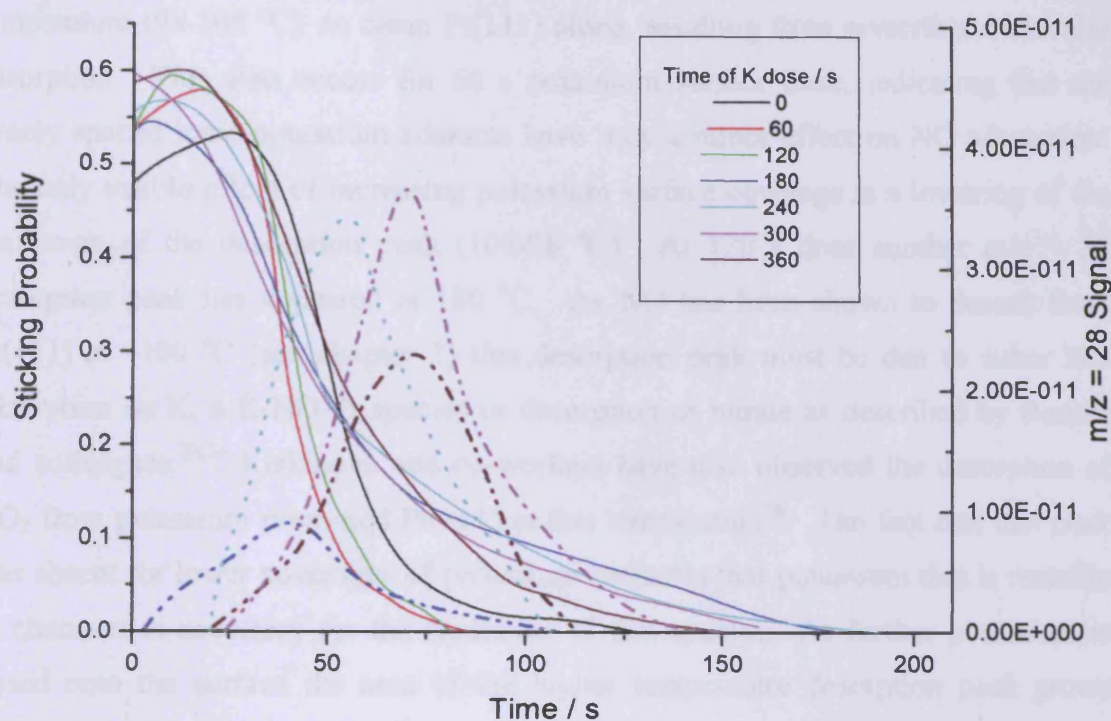


Figure 4.12 – The sticking profile of NO and the N_2 that is desorbed whilst beaming on to different potassium surface doses against experimental time (whilst beaming). Note that the solid lines represent sticking probabilities and the dotted lines N_2 desorbed from the surface.

As Figure 4.12 shows only potassium coverages of a monolayer or greater produce N_2 upon beaming NO. This implies that only metallic potassium is capable of reducing adsorbed NO, not potassium that is ionic in character or the platinum with increased electron density in the immediate vicinity of adsorbed potassium. However, the CO sticking data in Figure 4.6 implies that the transition from ionic to metallic potassium has occurred at approximately 2 minutes potassium surface dose. It therefore appears that the coverage of potassium that is required to reduce NO is less than a full Pt(111) crystal surface covering, possibly due to a mixture of both ionic and metallic potassium being present on the surface at this coverage. Kiskinova, Pirug and Bonzel have reported similar findings to these in that they found that for $\theta_K \geq 0.18$ NO starts to be decomposed by the surface with the formation of N_2 as well as an adsorbed NO_2 species with x-ray photoelectron binding energies in agreement with KNO_2 ¹⁸. This is examined in the temperature programmed desorption experiments following the molecular beam experiments shown in Figure 4.11 (Figure 4.13).

Figure 4.13 clearly shows NO desorbing with a single desorption peak at low temperature (98-108 °C) on clean Pt(111) alone, resulting from reversible molecular adsorption. This also occurs for 60 s potassium surface dose, indicating that the evenly spaced ionic potassium adatoms have only a minor effect on NO adsorption. The only visible effect of increasing potassium surface coverage is a lowering of the maximum of the desorption peak (108-98 °C). At 120 s dose another $m/z = 30$ desorption peak has appeared at 180 °C. As NO has been shown to desorb from Pt(111) at ~100 °C (see chapter 3) this desorption peak must be due to either NO adsorption on K, a K-NO-Pt species or desorption of nitrate as described by Bonzel and colleagues.^{20,34} Kiskinova and co-workers have also observed the desorption of NO₂ from potassium promoted Pt(111) at this temperature¹⁸. The fact that this peak was absent for lower coverages of potassium indicates that potassium that is metallic in character is necessary for the formation of this species. As further potassium is dosed onto the surface the area of the higher temperature desorption peak grows relative to that of the lower temperature peak and an oxygen desorption peak 420 - 470 °C becomes visible, demonstrating that NO has been broken down by the surface. The lower temperature NO desorption peak (from Pt(111)) is visible up to ~ 240 s K dosing time, possibly indicating a contraction of the overlayer in a similar manner to that seen for O₂ on K/Pt(111). If atomic oxygen is being produced from dissociative adsorption of NO it is reasonable to suppose that the reactive atomic species produced might react with surface potassium to form an oxide of potassium. The Pt(111) surface exposed by the oxide formation would then be able to adsorb incoming NO molecularly.

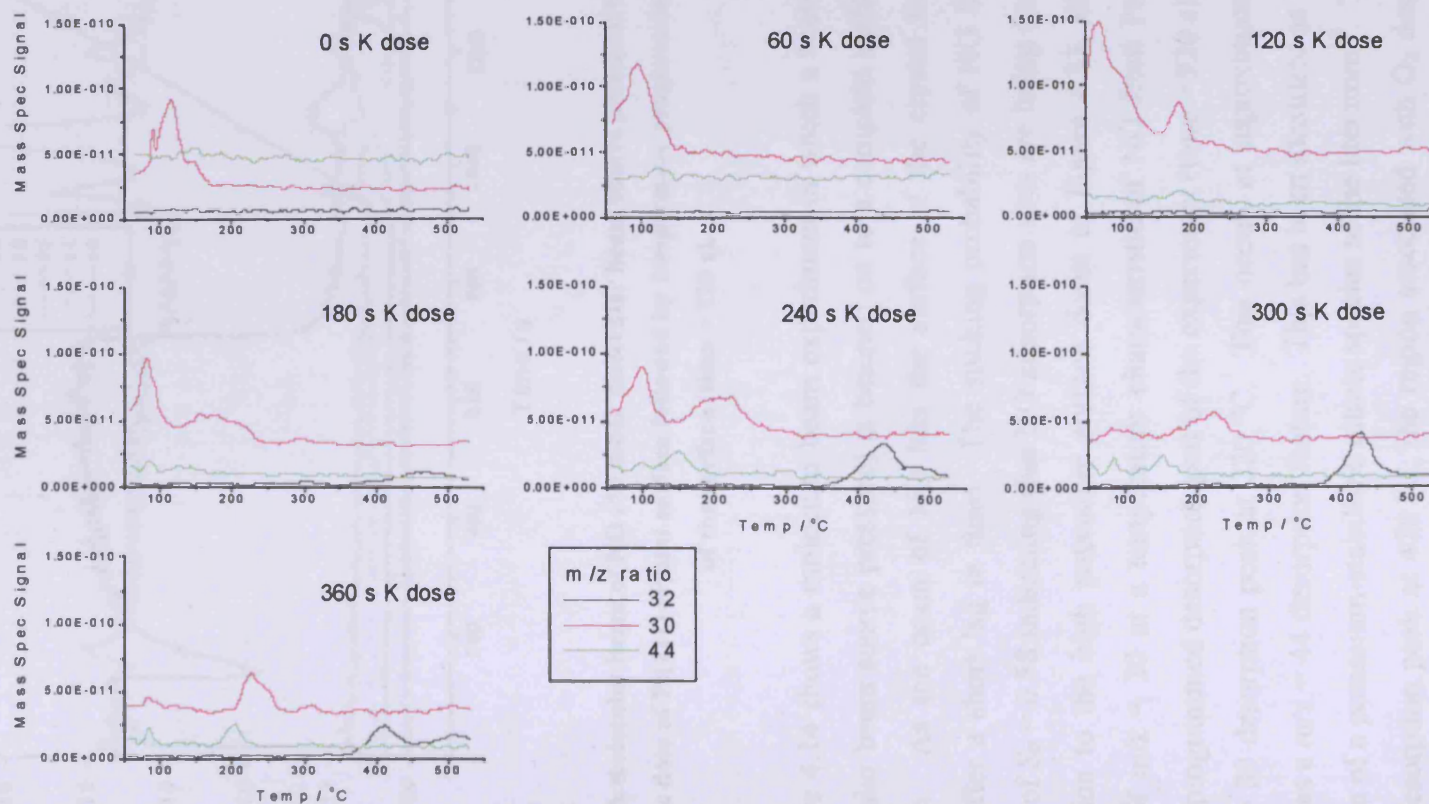


Figure 4.13 – Temperature programmed desorption of the crystal surface following the molecular beam experiments displayed in Figure 4.11. Note that $m/z = 28$ and 39 have been removed for clarity.

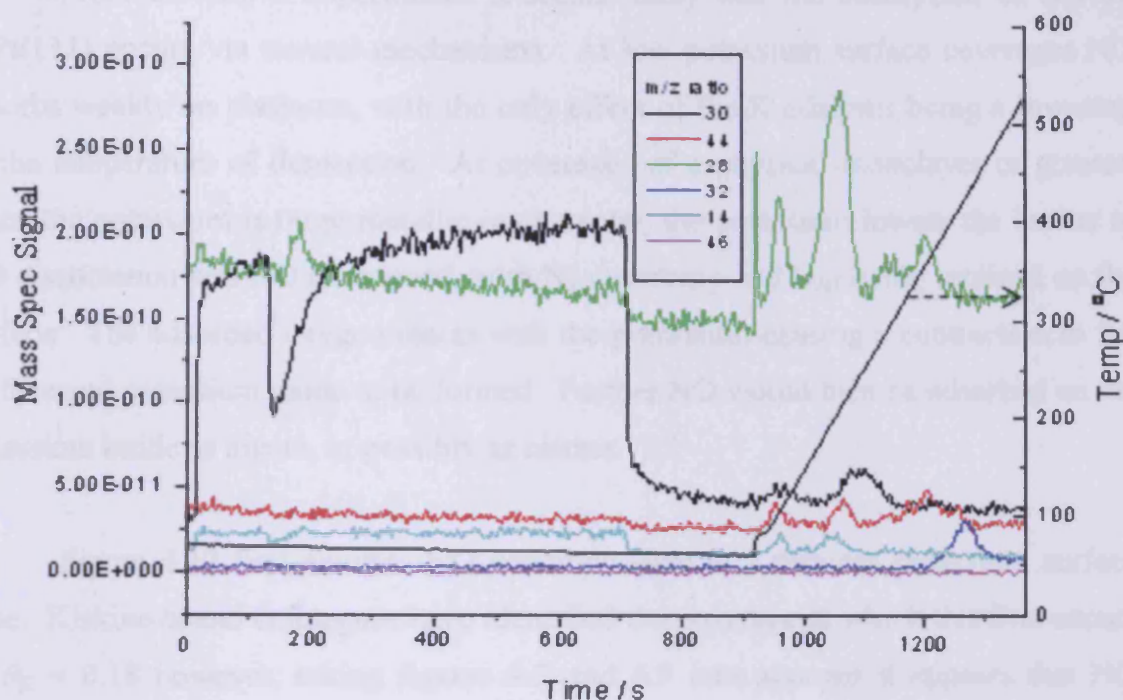


Figure 4.14 – A molecular beam of NO (50 mbar molecular beam source pressure) beamed onto 6 min K surface dose of Pt(111) crystal surface followed by temperature programmed desorption of the surface (time > 920 s).

Figure 4.14 shows a molecular beam experiment in which a beam of NO (50 mbar molecular beam source pressure) is beamed on to a complete surface coverage of potassium. As the beam of NO hits the surface of the crystal there is a N_2 desorption after a short lag in time. The sticking probability of NO falls from its initial value of $S_0 = 0.58$ indicating that NO adsorption sites are being occupied. In a similar fashion to the high potassium surface doses in Figure 4.13, there is some desorption of $m/z = 30$ at a temperature characteristic of NO from Pt(111) in the temperature programmed desorption part of the experiment (time > 920 s), but there is also a $m/z = 30$ desorption peak at 220 °C. This occurs at approximately the same temperature as a $m/z = 44$ desorption feature. This has been identified as being due to the formation of a potassium-stabilised nitrate species in the literature¹⁸. There is also an oxygen desorption peak at 420 °C, the region associated with O_2 desorbing from potassium carbonate (see figures 4.23, 4.25 and 4.27). The size of the $m/z = 28$ desorption peak at 195 °C makes it probable that this peak is due to the adsorption of CO from the background gases in the chamber over the whole crystal surface.

From the above experiments it seems likely that the adsorption of NO on K/Pt(111) occurs via several mechanisms. At low potassium surface coverages NO adsorbs weakly on platinum, with the only effect of the K adatoms being a lowering of the temperature of desorption. At coverages of a physical monolayer or greater, when the potassium is more metallic in character, the potassium lowers the barrier to NO dissociation and NO is reduced, with N₂ desorbing and O_(a) being retained on the surface. The adsorbed oxygen reacts with the potassium causing a contraction in the surface and potassium oxide to be formed. Further NO would then be adsorbed on the potassium oxide as nitrite, or possibly as nitrate.

Figure 4.12 first exhibits NO decomposition at 2 minutes potassium surface dose. Kiskinova and colleagues have identified the coverage at which this first occurs as $\theta_K = 0.18$ however, taking figures 4.3 and 4.9 into account it appears that NO decomposition occurs at nearer $\theta_K = 0.22$, assuming $\theta_K = 0.33$ at 3 minutes potassium surface dose (see sections 4.2.1-3)³⁶.

4.2.5 Molecular beams of NO on K/Pt(111) surface held at increasing surface temperature

Potassium was dosed onto surface for 2.5 minutes (roughly 5/6 of platinum surface covered by potassium assuming that 1 full layer of potassium ($\theta_K = 0.33$) has been deposited at 3 minutes surface dose) at 200 °C before the crystal was brought to the required temperature and NO (50 mbar molecular beam source pressure) beamed onto the surface.

As Figure 4.15 shows, the ability of the K/Pt(111) surface to dissociate NO is strongly temperature dependent. At 50 °C and 100 °C, NO binds to the surface with relatively high sticking probability ($S_0 = 0.5$ for 50 °C and 0.45 for 100 °C) and there is no sign of any immediate desorption features whilst beaming. When the temperature of the surface is raised to 150 °C however there are immediate $m/z = 44$ and 28 desorption peaks visible upon adsorption of NO onto the surface, likely due to the desorption of N₂O from the reduction of NO. At 200 °C the $m/z = 44$ desorption peak has disappeared and the $m/z = 28$ desorption peak has increased in size. The magnitude of the NO sticking has also decreased; this is likely to be due to the

temperature of the surface being above the desorption temperature of NO from K-Pt. As the temperature is increased further the $m/z = 28$ desorption peak decreases as a consequence of the reduction in NO sticking with increasing temperature.

The temperature programmed desorption data displayed in Figure 4.16 contains several features that aid clarification of the processes occurring in Figure 4.15. The temperature programmed desorption experiments with starting temperatures of 50 °C and 100 °C both show a $m/z = 30$ desorption peak at 85 °C resulting from the molecular desorption of NO from Pt(111), as well as a $m/z = 30$ desorption peak at approximately 200 °C, which must result from NO adsorbed on potassium. Both of these experiments also contain a $m/z = 44$ desorption peak at 95-120 °C, indicating that the $m/z = 44$ desorption peak present in the 150 °C molecular beam experiment in Figure 4.15 is from products that are present as adsorbed surface species in the lower temperature molecular beam experiments. The temperature programmed desorption experiments with initial starting temperatures of 50 °C and 100 °C also both show $m/z = 28$ desorption peaks below 150 °C, indicating that the products visible when beaming at 150 °C are present in an adsorbed surface state below this temperature. The experiments in Figure 4.16 that have starting temperatures below 200 °C also have a $m/z = 28$ desorption that occurs with a $m/z = 30$ desorption at 185-230 °C. This occurs with a $m/z = 14$ desorption (not shown) proving that the identity of the $m/z = 28$ species is nitrogen from the breakdown of surface species. The $m/z = 44$ desorption peak observed is probably due to the desorption of N₂O. All of the temperature programmed desorption experiments following the molecular beam experiments in which there is adsorption of NO show an O₂ desorption peak indicating that NO has been reduced by the surface; however the maximum of this desorption peak shifts to lower temperature with increasing surface dose. As the plot of the initial sticking probability against increasing surface temperature in Figure 4.15 shows, the sticking decreases slowly with increasing surface temperature up to 250 °C, where after it falls off rapidly until no sticking is observed for the surface held at 350 °C.

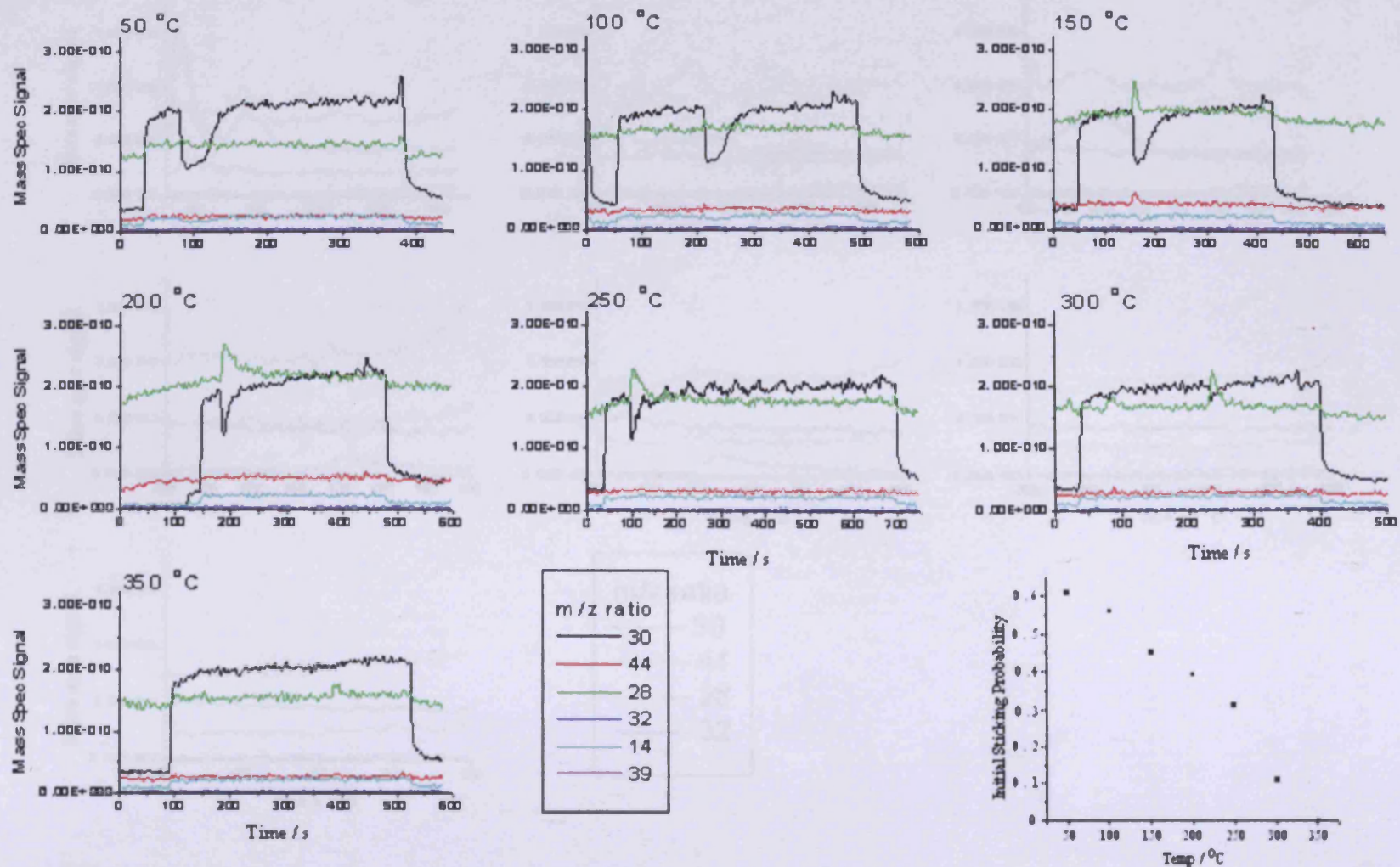


Figure 4.15 – Molecular beams of NO (50 mbar molecular beam source pressure) beamed onto 2.5 min K dosed Pt(111) held at increasing surface temperatures.

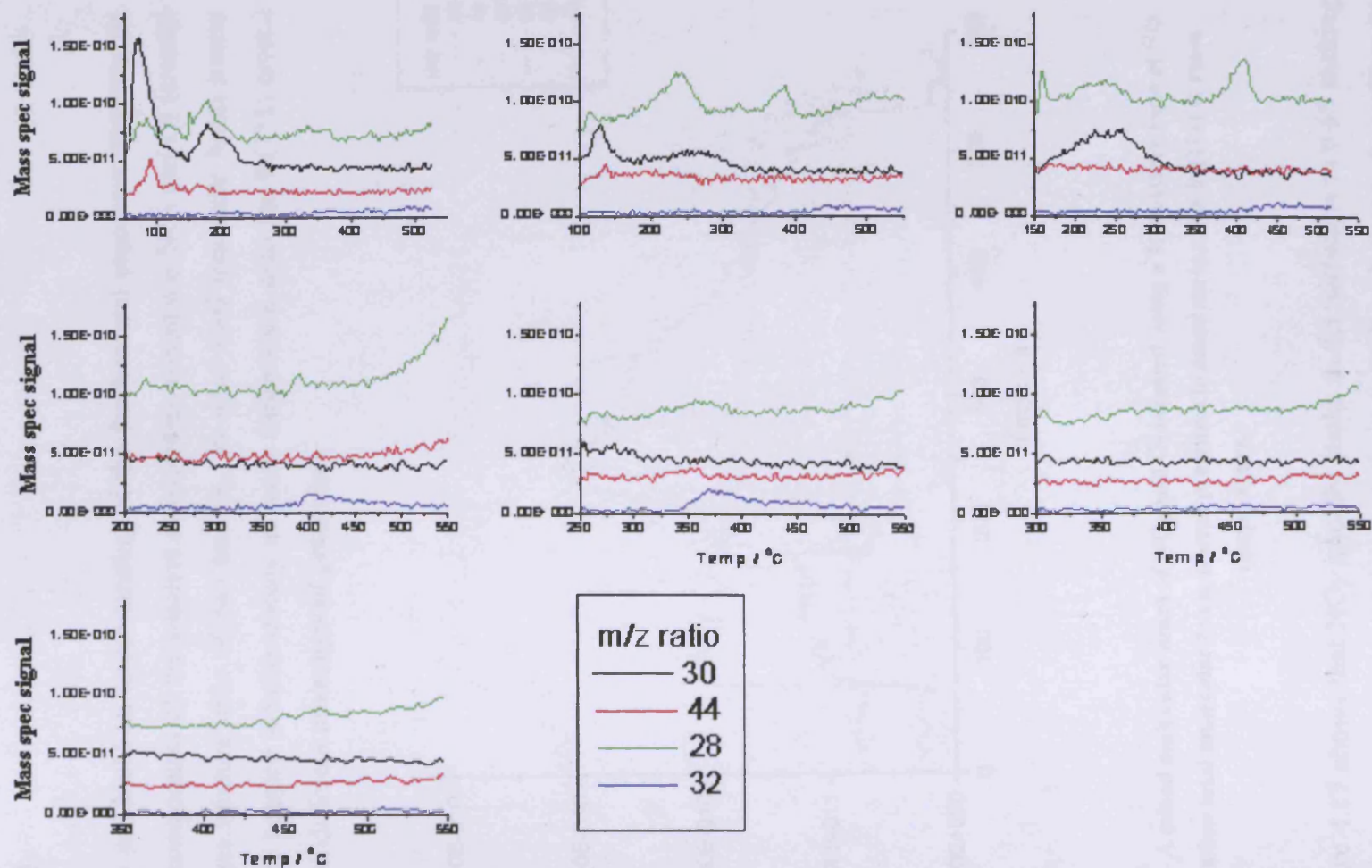


Figure 4.16 – Temperature programmed desorption of the crystal surface following the molecular beam experiments shown in Figure 4.15. Note that $m/z = 28$ trace has been reduced by a factor of 2 as a visual aid.

4.2.6 Mixed molecular beams of NO₂ and O₂ on different K coverages on the Pt(111) surface

Clean Pt(111)

To try and build an understanding of the fundamental processes occurring on the separate components of the catalyst in oxidising conditions NO₂ and O₂ (created using a 1:1 gas mixture ratio of NO and O₂, 50 mbar total molecular beam source pressure) were beamed simultaneously at room temperature onto the Pt(111) crystal pre-dosed with different coverages of potassium.

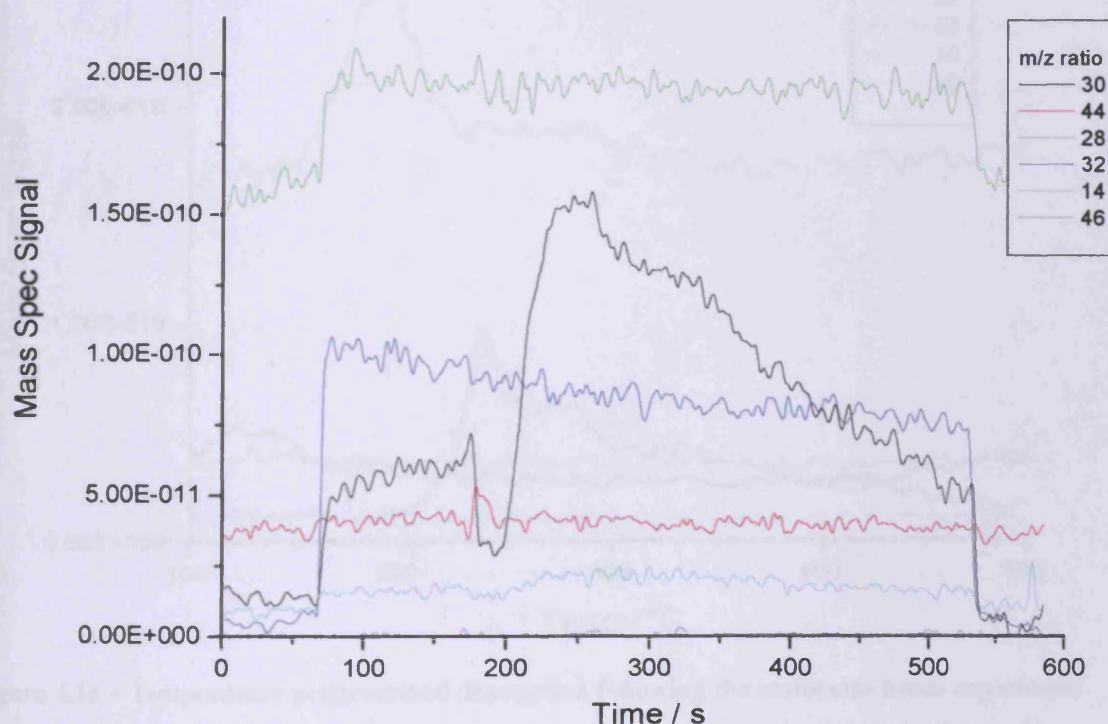


Figure 4.17 – A mixed molecular beam of NO₂ and O₂ (created using a 1:1 mixture ratio of NO and O₂, 50 mbar total molecular beam source pressure) beamed on to clean Pt(111) at room temperature.

Figure 4.17 shows that NO₂ initially sticks to the surface with 0.65 sticking probability. However, after an initial period, the m/z = 30 peak rises to three times its initial value. In concert with this rise there is an increase in the m/z = 14 peak. There is no apparent O₂ sticking and no changes in m/z = 46, 44 or 28 are obvious. This is

identical to the experiments shown in chapter 3 that prove that NO has reacted with O_2 in the gasline to form NO_2 . Therefore it is a mixture of NO_2 and O_2 that is being beamed on to the crystal surface (as equal pressures of NO and O_2 were used the mixture dosing the crystal was therefore 2 NO_2 : 1 O_2). The large rise in the $m/z = 30$ signal is a result of NO_2 being broken down and liberating NO and atomic oxygen, which adsorbs on to the crystal surface displacing adsorbed NO (although mass 30 is a cracking fragment of NO_2 , $m/z = 30$ is the molecular ion of NO, hence why the rise is $m/z = 30$ signal at 200 s is so large).

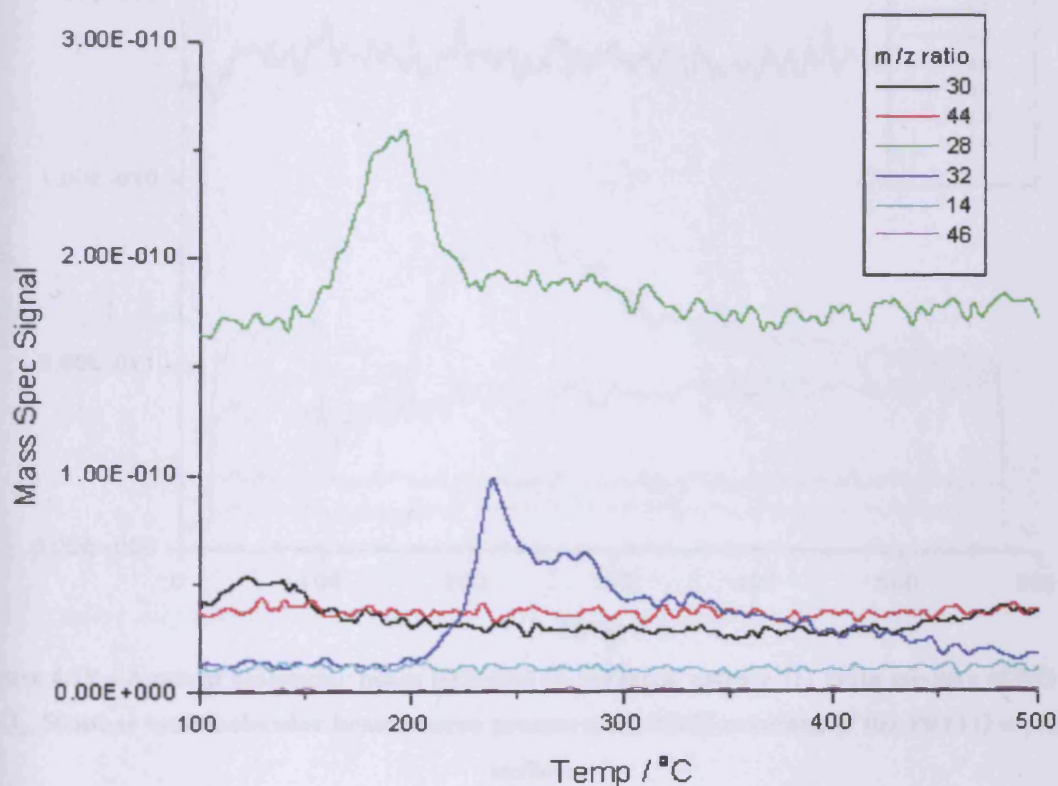


Figure 4.18 – Temperature programmed desorption following the molecular beam experiment shown in Figure 4.17. A temperature ramp of 1 K/s was used in the above figure.

Figure 4.18 shows a small $m/z = 30$ desorption peak at 125 °C, characteristic of NO desorbing from Pt(111)(see chapter 3), a large $m/z = 28$ desorption peak at 190 °C, characteristic of CO desorbing from Pt(111)(likely due to adsorption of background CO from background gases in the chamber), a sharp $m/z = 32$ desorption peak at 240 °C and another $m/z = 32$ desorption peak at 280 °C present as a shoulder on the larger desorption peak, due to O_2 desorbing from the Pt(111) surface. No other desorption peaks are evident.

Intermediate K surface dose

K was dosed onto surface for two minutes (roughly 2/3 of the platinum surface covered by potassium) and O_2 and NO_2 (created by using a NO/O_2 mixture, as described in chapter 3) beamed simultaneously (1:1 pressure ratio mixture, 50 mbar total molecular beam source pressure used).

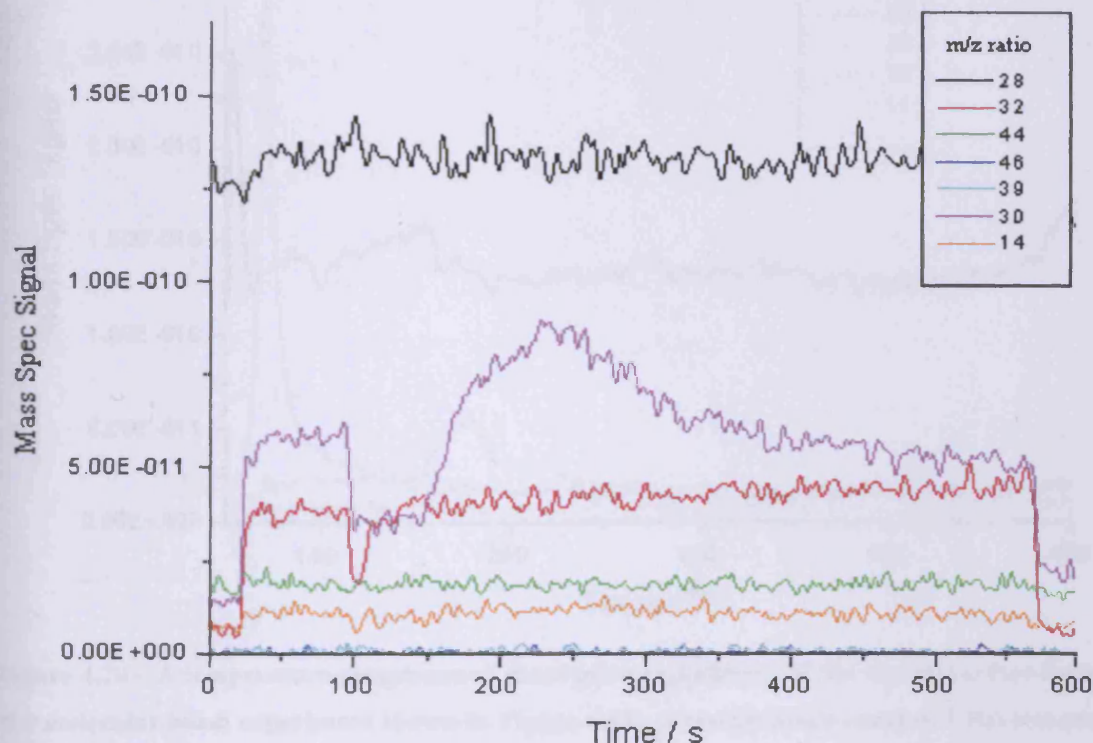


Figure 4.19 – A mixed molecular beam NO_2 and O_2 (created using a 1:1 ratio mixture of NO and O_2 , 50 mbar total molecular beam source pressure) on 2/3 K coverage of the $Pt(111)$ crystal surface.

The results of the mixed beam experiment displayed in Figure 4.19 appear similar to that shown in Figure 4.17, with initial sticking of $m/z = 30$ followed by a large $m/z = 30$ desorption peak. The magnitude of the $m/z = 30$ desorption peak is much less than seen in Figure 4.17. There is also adsorption of O_2 from the beam; however the O_2 adsorbs for a much shorter time period than the NO_2 (note that the pressure of O_2 is half that of the NO_2 in the beam). There is no desorption of nitrogen, which is to be expected as Figure 4.12 demonstrates that only potassium coverages of a monolayer or greater are capable of reducing NO . It is possible that what is occurring above is oxygen adsorbing on the potassium and NO_2 dissociatively adsorbing on the platinum in two separate reactions, or that NO_2 is reacting with

oxygen from the potassium-promoted dissociative adsorption of oxygen and dissociative adsorption of NO_2 , to form nitrate. The temperature programmed desorption after the experiment shown in Figure 4.19 is given below.

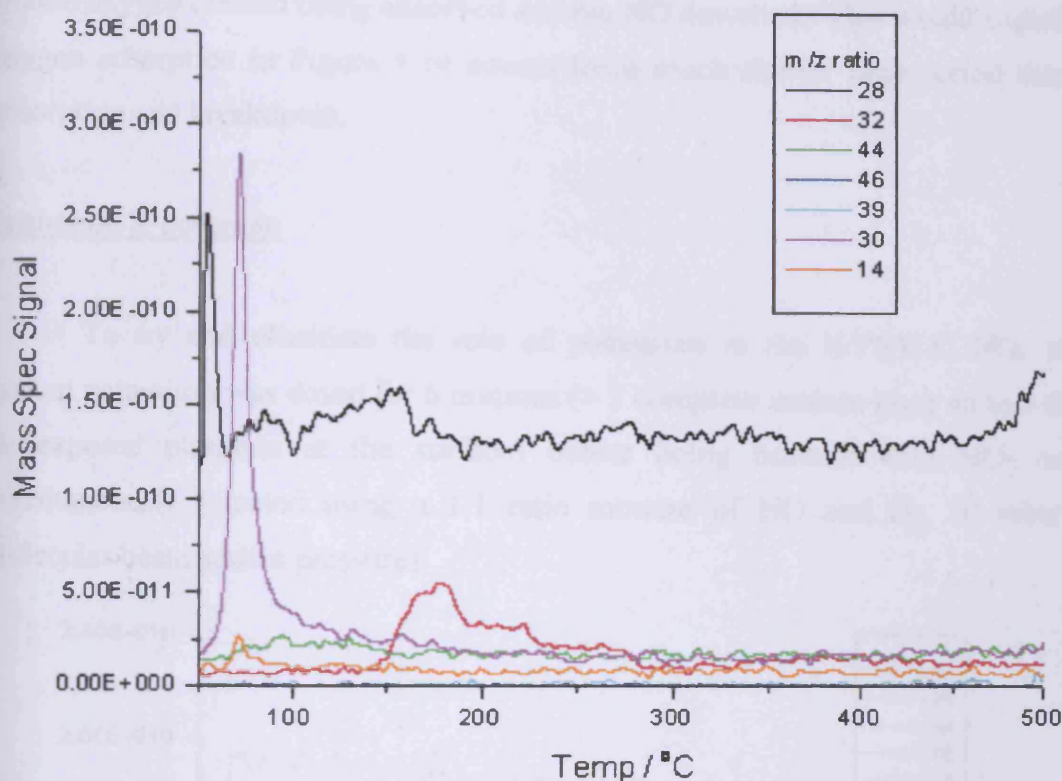


Figure 4.20 – A temperature programmed desorption experiment of the crystal surface following the molecular beam experiment shown in Figure 4.19. A temperature ramp of 1 K/s was used in the above figure.

Figure 4.20 is very similar to the temperature programmed desorption experiment shown in Figure 4.18. There is an initial sharp peak of $m/z = 30$ at the onset of heating, likely due to NO from Pt(111) sites, as well as a sharp $m/z = 28$ peak from flash desorption from the heater filaments. There is a small broad $m/z = 28$ peak occurring 120-155 °C, however this is smaller in magnitude than the corresponding CO-Pt(111) desorption feature in Figure 4.18 due to the correspondingly smaller area of free Pt(111) available for adsorption of background gases from the chamber. There is a $m/z = 32$ desorption peak at 170 °C with a shoulder at 210 °C in a similar manner to the oxygen desorption peaks seen in Figure 4.18; however the oxygen desorption peaks occur at a lower temperature for this potassium coverage. There is no high-temperature oxygen desorption peak (associated with potassium oxide species) visible. There is however a small, broad $m/z = 44$ desorption peak at 100 °C, possibly

as a result of NO_2^- breakdown to N_2O as shown earlier. A more likely explanation is that the adsorbed NO might react with oxygen that has adsorbed from the beam on to the potassium and forms NO_2 , which then breaks down on the platinum with the atomic oxygen created being adsorbed and the NO desorbed. This would explain why oxygen adsorption in Figure 4.19 occurs for a much shorter time period than NO_2 adsorption and breakdown.

Saturation K coverage

To try and elucidate the role of potassium in the K/Pt(111) NO_x storage system potassium was dosed for 6 minutes (> 1 complete surface layer so that there is no exposed platinum at the surface) before being beamed with NO_2 and O_2 simultaneously (created using a 1:1 ratio mixture of NO and O_2 , 50 mbar total molecular beam source pressure).

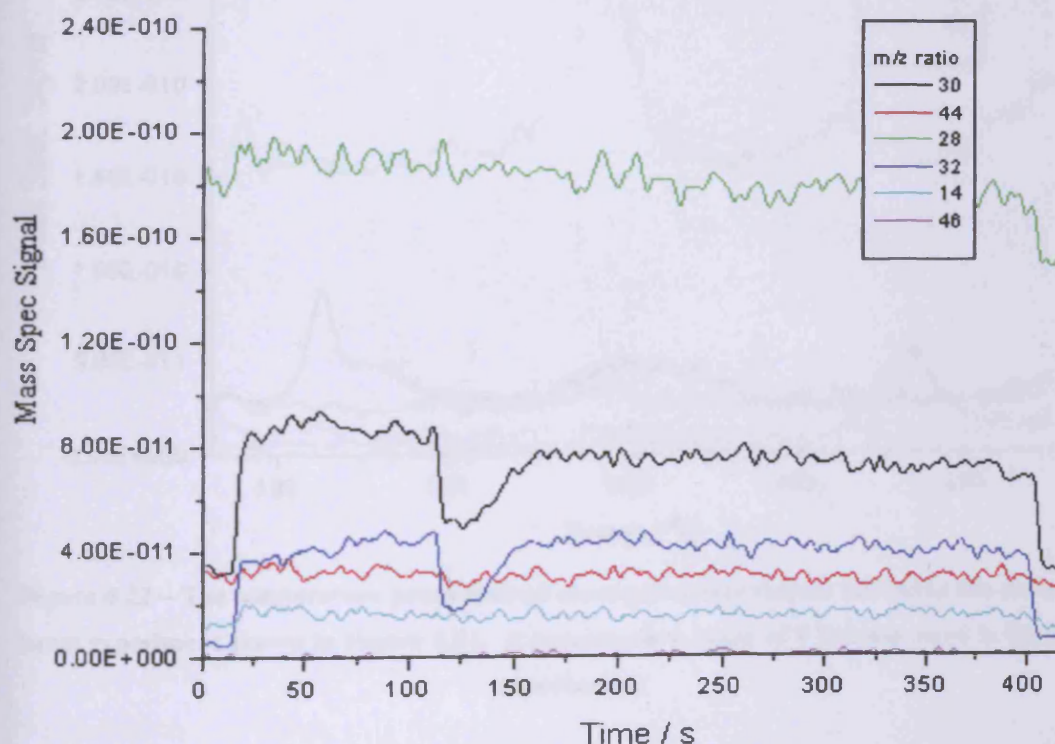


Figure 4.21 - Mixed molecular beam of NO_2 and O_2 (created using a 1:1 mixture ratio of NO and O_2 , 50 mbar total molecular beam source pressure) beamed on to 6 min K surface dose.

In the above molecular beam experiment both NO_2 and O_2 stick well with initial sticking coefficients of 0.65 and 0.64 respectively. However, unlike the previous two molecular beam experiments (Figure 4.17 and Figure 4.19) there is no

large $m/z = 30$ desorption peak as beaming continues, indicating that NO_2 is being adsorbed and not broken down by the surface. There are no desorption products visible whilst beaming which, when compared with Figure 4.14 indicates that NO_2 has not been broken down, since more than a monolayer of potassium reduces NO with the instantaneous desorption of N_2 (see Figure 4.12). The enhanced stability of adsorbed NO_2 species gained when dosing onto a potassium covered surface, as opposed to clean Pt(111) alone has been noted in the literature. This enhanced stability has been explained as being due to the increased back-donation of electrons from the potassium into a $6a_1$ molecular orbital on the NO_2 . Evidence is provided that the species formed is potassium nitrate, KNO_3 .¹⁸

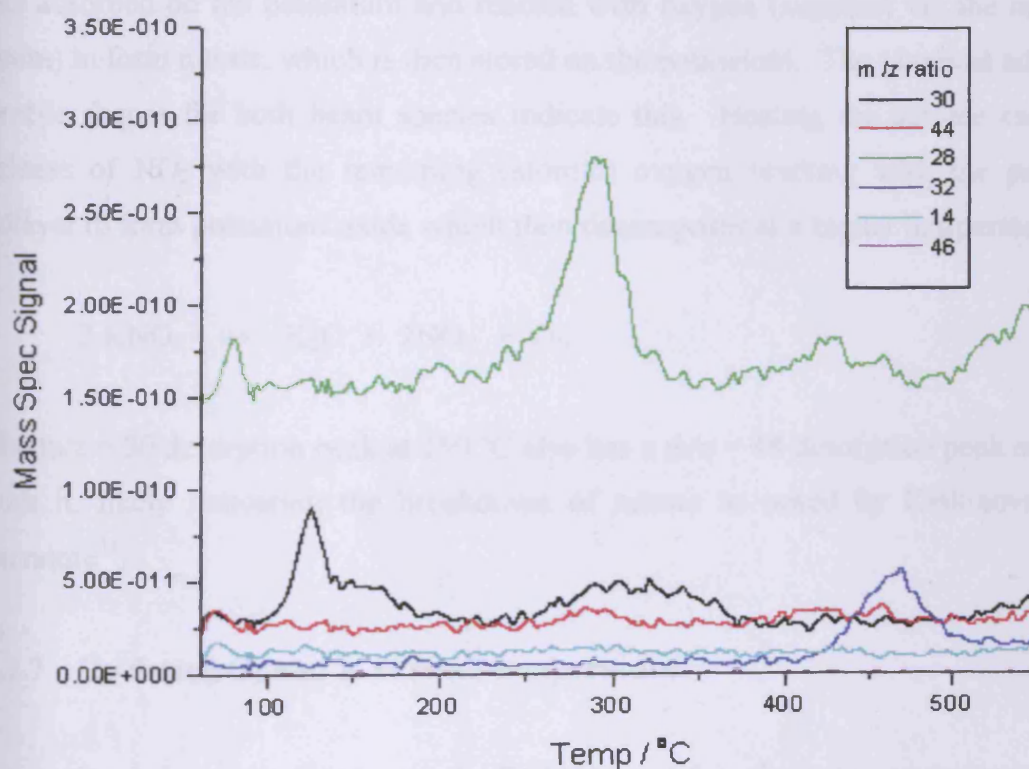
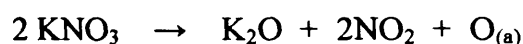


Figure 4.22 – The temperature programmed desorption experiment following the molecular beam experiment shown in Figure 4.21. A temperature ramp of 1 K/s was used in the above experiment.

Figure 4.22 shows the products of the molecular beam experiment shown in Figure 4.21. This figure contains several desorption features that are absent in previous temperature programmed desorption experiments (Figure 4.18 and Figure 4.20) indicating that metallic potassium is essential for this reactive behaviour. There is a sharp desorption peak of $m/z = 30$ at 130 °C and as well as a small broad

desorption peak at 250-320 °C. At 290 °C a $m/z = 28$ desorption peak is evident. There is also a $m/z = 32$ desorption peak at 450 °C. The $m/z = 32$ desorption peak is at a temperature characteristic of the desorption of oxygen from potassium oxide (see Figure 4.10 and Figure 4.33). Taking into account the contraction of the overlayer associated with potassium oxide formation, it is possible that the identity of the low temperature $m/z = 30$ desorption peak is NO (adsorbed on Pt(111) exposed from formation of potassium oxide) from the breakdown of NO₂ or adsorbed NO₂ itself. However NO₂ desorbing would be expected to give a $m/z = 46$ signal, which does not occur in the above temperature programmed desorption experiment. A more likely explanation however, as indicated by the similar desorption peak integrals, is that NO₂ has adsorbed on the potassium and reacted with oxygen (supplied via the molecular beam) to form nitrate, which is then stored on the potassium. The identical adsorption profile shapes for both beam species indicate this. Heating the surface causes the release of NO₂ with the remaining (atomic) oxygen reacting with the potassium adlayer to form potassium oxide which then decomposes at a higher temperature ie.



The $m/z = 30$ desorption peak at 250 °C also has a $m/z = 44$ desorption peak occurring with it, likely indicating the breakdown of nitrate as noted by Kiskinova in the literature³⁴.

4.2.7 Co-dosing O₂ and K at room temperature

Potassium was dosed onto the Pt(111) crystal surface at room temperature for five minutes (greater than a complete surface coverage of potassium or the contracted potassium oxide layer described in the literature¹⁰ assuming $\theta_{\text{K}} = 0.33$ at three minutes potassium dose as shown in figures 4.3, 4.6, 4.7 and 4.9) with differing background pressures of O₂.

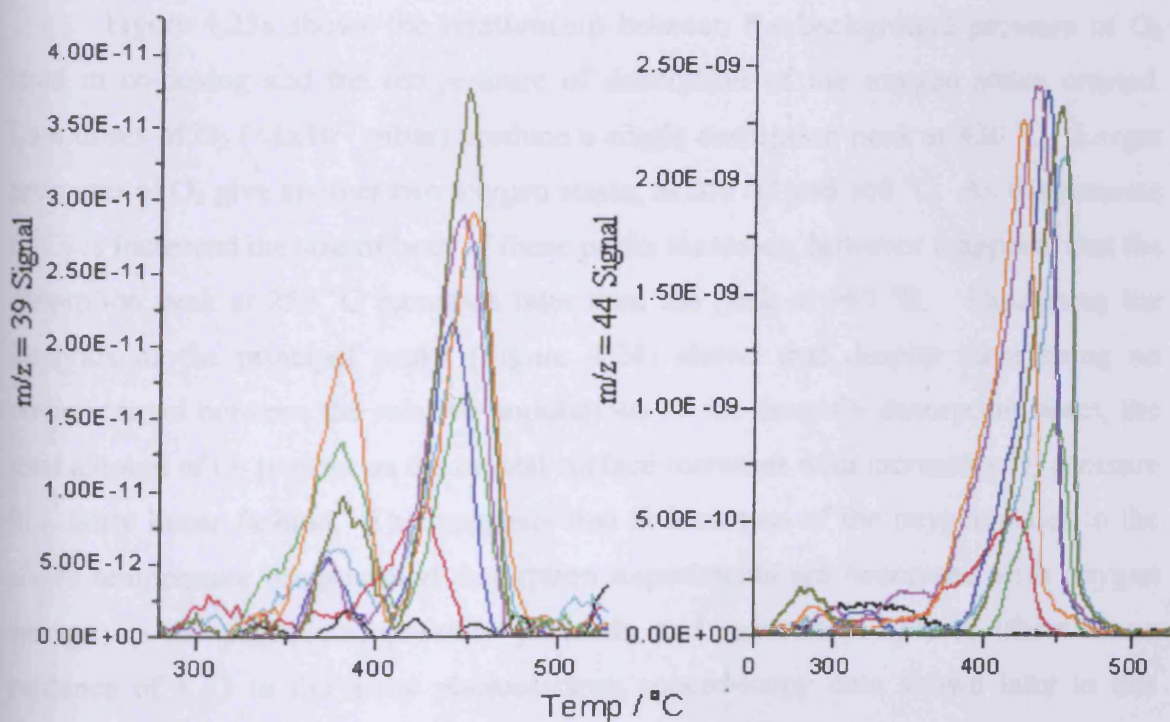
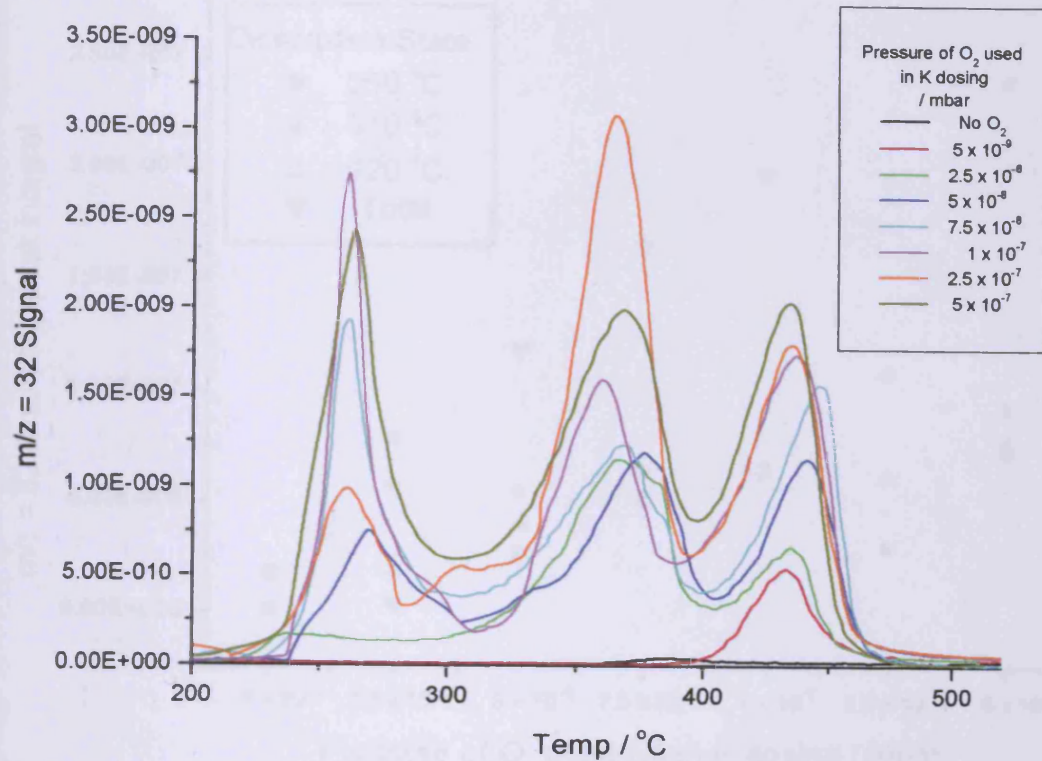


Figure 4.23 – The desorption of O_2 (a, top), K (b, bottom left) and CO_2 (c, bottom right) from K_2O_2/K_2CO_3 layer formed at room temperature.

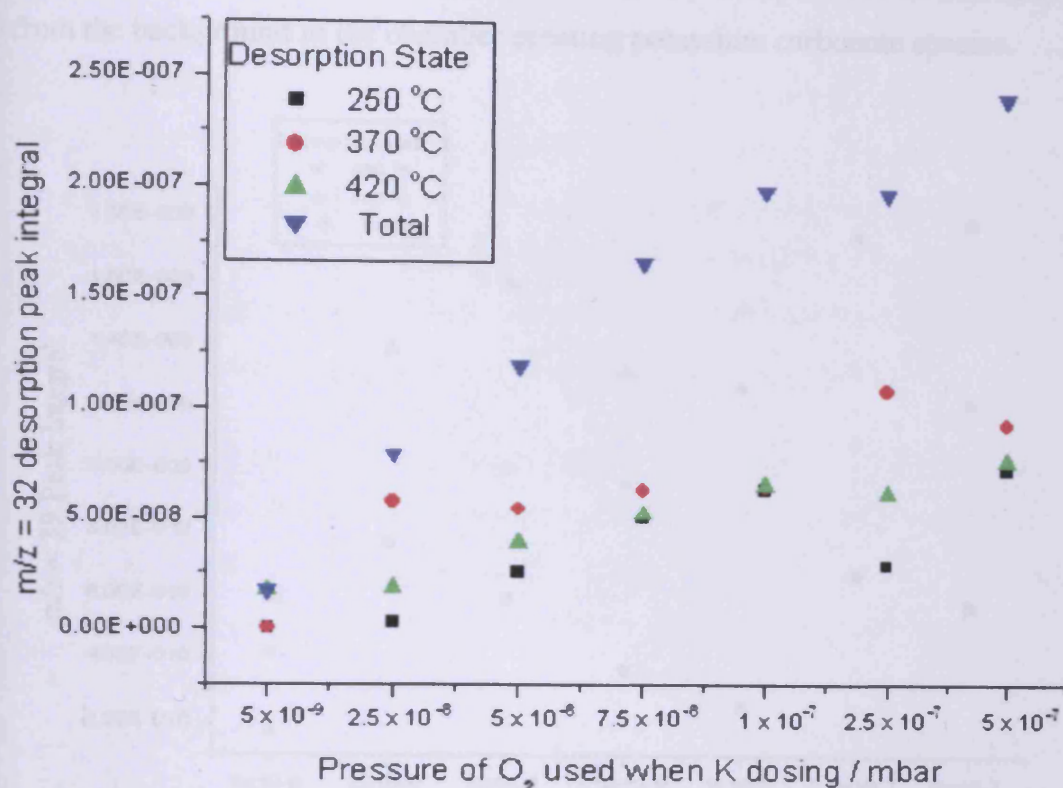


Figure 4.24 - The relative populations of each O₂ desorption state.

Figure 4.23a shows the relationship between the background pressure of O₂ used in co-dosing and the temperature of desorption of the oxygen states created. Low doses of O₂ ($<1 \times 10^{-8}$ mbar) produce a single desorption peak at 430 °C. Larger pressures of O₂ give another two oxygen states, at 250 °C and 360 °C. As the pressure of O₂ is increased the size of both of these peaks increases; however it appears that the desorption peak at 250 °C increases later than the peak at 360 °C. Examining the integrals of the principal peaks (Figure 4.24) shows that despite there being no obvious trend between the relative populations of the three O₂ desorption states, the total amount of O₂ present on the crystal surface increases with increasing O₂ pressure in a fairly linear fashion. This suggests that at least two of the oxygen states in the above temperature programmed desorption experiments are concerned with oxygen storage on the potassium, possibly peroxide and superoxide species (there is no evidence of K₂O in the x-ray photoelectron spectroscopy data shown later in this section and this has been confirmed in the literature¹⁰), with the superoxide being favoured at higher oxygen pressures. The fact that there is no clear trendline

however, suggests a random factor in the creation of the layer such as adsorption of CO from the background in the chamber creating potassium carbonate species.

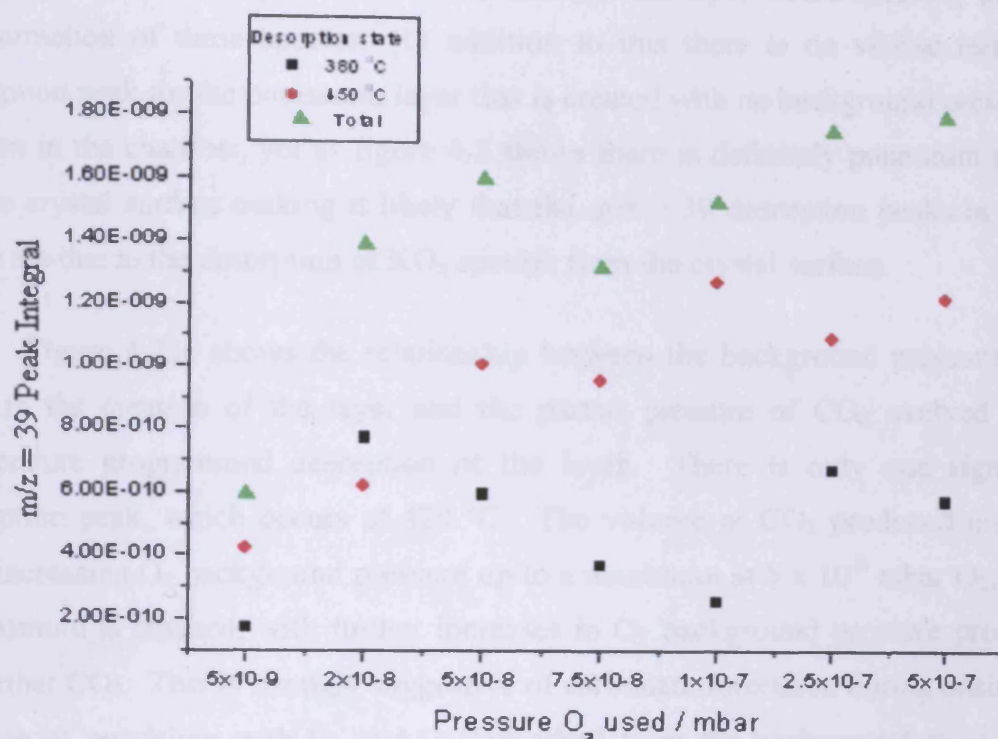


Figure 4.25 – The relative populations of each K desorption state.

Figure 4.23b shows the relationship between the background pressure of O₂ used in co-dosing and the temperature of desorption of the potassium states created. The main desorption peak appears at 450 °C and this peak grows in size with increasing O₂ pressure. This desorption peak is present for all oxygen pressures. At higher pressures of O₂ ($< 1 \times 10^{-8}$ mbar) another desorption peak becomes evident at lower temperature (~ 370 -380 °C). The size of this peak also grows with increasing potassium dose. It is apparent from the integrals of the potassium desorption peaks (Figure 4.25) that the total amount of potassium that is detected increases with increasing O₂ pressure used in co-dosing. Possible loss of potassium into the bulk during the initial stages of the deposition is not a factor for these experiments as the coverage used is greater than the coverage at which migration from sub-surface to surface sites occurs.^{8,9} It is possible that co-dosing oxygen with potassium enables the formation of an oxide of potassium that can saturate to a greater coverage than potassium alone or that co dosing with oxygen allows the formation of a more compressed surface state that enables more potassium to be 'packed into' the surface

in a potassium-oxygen bilayer. An alternative explanation is that the species being detected are K_2O_2 and K_2CO_3 that are desorbing from the surface. Increasing the background pressure of gas used in the creation of the layer would naturally promote the formation of these species. In addition to this there is no visible $m/z = 39$ desorption peak for the potassium layer that is created with no background pressure of oxygen in the chamber, yet as figure 4.3 shows there is definitely potassium present on the crystal surface making it likely that the $m/z = 39$ desorption peaks in Figure 4.23b are due to the desorption of KO_x species from the crystal surface.

Figure 4.23c shows the relationship between the background pressure of O_2 used in the creation of the layer and the partial pressure of CO_2 evolved in the temperature programmed desorption of the layer. There is only one significant desorption peak, which occurs at 420 °C. The volume of CO_2 produced increases with increasing O_2 background pressure up to a maximum at 5×10^{-8} mbar O_2 , where a maximum is reached, with further increases in O_2 background pressure producing no further CO_2 . This is strongly suggestive of carbonate formation during dosing, via reaction of potassium with O_2 and CO adsorbed from the background gases in the chamber. The limit on the volume of CO_2 that is desorbed from the surface with increasing surface potassium coverage in Figure 4.23c is hence due to the low background pressure of CO in the chamber limiting the amount of carbonate that can be formed. When Figure 4.23a, b and c are examined together it is apparent that many of the desorption peaks for different species occur at the same temperature, suggesting decomposition of surface species with desorption of the products. There is a high temperature desorption peak 420-450 °C that is present for all pressures in the temperature programmed desorption experiments suggesting that the species which decomposes and desorbs is potassium carbonate, K_2CO_3 . That this species forms in these series of experiments (Figure 4.23) and not in the earlier temperature programmed desorption experiment (Figure 4.7) suggests that CO is adsorbed on platinum or potassium oxide and reacts with potassium oxide to form carbonate. There is also a desorption peak in both the K and O_2 set of temperature programmed desorption experiments at 360-370 °C, suggesting the decomposition of potassium peroxide, K_2O_2 (see section 4.2.10). That this desorption of O_2 from K_2O_2 occurs at a higher temperature than seen previously (Figure 4.10) is likely due to enhanced stability associated with oxidising the complete surface coverage as opposed to just

the top surface layer. The lower temperature O₂ desorption in the temperature programmed desorption experiment is likely due to O₂ desorbing from Pt(111). The existence of oxygen in two separate environments, one associated with platinum and one with potassium, when adsorbing oxygen on a monolayer of potassium (where 1 ML equates to $\theta = 0.33$) has been noted by Pirug and colleagues, who ascribe the availability of the platinum environment to a contraction of the potassium layer in which the local potassium density rises from $\theta = 0.33$ to $\theta = 0.44$.¹⁰

An interesting feature in Figure 4.23b is that increasing the background pressure of oxygen appears to increase the amount of potassium adsorbed onto the surface. It is possible that this is due to the formation of a potassium oxide with a smaller unit cell, enabling more potassium to be 'packed into' the surface or that, as claimed by Somorjai and Garfunkel¹², multilayer formation of potassium is not possible on Pt(111) at room temperature, but it is possible to form more than a monolayer of potassium peroxide (or carbonate), trapping the extra potassium into multilayers. An alternative explanation could be that it is the desorption of potassium peroxide/carbonate that gives rise to the $m/z = 39$ desorption peaks in figure 4.23b. The fact that there are no desorption peaks visible when K dosing in the absence of oxygen in figure 4.23b adds weight to this alternative explanation. It is important to note that the impurity of the adlayer will have to be addressed in future experiments as it could potentially introduce complications into results.

The form of the potassium oxide species was examined using x-ray photoelectron spectroscopy on a separate ultrahigh vacuum system in collaboration with F. Grillo at Cardiff University.

0.4 ML (30 s dose)(where 1 ML = 1 K atom : 1 Pt atom) (calculated using atomic sensitivity factors and the relative ratios of potassium and oxygen integrals) was deposited onto the Pt(111) surface at room temperature both in vacuum and in the presence of O₂ (5×10^{-8} mbar). In both cases it was found that the potassium was present on the surface in oxidised form (a binding energy of 293.4 eV was recorded for the K 2p_{3/2} peak, compared to the 294.4 eV expected for pure potassium). It was found that when dosing potassium up to 120 s dose that the potassium was still present as K⁺ when being dosed in the vacuum, as well as in a background pressure of

O_2 (5×10^{-8} mbar). It is therefore evident that potassium deposited in vacuum is reacting with residual gases in the background of the chamber, possibly forming carbonate as evidenced in Figure 4.23 and the XPS below.

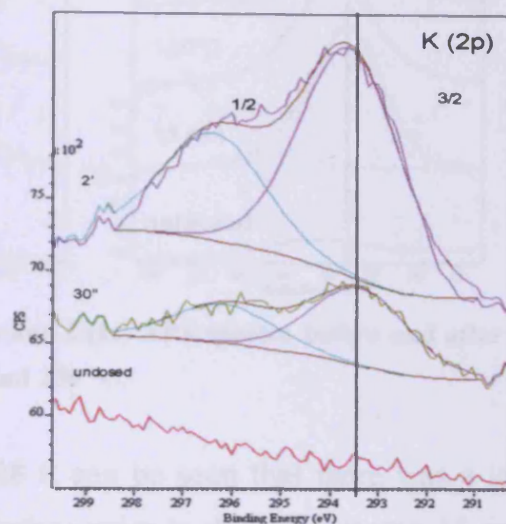


Figure 4.26 - K(2p) XPS spectra with peak fitting of clean Pt(111), and crystal surface after 30 s and 120 s of dosing K in 5×10^{-8} mbar O_2 . Spectra are offset for clarity.

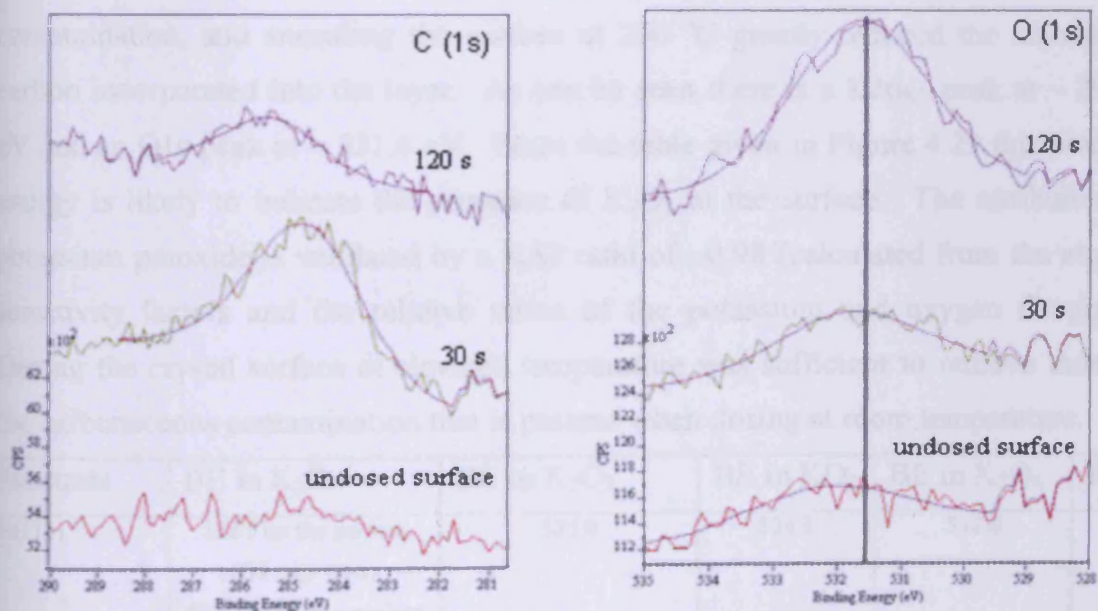


Figure 4.27 - C(1s) and O(1s) XPS spectra of clean Pt(111), and crystal surface after 30 s and 120 s of dosing K in 5×10^{-8} mbar O_2 . Spectra are offset for clarity.

To examine the effect of annealing potassium surfaces were created by dosing for 15 minutes onto the crystal surface held at $50^\circ C$ with 2×10^{-8} mbar O_2 background pressure and then annealing at both $150^\circ C$ and $250^\circ C$.

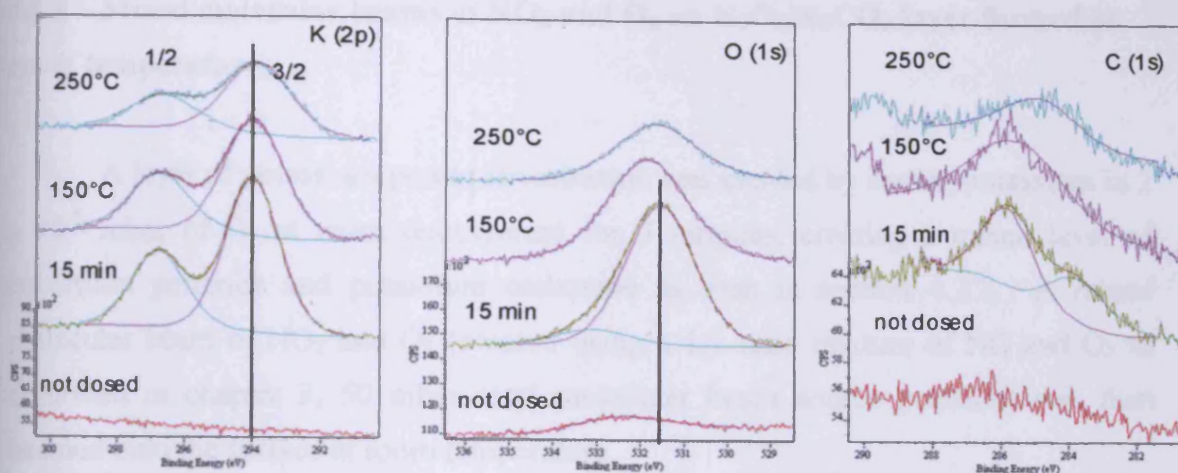


Figure 4.28 - K(2p), O(1s) and C(1s) XPS spectra before and after 15 minutes of K dosing and after annealing at 150 °C and 250 °C.

From Figure 4.28 it can be seen that there was a low level of carbonaceous contamination on the surface prior to dosing. Dosing 15 minutes of potassium in an oxygen atmosphere gave a large C1s peak in the recorded spectrum. However annealing the surface at 150 °C after dosing reduced the level of carbonaceous contamination, and annealing the surface at 250 °C greatly reduced the amount of carbon incorporated into the layer. As can be seen there is a K2p_{3/2} peak at ~ 294.0 eV and an O1s peak at ~ 531.6 eV. From the table given in Figure 4.29 this binding energy is likely to indicate the presence of K₂O₂ at the surface. The attribution to potassium peroxide is validated by a K/O ratio of ~0.98 (calculated from the atomic sensitivity factors and the relative ratios of the potassium and oxygen integrals). Dosing the crystal surface at elevated temperature was sufficient to remove most of the carbonaceous contamination that is present when dosing at room temperature.

Substrate	BE in K ₂ O	BE in K ₂ O ₂	BE in KO ₂	BE in K ₂ O ₃	Ref
Si(111)	528.3 on the surface (O ₂ exp < 4L) 527.2 under the surface (O ₂ exp > 4L)	531.0	534.3	532.0	46
Diamond (100)		531.1	534.3	534.2	47
		531.4 low coverage	534.2 high coverage		48
Ni(100)	529.5				49
NiO + K on Ag(100)	529.6	532.2	534.0		50

Figure 4.29 – The Binding Energy of O(1s) peak in different K compounds prepared on different substrates

4.2.8 Mixed molecular beams of NO₂ and O₂ on K₂O₂/K₂CO₃ layer formed at room temperature

A layer of potassium peroxide/carbonate was created by dosing potassium in 2×10^{-8} mbar of O₂ at room temperature for 5 minutes, creating a mixed layer of potassium peroxide and potassium carbonate as seen in section 4.2.7. A mixed molecular beam of NO₂ and O₂ (created using a 1:1 ratio mixture of NO and O₂ as described in chapter 3, 50 mbar total molecular beam source pressure) was then beamed onto the surface at room temperature.

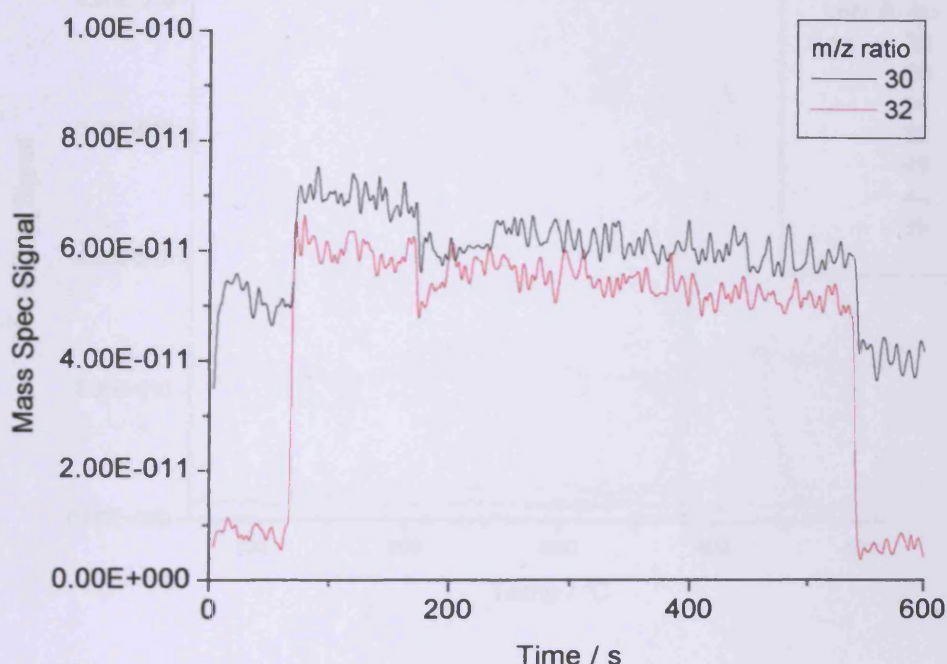


Figure 4.30 - A mixed molecular beam of NO₂ and O₂ (created using a 1:1 gas mixture ratio of NO and O₂, 50 mbar total molecular beam source pressure) on potassium peroxide/carbonate surface formed at room temperature.

The above molecular beam experiment shows that NO₂ and O₂ both stick moderately well with initial sticking probabilities of approximately 0.2 and 0.3 respectively. This represents an enhancement in the sticking of O₂ and a decrease in the sticking probability of NO₂ with regards to the clean Pt(111) surface or a decrease in initial sticking coefficient for both species with regards to the equivalent surface dose on clean potassium. That the beam of O₂ adsorbs is not surprising as the lower temperature desorption peak in Figure 4.23a appears for oxygen coverages greater

than were used in the creation of the layer used in the above experiment, making it likely that the oxygen from the beam has adsorbed on the platinum. No desorption products are obvious in the reaction indicating that NO_2 breakdown in a similar manner to the earlier Figure 4.17 and Figure 4.19 has not occurred. If one examines the mixed molecular beam scattering experiment shown in Figure 4.32 it is apparent that the O_2 from the mixed molecular beam has not adsorbed on the (identically created) layer. This strongly suggests that a surface reaction between NO_2 and O_2 has occurred in Figure 4.30.

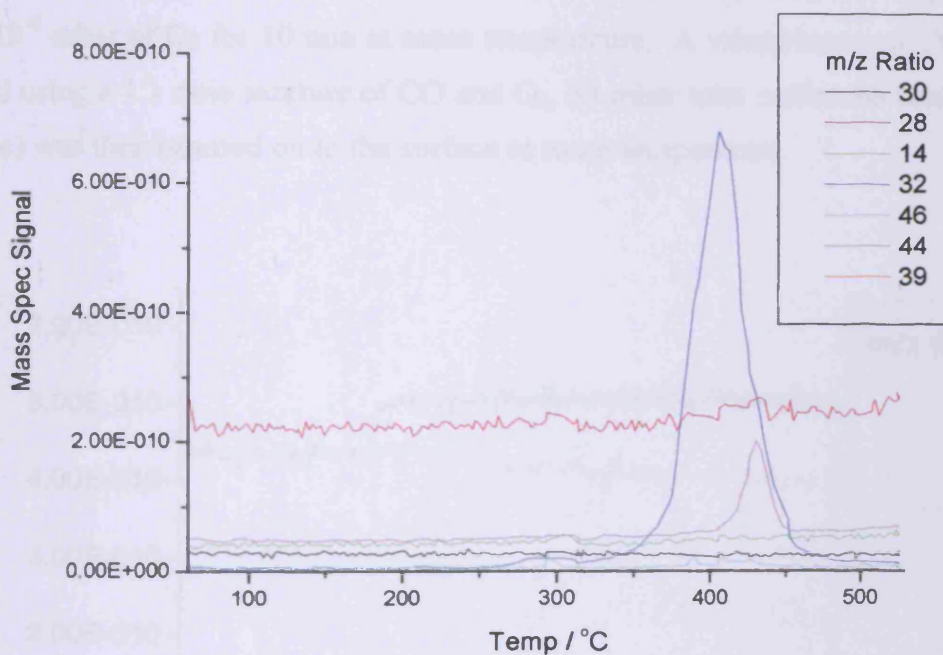


Figure 4.31 – Temperature programmed desorption of the crystal surface following the molecular beam experiment shown in Figure 4.30.

Figure 4.31 shows the temperature programmed desorption experiment after the molecular beam experiment displayed in Figure 4.30. There is a single broad $m/z = 32$ desorption peak present at 410 °C and a single, small $m/z = 44$ peak at 435 °C. There are no other desorption peaks in evidence. Correlating the oxygen and CO_2 desorptions with the earlier temperature programmed desorption experiments (Figure 4.23a and Figure 4.23c) it appears that these species are from the desorption of the surface $\text{K}_2\text{O}_2/\text{K}_2\text{CO}_3$ layer. It therefore appears as if the NO_2 (and possibly the O_2 from the beam experiment) have adsorbed transiently with a short surface lifespan. This is possibly evidenced by the adsorption of further O_2 after the layer has been

deposited in oxygen. The magnitude of the $m/z = 44$ desorption peak is much less when compared with the $m/z = 32$ desorption peaks that are seen in Figure 4.23a and Figure 4.23c, indicating that this layer is composed of more potassium peroxide than carbonate.

4.2.9 Mixed molecular beam of CO and O₂ on K₂O₂/K₂CO₃ layer formed at room temperature

A layer of potassium peroxide and carbonate was created by dosing potassium in 2×10^{-8} mbar of O₂ for 10 min at room temperature. A mixed beam of CO and O₂ (created using a 1:1 ratio mixture of CO and O₂, 50 mbar total molecular beam source pressure) was then beamed on to the surface at room temperature.

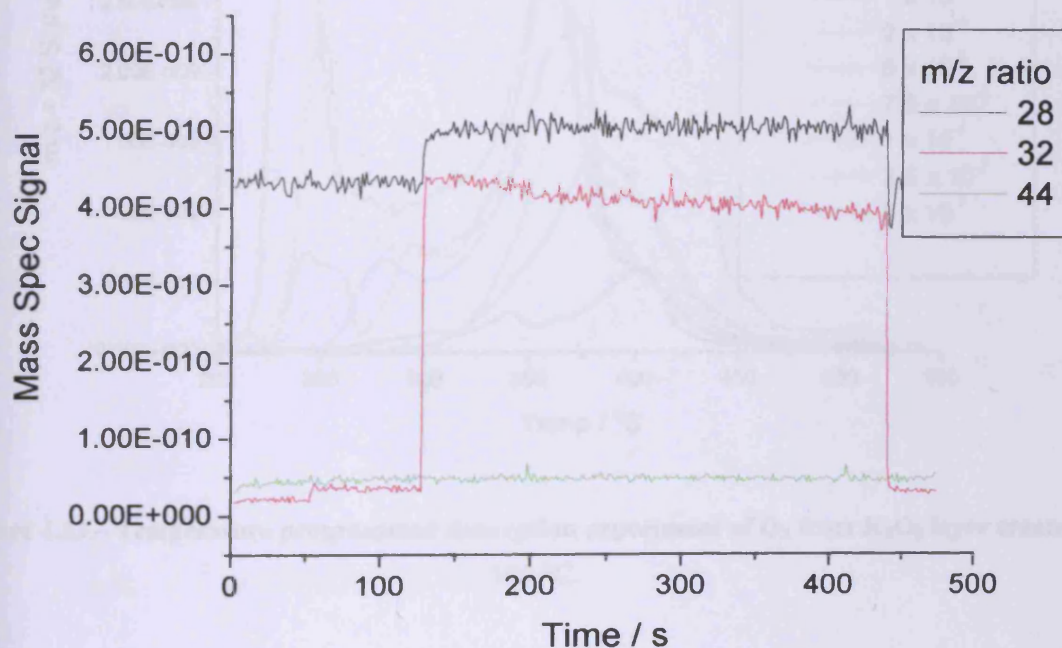


Figure 4.32 – A mixed molecular beam of CO and O₂ (1:1 ratio mixture, 50 mbar total molecular beam source pressure) beamed onto potassium peroxide/carbonate species at room temperature.

As is evidenced by Figure 4.32, neither CO nor O₂ stick to the mixed layer created to any appreciable degree. In addition to this there are no visible desorption products whilst beaming or during the temperature programmed desorption reaction

following the experiment (other than the desorption peaks associated with a mixed potassium peroxide/carbonate layer as seen in Figure 4.23), which is consistent with no adsorption of either of the reactants from the beam.

4.2.10 Co-dosing K and O₂ at 200 °C

To try and achieve a purer layer of potassium peroxide, potassium was dosed onto the crystal surface at 200 °C (above the desorption temperature of CO from the Pt(111) surface) for five minutes with differing background pressures of O₂.

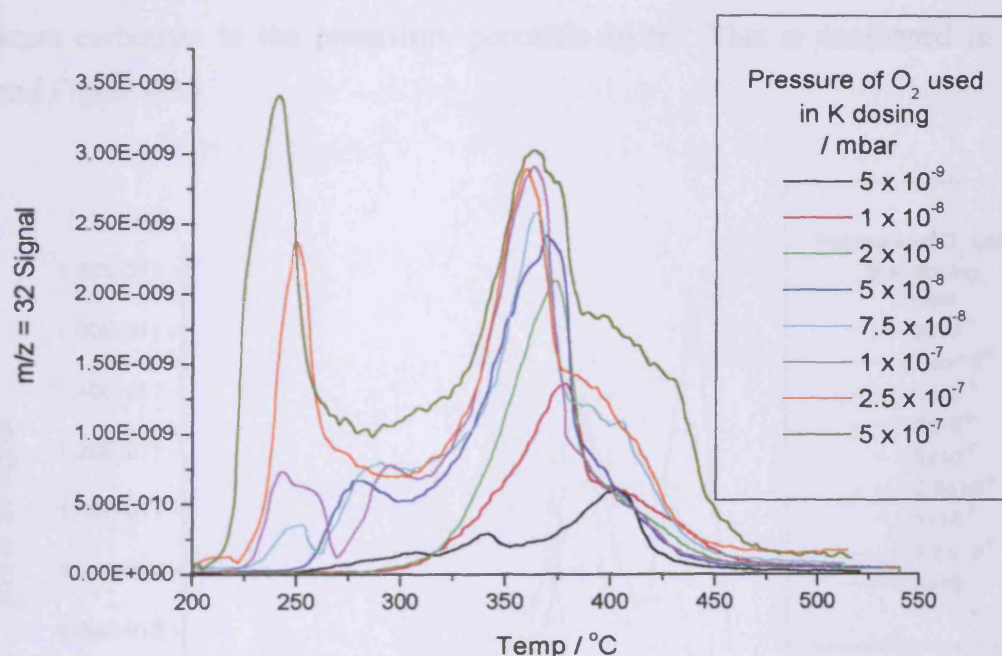


Figure 4.33 – Temperature programmed desorption experiment of O₂ from K₂O₂ layer created at 200 °C.

The above figure shows the variation of the temperature of desorption of O₂ with respect to the partial pressure of O₂ used in the creation of the layer. There is one major desorption peak for all pressures at between 360 and 380 °C, which appears to move to lower temperature with increasing O₂ pressure used in creation of the layer. For O₂ pressures above 5×10^{-8} mbar there is a second desorption peak at 240-250 °C, indicating the presence of another oxygen species on the surface. This peak also appears to shift to lower temperature with increasing O₂ background partial pressure. These two separate oxygen species have been noted by Brodén and

colleagues who assigned the lower temperature desorption state to oxygen desorbing from a platinum environment and the higher temperature desorption peak to oxygen desorbing from a potassium environment. They claim that the potassium is not in a K_2O form despite adsorption stoichiometries of 1:2¹⁰.

The temperature programmed desorption of the layer formed using 5×10^{-7} mbar of oxygen during its creation has a higher temperature shoulder on the desorption peak at 370 °C, a feature that is also present in the 2.5×10^{-7} and 7.5×10^{-8} mbar temperature programmed desorption experiments. Taking the data of the earlier Figure 4.23a into account it seems likely that this shoulder is due to the presence of potassium carbonate in the potassium peroxide layer. This is confirmed in Figure 4.34 and Figure 4.35.

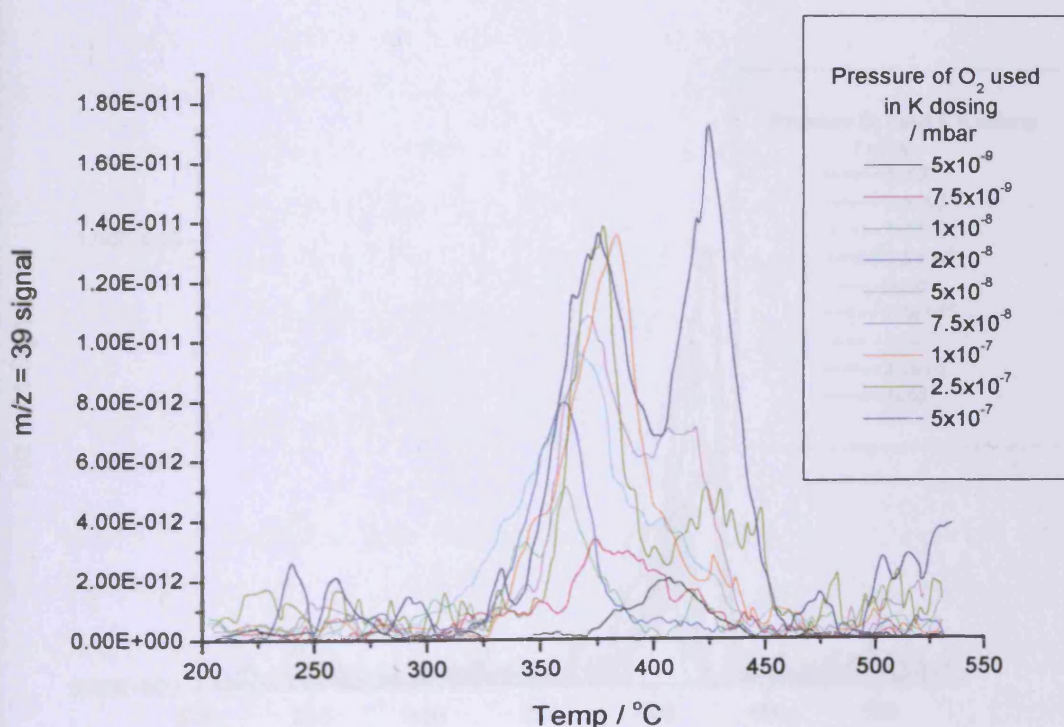


Figure 4.34 – Temperature programmed desorption experiment of K desorbing from K_2O_2 surface created at 200 °C.

Figure 4.34 shows the relationship between the background pressure of O_2 whilst dosing potassium and the amount of potassium incorporated into the surface layer. There is a single main desorption peak that is present for all O_2 pressures,

which occurs at 350-375 °C. As the background pressure of O₂ increases the size of this peak increases up to maximum at 1×10^{-7} mbar O₂. Above 7.5×10^{-8} mbar there appears to be a second site of K occupancy at 420-430 °C, indicating the presence of another potassium species on the surface. However this peak is much smaller than the lower temperature peak and does not appear for all traces, indicating that its origin is likely from background gases within the chamber. As the background pressure of O₂ whilst dosing is increased the area of the potassium desorption peak at 350-370 °C also increases, up to a limit at 1×10^{-7} mbar O₂, indicating that the presence of oxygen aids the uptake of potassium whilst dosing. However this seems counterintuitive as it is generally assumed that metal atoms from a doser adsorb at a constant rate with a sticking probability of close to unity. A more probable explanation for the increased uptake is that potassium peroxide is more stable on the Pt(111) surface than potassium, and is able to form multiple layers, unlike potassium alone.

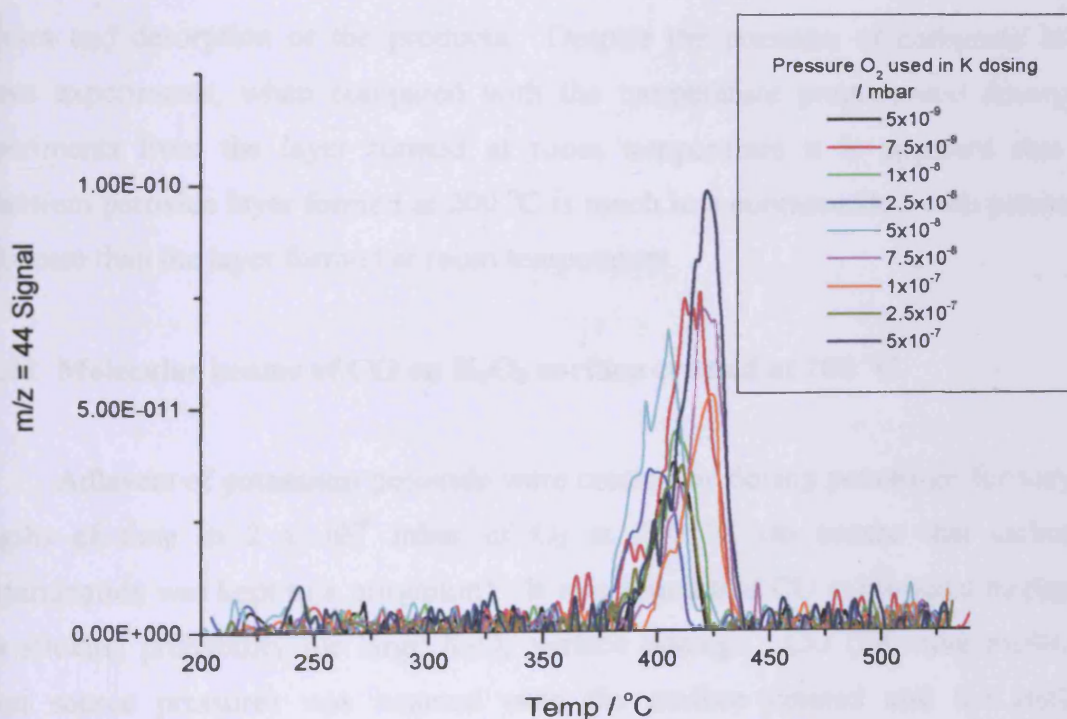


Figure 4.35 – A temperature programmed desorption experiment showing the amount of CO₂ desorbed from the K₂O₂ layer created at 200 °C.

Figure 4.35 shows the relationship between the temperature of desorption of CO₂ from the surface and the background pressure of O₂ used in the creation of the

layer. In a similar fashion to Figure 4.23c there is a single $m/z = 44$ desorption peak between 400 and 430 °C. However the scale of the desorption peak is approximately 1/25 of the desorption peak seen in the previous temperature programmed desorption experiment (Figure 4.23c), indicating that dosing at 200 °C is effective in reducing the carbonate contamination when creating a layer of potassium peroxide. It can therefore be concluded that the temperature programmed desorption peaks associated with potassium peroxide occur in the potassium temperature programmed desorption at 350-375 °C and the oxygen temperature programmed desorption at 360-380 °C. These conclusions are supported by similar experiments in the literature¹². The lower temperature O₂ desorption peak (230-250 °C) is most likely due to K/K₂O₂ –induced oxygen dissociation followed by spillover onto Pt(111) surface sites or by K/K₂O₂ –facilitated O₂ molecular dissociation and adsorption of atomic oxygen on Pt(111) surface sites. In addition to this the high-temperature K, O₂ and CO₂ desorption peaks seen in Figure 4.23a, b and c are due to dissociation of potassium carbonate surface species and desorption of the products. Despite the presence of carbonate in the above experiments, when compared with the temperature programmed desorption experiments from the layer formed at room temperature it is apparent that the potassium peroxide layer formed at 200 °C is much less contaminated with potassium carbonate than the layer formed at room temperature.

4.2.11 Molecular beams of CO on K₂O₂ surface created at 200 °C

Adlayers of potassium peroxide were created by dosing potassium for varying lengths of time in 2×10^{-8} mbar of O₂ at 200 °C (to ensure that carbonate contamination was kept to a minimum). It was found that CO exhibited a negligibly low sticking probability for large K₂O₂ surface dosings. CO (50 mbar molecular beam source pressure) was beamed onto the surface created and the sticking probability determined as a function of K/O₂ dosing time.

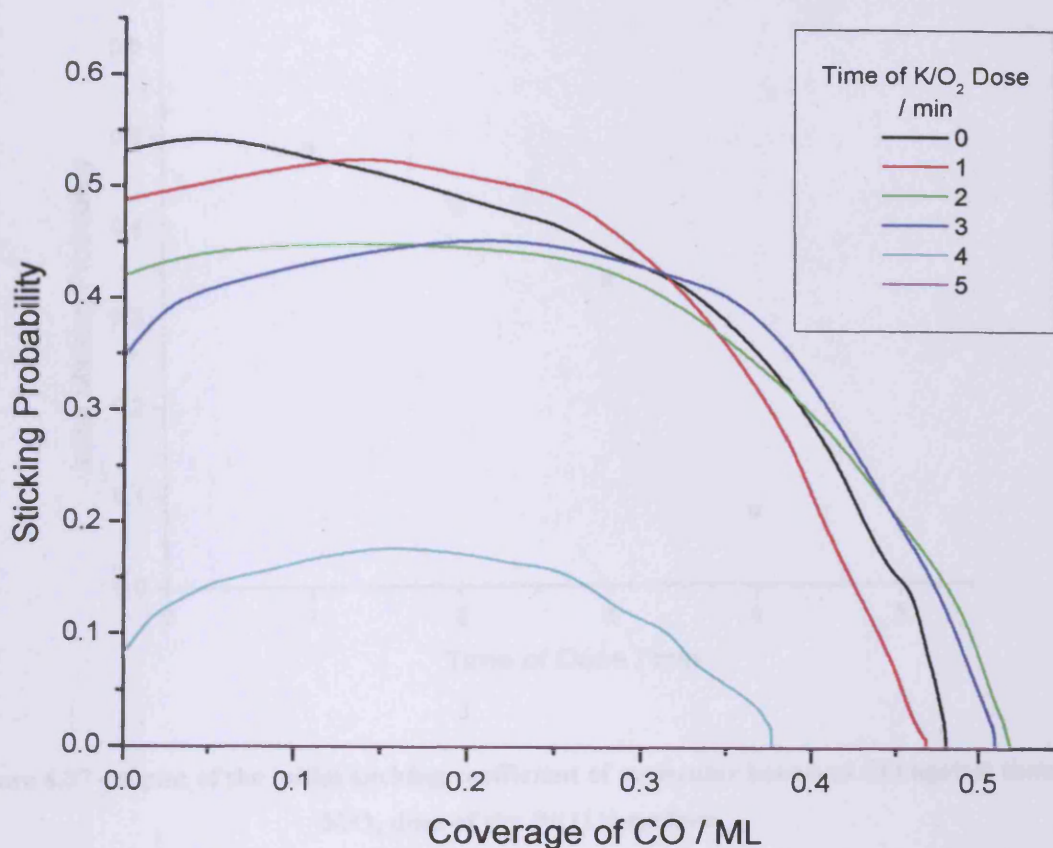


Figure 4.36 - The variation of sticking probability of molecular beams of CO (50 mbar molecular beam source pressure) with increasing time of K/O₂ dose of the Pt(111) surface.

As Figure 4.36 shows, dosing up to 2 minutes potassium peroxide onto the surface of the Pt(111) crystal has little effect on the saturation coverage and only a small reduction in the initial sticking coefficient. After that point both the initial sticking coefficient and the saturation coverage drop sharply, until there is no obvious CO adsorption by the surface after 5 minutes potassium peroxide surface dose.

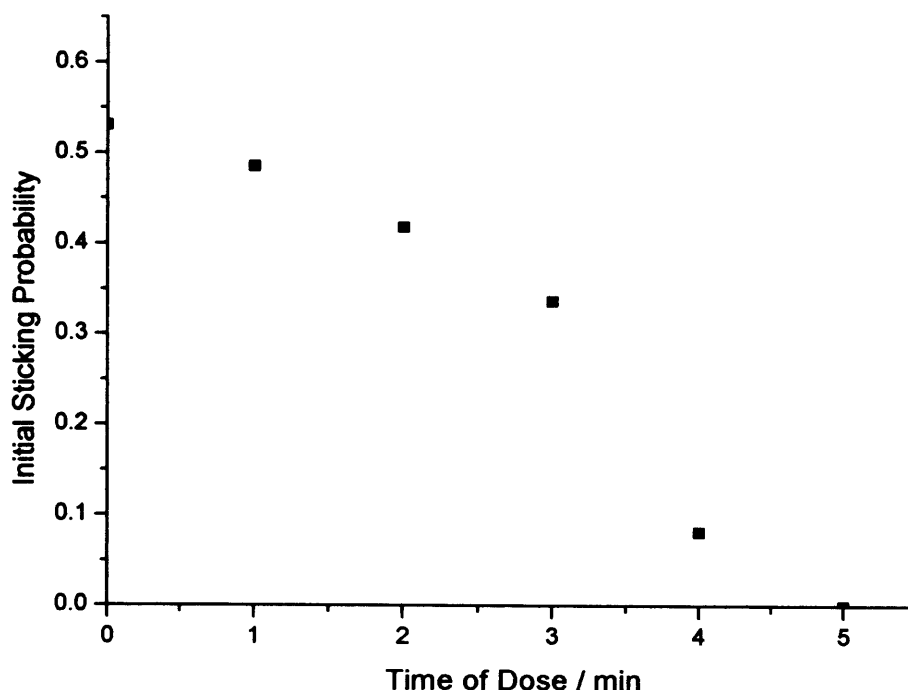


Figure 4.37 - A plot of the initial sticking coefficient of molecular beams of CO against time of K/O₂ dose of the Pt(111) surface.

Figure 4.37 clearly shows that although CO sticks with good initial sticking probability ($S_0 = 0.53$) on clean Pt(111), as the coverage of potassium peroxide is increased the initial sticking probability decreases. After 5 minutes no adsorption of the beam of CO is observed. There is a large difference in the initial sticking coefficients between three and four minutes dosing time, which is likely to be due to completion of the first layer. This occurs at a later time than seen previously for potassium adsorption (Figure 4.3, Figure 4.6 and Figure 4.9) which, assuming a constant flux from the potassium source and a constant sticking probability of potassium atoms on the surface, is likely due to the smaller size of potassium peroxide (made up of layering of K^+ and O_2^{2-}) allowing a greater surface packing into the layer. This agrees well with the smaller size of oxidised potassium recorded by Bonzel and colleagues¹⁰. CO sticks to K_2O_2 with a lesser sticking probability than on clean potassium alone, indicating competition between CO and O_2 adsorption.

4.2.12 Molecular beams of NO on K₂O₂ surface created at 200 °C

Different coverages of K₂O₂ were created by dosing potassium in 2×10^{-8} mbar of O₂ at 200 °C for varying amounts of time. The surface thus created was then cooled to room temperature and beamed with NO (50 mbar molecular beam source pressure).

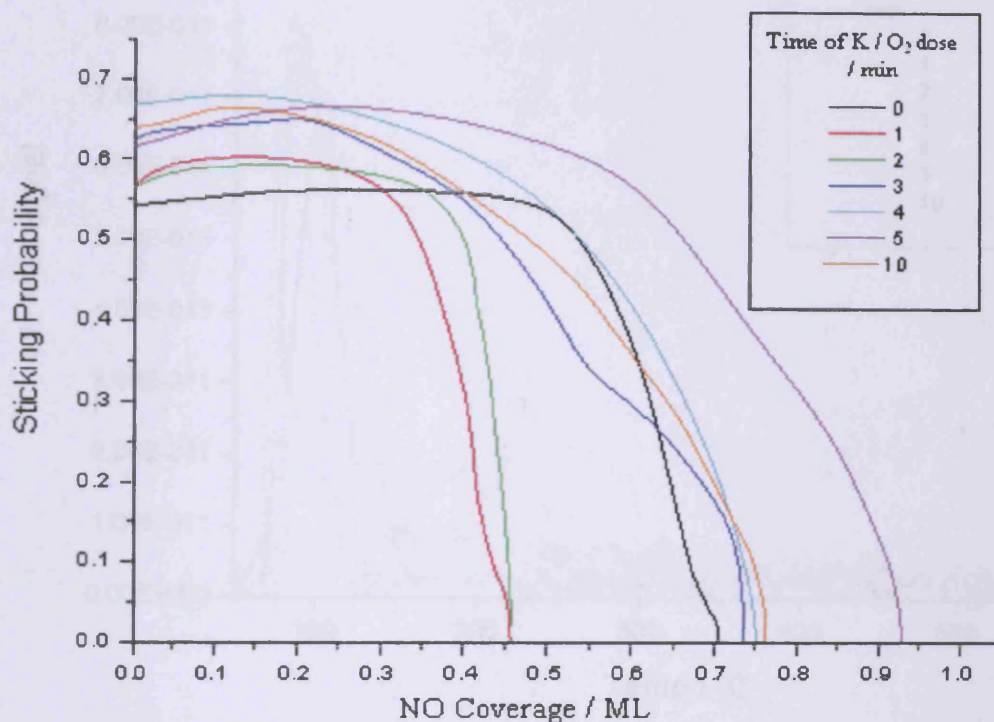


Figure 4.38 - The variation of sticking probability of molecular beams of NO (50 mbar molecular beam source pressure) with NO coverage for increasing time of K/O₂ dose of the Pt(111) surface.

In the above figure it can be seen that the presence of potassium oxide slightly increases the initial sticking probability of NO (and also seems to decrease the magnitude of the precursor effect in operation) up to 4 minutes of dose, where after no further increase in sticking probability is observed. There is an initial decrease in the coverage to which the beam saturates below a full surface layer of potassium peroxide; however as the Pt(111) surface coverage is increased further the maximum saturation coverage increases up to a maximum of 0.93 ML NO at 5 minutes K₂O₂ surface dose. Surface coverages of K₂O₂ greater than this decrease the saturation coverage close to that of the clean surface. Evolution of $m/z = 28$ was observed whilst beaming when beaming onto K/O₂ surface dosings of three minutes and

greater, which was assigned to N_2 desorbing from the surface. No $m/z = 44$ desorption peaks were observed, leading to the conjecture that the K_2O_2 surface was completely dissociating the NO with the nitrogen desorbing and the oxygen adsorbing onto the surface as seen earlier in Figure 4.36 and Figure 4.37.

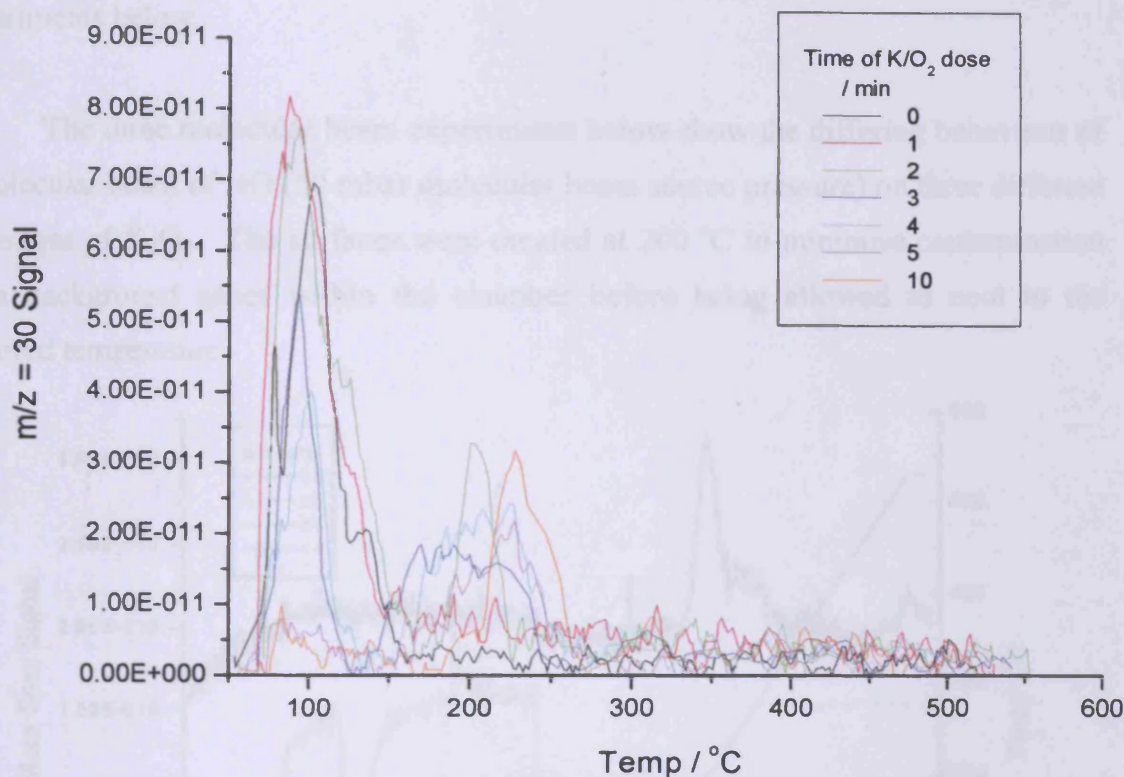


Figure 4.39 - Temperature programmed desorption of NO following the molecular beam experiments shown in Figure 4.38.

Figure 4.39 shows the temperature programmed desorption of the crystal surface following the molecular beam experiments shown in Figure 4.38. For doses of K_2O_2 of one minute and less there is a single desorption peak of NO at 90 °C, implying that the peroxide is present as a different surface state at smaller surface coverages. However, as Figure 4.38 showed, the sticking coefficient of NO for the surface actually increased, disproving the conjecture that the only adsorbed NO is that which is associated with platinum. As the surface coverage of K_2O_2 is increased a separate desorption peak at 200 °C becomes visible. This peak grows in area with increasing surface coverage at the expense of the lower temperature peak, which becomes smaller. Above five minutes of dosing the lower temperature desorption

peak disappears, suggesting that it is associated with NO adsorbed on Pt(111) and that completion of the monolayer has occurred by this point. However the surface reaction is more complicated than is implied by the above temperature programmed desorption experiments, with NO being broken down by the surface in a similar fashion to that seen on K/Pt(111). This is examined in the molecular beam experiments below.

The three molecular beam experiments below show the differing behaviour of a molecular beam of NO (50 mbar molecular beam source pressure) on three different coverages of K_2O_2 . The surfaces were created at 200 °C to minimise contamination from background gases within the chamber before being allowed to cool to the required temperature.

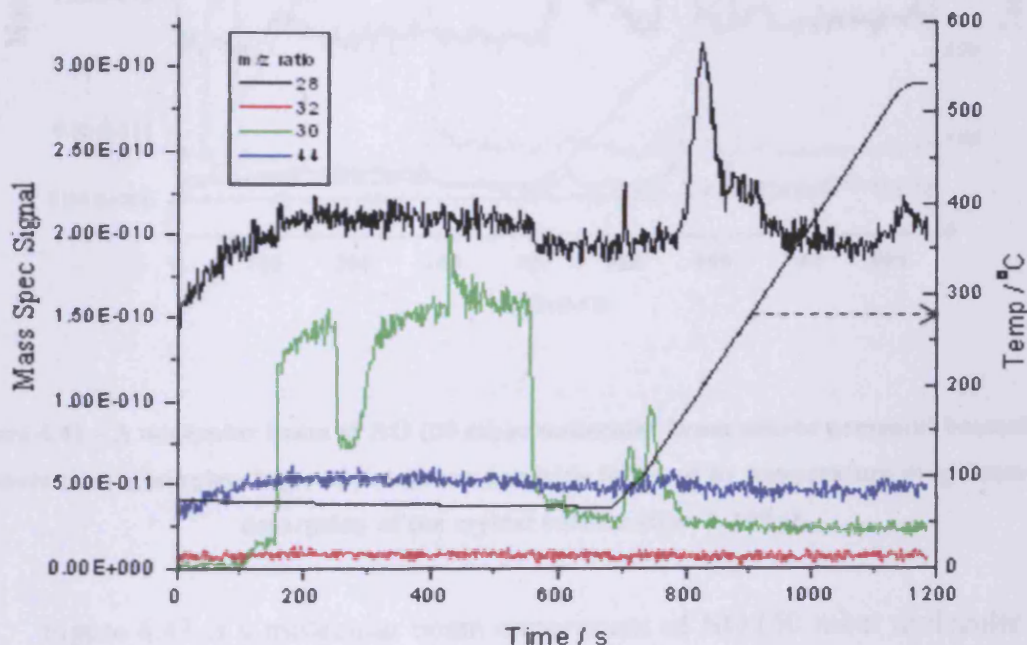


Figure 4.40 – A molecular beam of NO (50 mbar molecular beam source pressure) beamed onto the clean Pt(111) crystal surface followed by temperature programmed desorption of the surface (time > 700 s).

The above molecular beam experiment shows a molecular beam of NO on a clean Pt(111) surface at 60 °C. As seen in chapter 3, NO sticks moderately well to Pt(111) with $S_0 = 0.55$. There are no products immediately visible upon adsorption and ramping the temperature on the surface at a rate of 1 K/s (time > 685 s) produces two NO desorption peaks; a smaller peak immediately at the onset of heating (due to

flash desorption of NO from the heating filaments) and a larger peak at 95 °C due to NO desorbing intact from the crystal surface as a result of molecular adsorption. The integral of these two peaks is approximately equal to the coverage given by the area of the NO sticking peak. There is also a large $m/z = 28$ desorption peak at 210 °C that is due to CO adsorbing onto the rest of the crystal from the background gases within the chamber.

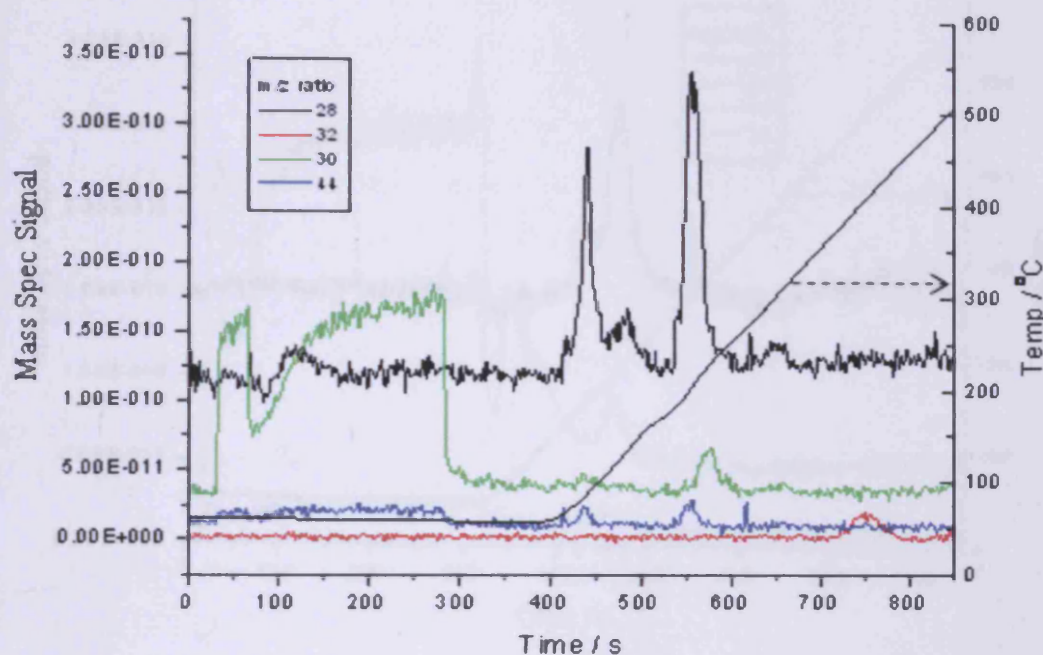


Figure 4.41 – A molecular beam of NO (50 mbar molecular beam source pressure) beamed onto more than a complete layer of potassium peroxide followed by temperature programmed desorption of the crystal surface (time > 400 s).

Figure 4.41 is a molecular beam experiment of NO (50 mbar molecular beam source pressure) beamed onto more than a complete surface covering of K_2O_2 (10 min dosing time). As can be seen, NO sticks well to the surface with $S_0 = 0.66$. The fact that there is a $m/z = 28$ desorption peak whilst beaming suggests that NO is adsorbing dissociatively, at least in part. The only $m/z = 30$ desorption peak in the temperature programmed desorption part of the experiment (time > 400 s) is at 240 °C, above the temperature associated with the molecular desorption of NO from Pt(111). There is also a $m/z = 44$ desorption peak at 200 °C, likely indicating the desorption of N_2O from the surface. The $m/z = 28$ desorption peak that occurs at 210 °C is likely due to the desorption of CO adsorbed from background gases during surface preparation and

during the course of the experiment. There is also a $m/z = 32$ desorption peak at 410 °C, either as a result of the decomposition and desorption of potassium carbonate from the surface or as a result of the desorption of adsorbed oxygen, possibly from the decomposition of nitrate at lower temperature in a similar manner to that seen on potassium alone.

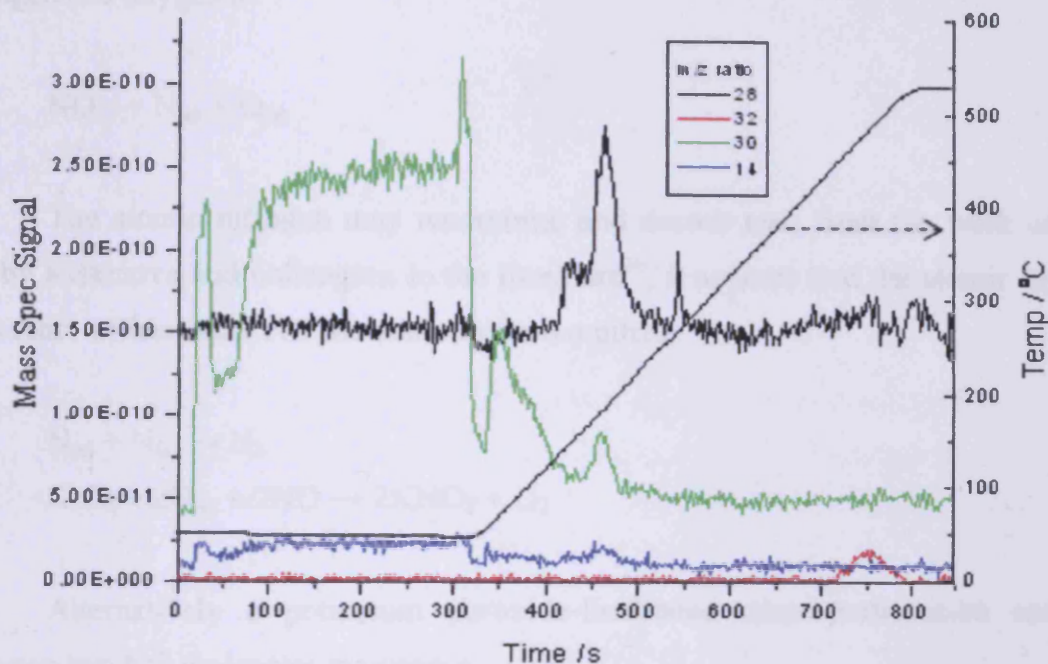
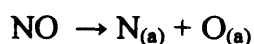


Figure 4.42 – A molecular beam of NO (50 mbar molecular beam source pressure) on intermediate K_2O_2 surface coverage followed by temperature programmed desorption of the crystal surface (time > 325 s).

The above figure shows a molecular beam experiment of a beam of NO (50 mbar molecular beam source pressure) beamed onto an intermediate surface covering of K_2O_2 (2 minutes surface dose). This surface dose was chosen so that there would be areas of potassium peroxide on the surface as well as areas of Pt(111), hopefully allowing any concerted reactions between the two components to be analysed. As can be seen, the beam of NO adsorbs to the surface with $S_0 = 0.6$ (higher than seen for clean Pt(111) – see Figure 4.38). Unlike in Figure 4.41, in Figure 4.42 there is no $m/z = 28$ desorption peak observed on beaming NO. In the temperature programmed desorption part of the experiment (time > 350 s) there appear to be two main $m/z = 30$ desorption peaks; one at 95 °C, characteristic of NO desorbing from the platinum and one at 180 °C. There is also a $m/z = 32$ desorption peak at 490 °C which is likely due to the desorption of oxygen from the potassium. The $m/z = 28$ desorption peak that is

visible at 195 °C is likely due to the desorption of CO which has adsorbed from the background gases within the chamber.

Taking the above three figures into account it is apparent that potassium peroxide has the effect of facilitating the dissociative adsorption of NO to atomic nitrogen and oxygen ie.



The atomic nitrogen may recombine and desorb and, from the work carried out by Kiskinova and colleagues in the literature³⁶, it appears that the atomic oxygen may react with another NO molecule to form a nitrite.



Alternatively a potassium peroxide-facilitated disproportionation reaction between two NO molecules may occur.



4.2.13 Mixed molecular beams of NO₂ and O₂ on K₂O₂ surface created at 200 °C

A layer of potassium peroxide was created by dosing potassium for 5 minutes in 2×10^{-8} mbar of O₂ at 200 °C. The layer was created at this temperature (above the desorption temperature of CO from Pt(111)) to reduce the presence of carbonate in the layer. The layer was then allowed to cool to room temperature and a mixed beam of NO₂ and O₂ (created using a 1:1 mixture ratio of NO and O₂ as described in chapter 3, 50 mbar total molecular beam source pressure) was beamed onto the surface.

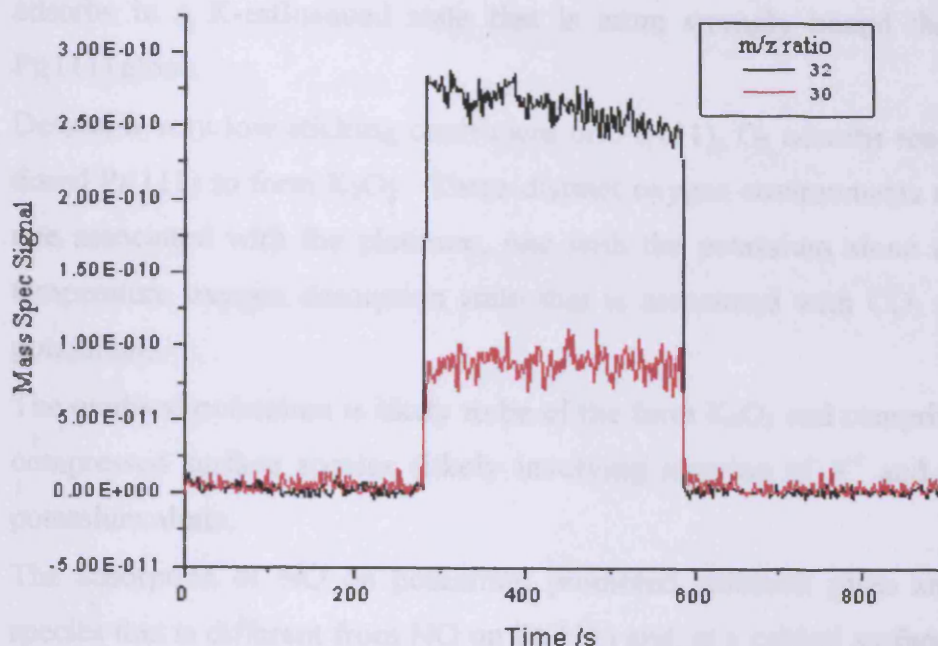


Figure 4.43 – A mixed molecular beam of NO_2 and O_2 (created using a 1:1 ratio of NO and O_2 , 50 mbar total molecular beam source pressure) beamed onto $\text{K}_2\text{O}_2/\text{Pt}(111)$ surface (created at 200 °C then allowed to cool to room temperature). Note that $m/z = 14, 28, 44$, and 46 have been eliminated for clarity.

The above molecular beam experiment shows that there is no visible sticking of either NO_2 or O_2 on the potassium peroxide surface. In addition to this there are no obvious products created whilst beaming and there were no features in the temperature programmed desorption experiment which followed the molecular beam experiment to suggest that a surface reaction had occurred.

4.3 Summary and conclusions

4.3.1 Platinum (111)/Potassium

- On $\text{Pt}(111)$, the growth of the potassium layer occurs via the initial completion of a full monolayer followed by island formation in Stranski-Krastanov fashion.
- The ionic character of the potassium on the surface has a large effect on the CO adsorption, with potassium that is largely ionic in character providing little obstacle to CO adsorption and potassium that is more metallic reducing the sticking coefficient of CO for the surface. CO that is adsorbed by the surface

adsorbs in a K-influenced state that is more strongly bound than CO on Pt(111) alone.

- Despite a very low sticking coefficient on Pt(111), O₂ adsorbs readily on K-dosed Pt(111) to form K₂O₂. Three distinct oxygen environments are visible, one associated with the platinum, one with the potassium alone and a high temperature oxygen desorption state that is associated with CO₂ as well as potassium.
- The oxidised potassium is likely to be of the form K₂O₂ and comprises a more compressed surface species (likely involving layering of K⁺ and O₂²⁻) than potassium alone.
- The adsorption of NO on potassium promoted platinum gives an adsorbed species that is different from NO on Pt(111) and, at a critical surface coverage of potassium, potassium-promoted NO begins to dissociate with the release of nitrogen. This is the same potassium surface coverage at which there is a drop in the initial sticking coefficient of CO on K/Pt. The dissociation leaves behind a surface species (identified in the literature as nitrite¹⁸) that breaks down ~ 200 °C and desorbs, leaving adsorbed oxygen.
- Dosing a complete monolayer of potassium onto the Pt(111) surface changes the adsorption characteristics of NO₂. Instead of being reduced to NO the NO₂ is stored by the surface, possibly as nitrate.

4.3.2 Platinum(111)/Potassium peroxide

- Co-dosing potassium and oxygen at room temperature produces an adlayer of potassium peroxide that is contaminated with carbonate from adsorption of CO from background gases in the chamber. The amount of carbonate in the peroxide layer can however be greatly reduced by dosing onto a surface held above the temperature of desorption of CO from Pt(111).
- Multiple oxygen species are visible in the temperature programmed desorption of the peroxide layer; one associated with potassium carbonate, one with peroxide and one with platinum. Increasing the pressure of oxygen appears to aid adsorption of potassium by the surface; this is assumed to be the result of multilayer formation.

- As with potassium, dosing potassium peroxide onto the surface reduces the adsorption of CO. Unlike with potassium however there is no separate CO adsorption site, adsorption is prevented via blocking of platinum CO adsorption sites.
- The peroxide surface is capable of breaking down NO in a similar manner to that seen for the potassium layer. Unlike potassium however the NO₂ is not adsorbed or broken down by the peroxide layer.

REFERENCES

1. Crowell, J.E., Garfunkel, E.L., Somorjai G.A., *Surf. Sci.*, **121**, 1982, 303.
2. Kudo, M., Garfunkel, E.L., Somorjai, G.A., *J. Phys. Chem.*, **89**, 1985, 3207.
3. Koyayashi, T., Yamada, T., Kayano, K., *SAE Technical Paper Series*, No. 970745, 1997.
4. Gurney, R.W., *Phys. Rev.* **47**, 1935, 479.
5. Windham, R.G., Bartram, M.E., Koel, B.E., *J. Phys. Chem.*, **92**, 1988, 2862.
6. Lehmann, J., Roos, P., Bertel, E., *Phys. Rev. B*, **54**, 1996, R2347.
7. Muller, J.E., Hannon, J.B., Giesen, M., Klunker, C., Schulze Icking-Konert, G., Stapel, D., Ibach, H., *Phys. Rev. Lett.*, **78**, 1997, 1094.
8. Moré, S., Berndt, W., Bradshaw, A.M., *Phys. Rev. B*, **57**, 1998, 9249.
9. Pirug, G., Winkler, A., Bonzel, H.P., *Surf. Sci.*, **163**, 1985, 153.
10. Pirug, G., Bonzel, H.P., Brodén, G., *Surf. Sci.*, **122**, 1982, 1.
11. Brodén, G., Pirug, G., Bonzel, H.P., *Chem. Phys. Lett.*, **73**, 1980, 506.
12. Garfunkel, E.L., Somorjai, G.A., *Surf. Sci.*, **115**, 1982, 441.
13. Lehmann, J., Roos, P., Bertel, E., *Phys. Rev. B*, **54**, 1996, 54.
14. Pirug, G., Bonzel, H.P., *Surf. Sci.*, **194**, 1998, 159.
15. Windham, R.G., Bartram, M.E., Koel, B.E., *J. Phys. Chem.*, **92**, 1988, 2862.
16. Pirug, G., Winkler, A., Bonzel, H.P., *Surf. Sci.*, **163**, 1985, 153.
17. Wenter, P., Memmel, N., *Surf. Sci. Lett.*, **513**, 2002, L419.
18. Kiskinova, M., Pirug, G., Bonzel, H.P., *Surf. Sci.*, **133**, 1983, 321.
19. Whitman, L.J., Ho, W., *J. Chem. Phys.*, **90**, 1989, 6018.
20. Bonzel, H.P., *Surf. Sci. Rep.*, **8**, 1987, 43.
21. Garfunkel, E.L., Maj, J.J., Frost, J.C., Farles M.H., Somorjai, G.A., *J. Phys. Chem.*, **87**, 1983, 3629.
22. Garfunkel, E.L., Crowell, J.E., Somorjai, G.A., *J. Phys. Chem.*, **86**, 1982, 310.
23. Ray, N.K., Anderson, B.A., *Surf. Sci.*, **803**, 1983, 125.
24. Wesner, D.A., Pirug, G., Cohen, F.P., Bonzel, H.P., *Surf. Sci.*, **178**, 608, 1986.
25. Hoffmann, F.M., de Paola, R.A., *Phys. Rev. Lett.*, **52**, 1984, 1697.
26. Lee, J., Arias, J., Hanrahan, C.P., Martin, R.M., Metiu, H., *Phys. Rev. Lett.*, **54**, 1985, 1440.
27. More, S., Berndt, W., Bradshaw, A.M., *Phys. Rev. B*, **57**, 1998, 9246.
28. Hannon, J.B., Giesen, M., Klunker, C., Schulze Icking-Konert, G., Stapel, D., Ibach, H., *Phys. Rev. Lett.*, **78**, 1997, 1094.
29. Ibach, H., *Surf. Sci.*, **29**, 1997, 193.
30. Gurney, R.W., *Phys. Rev.*, **47**, 1935, 479.
31. Goncalves, F., Figueiredo, J.L., *Appl. Catal. B: Environ.*, **50**, 2004, 271.
32. Harkness, I.R., Lambert, R.M., *J. Chem. Soc., Faraday Trans.*, **93**, 1425.
33. Garfunkel, E.L., Maj, J.J., Frost, J.C., Farias, M.H., Somorjai, G.A., *J. Phys. Chem.*, **87**, 1983, 3692.
34. Kiskinova, M.P., Pirug, G., Bonzel, H.P., *Surf. Sci.*, **140**, 1984, 1.
35. Goncalves, F., Figueiredo, J.L., *Appl. Catal. B: Environ.*, **62**, 2006, 181.
36. Kiskinova, M., Pirug, G., Bonzel, H.P., *Surf. Sci.*, **140**, 1, 1984.
37. Bonzel, H.P., *Surface Science Reports*, **8**, 1987, 43.
38. Dou, D., Balland, J., *SAE Technical Paper*, 2002-01-0734.
39. Gill, L.J., Blakeman, P.G., Twigg, M.V., Walker, A.P., *Top. Catal.*, **28**, 2004, 157.
40. Konsolakis, M., Yentekakis, I.V., *Appl. Catal. B*, **29**, 2001, 103.
41. Neal, L.G., Haslbeck, J.L., Tseng, H., *US Patent 475,599*, 1998.

-
42. Epling, W.S., Campbell, L.E., Yezerets, A., Currier, N.W., Parks, J.E., *Catal. Rev.*, **46**, 2004, 163.
 43. Liu, Z.M., Zhou, Y., Solymosi, F., White, J.M., *J. Phys. Chem.*, **93**, 1989, 4384.
 44. Cassuto, A., Schmidt, S., Mane, M., *Surf. Sci.*, **284**, 1993, 273.
 45. Brown, J.K, and Luntz, A.C., *Chem. Phys. Lett.*, **186**, 2-3, 1991, 125.
 46. Lamontagne, B., Semond, F., Roy, D., *Surf. Sci.*, **327**, 1995, 371.
 47. Petrick, S., Benndorf, C., *Diamond and Relat. Mat.*, **10**, 2001 519.
 48. Puglia, C., Bennich, P., Hasselstrom, J., Bruhwiler, P.A., Nilsson, A., Li Y., Rudolf, P., Martensson, N., *Surf. Sci.*, **488**, 2001, 1.
 49. Finetti, P., Scantelbury, M.J., McGrath, R., Borgatti, F., Sambì, M., Zaratini, L., Granozzi, G., *Surf. Sci.*, **461**, 2000, 240.
 50. Schulze, M., Reissner, R., *Surf. Sci.*, **507**, 2002, 8518.

5. THE EFFECT OF Ba AND BaO ON THE SURFACE CHEMISTRY OF NO, CO AND O₂ ON Pt(111), AND THE SUITABILITY OF BaO AS A NO_x STORAGE COMPONENT IN THE NSR CATALYST

5.1	<i>Literature review</i>	186
5.2	<i>Results and discussion</i>	190
5.2.1	<i>Sticking of O₂ on Ba dosed Pt(111)</i>	190
5.2.2	<i>LEED of the Ba layer</i>	192
5.2.3	<i>Sticking of CO on increasing Ba surface dosings of Pt(111)</i>	194
5.2.4	<i>Adsorption of molecular beams of NO on increasing Ba coverage</i>	197
5.2.5	<i>Mixed molecular beams of NO₂ and O₂ on increasing Ba coverages</i>	198
5.2.6	<i>Mixed molecular beams of NO and CO on Ba dosed Pt(111)</i>	202
5.2.7	<i>X-ray photoelectron spectroscopic analysis of barium oxide</i>	203
5.2.8	<i>Adsorption of molecular beams of CO on increasing BaO coverages of the Pt(111) crystal surface</i>	205
5.2.9	<i>Temperature programmed desorption of O₂ from different BaO surface coverages</i>	211
5.2.10	<i>Adsorption of NO onto different BaO coverages Of Pt(111)</i>	213
5.2.11	<i>NO decomposition by BaO with increasing surface temperature</i>	220
5.2.12	<i>Mixed molecular beams of NO and CO on BaO layers held at increasing surface temperatures</i>	223
5.2.13	<i>Molecular beams of NO₂ on increasing BaO coverages of the Pt(111) surface</i>	226
5.3	<i>Summary and conclusions</i>	229
	REFERENCES	231

5.1 Literature Review

There is relatively little information in the literature focusing on the characterisation of barium and barium oxide under ultrahigh vacuum conditions, research efforts having been more concentrated on NO_x storage and reaction in catalytic reactor studies. There is considerably more information on MgO, a similar material, however one should be wary of drawing too close a parallel between the two species as BaO is considerably more ionic in nature than MgO and also much larger, with a lattice constant approximately 30% greater than MgO¹.

Under standard conditions barium oxide is an oxide with a cubic sodium chloride-like bulk structure with a lattice constant of 5.59 Å and it possesses a high degree of ionicity¹⁰. The large lattice parameter leads to a lower restoring Madelung potential when compared to similar alkaline earth metal compounds. This is important with regards to NO_x storage as it implies that O anions in a BaO lattice would be more easily oxidised by the presence of an oxidant (NO₂ is particularly relevant in this system) than comparable compounds¹⁰. Barium oxide is known to have a very low work function, implying that it forms with negative ions inward and the positive barium centres towards the vacuum^{7,2}.

The growth of the barium layer on Pt(111) has been found to proceed in a Stranski-Krastanov manner, in which a single monolayer of Ba is deposited and completed before nanoparticles and islands of Ba begin to form on top of the layer.³ Stranski-Krastanov growth is characterised by the simultaneous presence of two different adatom environments; both as particles and as a complete physical monolayer. It is interesting to note that in the Pt(111)/Ba system these different barium environments exhibit different behaviour when oxidised. Oxidation of the barium particles on top of the layer irreversibly produces BaO whilst oxidation of the barium in the layer reversibly produces BaO₂⁶.

Calculations involving the relative atomic radii of platinum and barium atoms indicate that the most densely-packed barium surface adlayer would be (2 x 2) in structure, corresponding to a monolayer coverage of 0.25 ML (where a 1 ML coverage would correspond to 1 adsorbate atom per 1 substrate atom)⁶. STM

measurements of a barium oxide surface have verified that the barium-oxygen spacing is twice the spacing of 0.39 nm that would be expected for a (1 x 1) BaO structure, forming a (2 x 2)-BaO layer⁷, implying a reconstructed BaO(111) surface layer as predicted by theory^{3,4} and seen for other fcc metal surfaces⁵. However, due to strain between the platinum surface and the barium/barium oxide adlayers and the disorder within the adlayers no LEED patterns were observable^{6,7}. The (2 x 2) reconstruction leads to a BaO surface layer that is terminated by three-sided pyramids composed of a barium ion at the apex bonded to three oxygen atoms at the base of the pyramid, which in turn are bonded to the four nearest Ba ions in the manner predicted for rocksalt-structure materials^{7,8}. The sides of these pyramids are BaO(100) surfaces⁷. Larger (4 x 4) surface reconstructions have been shown to form larger pyramids; however these are much less common than the (2 x 2) reconstructions mentioned earlier, either due to this being the favoured phase or for the greater amount of BaO needed for the larger pyramids not being present in thinner films⁷.

It has been shown that NO storage on BaO/Pt(111) is only able to occur when both NO and O₂ are present⁶. However, according to the model postulated by the authors, NO oxidation does not occur over the platinum, and exposed platinum is not necessary for NO_x storage. This is in direct disagreement with the generally accepted model in which oxidation of NO occurs over the platinum metal centre before storage as nitrate on the BaO^{9,10}. However, both NO and NO₂ have been shown to adsorb on barium oxide in the absence of the noble metal present in the NSR catalyst. The amount of NO₂ adsorbed is much greater than the amount of NO in the absence of platinum however, implying that the oxidation of NO is an important first step in the NSR process^{11,15}. It may be that the first step of the NO_x storage mechanism is the production of barium peroxide, which may then go on to react with NO and hence store NO_x.

Theoretical and experimental studies have shown that the identity of the stored NO_x is likely to be Ba(NO₃)₂^{9,12,13}. The mechanism of the formation of the barium nitrate is still a matter of controversy however. On bulk barium oxide theoretical studies have shown that NO₂ has little energetic preference with regards to adsorbing on the Ba or O centres. The site of adsorption has however been shown to influence the species formed, with adsorption of NO₂ on oxygen being shown to favour nitrate

species (NO_3^-) whereas adsorption of NO_2 on Ba forms adsorbed nitrites (NO_2^-). The authors show that there is an ionic interaction between the adsorbed nitrites and the barium centre, making it an important step in the storing of NO_x . This step indicates a difference in the mechanism behind the storing of NO_x and the unwanted poisoning of the catalytic surface by SO_x ¹⁰. Surface nitrite species have been shown to be more thermally stable than surface nitrates⁹.

One possible adsorption sequence is the formation of nitrites followed by the formation of pairs of nitrite-nitrates and nitrate-nitrites along with pairs of nitrates. This is supported by evidence from flow-reactor studies in which the adsorption of NO_2 is shown to give NO as a product on $\text{BaO}/\text{Al}_2\text{O}_3$ ¹⁰. The formation of NO may also be indicative of the formation of peroxide species at the surface.

Sedlmair *et al.*⁹ have produced IR information that shows that two distinct types of nitrites are formed; linear and bridged. They account for this as being due to δ^+ N atoms in the NO interacting with δ^- O atoms in the BaO and creating a linear nitrite species. However if this occurs on a BaO oxygen that is less well coordinated (for instance one perpendicular from the plane of the surface) the free oxygen of the NO could interact with another Ba atom, creating a bridged species⁹.

Taking these results together it seems as if the initial adsorption of NO_2 on BaO produces an adsorbed nitrite species. This requires transfer of an electron from the oxygen present in the surface. The transfer of the electron leaves a vacant hole in the O(2p) electron energy level, facilitating adsorption of another NO_2 molecule. This second NO_2 molecule adsorbs as nitrate at the thus activated surface oxygen, forming a nitrite-nitrate linked pair. A further NO_2 molecule oxidises the nitrite of the pair, producing $\text{Ba}(\text{NO}_3)_2$ and a gas phase NO molecule^{10,14}.

It has been hypothesised that the formation of BaO_2 is essential in the oxidation of NO to nitrate, as a source of highly reactive oxygen is required⁹. However it has also been predicted that BaO_2 and a nitrite is formed by the dissociative adsorption of NO_2 and that bridging nitrites are capable of being oxidised to NO_2 by gas phase NO¹⁵. A species that is thought to be BaO_2 can be seen via scanning tunnelling microscopy to form readily at 573 K whilst dosing O_2 onto a

barium adlayer. Such species are unstable with a transient lifetime however; when the background pressure of O_2 is removed the islands formed can be seen to shrink before disappearing⁶. It is possible to form stable islands of BaO_2 at lower temperature by exposure to high pressures of oxygen, allowing distinct images of the BaO_2 structure to be produced⁶.

Schmitz *et al.*¹⁵ have provided x-ray photoelectron spectroscopic experimental data that suggests that NO_2 dissociatively adsorbs onto BaO . They account for this as possibly being due to the NO_2 dissociating to form BaO_2 and linearly bonded nitrites. These nitrite intermediates may then go on to form predominantly nitrates for higher coverages of NO_2 . They hypothesise that nitrate formation might occur via a trimer of two adsorbed nitrites and a molecularly adsorbed nitrate. NO , on the other hand, adsorbs molecularly to form a nitrite¹⁵.

It has been found that the breakdown of $Ba(NO_3)_2$ which is desirable under anaerobic conditions is inhibited by the presence of O_2 , which stabilises the compound and raises the temperature at which it desorbs. The presence of CO_2 however facilitates the release of the stored NO_x by promoting formation of $BaCO_3$ ^{16,17}. $BaCO_3$ has been shown to exist in chelating, bridged and monodentate forms⁹.

Stored CO_2 in the form $BaCO_3$ has been shown to be released in the presence of NO or $NO + O_2$ but not in the presence of NO_2 . From this it can be inferred that it is the NO which has a vital role in the decomposition of $BaCO_3$ ⁹.

5.2 Results and Discussion

Only a very small signal was detected due to barium with Auger electron spectroscopy due to the low sensitivity of barium for this surface analysis technique. This effect has been noted in the literature⁶. This made it impossible to use Auger electron spectroscopy to chart the growth of the barium surface in a similar manner to that seen for potassium in chapter 4.

5.2.1 Sticking of O₂ on Ba dosed Pt(111)

Barium was dosed onto the surface at 200 °C for increasing lengths of time using a custom built SAES getter source heated to over 900 °C and positioned in front of the crystal. After outgassing the differential pressure rise was 1×10^{-9} mbar during the course of the depositions, the majority of which was due to hydrogen and CO desorption from the doser. The crystal surface was held at elevated temperature to reduce the adsorption of background gases during the dosing. The surface was sputtered and annealed for multiple cycles in between each dosing to make certain of the removal of all the barium used in previous experiments from the surface.

O₂ sticks with a low initial sticking probability on pure Pt(111) ($S_0 = 0.06$, see chapter 3). However it was found that the addition of barium to the surface increased the initial sticking coefficient of the beam of oxygen. This allowed the growth of the barium adlayer to be examined.

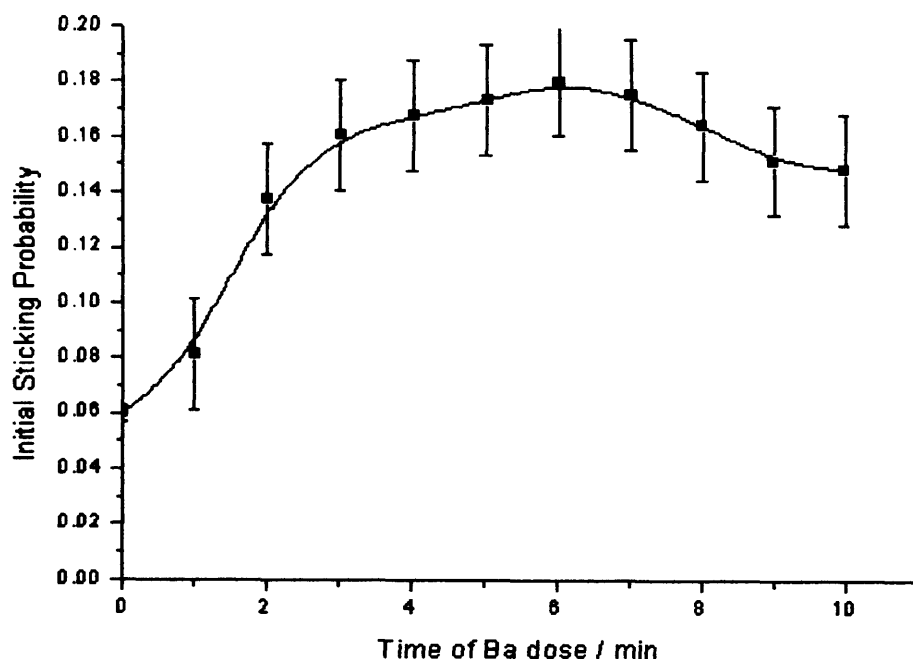


Figure 5.1 - The initial sticking probability of a beam of O₂ (50 mbar molecular beam source pressure) with increasing barium coverage of the Pt(111) surface.

Figure 5.1 is a plot of the initial sticking probability of the beam of oxygen against the time of barium surface dose. As can be seen there is an initial steep rise in sticking probability up to 3 minutes dosing time, after which the curve levels off to form a plateau (within experimental error). Unlike for potassium it is difficult to use oxygen sticking to determine the point at which a complete monolayer of barium is deposited due to the error inherent in the above figure. Alternatively the shape of the above graph may indicate a degree of contamination of the surface. If however the barium film was contaminated is unlikely that the level of contamination was high as the crystal was held at elevated temperature during dosing to reduce the adsorption of background gases onto the crystal surface during dosing and the background pressure of the system was low (base pressure $< 2 \times 10^{-10}$ mbar). In addition to this it would be expected that oxygen would not readily adsorb onto a contaminated surface.

Taking Figure 5.7 into account it is apparent that a complete physical monolayer has occurred by four minutes barium dosing time. Figure 5.1 would seem to argue that a monolayer has been deposited by three minutes barium dosing time; however, as mentioned earlier, due to the error in Figure 5.1 an accurate determination of the point of monolayer formation is problematic. The initial steep

portion of Figure 5.1 is likely to be due to the adsorption of barium that is ionic in character and the levelling off due to barium becoming more metallic in character as it is packed more tightly into the surface. There were no desorption products visible in the temperature programmed desorption of the crystal surface following the molecular beam experiment indicating that stable surface species have been formed.

5.2.2 LEED of the Ba layer

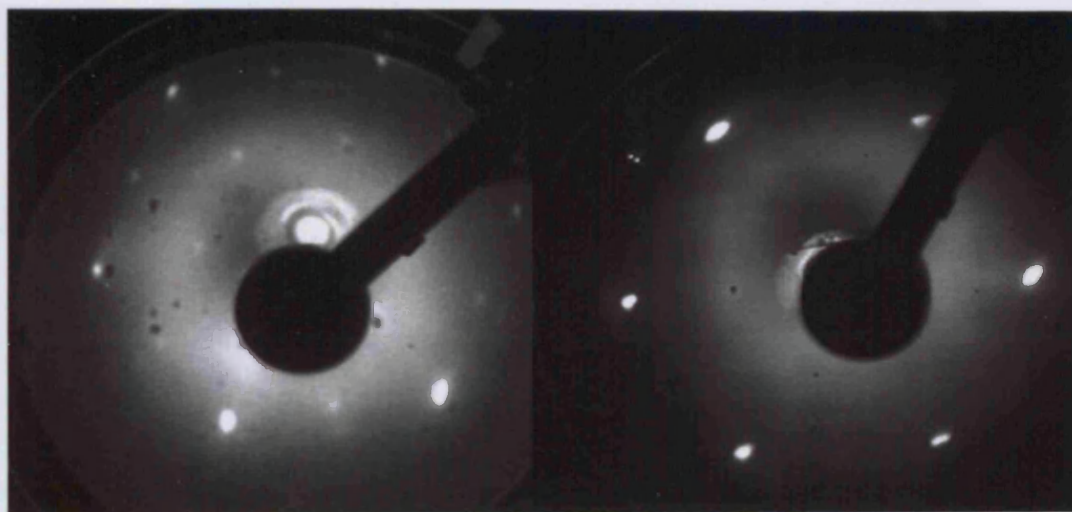


Figure 5.2 - LEED pictures taken at 76 eV of 5 min Ba dose (left) and clean Pt(111) surface as a reference (right).

Figure 5.2 comprises two LEED photos, one of the clean Pt(111) surface and one of the Pt(111) surface after a 5 min dose of barium. As would be expected after the addition of an adsorbate, the LEED photo of the barium adlayer has additional spots, arranged in a (2x2) pattern. This is shown in the schematic below.

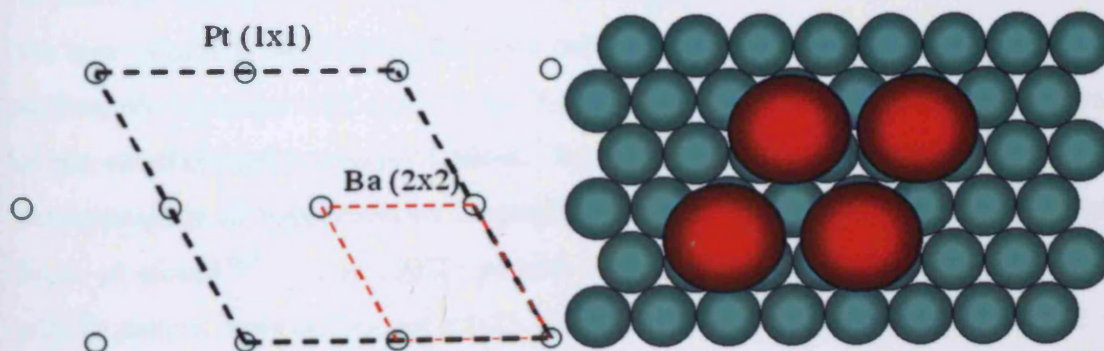


Figure 5.3 – The Pt(111) (1x1) and Ba(2x2) unit cells from the LEED pattern shown in Figure 5.2 and the corresponding real-space structures.

Some of the additional spots that are due to the adsorption of barium in Figure 5.2 appear to be split into pairs (most clear is the (2x2) spot due to barium that appears directly below the zero order spot). With larger doses of barium to the surface these were resolved into ring structures as seen in Figure 5.4 below.

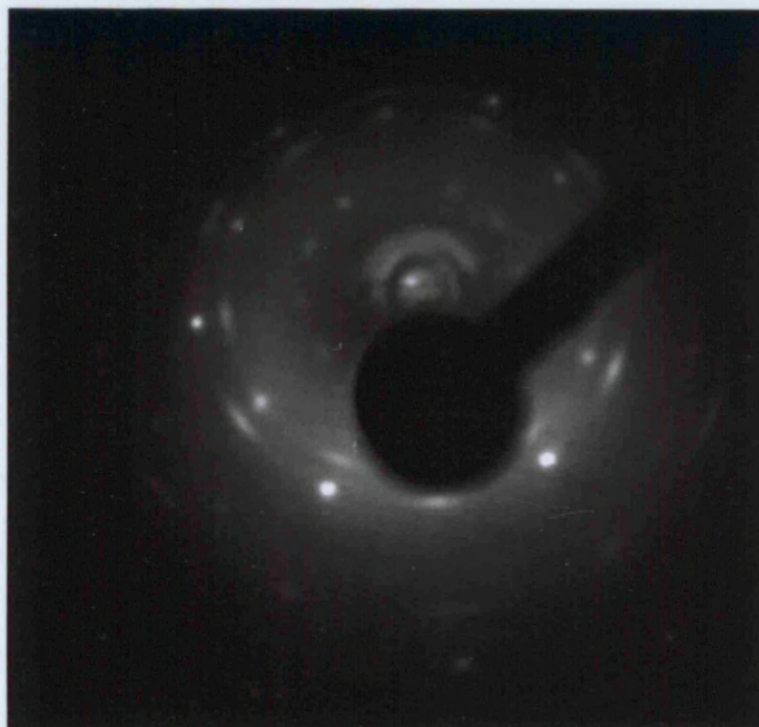


Figure 5.4 – LEED picture of 10 min Ba dose, taken at 123 eV.

The above LEED structure appears to be a (2x2) pattern with additional rings and diffraction spots arranged radially around the central beam spot. The streaking of LEED spots is generally due to the one-dimensional disorder in the overlayer lattice in the real space direction that corresponds to the direction of the streaking, for instance as is seen by adsorption of low coverages of O₂ on Cu(110)^{18,19}. However, if the base planes of the crystallites are randomly rotated around the axis normal to the surface, the disorder will exist in the dimensions of the mutual azimuthal orientation of the substrate and overlayer lattices. Such ring systems are commonly seen for the decomposition of hydrocarbons to graphite and adsorption of alkali metals on certain faces of nickel^{20,21}. The LEED pattern seen in Figure 5.4 appears to be due to a p(2x2) pattern with additional (2x2) structure rotated 30° with respect to the main crystallographic axis. There also appears to be an additional (1x1) lattice that is rotated 30° with respect to the main crystallographic axis. As with the rotated (2x2)

structure there is radial streaking of these additional spots indicating that the features that give rise to these additional spots are not perfectly ordered and that there is a degree of rotational disorder.

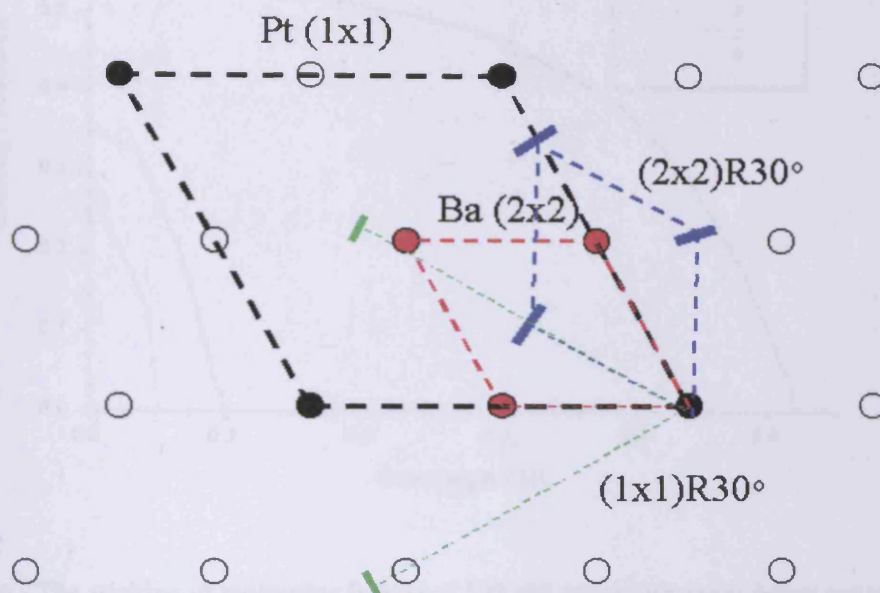


Figure 5.5 – Schematic of the individual features making up the LEED pattern seen in Figure 5.4.

5.2.3 Sticking of CO on increasing Ba surface dosings of Pt(111)

As shown in chapter 3, CO adsorbs with relatively high initial sticking probability ($S_0 = 0.45 \pm 0.02$) on Pt(111) at room temperature. It was found that the initial sticking probability of CO on high doses of barium was negligibly small.

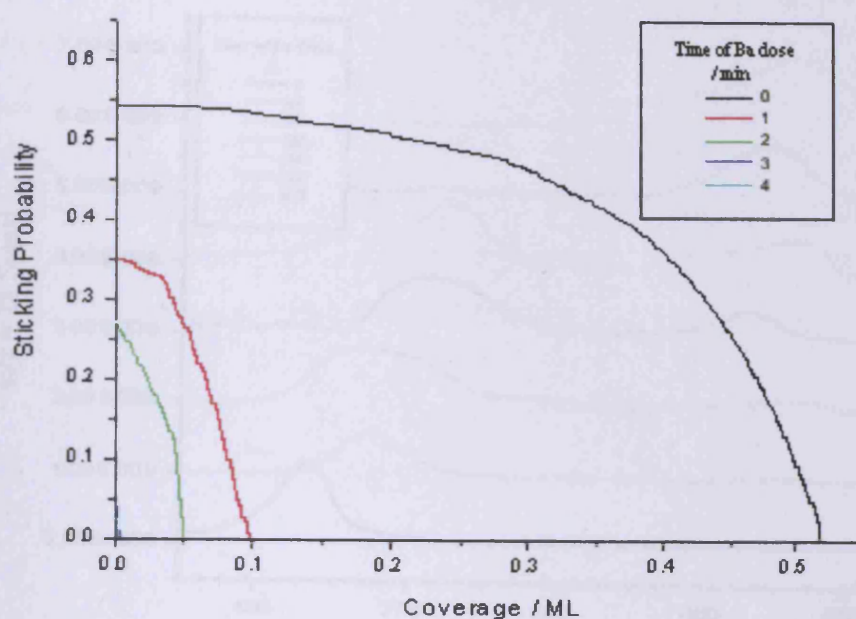


Figure 5.6 - The sticking of molecular beams of CO (50 mbar molecular beam source pressure) on increasing barium coverage of the Pt(111) surface.

From the above figure it is apparent that both the initial sticking probability and the saturation coverage of CO decrease rapidly with increasing surface barium coverage. There is a very large decrease in both the initial sticking probability and saturation coverage between 0 and 1 minutes barium dose, reflecting a difference in the sticking coefficient of CO on platinum and barium. There is no visible CO adsorption in the beam experiment itself for barium coverages of greater than four minutes; however CO adsorption has still taken place (from background gases within the chamber during deposition) as is reflected in the temperature programmed desorption experiments displayed in Figure 5.7 below (note that CO adsorption from the background occurs over the entirety of the crystal surface as well as the molecular beam spot). The lack of sticking in the molecular beam experiments indicates that the surface has been saturated by the background gases during Ba dosing.

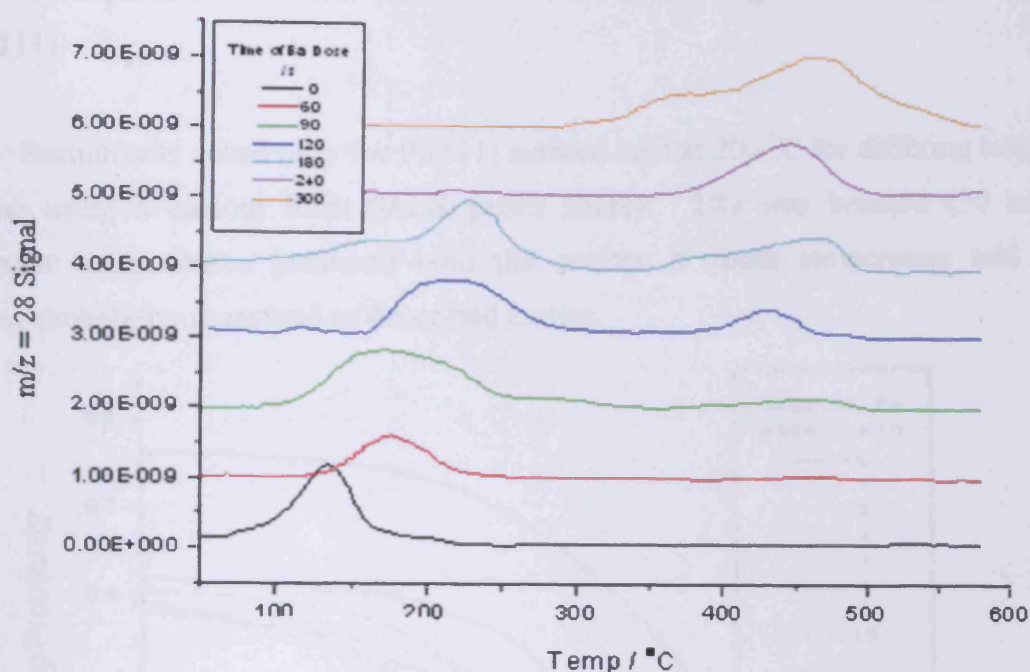


Figure 5.7 – Temperature programmed desorptions from the crystal surface following the molecular beam experiments shown in Figure 5.6.

Figure 5.7 shows that, contrary to as is implied by Figure 5.6, CO has been adsorbed by barium surface doses up to 6 minutes. Two separate adsorption states are visible; a low temperature desorption state that occurs on clean platinum and is hence due to CO on Pt(111). This desorption state increases to higher temperature with increasing barium surface coverage indicating increasing strength of the Pt-CO bond due to increased electron density at the platinum (from the barium). There is also a higher temperature CO desorption peak at ~ 430 °C that is first visible at 120 s barium surface dose. This desorption peak has disappeared by 240 s barium surface dose, indicating completion of a Ba surface layer by this point. As there is no visible sticking in Figure 5.6 for barium surface coverages that are greater than this, yet as CO desorption from these larger coverages has occurred in Figure 5.7 it is obvious that CO has been adsorbed from the background and has saturated the barium layer in the time taken to cool to 50 °C. There was no sign of any CO₂ evolution either whilst beaming or during the temperature programmed desorption experiments that followed the molecular beam experiment.

5.2.4 Adsorption of molecular beams of NO on increasing Ba surface coverage of Pt(111)

Barium was dosed onto the Pt(111) surface held at 200 °C for differing lengths of time using a custom built SAES getter source. NO was beamed (50 mbar molecular beam source pressure) onto the surface at room temperature and the sticking probability measured as described earlier.

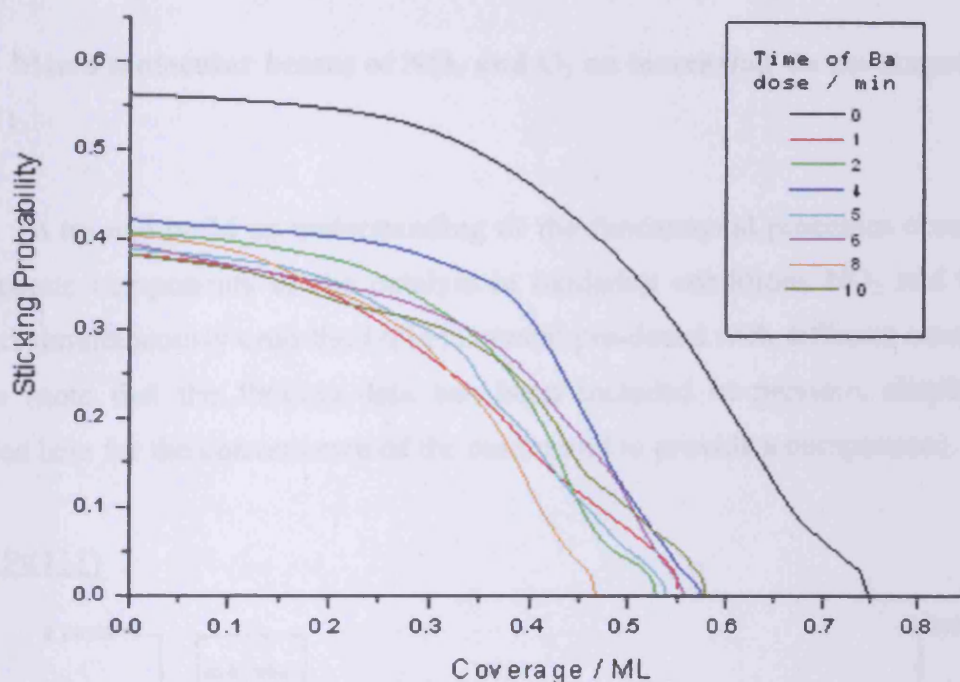


Figure 5.8 - The sticking of molecular beams of NO (50 mbar molecular beam source pressure) on increasing barium coverage of the Pt(111) surface.

Figure 5.8 shows that there is a reduction in both the initial sticking probability and saturation coverage of NO on all barium coverages when compared to the clean Pt(111) surface. It is surprising that there is no clear trend in the reduction in sticking probability and saturation coverage; with 1 min barium dose S_0 decreases from 0.57 to 0.40 (± 0.03) and there after S_0 remains constant within experimental error. This likely reflects a reduction in NO adsorption due to ionised barium at the surface and a coincidentally similar sticking probability of NO on larger barium doses also. As with the earlier experiments of O₂ on barium, there was no NO desorption visible in the temperature programmed desorption experiment following the molecular beam experiment and, as with CO on barium, there was no sign of any decomposition products either whilst beaming or in the temperature programmed

desorption experiment following the molecular beam experiment. In addition to this there was no sign of NO displacing CO from the surface. If the barium surface was left to allow adsorption of CO from the background gases within the chamber on to the barium layer, the adsorbed CO was displaced by the beam of NO whilst beaming, reflecting the enhanced stability of adsorbed NO over adsorbed CO. It was possible to distinguish this desorbing CO from N₂ (from NO reduction) by the lack of a $m/z = 14$ desorption peak in molecular beam experiment.

5.2.5 Mixed molecular beams of NO₂ and O₂ on increasing Ba coverages of Pt(111)

To try and build an understanding of the fundamental processes occurring on the separate components of the catalyst in oxidising conditions NO₂ and O₂ were beamed simultaneously onto the Pt(111) crystal pre-dosed with different coverages of barium (note that the Pt(111) data has been included in previous chapters; it is included here for the convenience of the reader and to provide a comparison).

Clean Pt(111)

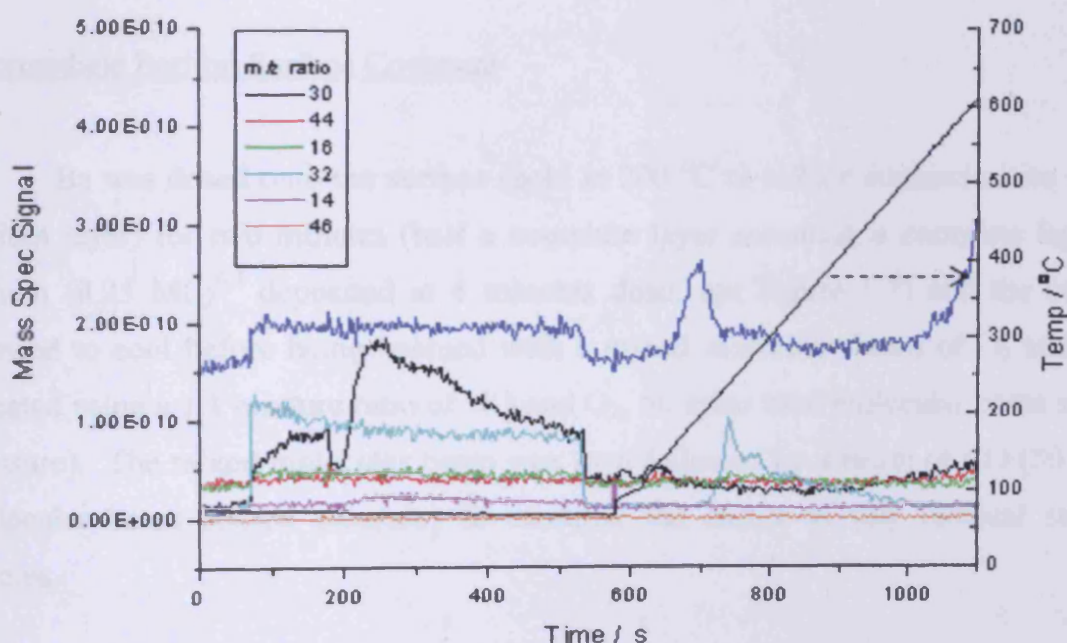


Figure 5.9 – A mixed molecular beam of NO₂ and O₂ (created by a using 1:1 gas mixture ratio of NO and O₂ as described in chapter 3, 50 mbar total molecular beam source pressure) on clean Pt(111) followed by temperature programmed desorption of the crystal surface (time > 580 s).

Figure 5.9 shows that NO_2 initially sticks to the surface with $S_0 = 0.65$. However, after an initial period in which an attenuation of the $m/z = 30$ signal is observed, the $m/z = 30$ signal rises to two and a half times its initial value. There is no apparent O_2 sticking and no changes in $m/z = 46$, 44 or 28 are obvious. This is identical to the experiments shown in chapter 3 that prove that NO has reacted with O_2 in the gasline to form NO_2 . Therefore it is a mixture of NO_2 and O_2 that is being beamed on to the crystal surface (as equal pressures of NO and O_2 were used the mixture dosing the crystal was therefore 2 NO_2 :1 O_2). The large rise in the $m/z = 30$ signal is a result of NO_2 being broken down and liberating NO and atomic oxygen which adsorbs on to the crystal surface, displacing adsorbed NO (although $m/z = 30$ is a cracking fragment of NO_2 , $m/z = 30$ is the molecular ion of NO, explaining why the rise in $m/z = 30$ signal is so large). The temperature programmed desorption portion of the spectra (> 580 s) shows a large $m/z = 28$ desorption peak due to the adsorption of CO from the background gases on the rest of the crystal outside the beam spot as well as a $m/z = 44$ desorption peak from the oxidation of background CO by atomic oxygen from the breakdown of NO_2 . There is also a $m/z = 32$ desorption peak at 360°C due to the desorption of O_2 from Pt(111) as a result of NO_2 decomposition and adsorption of atomic oxygen.

Intermediate Barium Surface Coverage

Ba was dosed onto the surface (held at 200°C to reduce contamination of the barium layer) for two minutes (half a complete layer assuming a complete layer of barium $(0.25 \text{ ML})^{6,7}$ deposited at 4 minutes dose, see Figure 5.7) and the surface allowed to cool before being beamed with a mixed molecular beam of O_2 and NO_2 (created using a 1:1 mixture ratio of NO and O_2 , 50 mbar total molecular beam source pressure). The mixed molecular beam was then followed by a beam of CO (50 mbar molecular beam source pressure) to examine the nature of any residual surface species.

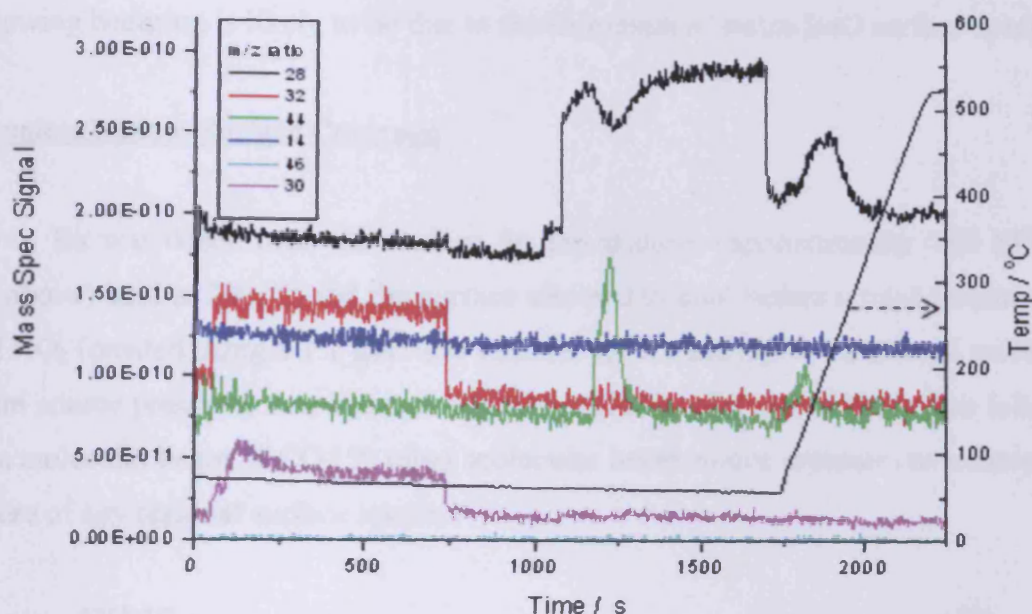


Figure 5.10 – A mixed molecular beam of NO_2 and O_2 (created using a 1:1 ratio mixture of NO and O_2 , 50 mbar total source pressure) followed by a beam of CO (50 mbar molecular beam source pressure) on 0.13 ML Ba surface coverage. Following the molecular beam experiment the temperature of the surface was ramped (time > 1750 s) as an aid to identify any remaining surface species.

The above molecular beam experiment appears very similar to the experiment shown in Figure 5.9. NO_2 initially adsorbs onto the surface but is broken down with the release of NO and the storage of $\text{O}_{(\text{a})}$ on the surface, as is evidenced by the CO_2 desorption when beaming CO . Other than the oxygen from the NO_2 there is no evidence of O_2 adsorption from the beam. The only features in the temperature programmed desorption part of the experiment (time > 1750 s) is a $m/z = 28$ desorption peak at around 235 °C (similar in temperature to the CO desorption peak seen for two minutes barium dose in Figure 5.7 and is therefore likely to be due to the adsorption of CO on to barium-effected platinum sites from background gases in the chamber as well as from the molecular beam) as well as a $m/z = 44$ desorption peak at approximately 100 °C (likely to be N_2O from the release of stored NO_2). That no O_2 adsorption from the beam occurs is surprising as, according to Figure 5.1, there should be measurable O_2 adsorption on the barium. It is likely that oxygen is adsorbed on the barium from the breakdown of NO_2 as this is more energetically favourable due to there being less of an energy barrier to dissociation to overcome.

As stated earlier the lack of O_2 in the temperature programmed desorption experiment following beaming is likely to be due to the formation of stable BaO surface species.

Complete Barium Surface Coverage

Ba was dosed onto the surface for ten minutes (approximately 0.63 ML Ba, see above) held at 200 °C and the surface allowed to cool before a mixed beam of O_2 and NO_2 (created using a 1:1 gas ratio mixture of NO and O_2 , 50 mbar total molecular beam source pressure) was beamed onto the surface. The mixed beam was followed by a molecular beam of CO (50 mbar molecular beam source pressure) to examine the nature of any residual surface species.

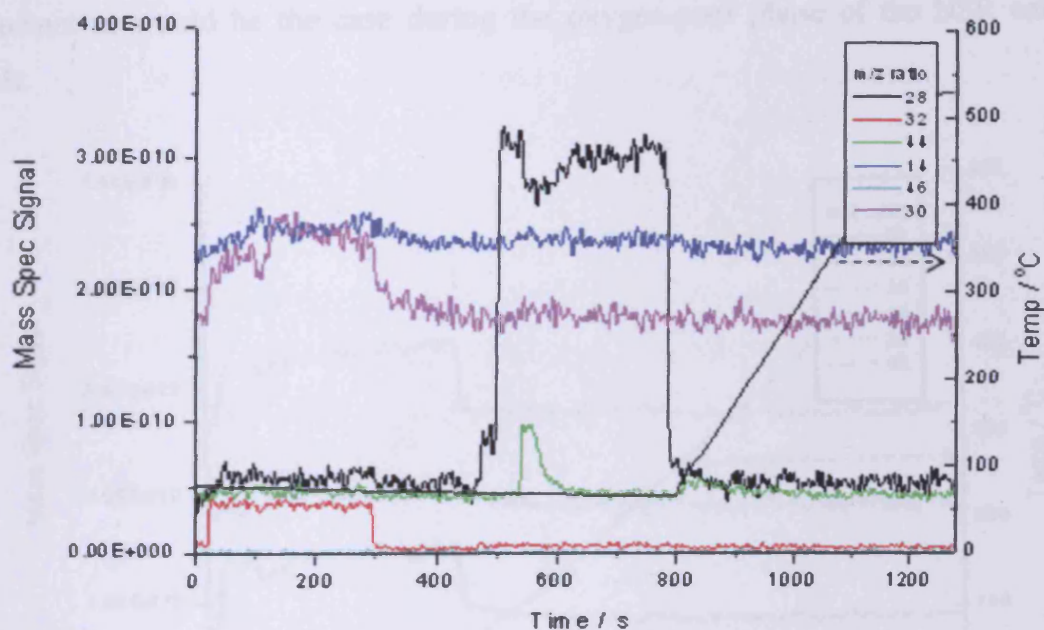


Figure 5.11 – A mixed molecular beam of NO_2 and O_2 (created using a 1:1 mixture ratio of NO and O_2 , 50 mbar total molecular beam source pressure) followed by a molecular beam of CO on 0.63 ML Ba surface coverage. Following the molecular beam experiments the temperature of the crystal surface was steadily ramped as an aid to identifying any residual surface species (time > 800 s).

As with Figure 5.10, Figure 5.11 appears to behave in a very similar manner to the Pt(111) clean surface, in that NO_2 is broken down by the surface with the desorption of NO and the storage of atomic oxygen. Unlike Figure 5.10 there is a slight adsorption of the O_2 in the beam, likely to be due to the time delay between the

adsorption of NO_2 and desorption of NO providing a time window in which oxygen from the beam may adsorb. The $m/z = 28$ desorption peak due to CO from platinum that is visible in Figure 5.10 is not present in the above figure, indicating that the platinum surface is completely covered with barium.

5.2.6 Mixed molecular beams of NO and CO on Ba dosed $\text{Pt}(111)$

Barium was dosed onto the surface for ten minutes (approximately 0.63 ML Ba assuming a constant dosing rate and a complete layer of barium deposited at 4 minutes dose, see section 5.2.5 and Figure 5.7) and CO and NO (1:1 ratio mixture, 50 mbar total molecular beam source pressure) beamed onto the crystal surface at room temperature to determine if there was any reaction of NO in the presence of a reductant as would be the case during the oxygen-poor phase of the NSR catalyst cycle.

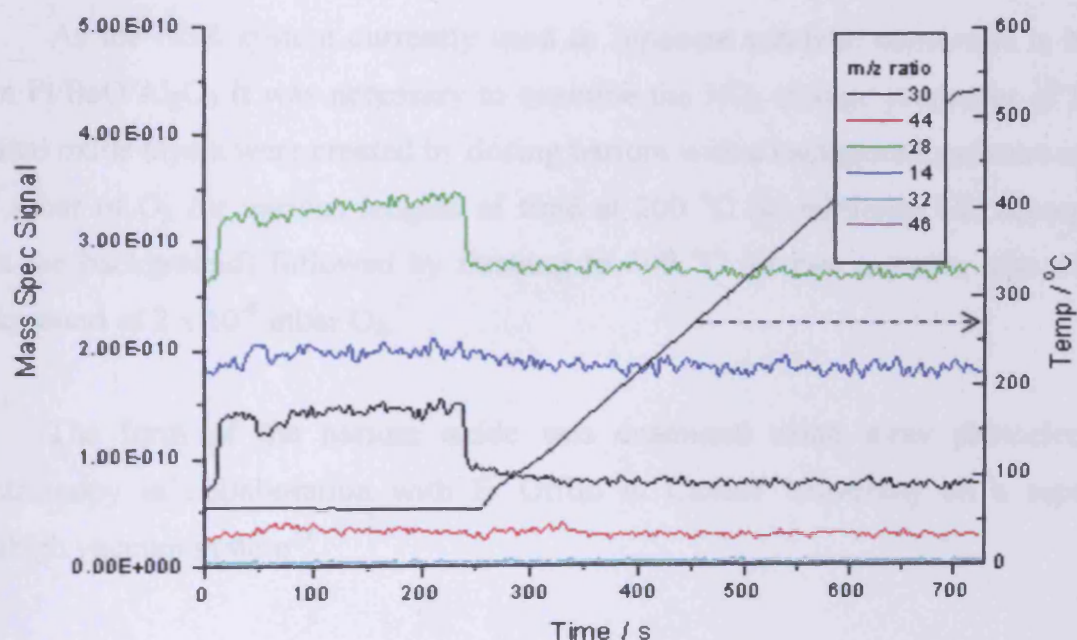


Figure 5.12 – A mixed molecular beam experiment of NO and CO (created using a 1:1 gas ratio mixture of NO and CO , 50 mbar total molecular beam source pressure) on 0.63 ML barium followed by temperature programmed desorption of the crystal surface (time > 255 s) as an aid to identifying any residual surface species.

From the above experiment it can be seen that the NO adsorbs with a sticking coefficient characteristic of that seen for NO adsorbing on a complete layer of barium

and that the CO adsorbs with a higher sticking coefficient than would be expected from Figure 5.6 ($S_0 = 0.2$, in figure 5.6 no CO adsorption is observed for coverages of Ba of larger than 4 minutes dose). However this is not necessarily due to a surface reaction between adsorbed NO and CO species, as Figure 5.7 indicates that CO is adsorbed by the surface, making it likely that the non-adsorption of CO seen for high coverages of barium in Figure 5.6 is due to the surface becoming saturated with CO whilst dosing barium. There is no desorption of either reactant species or products of a reaction between the two whilst beaming or in the temperature programmed desorption part of the experiment (time > 255 s), indicating that both NO and CO have reacted (either singly or together) with the barium on the surface and formed stable surface species that desorb outside of the temperature range used in the temperature programmed desorption experiments.

5.2.7 X-ray photoelectron spectroscopic analysis of barium oxide

As the NSR system currently used in Japanese catalytic converters is based upon Pt/BaO/Al₂O₃ it was necessary to examine the NO_x storage properties of BaO. Barium oxide layers were created by dosing barium with a background pressure of 2×10^{-8} mbar of O₂ for various lengths of time at 200 °C (to minimise CO adsorption from the background) followed by flashing to 500 °C for two minutes, also with a background of 2×10^{-8} mbar O₂.

The form of the barium oxide was examined using x-ray photoelectron spectroscopy in collaboration with F. Grillo at Cardiff University on a separate ultrahigh vacuum system²².

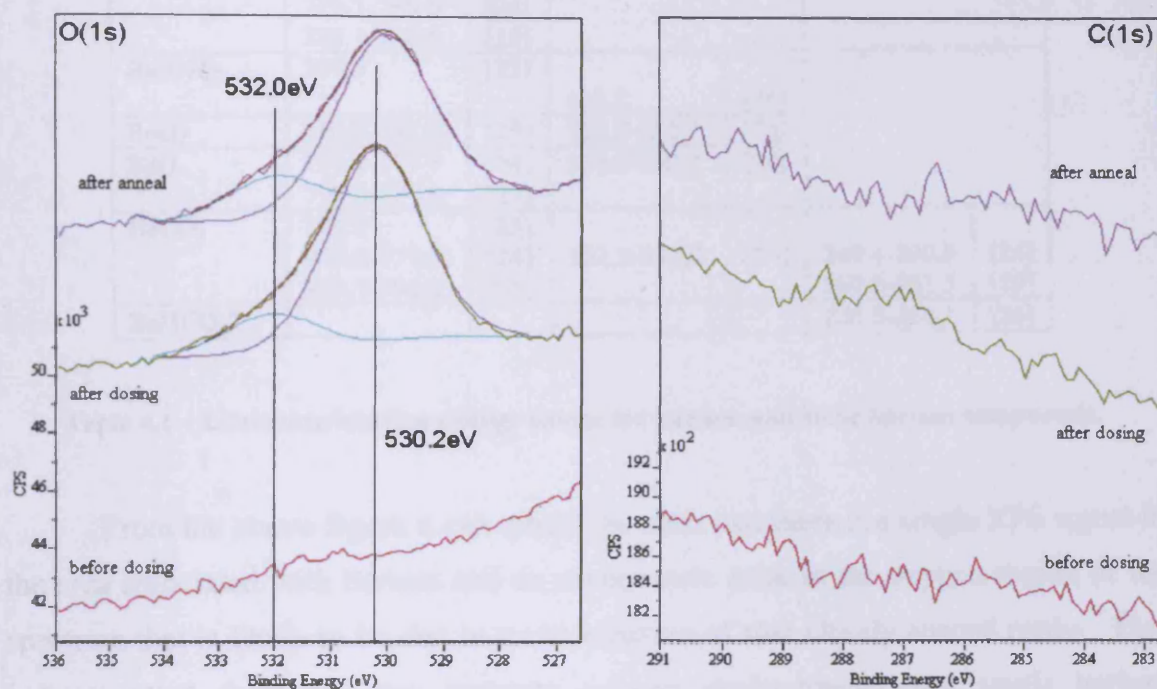


Figure 5.13 – O(1s) and C(1s) XPS spectra of crystal prior to dosing (red), immediately post dosing (light brown) and after annealing at 500 °C (pink).

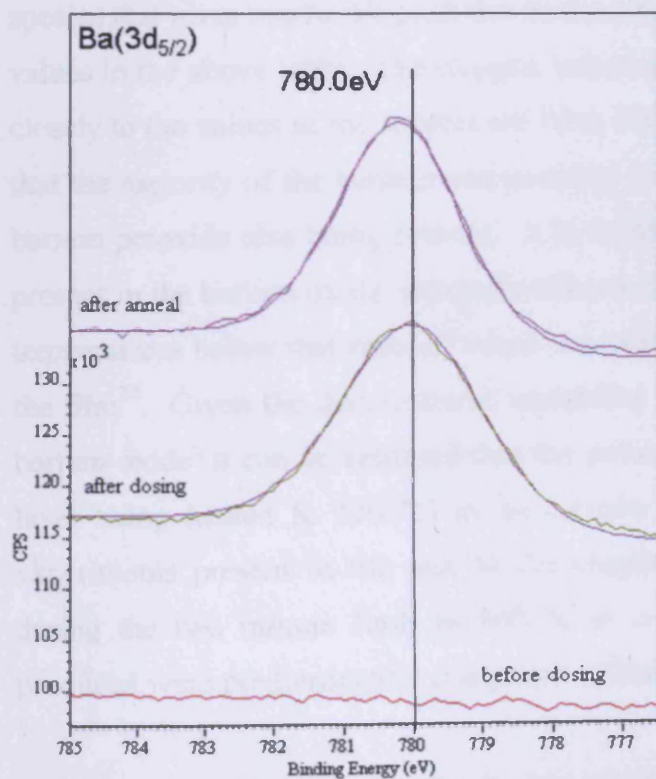


Figure 5.14 - Ba(3d_{5/2}) and O(1s) XPS spectra of Pt(111) surface before dosing Ba and O₂ (red), immediately after dosing (light brown) and post anneal (pink).

Compound	Ba(3d _{5/2})		O(1s)		C(1s)	
Ba	779.3-780.5	[23]				
	779.3-780.6	[24]				
	780.1-780.6	[25]				
Ba(OH) ₂	779.5	[23]	531.2	[24]		
BaO ₂	780.3-781.2	[25]	532.0-532.7	[25]		
BaO	779.1-779.9 779.2-779.8	[24] [25]	528.3-530.2	[24]		
BaCO ₃	779.7	[23]	531.1-532.2	[24]	289.4-290.8	[24]
	779.8-779.9	[24]			289.0-291.5	[25]
	779.7-780.2	[25]				
BaHCO ₃ ⁱⁱ					285.5-286.1	[26]

Table 4.1 – Literature binding energy values for barium and some barium compounds.

From the above figure it can clearly be seen that there is a single XPS signal in the area associated with barium and an asymmetric peak in the oxygen region of the spectrum that is likely to be due to a combination of two closely spaced peaks. This indicates that there are two separate oxygen environments and single barium environment. There is insufficient resolution in Figure 5.14 to determine the barium species that gives rise to the peak due to the close proximity and overlap of the barium values in the above table. The oxygen values given in table 4.1 that correspond most closely to the values in the spectra are from BaO₂ and BaO. From this it seems likely that the majority of the surface composition is mainly barium oxide with a degree of barium peroxide also being present. It is worth noting that Ba(OH)₂ is unlikely to be present in the barium oxide/ peroxide adlayer due to Ba(OH)₂ decomposing at surface temperatures below that reached when annealing the crystal during the preparation of the film²⁷. Given the demonstrated instability of barium peroxide when compared to barium oxide⁶ it can be assumed that the peroxide present in the layer was due to the layer being heated to 500 °C in an oxygen environment. As the barium dosing experiments present in the rest of the chapter did not use an oxygen background during the two minute flash to 500 °C it is reasonable to assume that the layers produced were predominantly composed of BaO.

5.2.8 Adsorption of molecular beams of CO on increasing BaO coverages of the Pt(111) crystal surface

Layers of barium oxide were created by dosing the Pt(111) crystal surface held at 200 °C (to minimise CO adsorption from the background) with barium in a

background pressure of 2×10^{-8} mbar of O_2 for differing lengths of time, followed by removing the oxygen and flashing the crystal $500^\circ C$ for two minutes. The crystal was then allowed to cool and CO (50 mbar molecular beam source pressure) beamed onto the surface held at $50^\circ C$.

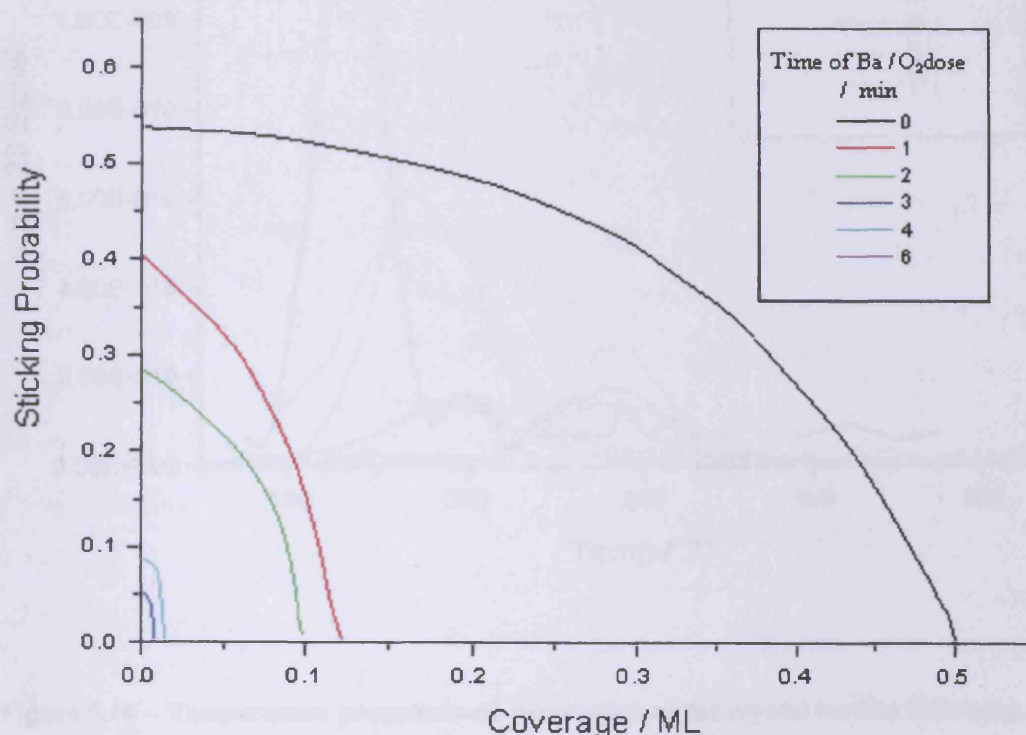


Figure 5.15 –The sticking probability against time and coverage for a molecular beam of CO (50 mbar molecular beam source pressure) on increasing BaO coverage of Pt(111).

The above figure shows the effect of increasing surface coverages of barium oxide on the sticking probability of a beam of CO (50 mbar molecular beam source pressure) and the maximum coverage to which it saturates. From the above figure it can clearly be seen that dosing BaO onto the surface greatly reduces both the initial sticking of CO and the maximum coverage to which it saturates. There is a decrease in sticking probability from 0-3 minutes barium oxide surface dose. As the surface dose is increased to four minutes BaO the initial sticking probability and saturation coverage remain constant (within experimental error). After six minutes of dosing the surface no appreciable sticking of the beam of CO is observed.

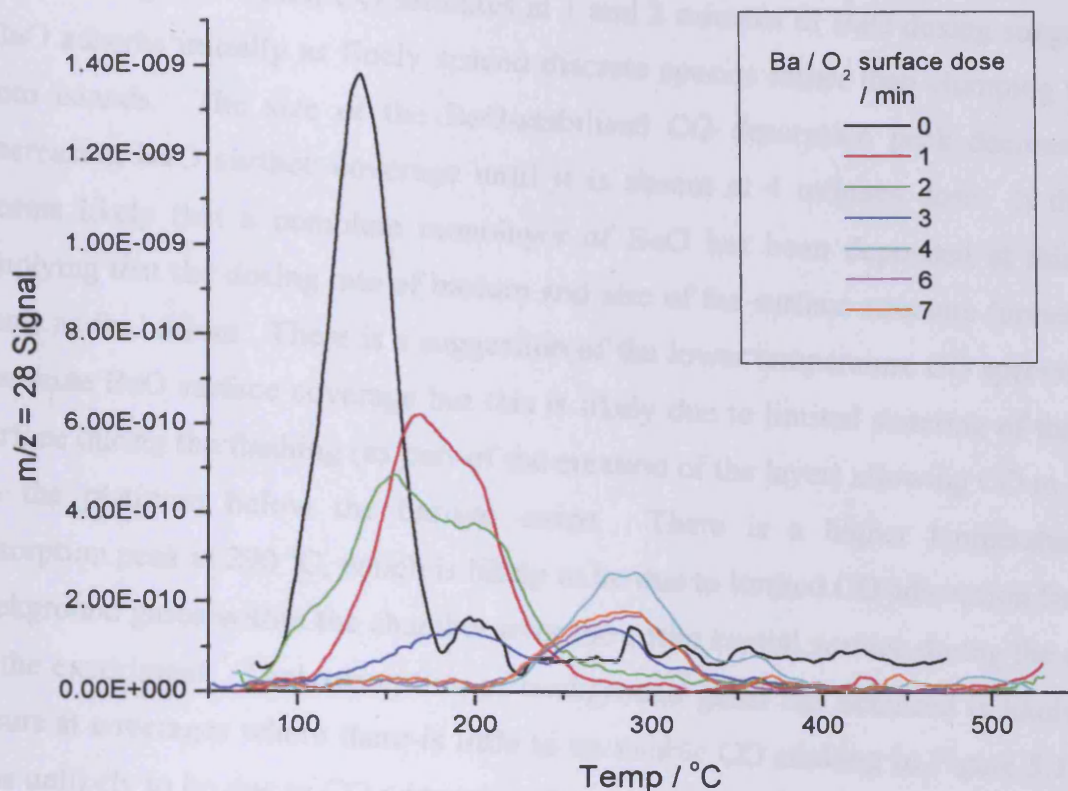


Figure 5.16 – Temperature programmed desorption of the crystal surface following the molecular beam experiments shown in Figure 5.15.

Figure 5.16 shows the relationship between the amount of BaO present at the crystal surface and the temperature of desorption of the adsorbed CO. CO adsorbing on just the Pt(111) surface gives a single CO desorption peak at 139 °C. However, the addition of BaO to the surface shifts the maximum of this desorption peak to higher temperatures and reduces it in height. The shift in temperature is likely due to attractive interactions between adsorbed BaO and CO on platinum stabilising the adsorbed species and increasing the energy required for desorption. The reduction in peak area is not consistent with the reduction in sticking probability seen in Figure 5.15, indicating that adsorption of CO from background gases has occurred. However, when one takes into account the differences in area between the CO desorption peaks for the clean surface and 6 minutes barium dose (bearing in mind the difference in area between the area of the beam spot and the area of the whole crystal surface) it is apparent that dosing Ba/O₂ at 200 °C has limited the CO contamination of the layer. The fact that there is little difference between the sticking coefficients

and coverages to which CO saturates at 1 and 2 minutes of BaO dosing suggests that BaO adsorbs initially as finely spaced discrete species rather than clumping together into islands. The size of the BaO-stabilised CO desorption peak decreases with increasing BaO surface coverage until it is absent at 4 minutes dose. It therefore seems likely that a complete monolayer of BaO has been deposited at this point, implying that the dosing rate of barium and size of the surface structure formed is the same as for barium. There is a suggestion of the lower temperature CO species in the 5 minute BaO surface coverage but this is likely due to limited sintering of the oxide surface during the flashing (as part of the creation of the layer) allowing CO to adsorb on the platinum below the barium oxide. There is a higher temperature CO desorption peak at 290 °C, which is likely to be due to limited CO adsorption from the background gases within the chamber over the entire crystal surface during the course of the experiment. That adsorption of background gases has occurred is likely as it occurs at coverages where there is little to no visible CO sticking in Figure 5.15 and so is unlikely to be due to CO adsorption from the beam. The size of this peak grows slightly with increasing time of BaO dose, indicating that it is BaO that the CO is adsorbing on. This CO adsorption environment gives a desorption peak that is comparable in magnitude to the desorption peaks from the CO that has been beamed onto the crystal due to the fact that the beam spot only comprises a fraction of the total crystal surface area whereas BaO was deposited over the entirety of the surface.

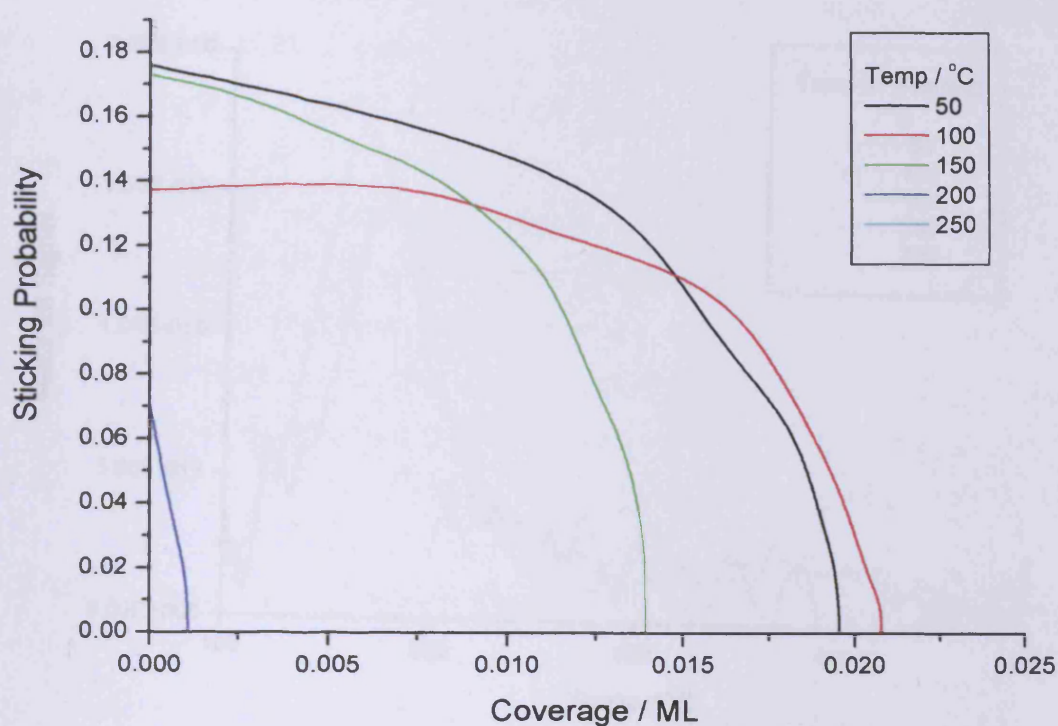


Figure 5.17 – The variation of sticking probability with CO coverage for molecular beams of CO (50 mbar molecular beam source pressure) on a complete BaO coverage of the Pt(111) surface (4 min dose, see Figure 5.16) held at increasing surface temperatures.

As Figure 5.17 shows, the initial sticking probability of CO remains fairly constant ($\sim 0.14 - 0.15$, within experimental error) from 50 °C to 150 °C. CO appears to saturate to the highest coverage when beamed at 100 °C. This is likely due to the increased time of cooling to 50 °C after flashing to 500 °C allowing more time for adsorption of background gases, with a consequent occupancy of surface adsorption sites. However, as the surface temperature is increased above 100 °C the maximum saturation coverage exhibits a definite reduction. This trend continues as the temperature is raised to 200 °C, along with a decrease in the sticking probability. No CO adsorption was observed for surface temperatures of 200 °C and above.

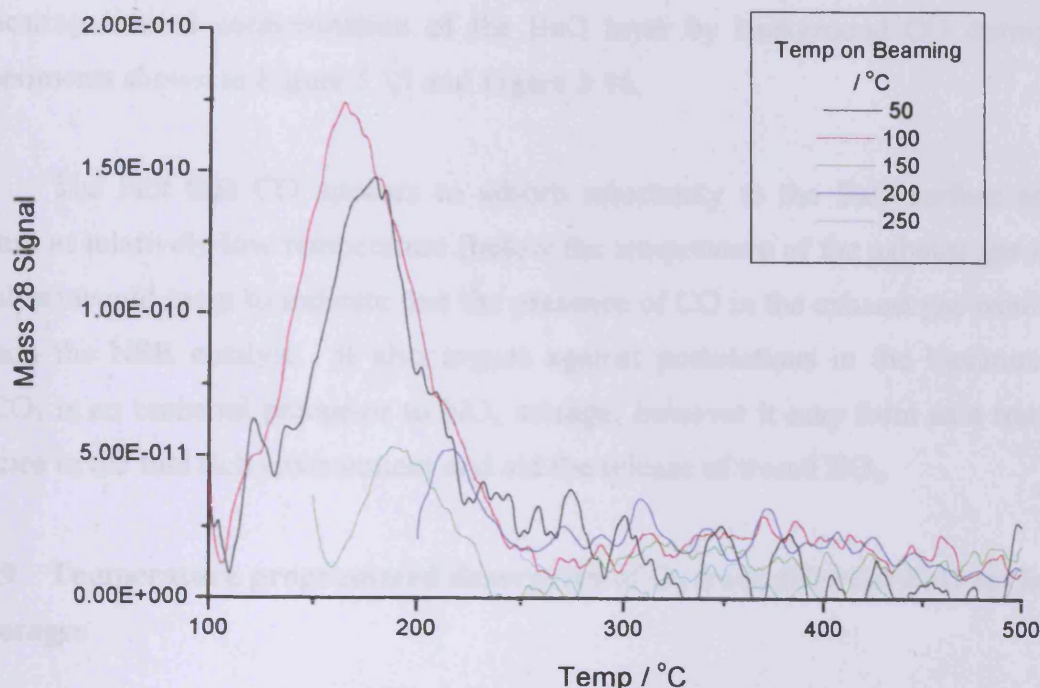


Figure 5.18 – Temperature programmed desorption of CO from the crystal surface following the molecular beam experiments shown in Figure 5.17

The above figure shows the temperature programmed desorption experiments following the molecular beam experiments shown in Figure 5.17. As can be seen the largest desorption peak occurs when beaming at 100 °C. This is consistent with Figure 5.17, in which the beaming at 100 °C saturates to the highest coverage. The desorption peak at 100 °C dosing temperature also desorbs at a slightly lower temperature than the one at 150 °C, again consistent with a higher saturation coverage. At 150 °C and above the quantity of desorbing molecules is much less; this is reflected in the decreased sticking probabilities and saturation coverages seen in Figure 5.17. At 250 °C no CO desorption peak is evident, corresponding with the lack of sticking seen in Figure 5.17.

The position of the maximum of the CO desorption peaks from the Pt/BaO surface would seem to imply that the desorption features are a result of the adsorption of CO on the Pt(111) surface. There is no indication of any BaO-CO species and the reduced sticking probability would seem to indicate that the observed CO sticking occurs on Pt(111) with BaO serving to block adsorption sites. However there is no

CO desorption at ~ 300 °C, which would be expected from Figure 5.16, likely indicating limited contamination of the BaO layer by background CO during the experiments shown in Figure 5.15 and Figure 5.16.

The fact that CO appears to adsorb reluctantly to the BaO surface and to desorb at relatively low temperature (below the temperature of the exhaust gas in the catalyst) would seem to indicate that the presence of CO in the exhaust gas would not poison the NSR catalyst. It also argues against postulations in the literature that BaCO₃ is an essential precursor to NO_x storage; however it may form as a transient species in the fuel rich environment and aid the release of stored NO_x.

5.2.9 Temperature programmed desorption of O₂ from different BaO surface coverages

Barium oxide layers were created by dosing the Pt(111) crystal surface held at 200 °C (to minimise CO adsorption from the background) with barium in a background pressure of 2×10^{-8} mbar of O₂ for differing lengths of time, followed by flashing to 500 °C for two minutes. The surface was then allowed to cool and O₂ (50 mbar molecular beam source pressure) beamed onto the surface held at 50 °C.

As stated in chapter 3, O₂ adsorbs on clean Pt(111) with an almost negligibly small initial sticking probability ($S_0 = 0.06$). It was found that dosing barium oxide onto the platinum surface had the effect of decreasing this further, such that there was no appreciable adsorption of O₂ molecular beams (within experimental error) for all surface coverages of BaO. From this it can be inferred that there is no BaO-promoted O₂ dissociation followed by the spillover of atomic oxygen to surface platinum adsorption sites in the manner postulated for K⁺ on Pt(111) (see section 4.2.3), and that the deposited barium has been saturated with oxygen during the creation of the layer. There were also no obvious O₂ or CO desorption peaks in the temperature programmed desorption experiments following the molecular beam experiments, indicating that the BaO surface created broke down outside the temperature range of the experiment (it was found that it could only be removed via sputtering) and was relatively uncontaminated by background CO. It was found however that background-dosing O₂ onto a BaO layer (6 minutes Ba dose, 2×10^{-8} mbar O₂

background pressure, 200 °C) gave rise to oxygen desorption peaks when heated (see Figure 5.19, below).

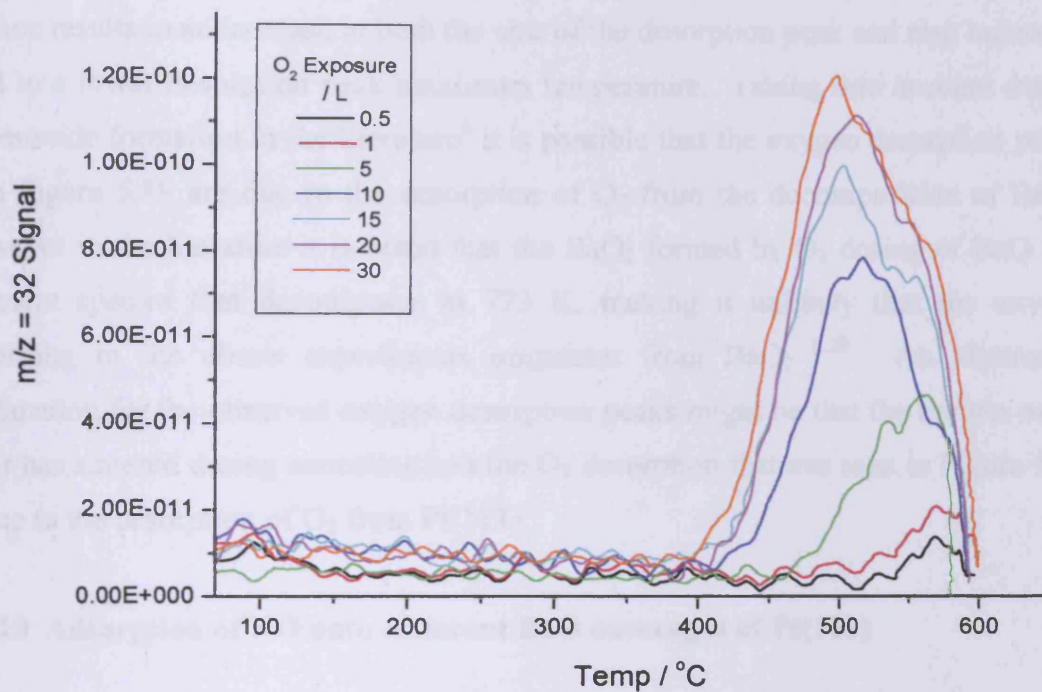


Figure 5.19 – Temperature programmed desorption of O₂ from BaO layer.

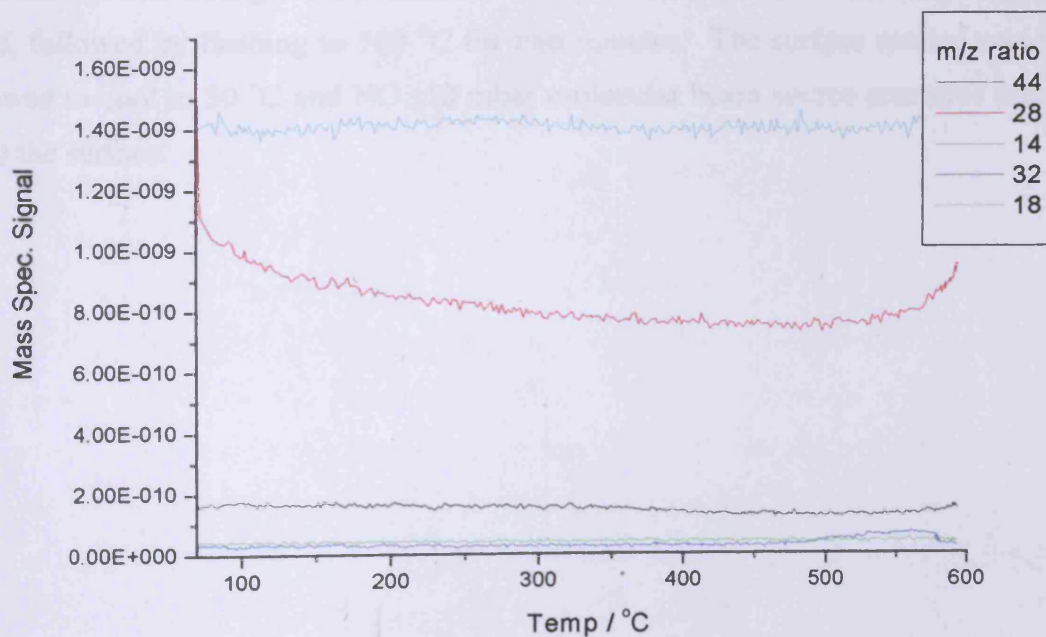


Figure 5.20 – Temperature programmed desorption of 5L O₂ exposure from BaO layer showing m/z = 14, 18, 28, 32 and 44.

From figure 5.19 it is evident that at low exposures there is a single O₂ desorption environment at 560-570 °C. As Figure 5.20 shows, no other desorbing species were evident during the experiment. Increasing the dose of oxygen onto the surface results in an increase in both the size of the desorption peak and also induces a shift to a lower desorption peak maximum temperature. Taking into account details of peroxide formation in the literature⁶ it is possible that the oxygen desorption peaks seen Figure 5.19 are due to the desorption of O₂ from the decomposition of BaO₂. However in the literature it is noted that the BaO₂ formed by O₂ dosing of BaO is a transient species that decomposes at 723 K, making it unlikely that the oxygen desorbing in the above experiments originates from BaO₂^{6,28}. An alternative explanation for the observed oxygen desorption peaks might be that the barium oxide layer has sintered during annealing and the O₂ desorption features seen in Figure 5.19 is due to the desorption of O₂ from Pt(111).

5.2.10 Adsorption of NO onto different BaO coverages of Pt(111)

Barium oxide layers were created by dosing the Pt(111) crystal surface held at 200 °C (to minimise CO adsorption from the background gases within the chamber) with barium in a background pressure of 2×10^{-8} mbar of O₂ for differing lengths of time, followed by flashing to 500 °C for two minutes. The surface created was then allowed to cool to 50 °C and NO (50 mbar molecular beam source pressure) beamed onto the surface.

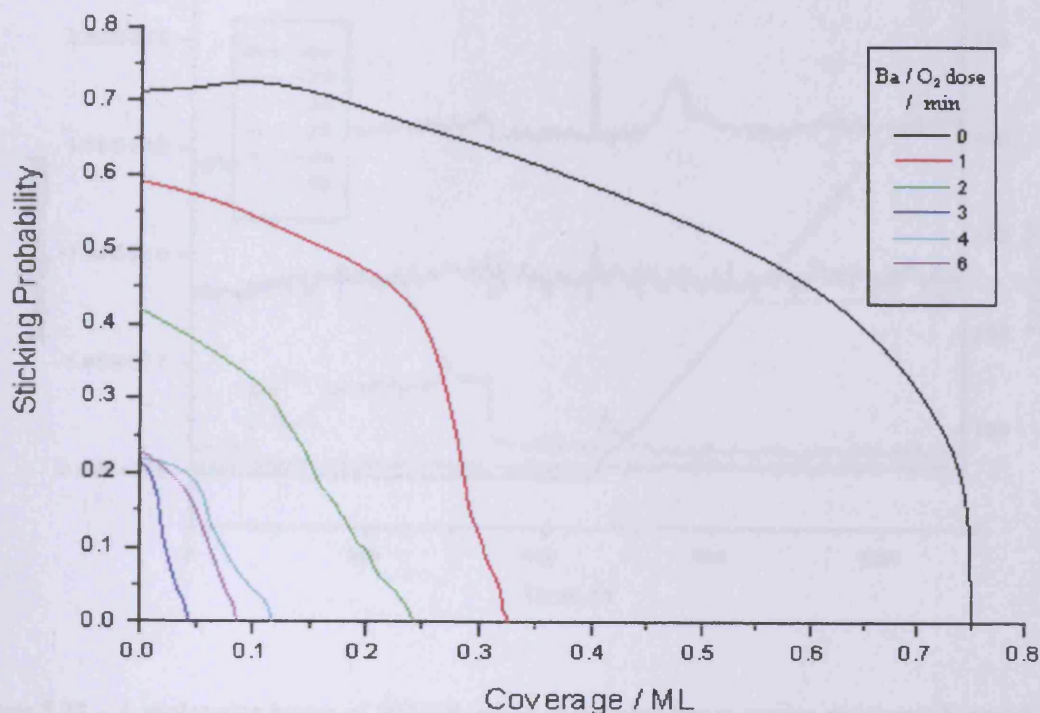


Figure 5.21 – The variation of the sticking probability of molecular beams of NO (50 mbar molecular beam source pressure) with NO coverage for increasing BaO surface coverages of the Pt(111) crystal.

Figure 5.21 shows that NO sticks well on Pt(111) alone with high initial sticking probability ($S_0 = 0.71$). From the above figure it is apparent that increasing the surface coverage of barium oxide decreases both the initial sticking coefficient and the maximum saturation coverage, to a minimum of $S_0 = 0.21$ at 3 minutes Ba/O₂ dosing time. Further increases in the barium oxide surface coverage have no effect on the sticking probability (within experimental error). However when one examines the actual individual molecular beam experiments it is apparent that the situation is more complicated than simple reversible adsorption occurring (see figures 5.24 and 5.24). The reduction in sticking of NO with increasing amounts of barium oxide on the surface agrees with STM and pulse-flow reactor studies in which it has been found that NO_x is only stored in the presence of both NO and O₂^{6,29}.

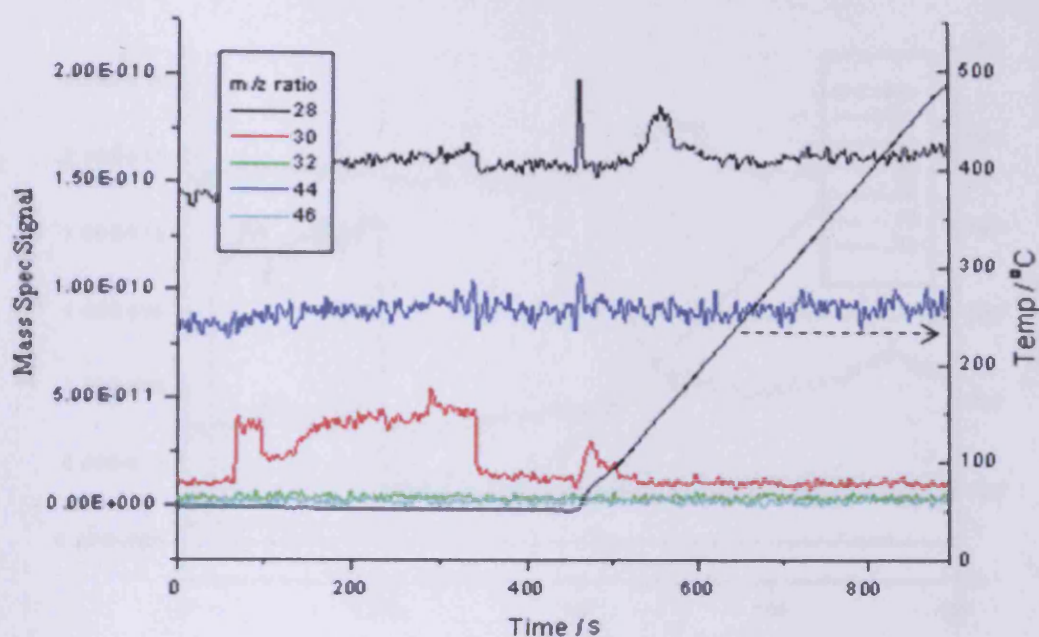


Figure 5.22 – A molecular beam of NO (50 mbar molecular beam source pressure) beamed onto clean Pt(111) surface followed by temperature programmed desorption of the surface (time > 450 s).

In Figure 5.22 NO (50 mbar molecular beam source pressure) has been beamed onto the Pt(111) crystal with no BaO surface coverage (note that this data has been displayed in chapter 3, it is included here as an aid for comparison). There is no obvious NO decomposition (no $m/z = 28$ or 44 desorption peaks are evident whilst beaming) and NO desorbs from the crystal surface almost as soon as the crystal is heated (~ 80 °C). It is therefore evident that NO adsorbs weakly and reversibly with a large sticking coefficient ($S_0 = 0.71$) in a molecular state at room temperature. As NO adsorbs so weakly yet with a large sticking coefficient at room temperature is likely that the adsorbed NO is surface mobile.

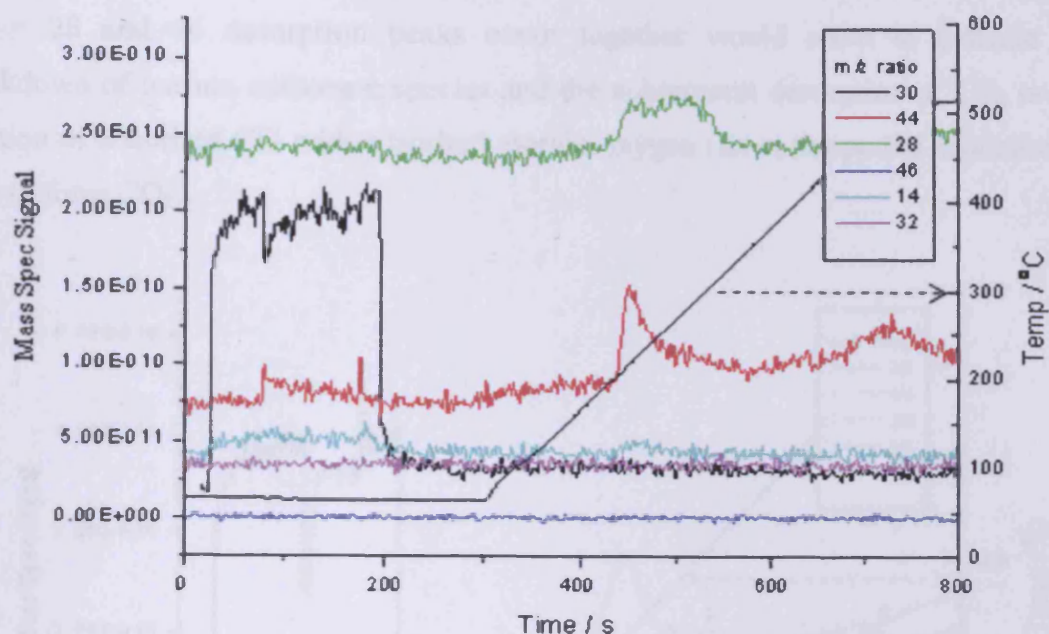


Figure 5.23 – A molecular beam of NO (50 mbar molecular beam source pressure) beamed onto 6 min Ba/O₂ surface dose of the Pt(111) crystal surface followed by temperature programmed desorption of the surface (time > 300 s).

In Figure 5.23 the Pt(111) crystal surface has been completely covered with more than a complete layer of BaO (6 min surface dose). It is immediately apparent that the sticking coefficient of NO is greatly reduced ($S_0 = 0.18$ as opposed to 0.71 for clean Pt(111)). In addition to this there is also no $m/z = 30$ desorption peak visible in the temperature programmed desorption part of the experiment (time > 300 s), suggesting irreversible NO adsorption or decomposition. There is a $m/z = 44$ desorption peak that appears immediately upon beaming, lending itself to the explanation that two NO molecules have been broken down to N₂O, which then desorbs from the surface at room temperature. Alternatively the $m/z = 44$ peak could be due to the desorption of CO₂ formed by reaction between CO adsorbed from background gases during the creation of the layer and oxygen from the reduction of NO. If NO has been reduced this would leave oxygen present on the crystal, possibly occupying adsorption sites and bringing the reaction to a halt as seen for NO dissociation on Pt(110)³⁰. There is no sign of this oxygen present in the temperature programmed desorption, however there is a large $m/z = 44$ desorption peak at 220 °C. It therefore seems likely that the adsorbed oxygen has reacted with CO adsorbed as barium carbonate and desorbed as CO₂. There is also a $m/z = 28$ desorption peak at

260 °C, also likely due to the desorption of CO gases from the BaO layer. That the $m/z = 28$ and 44 desorption peaks occur together would seem to indicate the breakdown of barium carbonate species and the subsequent desorption of CO_x or the reaction of adsorbed CO with adsorbed atomic oxygen (from the partial reduction of NO) to form CO_2 .

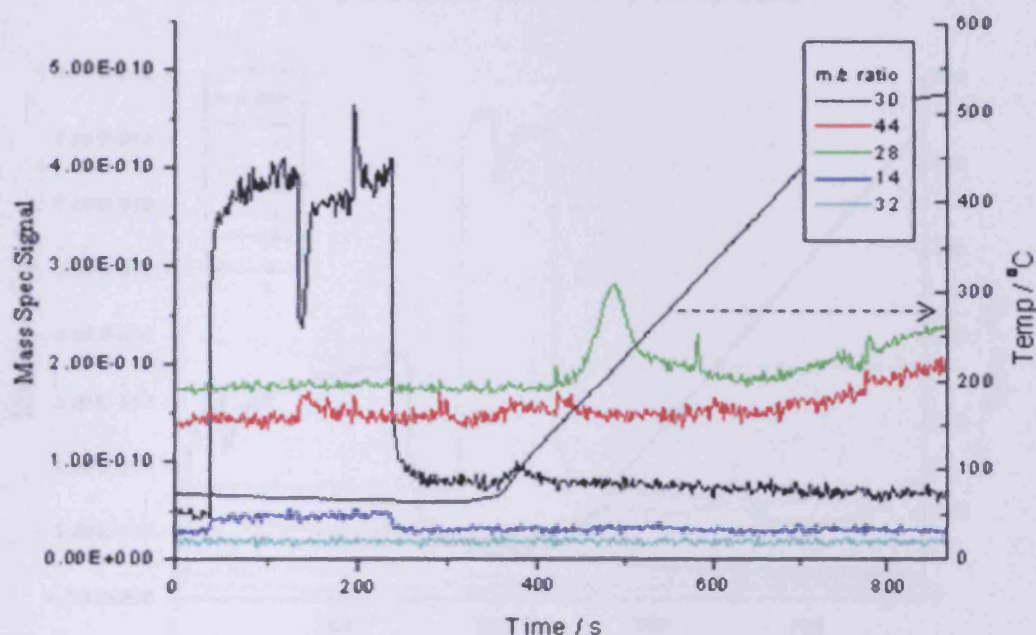


Figure 5.24 – A molecular beam of NO (50 mbar molecular beam source pressure) beamed onto Pt/BaO (2 min Ba/O₂ dose) followed by temperature programmed desorption of the crystal surface (time > 350 s).

Figure 5.24 is a molecular beam of NO onto an intermediate BaO coverage, with areas of BaO and Pt(111) both present at the surface. NO sticks to the mixed surface with a sticking coefficient ($S_0 = 0.49$) in between the two extremes of no surface BaO and complete BaO surface coverage. In a similar manner to Figure 5.23 there is a $m/z = 44$ desorption peak immediately on NO adsorption indicating partial NO reduction and the oxidation of CO adsorbed from background gases in the chamber. There is also a $m/z = 30$ desorption peak at approximately 80 °C in the temperature programmed desorption part of the experiment indicating that NO has also adsorbed reversibly on the Pt(111). There is also a $m/z = 28$ desorption peak at 210 °C present in the temperature programmed desorption, likely due to incorporation of background CO into the BaO during the creation of the layer. This desorption peak

is a single peak, unlike that seen in Figure 5.23, possibly due to the lesser thickness of the barium oxide layer.

In order to investigate the nature of the residual surface species the NO molecular beam decomposition reactions were followed with beams of O₂ and CO (50 mbar molecular beam source pressures were used for all species).

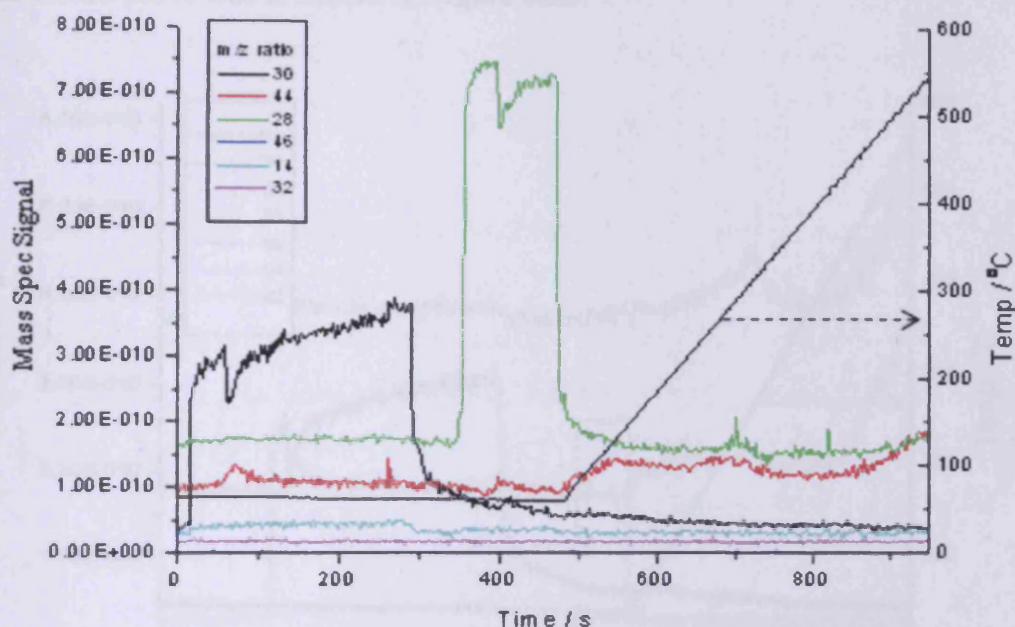
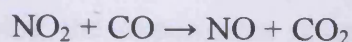


Figure 5.25 – A molecular beam of NO (50 mbar molecular beam source pressure) beamed onto more than a complete surface covering of BaO (10 min Ba/O₂ surface dose), followed by a molecular beam of CO (50 mbar molecular beam source pressure) (CO trace reduced by a factor of four as a visual aid) and a temperature programmed desorption of the crystal surface (time > 490 s).

Figure 5.25 is a molecular beam experiment to attempt to probe the nature of the residual species on the surface after beaming NO onto more than a complete surface covering of BaO, by using a molecular beam of CO. NO is broken down by the surface in a similar manner to that seen in Figure 5.23 as is evidenced by the $m/z = 44$ desorption peak immediately upon adsorption. There is a second immediate $m/z = 44$ desorption peak when CO is beamed onto the surface. It is possible that this is due to a reactive oxygen species being left at the surface. However, there is also a minor $m/z = 30$ desorption peak that occurs as well as the $m/z = 44$ desorption peak on beaming the CO, possibly due to NO₂ or N₂O being adsorbed on the BaO and a disproportionation reaction occurring ie.



An alternative scenario might be that the surface has sintered and that NO has adsorbed on the Pt(111) beneath the BaO, from which it is then displaced by the beam of CO. However the low temperature desorption peak characteristic of CO on Pt(111) which would prove this is absent in Figure 5.25.

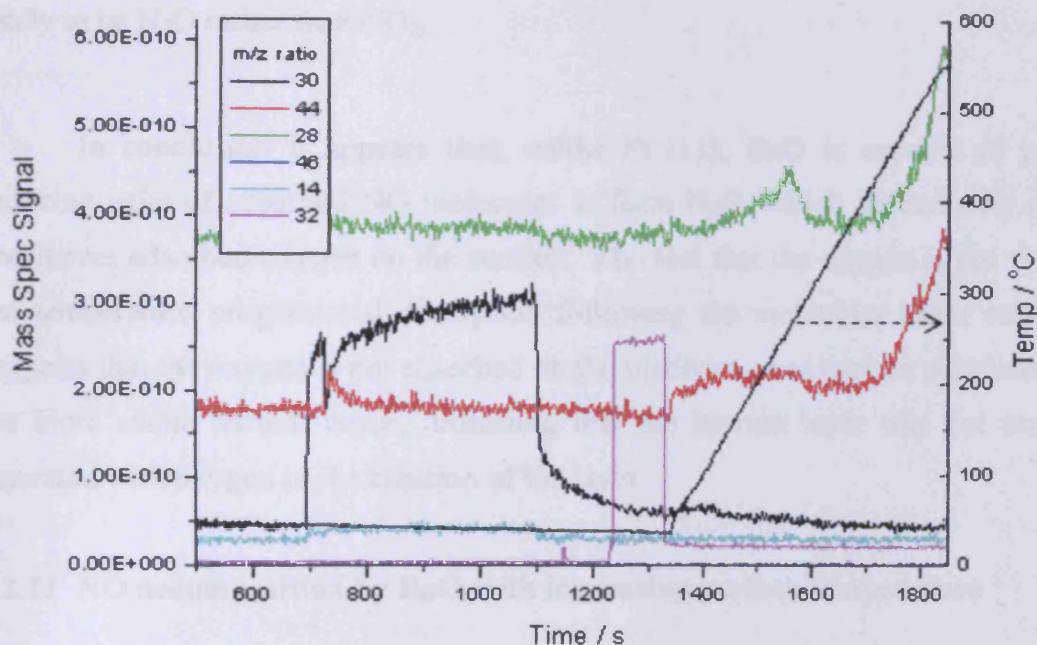


Figure 5.26 – A molecular beam of NO (50 mbar molecular beam source pressure) beamed onto more than a complete surface layer of BaO (10 min Ba/O₂ surface dose), followed by a molecular beam of O₂ (50 mbar molecular beam source pressure) and a temperature programmed desorption of the crystal surface (time > 1350 s).

Figure 5.26 shows a molecular beam of NO (50 mbar molecular beam source pressure) beamed on to more than a complete layer of BaO (10 min Ba/O₂ surface dose), followed by a molecular beam of O₂ (50 mbar molecular beam source pressure) to attempt to induce a surface reaction as an aid to identifying adsorbed surface species.

NO is partially decomposed by the surface with the release of N₂O as seen in Figure 5.26. There is no obvious O₂ adsorption from the beam and no desorption

products are released on beaming. The temperature programmed desorption following the experiment reveals a broad $m/z = 44$ desorption peak (or possibly several overlapping features) between 80 °C and 260 °C. There is also a $m/z = 28$ desorption peak at 160 °C. There are no additional features in the temperature programmed desorption part of the experiment other than those than seen in Figure 5.25, enabling the conclusion that the remnants of the decomposed NO on the surface are inert to oxidation and are hence likely to be atomic oxygen. This would make the identity of the $m/z = 44$ desorption peak that is observed on adsorption of NO more likely to be N_2O rather than CO_2 .

In conclusion it appears that, unlike Pt(111), BaO is capable of partially reducing pairs of adsorbed NO molecules to form N_2O , which immediately desorbs and leaves adsorbed oxygen on the surface. The fact that the oxygen is not visible in the temperature programmed desorption following the molecular beam experiment suggests that the oxygen is not adsorbed on the platinum or as barium peroxide, but as the more stable barium oxide, indicating that the barium layer was not originally saturated with oxygen in the creation of the layer.

5.2.11 NO decomposition by BaO with increasing surface temperature

Barium oxide layers were created by dosing the Pt(111) crystal surface held at 200 °C (to minimise CO adsorption from the background) with barium in a background pressure of 2×10^{-8} mbar of O_2 for five minutes (0.31 ML), followed by flashing to 500 °C for two minutes. The surface was then allowed to cool to the temperature required for each molecular beam experiment.

Figure 5.27 shows that at 50 °C NO sticks with to the BaO surface with a lesser initial sticking probability than seen for a molecular beam of NO beamed on to clean Pt(111) ($S_0 = 0.27$ compared to 0.71). However it appears that whereas on clean Pt(111) NO adsorbs reversibly, a $m/z = 44$ desorption peak is observed immediately on adsorption of NO on BaO. As with the earlier NO decompositions it is likely that the identity of this species is N_2O . If NO is being reduced by the surface it is reasonable to assume that oxygen is left behind and ties up adsorption sites, hence

poisoning the reaction in a similar manner to that seen for NO breakdown on Pd(110) and Pd(111) at elevated temperature³⁰. This continues up to 300 °C with the only noticeable difference being a reduction in the NO sticking coefficient. However at 300 °C there is a $m/z = 28$ desorption peak observed. The $m/z = 28$ desorption peak is accompanied by a $m/z = 14$ desorption peak, making it likely that the identity of the desorbing species is nitrogen. Above this temperature there is a large reduction in the NO sticking coefficient, reducing the quantity of products produced. As the temperature is raised to 400 °C the magnitude of both desorption peaks is reduced, and at 500 °C there is no obvious $m/z = 44$ desorption peak, only a $m/z = 28$ desorption peak.

The above observations would seem to suggest that the extent to which the NO decomposition occurs is heavily influenced by the temperature at which the adsorption of NO occurs, with a more complete NO reduction process occurring at higher temperatures. If NO is dissociated upon adsorption, adsorbed atomic oxygen and atomic nitrogen is created. The atomic nitrogen is free to react with incoming NO molecules whereas the adsorbed oxygen builds up on the catalytic surface, thus poisoning it. The observed variation in product selectivity could therefore be due to a decreased NO surface lifetime at higher temperatures, making it less likely that weakly held NO species encounter surface-adsorbed nitrogen to form N_2O , as reported for Pd(110)³⁰. It is worth noting that if adsorbed oxygen does occupy NO adsorption sites and poisons the reaction a more complete reduction to N_2 rather than N_2O would result in twice as much oxygen adsorbed, reducing the NO adsorption by half.

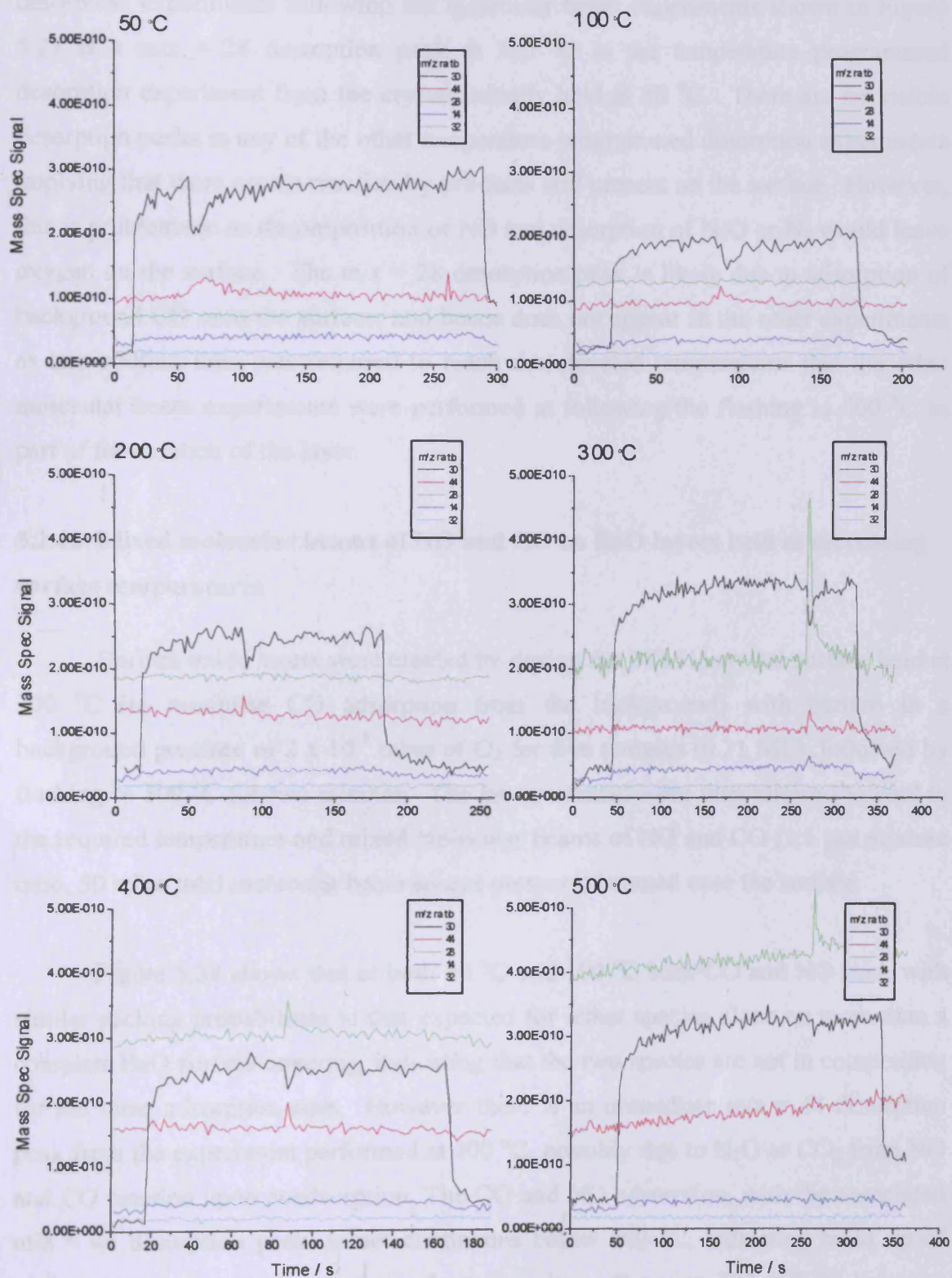


Figure 5.27 – Molecular beams of NO (50 mbar molecular beam source pressure) on 0.31 ML BaO held at increasing surface temperatures.

The only significant desorption peak present in the temperature programmed desorption experiments following the molecular beam experiments shown in Figure 5.27 is a $m/z = 28$ desorption peak at 280 °C in the temperature programmed desorption experiment from the crystal initially held at 50 °C. There are no visible desorption peaks in any of the other temperature programmed desorption experiments implying that there are no reaction by-products still present on the surface. However, this is problematic as decomposition of NO and desorption of N₂O or N₂ would leave oxygen on the surface. The $m/z = 28$ desorption peak is likely due to adsorption of background CO onto the surface, and hence does not appear in the other experiments as less cooling time was required to reach the elevated temperatures that the other molecular beam experiments were performed at following the flashing to 500 °C as part of the creation of the layer.

5.2.12 Mixed molecular beams of NO and CO on BaO layers held at increasing surface temperatures

Barium oxide layers were created by dosing the Pt(111) crystal surface held at 200 °C (to minimise CO adsorption from the background) with barium in a background pressure of 2×10^{-8} mbar of O₂ for five minutes (0.31 ML), followed by flashing to 500 °C for two minutes. The layers created were then allowed to cool to the required temperature and mixed molecular beams of NO and CO (1:1 gas mixture ratio, 50 mbar total molecular beam source pressure) beamed onto the surface.

Figure 5.28 shows that at both 50 °C and 100 °C both CO and NO stick with similar sticking probabilities to that expected for either species alone on more than a complete BaO surface covering, indicating that the two species are not in competition for the same adsorption sites. However there is an immediate $m/z = 44$ desorption peak from the experiment performed at 100 °C, possibly due to N₂O or CO₂ from NO and CO reaction upon coadsorption. The CO and NO adsorption, with the associated $m/z = 44$ desorption peak, is not continuous below 200 °C, indicating build up of surface species occupying surface adsorption sites. Between 300-400 °C however there is constant evolution of $m/z = 44$, due to a mixture of CO₂ and N₂O being produced. As both products desorb there is no tying up of surface sites and so the reaction is continuous. It is worth noting that the rate of reaction is much reduced at

400 °C due to the lowered sticking probabilities of both species in the mixed beam. At 500 °C there is no obvious sticking of either species in the beam and so the reaction has essentially ceased.

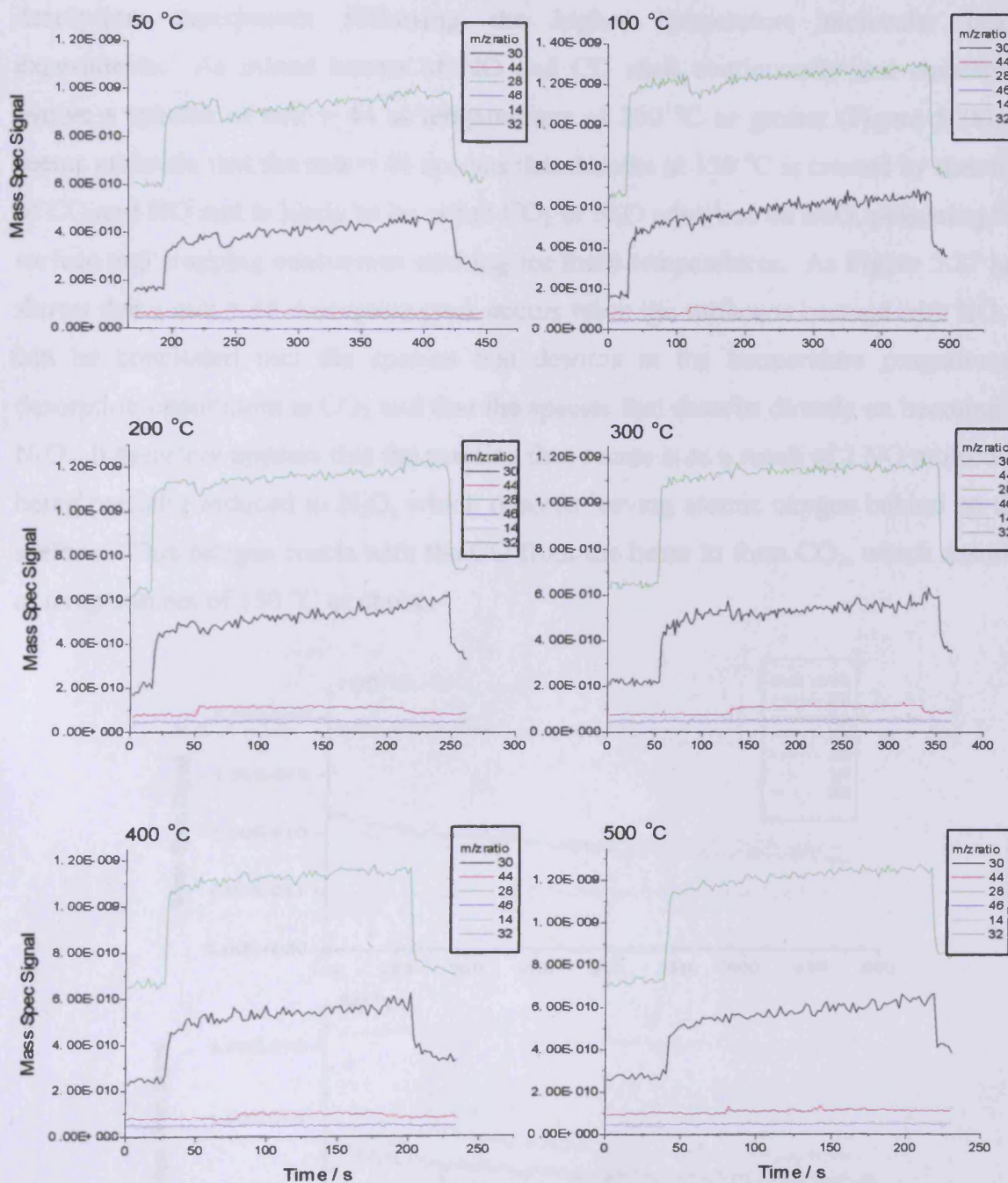


Figure 5.28 - Mixed molecular beams of NO and CO (1:1 gas mixture ratio, 50 mbar total molecular beam source pressure) on 0.31 ML BaO coverage of Pt(111).

Figure 5.29 shows the temperature programmed desorption data recorded after the mixed molecular beam experiments featured in Figure 5.28. As can be seen the dosings performed at 50 and 100 °C both exhibit a $m/z = 44$ desorption peak at 150 °C. There are no features of interest in any of the other temperature programmed desorption experiments following the higher temperature molecular beam experiments. As mixed beams of NO and CO stick continuously and constantly evolve a species of $m/z = 44$ at temperatures of 200 °C or greater (Figure 5.28), it seems probable that the $m/z = 44$ species that desorbs at 150 °C is created by reaction of CO and NO and is likely to be either CO_2 or N_2O adsorbed on BaO, poisoning the surface and stopping continuous sticking for these temperatures. As Figure 5.27 has shown that a $m/z = 44$ desorption peak occurs when the surface is beamed with NO, it can be concluded that the species that desorbs in the temperature programmed desorption experiment is CO_2 and that the species that desorbs directly on beaming is N_2O . It therefore appears that the reaction that occurs is as a result of 2 NO molecules being partially reduced to N_2O , which desorbs leaving atomic oxygen behind on the surface. This oxygen reacts with the CO from the beam to form CO_2 , which desorbs at temperatures of 150 °C or above.

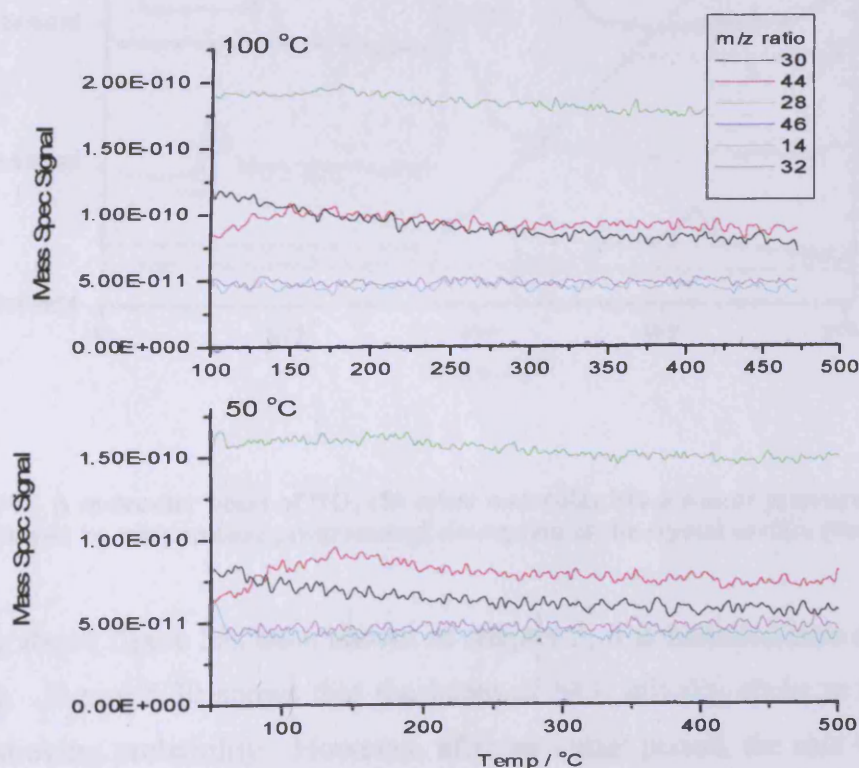


Figure 5.29 - Temperature programmed desorption experiments following the mixed NO and CO molecular beam experiments shown in Figure 5.28.

5.2.13 Molecular beams of NO₂ on increasing BaO coverages of the Pt(111) surface

To try and build an understanding of the fundamental processes occurring on the separate components of the catalyst during the NO_x storage phase of operation molecular beams of NO₂ (50 mbar molecular beam source pressure) were beamed onto the Pt(111) crystal pre-dosed with three different coverages of barium oxide. The BaO layers were created by dosing barium onto the crystal surface held at 200 °C in a background pressure of 2×10^{-8} mbar of O₂. The layers created were then flashed to 500 °C for two minutes before being allowed to cool to 75 °C.

Clean Pt(111)

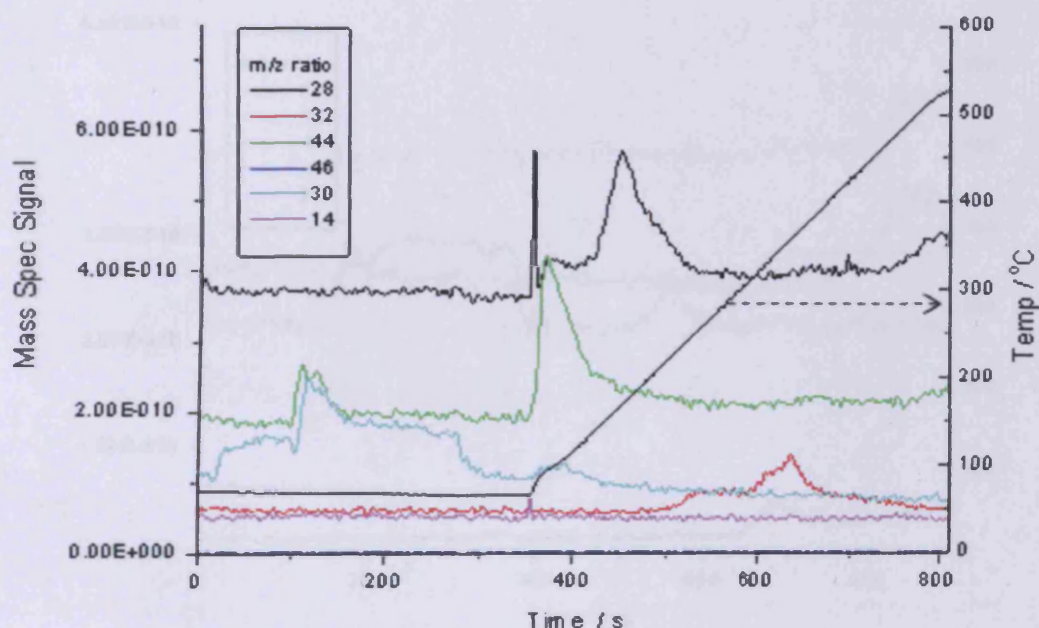


Figure 5.30 – A molecular beam of NO₂ (50 mbar molecular beam source pressure) on clean Pt(111) followed by temperature programmed desorption of the crystal surface (time > 355 s).

The above figure has been shown in chapter 3; it is included here as an aid to comparison. Figure 5.30 shows that the beam of NO₂ initially sticks to the surface with 0.65 sticking probability. However, after an initial period, the $m/z = 30$ signal rises to three times its initial value. There are no apparent changes in $m/z = 46$, 32 or 28, however there is a large $m/z = 44$ desorption peak that is likely due to the

oxidation of adsorbed CO from the background gases in the chamber by atomic oxygen from the breakdown of NO_2 . The large rise in the $m/z = 30$ signal is a result of NO_2 being broken down and liberating NO and atomic oxygen, which adsorbs on to the crystal surface, displacing adsorbed NO (although $m/z = 30$ is a cracking fragment of NO_2 , $m/z = 30$ is the molecular ion of NO, hence why the rise in $m/z = 30$ signal at 200 s is so large). The temperature programmed desorption portion of the experiment (time > 355 s) shows a large $m/z = 28$ desorption peak due to the adsorption of CO from the background to the rest of the crystal as well as a $m/z = 44$ desorption peak from the oxidation of background CO by atomic oxygen from the breakdown of NO_2 .

Complete BaO surface coverage

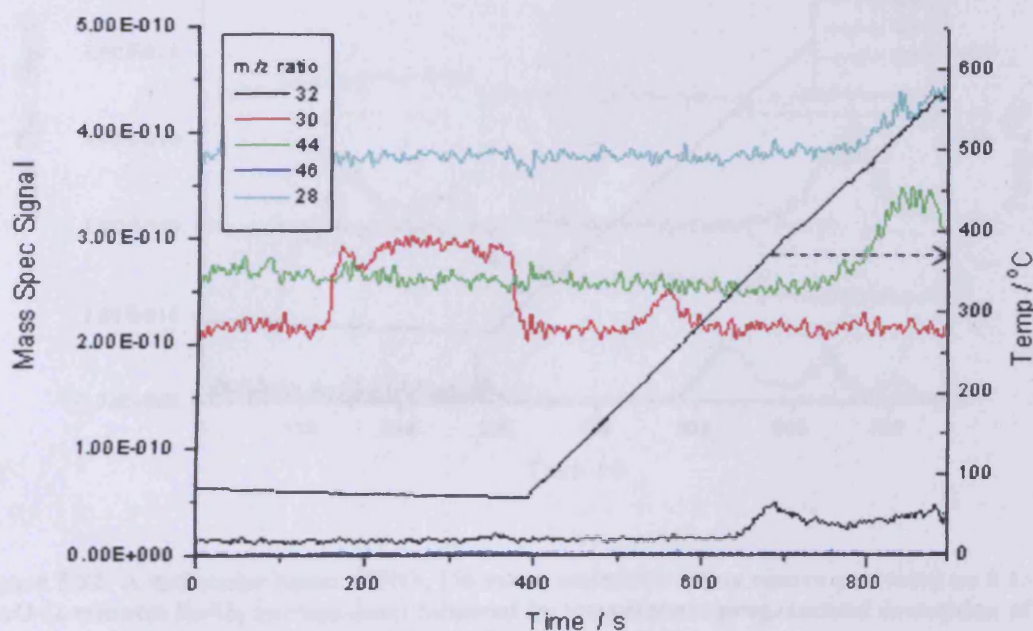


Figure 5.31 – A molecular beam NO_2 (50 mbar molecular beam source pressure) on 0.63 ML BaO (10 minutes Ba/ O_2 dose) followed by temperature programmed desorption of the crystal surface (time > 395 s).

In Figure 5.31 the Pt(111) crystal surface has been covered with 0.63 ML BaO (10 minutes Ba dose, 2×10^{-8} mbar O_2) before being beamed with a molecular beam of NO_2 . From the above it appears that NO_2 adsorbs intact to the BaO surface without the characteristic $m/z = 30$ peak given by NO_2 breakdown on Pt(111). That NO_2 has adsorbed to the surface is confirmed by the $m/z = 30$ desorption peak at 220

°C. There is a $m/z = 32$ desorption peak at ~ 370 °C indicating that the $m/z = 30$ desorption peak at 220 °C is the result of NO desorbing not as a result of the desorption of NO_2 . That the O_2 is desorbed at a higher temperature than the NO indicates that adsorption of the oxygen from the decomposition of the stored NO_2 has occurred, possibly via BaO_2 formation, which has been shown to be metastable at this temperature with STM⁶.

Intermediate BaO Surface Coverage

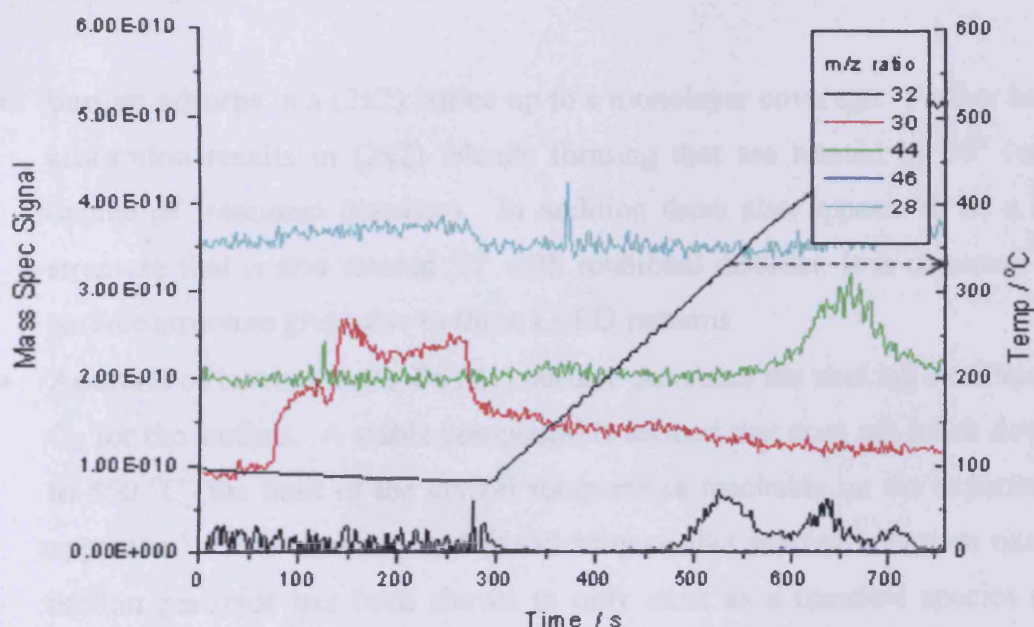
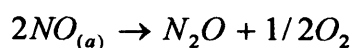
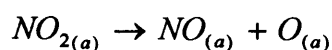


Figure 5.32- A molecular beam of NO_2 (50 mbar molecular beam source pressure) on 0.13 ML BaO (2 minutes Ba/ O_2 surface dose) followed by temperature programmed desorption of the crystal surface (time > 300 s).

Figure 5.32 shows a molecular beam experiment in which a molecular beam of NO_2 is beamed onto a 0.13 ML BaO layer (2 minutes Ba dose, 2×10^{-8} mbar O_2). This coverage was chosen so that there was both exposed Pt(111) and BaO present at the surface. From the above figure it is apparent that NO_2 is broken down, with the immediate release of NO, by the mixed layer in a similar manner to that seen in Figure 5.30. There are no other features of interest in the molecular beam part of the experiment, however during the temperature programmed desorption following the molecular beam experiment (time > 300 s) several desorption peaks are evident.

There is a $m/z = 32$ desorption peak at 310 °C that is due to the desorption of oxygen from Pt(111) as seen in Figure 5.30 and $m/z = 32$ and $m/z = 44$ desorption peaks that both occur at 440–455 °C. These desorption peaks are possibly due to the desorption of N_2O and O_2 from the release of stored NO_2 from the BaO storage component followed by its breakdown on Pt(111) ie. (assuming that the NO_2 is stored as nitrate)



5.3 Summary and Conclusions

- Barium adsorbs in a (2x2) lattice up to a monolayer coverage. Further barium adsorption results in (2x2) islands forming that are rotated by 30° (with a degree of rotational disorder). In addition there also appears to be a (1x1) structure that is also rotated 30° with rotational disorder. It is unknown what surface structure gives rise to these LEED patterns.
- Addition of barium to the Pt(111) surface increases the sticking coefficient of O_2 for the surface. A stable compound is formed that does not break down up to 550 °C (the limit of the crystal temperature reachable on the experimental apparatus). It is assumed that the identity of this species is barium oxide as barium peroxide has been shown to only exist as a transient species under UHV conditions⁶ and barium hydroxide would be expected to decompose at the elevated temperature used in the flashing of the crystal during the creation of the layer²⁷. XPS analysis confirms that the likely identity of this species is barium oxide, with barium peroxide also being present when layer is flashed to 500 °C in oxygen.
- CO will only adsorb on barium that is metallic in character, not the ionic barium that forms during the initial stages of Ba deposition. The addition of ionic barium to the Pt(111) surface increases the temperature of desorption of CO from the Pt(111). CO adsorbed on metallic barium is stable to higher temperatures than CO on Pt(111).
- Dosing barium onto the Pt(111) surface decreases the sticking probability and saturation coverage of NO for the surface when compared to clean Pt(111).

Despite this there is little change in the adsorptive behaviour of NO_2 for a barium-modified Pt(111) surface, with dissociation to NO and O_2 occurring on adsorption.

- Dosing BaO onto the crystal surface decreases the affinity of CO for the surface. Despite this some CO adsorption still occurs, forming a compound with a lower desorption temperature than CO on Ba but higher than CO on Pt(111). It is likely that the identity of this species is barium carbonate.
- Increasing the amount of BaO on the Pt(111) surface decreases the sticking probability of O_2 for the surface. Despite this O_2 adsorption can occur when using high background pressures of oxygen. It is likely that this oxygen adsorbs via barium peroxide formation, or possibly as a result of barium that has not been oxidised in the creation of the layer.
- In a similar manner to potassium, dosing BaO onto the Pt(111) crystal surface facilitates the reduction of NO, with N_2O being desorbed. The extent of the reduction process can be increased by increasing the temperature of the reactive surface, with elevated temperatures favouring a more complete reduction process to N_2 at the expense of N_2O production. The presence of a reductant such as CO has no effect on the selectivity of the reduction however.
- BaO is capable of storing NO_2 , likely as a nitrate species³¹. Stored NO_2 is released when heated as nitric oxide and oxygen. In a mixed system where both Pt and BaO are present at the surface there is an additional oxygen desorption environment, likely as the result of the desorption of stored atomic oxygen from Pt(111).

From the above list of conclusions it is obvious that the proposed reaction scheme for the NSR catalyst (see chapter 1) is valid in that barium oxide is capable of storing nitrogen dioxide and releasing the stored nitrogen dioxide as nitric oxide and oxygen (see Figure 5.31 and Figure 5.32). In addition to this the barium oxide component of the catalyst would appear to also be able to assist in the reduction of NO to N_2 at catalyst operating temperatures (Figure 5.27).

REFERENCES

1. Grönbeck, H., Broqvist, P., *J. Chem. Phys.*, **119**, 2003, 3896.
2. Thornton, G., Owen, I.W., Richardson, C.H., Norman, D., Tuck, R.A., Skinner, H.B., Wasdsworth, P.J., Gardiner, T.M., *Vacuum*, **38**, 1998, 401.
3. Onishi, H., Egawa, T., Aruga, T., Iwasawa, Y., *Surf. Sci.*, **191**, 1987, 479.
4. Tasker, P.W., *J. Phys. C: Solid State Phys.*, **12**, 1979, 4977.
5. Rohr, F., Wirth, K., Libuda, J., Cappus, D., Baumer, M., Freund, H.-J., *Surf. Sci.*, **315**, 1994, L977.
6. Stone, P., Ishii, M., Bowker, M., *Surf. Sci.*, **537**, 2003, 179.
7. Bowker, M., Stone, P., Smith, R., Fourre, E., Ishii, M., de Leeuw, N.H., *Surf. Sci.*, **600**, 2006, 1973.
8. Shi, A.C., Wortis, M., *Phys. Rev. B*, **37**, 1988, 7793.
9. Sedlmair, Ch., Seshan, K., Jentys, A., Lercher, J.A., *J. Catal.*, **214**, 2003, 308.
10. Broqvist, P., Grönbeck, H., Fridell, E., Panas, I., *Catal. Today*, **96**, 2004, 71.
11. Mahzoul, H., Brilhac, P., Gilot, P., *Appl. Catal. B: Environ.*, **20**, 1999, 47.
12. Westerberg, B., Fridell, E., *J. Mol. Cat. A: Chem*, **165**, 2001, 249.
13. Prinetto, F., Ghiotti, G., Nova, I., Lietti, L., Tronconi, E., Forzatti, P., *J. Phys. Chem. B*, **105**, 2001, 12732.
14. Schneider, W.F., Hass, K.C., Miletic, M., Gland, J.L., *J Phys. Chem. B*, **106**, 2002, 7405.
15. Schmitz, P.J., Baird, R.J., *J. Phys. Chem. B.*, **106**, 2002, 4172.
16. Amberntsson, A., Persson, H., Engstrom, P., Kasemo, B., *Appl. Catal. B: Environ.*, **31**, 2001, 27.
17. Kabin, K.S., Muncrief, R.L., Harold, M.P., *Catal. Today*, **96**, 2004, 79.
18. Simmons, G.W., Mitchell, D.F., Lawless, K.R., *Surf. Sci.*, **8**, 1967, 130.
19. Ertl, G., *Surf. Sci.*, **6**, 1967, 208.
20. Gerlach, R.L., Rhodin, T.N., *Surf. Sci.*, **17**, 1969, 32.
21. Ertl, G., *Molecular Processes on Solid Surfaces*, McGraw Hill, New York 1969, 147.
22. Grillo, F., PhD thesis, Cardiff University, 2007.
23. <http://www.lasurface.com/>, web-based XPS database.
24. <http://srdata.nist.gov/xps/>, X-ray Photoelectron Spectroscopy Database 20, Version 3.0, National Institute of Standards and Technology, Gaithersburg, MD.
25. Moulder, J.F., Stickle, W.F., Sobol, P.E., Bomben, K.D., Chastain J. (Ed.), *Handbook of X-ray Photoelectron Spectroscopy*, 2nd ed., Perkin-Elmer Corp. (Physical Electronics), 1992.
26. Tanaka, K., Miyahara, K., Toyoshima, I., *J. Phys. Chem.*, **88**, 1984, 3504.
27. Tsami, A., Grillo, F., Bowker, M., Nix, R., *Surf. Sci.*, **600**, 2006, 3403.
28. Lide, D.R. (Ed.), *Handbook of Chemistry and Physics*, 73rd ed., CRC Press, 1992.
29. Matsumoto, S., *Cattech*, **4**, 2000, 102.
30. Sharpe, R.G., Bowker, M., *Surf. Sci.*, **360**, 1996, 21.
31. James, D., Fourré, E., Ishii, M., Bowker, M., *Appl. Cat. B Environ.*, **45**, 2003, 147.

6. CONCLUSIONS AND FUTURE WORK

6.1 Overall Conclusions 233

6.2 Future Work 240

REFERENCES 240

6.1 Overall Conclusions

By a combination of molecular beam, TPD, LEED and AES methods a detailed examination of the interactions and reactions of certain automobile exhaust pollutants has been carried out on a model Pt(111)/BaO exhaust catalyst as well as the separate Pt(111) (NO_x oxidation/reduction) and BaO (NO_x storage) components of the catalyst. Also examined was an alternative Pt(111)/K and Pt(111)/K₂O₂ system to examine the effect of a more basic NO_x storage component on the NO_x storage ability of the catalyst.

Adsorption and desorption characteristics of NO, CO, NO₂ and O₂ have been studied on Pt(111) and the NO-O₂, CO-O₂ and NO-CO reaction systems have been investigated. The focus of this work has been to examine the data received in relation to the proposed Matsumoto model for NO_x storage and reduction under oxidising and reducing environments.

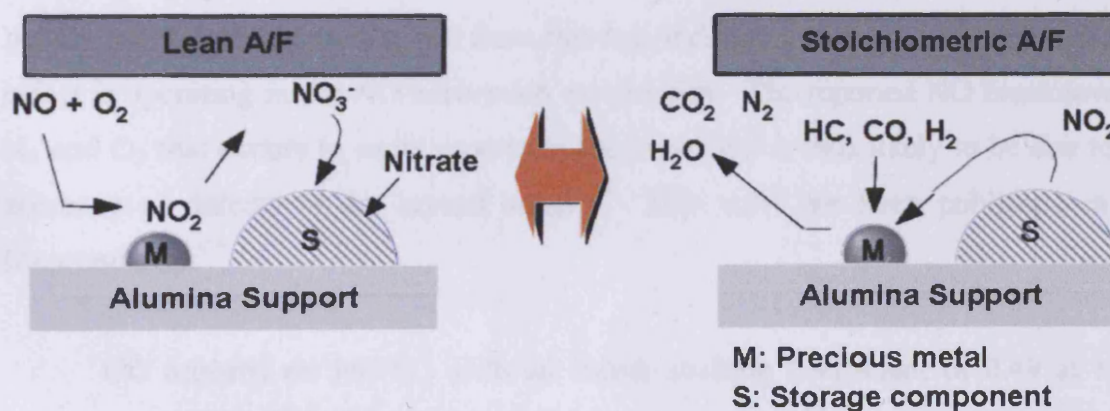
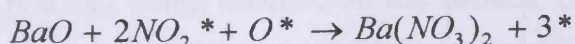
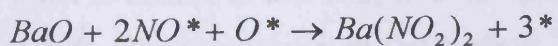
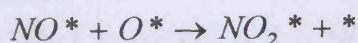
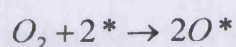
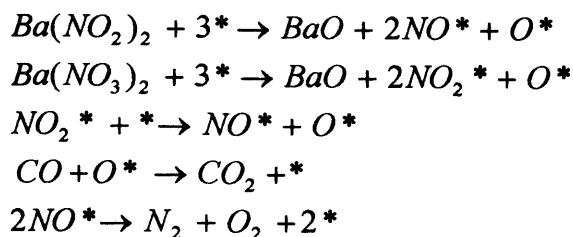


Figure 6.1 - The Matsumoto model for the NSR process^{1,2}

From the above it can be seen that the Matsumoto model for NO_x storage and reduction can be broken up into a number of separate reactions ie.



Equation 1- Oxygen-rich condition reactions.



Equation 2 - Fuel-rich condition reactions

The main conclusions from each chapter and group of experiments will be summarised below and analysed with respect to the reactions given above to assess the suitability of Pt(111), K/Pt(111), K₂O/Pt(111), Ba/Pt(111) and BaO/Pt(111) as NO_x storage and reduction catalysts.

NO adsorbs on Pt(111) with an initial sticking coefficient of 0.73 at room temperature. Temperature programmed desorption experiments provide no evidence of multiple adsorption sites and adsorption is reversible with no NO decomposition. Adsorbed NO is weakly held and desorbs at relatively low temperature. A Kisliuk parameter of 0.18 can be derived from the data indicating that a substantial precursor effect is operating in the NO adsorption mechanism. The reported NO breakdown to N₂ and O₂ that occurs in some reports in the literature³ is thus likely to be due to the presence of defects in the crystal surface. This view has been published in the literature also.^{4,5}

CO adsorbs on Pt(111) with an initial sticking coefficient of 0.49 at room temperature. As with NO, there is no evidence of multiple adsorption sites and adsorption occurs reversibly with the adsorbate being fairly weakly held, although not as weakly as NO. The Kisliuk parameter of 0.1 that was obtained indicates that precursor kinetics play a large part in the adsorption of CO on Pt(111).

Due to the behaviour of NO₂ adsorbing on Pt(111), obtaining Kisliuk parameters and a value for the sticking coefficient for the adsorption is problematic. What is certain is that NO₂ is decomposed by the surface with the desorption of NO and O_(a) being retained on the surface. As there is no evidence that any of the NO from the breakdown of NO₂ is retained on the surface it is logical to assume that NO

is displaced from the surface by the atomic oxygen. In the Matsumoto model the stored nitrate is released as NO_2 under fuel-rich conditions before being reduced to NO and O over the platinum metal centre; our results have confirmed the validity of this latter step. The inclusion of rhodium in the NSR catalyst is likely responsible for the reduction of NO that occurs.

The atomic oxygen left on the surface by the breakdown of NO_2 is highly active in the oxidation of CO, unlike the case for mixed beams of CO and O_2 , from which it can be inferred that the limiting step is the dissociative adsorption of O_2 rather than the adsorption of CO or the oxidation reaction itself. This is borne out in the extremely low initial sticking coefficient of O_2 on Pt(111) ($S_0 \sim 0.06$) which is probably due to adsorption on defect sites.^{6,7} The low sticking coefficient of O_2 on the platinum would not be a problem in the NSR catalyst due to the relatively high partial pressures of O_2 in the exhaust feed under lean operating conditions, and as shown CO oxidation occurs readily on Pt(111), making the catalyst efficient at removing CO from the exhaust gases.

Unlike the oxidation of CO by pre-adsorbed atomic oxygen, NO oxidation via pre-adsorbed oxygen does not occur under these conditions. This is surprising due to the fact that NO and O_2 react spontaneously together at room temperature in a gas-phase reaction (as shown in chapter 3), proving that the reaction is thermodynamically favourable. It is likely that oxidation of NO does occur by the adsorbed atomic oxygen but the back reaction is so favourable due to the strength of the Pt-O bond that the NO_2 formed immediately dissociates back to NO and atomic oxygen, with the NO desorbing into the gas phase and hence demonstrating little sticking of the beam. It is likely that this is not a problem in the actual NSR catalyst due to the relatively high partial pressures of NO_x and O_2 in the exhaust under lean burn conditions and the elevated temperature at which the catalyst operates.

There is no evidence of NO reduction by CO in a mixed beam reaction. This is not surprising as the first step of the proposed NSR reaction is the breakdown of NO by the surface with the desorption of N_2 , followed by the removal of the oxygen left on the surface by the CO in an oxidation reaction, and NO is not easily decomposed by the Pt(111) surface as was demonstrated earlier. This however has

implications for the Matsumoto NSR catalyst model, in which, under fuel-rich operating conditions released NO_x is reduced to N_2 (or more likely to N_2O , the species normally observed during model catalytic reactor studies and during our own studies. The rhodium included in the catalyst is then likely to be responsible for the reduction of N_2O to N_2 , as well as producing N_2 directly). As it has been shown, under UHV conditions at least, that this is not catalysed by Pt(111), the breakdown of NO that occurs must be catalysed by the BaO NO_x storage component (or possibly by the alumina support in the real-world catalyst). This was confirmed during our studies.

In contrast to the adsorptive behaviour of O_2 on Pt(111), O_2 readily adsorbs on K/Pt(111), with a maximum initial sticking probability of 0.65 on a monolayer of potassium. Adsorption of O_2 on the surface was conjectured to occur via potassium-induced O_2 dissociation at low potassium surface coverages followed by spillover onto platinum surface sites and via formation of a potassium oxide at higher potassium surface coverages (XPS showed the probable identity of this species to be potassium peroxide). Formation of the oxide species caused a contraction in the potassium layer allowing potassium induced dissociation of O_2 and adsorption on the platinum as described earlier.

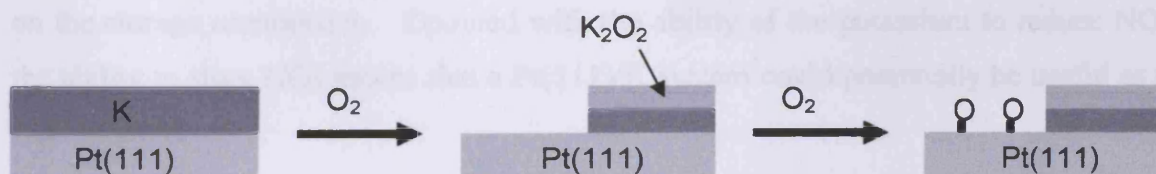


Figure 6.2 – The formation of potassium peroxide and adsorption of further oxygen

The promotional effect of potassium on the adsorption of O_2 on Pt(111) is inversely mirrored by the behaviour of CO adsorbing on a potassium-promoted Pt(111) surface. Potassium blocks Pt-CO adsorption sites and although some adsorption of CO on potassium does occur, sticking is much less than seen on the Pt(111) surface.

Dosing different potassium surface coverages onto the Pt(111) surface has little effect on the sticking coefficient of NO on the Pt(111) surface. The state of the potassium does however affect the mode of adsorption, with a monolayer of potassium causing the NO to adsorb dissociatively with the immediate evolution of N_2

and the adsorption of $O_{(a)}$ on the potassium. NO also adsorbs in a non-dissociative fashion onto K coverages of the Pt(111) surface of up to five minutes K dosing time, with a temperature of desorption that is higher than observed on clean Pt(111); this is likely due to an oxygen-induced potassium surface contraction exposing the platinum beneath the potassium, followed by NO adsorption on Pt(111). The Pt(111)-NO however is affected by the presence of the potassium in the immediate vicinity, accounting for the increased temperature of desorption. This ability of the potassium to catalyse the reduction of NO complements the Pt(111) in the NSR catalyst which, as shown earlier, is not effective in the reduction of NO. Coverages of potassium of a monolayer or greater also show evidence of another species in the TPD; this has been identified in the literature as a nitrite, formed by the reaction of oxygen from the breakdown of NO with another NO molecule.⁸

Unlike when NO_2 is adsorbed on clean Pt(111), when NO_2 is adsorbed on a potassium-promoted Pt(111) surface there is no evidence of reduction of NO_2 to NO upon adsorption. Evidence is provided in the literature that nitrite species are stable on K/Pt(111) making potassium nitrite the possible identity of the stored NO_2 .^{9,8} This however disagrees with the Matsumoto model in which the NO_2 is adsorbed as nitrate on the storage component. Coupled with the ability of the potassium to reduce NO, the ability to store NO_2 means that a Pt(111)/K system could potentially be useful as a NSR catalyst.

In a similar manner to that seen on potassium only, dosing potassium peroxide onto the Pt(111) surface has the effect of decreasing the sticking coefficient of CO for the surface. Unlike pure potassium however, on which CO adsorption occurs on surface coverages of greater than a monolayer (albeit with a significantly reduced sticking probability when compared to the clean surface), no CO adsorption occurs on K_2O_2 surface coverages of a monolayer or greater.

As with pure potassium on Pt(111), potassium peroxide (or possibly carbonate) was shown to be able to catalyse the reduction of NO with the immediate release of nitrogen when beaming at room temperature (section 4.2.12). As with coverages of potassium of greater than a monolayer the oxygen is adsorbed by the surface and there is evidence of an additional species that has been identified in the

literature as a nitrite.¹⁰ With consideration it is to be expected that potassium and potassium peroxide would behave in a similar fashion as the first step in potassium nitrate storage is the reduction of NO with the oxygen liberated reacting with the potassium layer to form peroxide. Unlike pure potassium however there is no NO₂ adsorption on a potassium peroxide surface. From this it may be concluded that whilst potassium has potential as a replacement for the barium oxide NO_x storage component in the NSR catalyst, potassium oxide is unable to store NO_x during the excess oxygen phase of engine operation and would therefore be ineffective as a component in the catalyst.

Dosing barium on to the Pt(111) surface increased the sticking coefficient of O₂ for the surface in a similar manner to that seen when dosing potassium onto the surface. However the magnitude of the increased oxygen sticking was less for barium than was seen for potassium. The adsorbed oxygen forms a stable compound that XPS has shown is likely to be barium oxide with higher pressures of oxygen creating an additional unstable barium peroxide species.

As with potassium and potassium peroxide, dosing barium onto the Pt(111) crystal decreases the sticking coefficient of CO for the surface, although, in a similar manner to potassium, a barium-CO compound is formed with a higher temperature of desorption than CO desorbing from Pt(111) alone. Unlike potassium and potassium oxide however, NO adsorbed irreversibly on barium (rather than being dissociated with the immediate desorption of N₂), forming a stable compound that desorbed outside the temperature range employed during the experiments contained in this thesis. In addition to this, as shown earlier, Pt(111) does not catalyse the breakdown of NO to its constituent elements, making the ability to reduce NO an essential part of the NO_x storage component in the NSR catalyst. As metallic barium does not facilitate the decomposition of NO (as shown in chapter 5), its inclusion in the exhaust catalyst would be suspect (also metallic barium is very reactive and would not remain as a metal under catalyst operating conditions)

Platinum surface coverages of half a complete layer as well as a full complete layer of barium have been shown to break down NO₂ with NO desorbing and leaving reactive oxygen on the surface in a manner similar to that seen for clean Pt(111). This

inability of barium to store NO_2 in an oxidising environment (as well as its high reactivity) would make barium metal unsuitable as a replacement for barium oxide in the NSR catalyst. However as NO_2 breakdown results in the adsorption of atomic oxygen, presumably via reaction with the barium to form barium oxide, which was shown to store NO_2 , it is possible that the barium surface was contaminated with carbonaceous compounds to a certain extent.

As with metallic barium, barium oxide was found to decrease the sticking of CO to the Pt(111) crystal surface. In a similar manner to the metal, limited CO adsorption did occur, forming a CO species that desorbed at a lower temperature than the CO species on Ba. The magnitude of the CO adsorption that occurred on BaO was much less than the CO adsorption that occurs on Ba.

Unlike metallic barium, the presence of barium oxide on the crystal surface reduced the (already minimal) sticking of O_2 substantially. With large background doses of O_2 it was possible to form an adsorbed O_2 species that was stable to $\sim 500\text{--}550^\circ\text{C}$; it was surmised that this was the oxygen from barium peroxide. An alternative explanation however might be that sintering of the barium oxide had occurred during annealing and that the O_2 desorbed was from O_2 adsorbed on Pt(111) as a result of barium-oxide facilitated O_2 dissociation ($\text{O}_{(\text{a})}$ on Pt(111) has been shown to desorb from Pt(111) in the temperature range employed in the temperature programmed desorption experiments contained in this thesis, see chapter 3).

As commented upon earlier in this section, given the fact that Pt(111) does not reduce NO to N_2 and O_2 , an essential aspect of any NSR catalyst would be the ability of the NO_x storage component of the catalyst to reduce NO. BaO is capable of reducing NO, however the reduction is not complete; N_2O is formed instead of N_2 , even with the presence of a reductant such as CO. NO_2 however is stored and not broken down on the BaO, an important aspect of the exhaust catalyst.

Perhaps the most interesting result in this thesis is the non-reduction of NO by Pt(111). This would appear to be in direct contradiction to the Matsumoto model for a Pt/BaO/ Al_2O_3 catalyst; however as mentioned earlier rhodium is a common additive in the NSR catalyst. It is therefore likely that rhodium is the active species in the

reduction of N_2O to N_2 , as well as being responsible for the reduction of NO to N_2 . If rhodium does not play an active role in the reduction of N_2O this has profound implications for the choice of NO_x storage material as it must be capable of reducing NO under anerobic conditions. Also of interest was the apparent potential of potassium as an alternative NO_x storage medium to barium oxide, as it demonstrates a greater NO_2 storage ability and reduces NO more completely.

6.2 Future Work

From the above it is apparent that a more detailed examination would be useful to aid characterisation of the K/Pt(111) and BaO/Pt(111) systems described. In particular additional XPS and IR data would be useful in examining the nature of the stored NO_2 on K and BaO and partially reduced NO species on BaO as an aid in mechanistic determination.

REFERENCES

1. Matsumoto, S., Ikeda, Y., Suzuki, H., Ogai, M., Miyoshi, N., *Appl. Catal. B.*, **25**, 2000, 115.
2. Masahiko, T., Matsumoto, S., *Topics in Catalysis*, **28**, 2004, 151.
3. Comrie, C.M., Lambert, R.M., *Surf. Sci.*, **46**, 1974, 61.
4. Hayden, B.E., *Surf. Sci.*, **131**, 1983, 419.
5. Gland, J.L., Sexton, B.A., *Surf. Sci.*, **94**, 1980, 355.
6. Campbell, C.T., Ertl, G., Kuipers, H., Segner, J., *Surf. Sci.*, **107**, 1981, 207.
7. Gland, J.L., *Surf. Sci.*, **75**, 1978, 733.
8. Kiskinova, M., Pirug, G., Bonzel, H.P., *Surf. Sci.*, **133**, 1983, 321.
9. Bonzel, H.P., *Surf. Sci. Rep.*, **8**, 1987, 43.
10. Kiskinova, M.P., Pirug, G., Bonzel, H.P., *Surf. Sci.*, **140**, 1984, 1.

